Author:
Salter, N

Title:
Creep-feed cylindrical grinding of deep forms.

CREEP-FEED CYLINDRICAL GRINDING OF DEEP FORMS

BY

NIGEL SALTER

A dissertation submitted for the Degree of Doctor of Philosophy at the University of Bristol

March 1985

"Science and Engineering produce 'know-how';
but 'know-how' is nothing by itself; it is
a means without an end, a mere potentiality,
an unfinished sentence."

E F Schumacher

'Small is Beautiful'

SUMMARY

Creep-feed grinding is a method of grinding which employs larger depths of cut (1mm upwards) and correspondingly lower feed rates than conventional grinding.

Having become established as an effective method of grinding 'difficult-to-grind' materials such as Nickel-based alloys, creep-feed grinding is now being increasingly used to grind deep forms in comparatively 'easy-to-grind' materials. Complete profiles can be ground to reasonable tolerances in pre-hardened steel components without having to pre-cut the form before heat treatment.

The work reported in this thesis considers one particular potential application - the grinding of ballscrew tracks.

Established relationships between the relevant parameters in creep-feed grinding are reviewed and experimental results show how these can be extended to form grinding applications.

Workpiece temperatures are of particular interest in ballscrew grinding if errors due to thermal expansion are to be avoided. A new method of measuring how much of the heat generated in the creep-feed grinding process enters the bulk of the workpiece was therefore developed and some interesting results obtained. These results suggest that there is a limit to the mean workpiece surface temperature which can be sustained without burning occuring. This temperature is shown to depend on the type of grinding fluid used and on the workpiece material. The fraction of the heat generated which is conducted away through the workpiece under stable grinding conditions was measured at less than 2.5% for a water-based grinding fluid and at approximately 13% for an oil-based fluid.

The consequences of these results are investigated with the

aid of a theoretical heat flow model which demonstrates the effect of various geometrical factors on the limiting power flux which can be dissipated before the critical temperature is exceeded.

Further experimental work investigated the influence of the type of grinding fluid used and workpiece material properties on grinding performance.

MEMORANDUM

The accompanying dissertation "Creep-feed Cylindrical Grinding of Deep Forms" is submitted in support of an application for the Degree of Doctor of Philosophy at the University of Bristol.

The work has not been submitted for any other degree in this University nor for an award of a Degree or Diploma of any other institution.

The dissertation is based on independent work by the candidate - all contributions from others being acknowledged in the dissertation itself.

I hereby declare that the above statements are true.

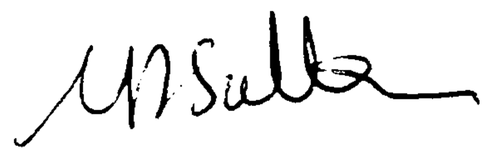

NIGEL SALTER

ACKNOWLEDGEMENTS

I would firstly like to thank Dr T D Howes for his advice and encouragement throughout the period of this research work. I would also like to thank Dr T R A Pearce for his useful and constructive discussions and Dr J M Morgan for his help with the metallurgical aspects.

Thanks are also due to the technical staff of the Mechanical Engineering Department for producing all the test specimens and for helping to maintain and develop the test rig. In particular I would like to thank Clive Calder for his help in this respect.

Of the industrial companies that have contributed I should like to thank T I Matrix for their sponsorship of the work, J K Smit & Sons for providing the diamond roll dressers, the Universal Grinding Wheel Company for the grinding wheels used and P G M Ballscrews Ltd for the information on ballscrew grinding and for providing some of the material used. Also I should like to acknowledge the Science and Engineering Research Council for the provision of my Industrial Studentship.

Thanks as always go to Nikki, without whom this thesis would never have been completed.

CONTENTS

TABLES

PLATES

FIGURES

NOMENCLATURE

a	(mm)	Depth of cut
C_L	(W/m²/°C)	Heat Loss coefficient
C_p	(J/Kg/°C)	Specific heat coefficient
d	(mm)	Diameter of pin (pin tests)
d_s	(mm)	Diameter of grinding wheel
d_w	(mm)	Diameter of workpiece
e	(J/mm³)	Specific grinding energy
e_c, e_s	(J/mm³)	Cutting and sliding components of specific grinding energy respectively
F_N, F_T	(N)	Normal and tangential force components respectively
F'_N, F'_T	(N/mm)	Normal and tangential force components per mm width of cut
F_{NC}, F_{TC}		Normal and tangential components of cutting force
F_{NS}		Normal sliding force component
H	(W/mm²)	Mean power flux in the arc of cut
H_b	(W/mm²)	Mean power flux at onset of burn
h	(W/m²/°C)	Convective heat transfer coefficient
k	(W/m/°C)	Thermal conductivity
ℓ_c		Length of wheel - workpiece contact arc
q_w, q_v		Energy partitioning parameters
R_a	(μm)	Surface roughness
T	(°C)	Temperature
T_a	(°C)	Ambient temperature
T_b	(°C)	Surface temperature of pin
T_B	(°C)	Surface temperature of pin at onset of burn
T_c	(°C)	Coolant temperature

t	(°C)	Temperature rise above ambient
V_d	(μm/rev)	Local normal dresser infeed rate
V_D	(μm/rev)	Radial dresser infeed rate
V_f	(mm/min)	Table speed (surface grinding)
V_n	(mm/min)	Local normal infeed rate
V_N	(mm/min)	Maximum normal infeed rate (MNIR)
V_p	(mm/min)	Plunge feed rate (pin tests)
V_s	(m/s)	Grinding wheel surface speed
V_w	(mm/min)	Workpiece surface speed (cylindrical grinding)
Z	(mm^3/sec)	Stock removal rate
Z'	(mm^3/mm/sec)	Normalised stock removal rate
α		Angle subtended by grinding arc at workpiece axis
OR	(m^2/sec)	Thermal diffusivity
β		Angle subtended by grinding arc at axis of grinding wheel
γ		Angle of ground face relative to workpiece axis
Λ		Grinding parameter (after Hahn Reference [16])
ρ	(Kg/m^3)	Density
σ_n, σ_t	(N/mm^2)	Local grinding stresses
η		Ratio of tangential to normal stresses
μ		Coefficient of friction

Additional symbols are used which are relevant in each appendix only, and are fully described where used.

CHAPTER 1

Introduction

1.1 Background

Creep-feed grinding is a high stock removal rate grinding process which has proved to be especially effective for grinding 'difficult-to-grind' materials. The principal difference between creep-feed and conventional grinding is the depth of cut. Indeed, creep-feed is often descriptively referred to as 'deep grinding'. Conventional or shallow-cut grinding employs small depths of cut, usually in the order of 10 - 20μm, and many passes of the grinding wheel to remove the material, whereas creep-feed grinding is typically carried out with depths of cut between 1mm and 20mm and only one or maybe two passes. The feed rate is much reduced compared with conventional grinding, hence the name creep-feed.

Creep-feed grinding is an abrasive machining process; that is, it is generally a stock removal operation rather than a finishing one, although for many applications an adequate surface finish is attainable.

One successful application of creep-feed grinding has been the grinding of turbine blades for gas turbine engines. These blades are cast in Nimonic alloy, which is recognised as being difficult to machine, and creep-feed grinding is then used to produce the 'fir-tree' form on the blade roots. Research into this application has been particularly fruitful and useful advances have been made. [1] *

However, the use of creep-feed grinding is not limited to

* Numbers in brackets refer to references which are listed on pages 121-129.

difficult materials. It has been found to be an effective way of grinding 'easy-to-grind' materials in certain cases, especially where forms are concerned, and machine tool manufacturers are now producing machines for this purpose. [2,3,4]

Grinding deep slots in relatively short components is one example where creep-feed appears to show an advantage over conventional grinding. When grinding a short component the time lost in reversing the table direction at the end of each pass, during which the grinding wheel is not actually grinding, is a significant proportion of the total grinding time; the shorter the grinding pass, the greater the time lost. If a single pass creep-feed method is used the time wasted is reduced and overall grinding times can be reduced, even for the same metal removal rate. [5]

In cylindrical grinding this advantage will not apply, but other factors may become more relevant. For example, the low rotational speeds employed enable large asymetric components to be ground without any out of balance problems arising.

One specific advantage of creep-feed that recommends it for form grinding is its accepted ability to maintain form profiles over a longer grinding time than is the case in conventional grinding. This allows more material to be removed without redressing the grinding wheel. As a consequence, either full forms can be ground from a plane workpiece in a single pass or more components can be ground between dressing cycles depending on the individual case.

Many processes involve rough cutting a form in a soft steel component, hardening it, and then finish grinding the form, often in several passes. Using creep-feed

allows the complete form to be ground directly in a hardened steel blank, thereby removing one complete operation. The even wheel wear characteristics ensure that the profile can be maintained whilst large amounts of material are removed.

1.2 Ballscrew Grinding

The industrial sponsors of this work (T I Matrix) have been producing what are effectively creep-feed thread and tap grinders for many years. Creep-feed is used not only because of its good form holding capabilities, but also because it alleviates the need to keep rewinding the thread. Each grinding pass, under conventional grinding practice, would normally have to be made in the same direction or else backlash and elastic deflections in the machine would introduce inaccuracies. Using a creep-feed single pass there is no time lost in rewinding.

These problems become more significant when greater accuracy is required and especially so on long components. Leadscrews, and in particular ballscrews, are one such type of component where this is so. Ballscrews, for recirculating ballscrew assemblies, can often be over 1m long yet cumulative pitch tolerances of 15μm for a 1m thread may still be required. [6]

At the outset of this project there was evidence of a growing market for recirculating ballscrews. [7] One of the main applications for this type of component is for the control of machine tool slideways, and the ever-increasing number of CNC tools being produced demands more ballscrews. Of the two industrial companies visited (Appendix 1) both were engaged in ballscrew production, and both were expanding their facilities. This application is of special interest to the industrial sponsor of the work as a manufacturer of ballscrew

grinding machines; the research was therefore structured with this application in mind.

Of the two companies contacted, each approaches the problem of producing ballscrew tracks differently. One pre-cuts the rough track from ground stock bar, case hardens it, and then finish grinds both the outside diameter and the track form. The disadvantage of this method centres largely on the distortion caused by heat treatment. After this operation the bar has to be straightened back to within approximately 50μm for a screw 50mm in diameter by 600mm in length. Even after this ,grinding times for a typical screw (600mm length x 50mm diameter x 5mm pitch) are around 3-3½ hours.

The second method is to case harden a stock bar to a depth below the deepest point of the form and then to grind the complete form in many passes from a solid bar. Grinding times are again very long and although the errors caused by heat treatment are avoided, the cumulative heat input to the bar over many grinding passes can cause significant pitch errors.

There are two main problems with both methods: firstly, the need to grind in many passes makes it necessary to rewind the screw and to grind in the same direction to avoid the backlash problems already mentioned. The necessity to maintain accuracy over many cycles places strict requirements on some machine design features, such as thermal stability of the machine base, leadscrew and the component. Secondly, warming of the bar can easily be sufficient to cause excessive pitch inaccuracies. Both heat generated in the grinding zone and from friction on the steadies when rewinding the thread can contribute to this temperature rise. Furthermore, uneven temperature distributions can cause the bar to bend. The use of delicate grinding practice and

refrigerated grinding fluids enable these tolerances to be maintained, but it is a slow and highly skilled process.

A single uni-directional creep-feed grinding pass in the case hardened bar would eliminate the problem of backlash and the time wasted in rewinding. Furthermore, creep-feed grinding is claimed to result in lower workpiece temperatures than conventional grinding, which would be particularly beneficial in this case. On the other hand, previous studies in creep-feed grinding suggest that the increased grinding forces encountered would require greater machine stiffness, greater spindle motor power and more efficient coolant application.

1.3 Aims of the Research

Research so far carried out at the University of Bristol into the creep-feed grinding process has established some fundamental relationships for creep-feed grinding plane workpieces [8]. However, as illustrated in the previous sections creep-feed has particular advantages in form grinding applications. The first objective of this work therefore is to extend the understanding of the process so that it can be applied to form grinding operations.

One factor which is going to be significant in the process is the method of dressing used. The technique often currently used to generate the form on the grinding wheel is to traverse a single point diamond across the wheel guided by a former plate. This method is relatively slow and is not always reliable. As the diamond wears, the form accuracy is lost unless constantly checked.

Increasingly diamond roll dressers are being used. These consist of a roll with the required form reproduced

in it, which is plated with many small diamonds. This is rotated and plunged into the rotating grinding wheel to both generate the form and to condition the grinding wheel. There are several types of roll, each for different applications, but the one used for high accuracy is a reverse electroplated type capable of producing a form to an accuracy of 2μm. Although the initial cost of such a roll is high, they can reliably reproduce profiles quickly and for many dressing cycles without the need for constant inspection. This method of dressing has been employed throughout the work since it is likely to be used on any dedicated automated machine. Special emphasis has been placed on the consequences of its use for dressing forms.

A method known as 'continuous dressing' by which the wheel is continuously dressed whilst it is grinding has proved to be beneficial in increasing the stock removal rate when grinding difficult-to-grind materials [9]. For form grinding applications the technique has the added advantage that there can be no deterioration in the shape of the profile being ground under normal grinding conditions since it is being constantly dressed. However, the amount of wheel used will be high and the use of this technique may well only be justified when grinding certain types of material.

The material to be considered in this case is a 1% Chromium steel, typical of that used in ballscrew production. It is considered to be an easy-to-grind material.

A further aim of the work is therefore to assess the grindability of steels relative to that of a difficult-to-grind material such as Nimonic alloy. This will not only help in judging the desirability of continuous dressing, but will also produce useful information on the creep-feed grinding of steels.

Workpiece temperatures have already been shown to be of particular interest in this piece of work. For many years researchers have been producing widely varying estimates, under both creep-feed and conventional grinding conditions, of what the actual workpiece temperatures will be under any grinding conditions. The essence of the problem is to determine how much of the energy used in the grinding process actually enters the workpiece as heat.

The reasons for doing further research into the field of workpiece temperatures are twofold..

The successful application of creep-feed grinding depends upon the ability of the coolant to remove heat from the grinding zone. It appears that if the workpiece surface exceeds a certain critical temperature a change in the heat transfer mechanism results in a drastic reduction in this ability. Knowing how much heat is going into the workpiece enables the temperatures to be calculated and, hence, the limiting stock removal rate. In addition to this general limitation there is a further need to understand the thermal aspects of the process in the ballscrew application where workpiece temperatures have been shown to be an important factor if accuracy is to be maintained.

One of the major aims of this work then is to establish how much of the energy used in the grinding process does enter the workpiece as heat and what factors influence it.

A further question which arises in the field of thread form and ballscrew grinding is the type of grinding fluid to use. Such operations are often carried out using a neat oil. However the cost and health problems associated with this make water based fluids look increasingly attractive.

The type of fluid used is going to influence the rate of wheel wear, the surface finish and the limiting stock removal rate. It would also be expected to influence the temperatures reached and is therefore of particular interest to this study.

In summary the aims of the research programme can be broadly divided into four sections:

1 To extend existing understanding of the creep-feed grinding process to form grinding applications.

2 To investigate the grindability of steels under creep-feed conditions.

3 To determine the fraction of the grinding energy which enters the workpiece as heat, and to assess the implications of this on workpiece temperature.

4 To compare oil and water based grinding fluids with respect to workpiece temperatures, limiting stock removal rates and surface finish.

The sections given above are not meant to imply a format to each of the chapters. Because of the interconnection between these topics a more general structure has often been adopted, particularly in Chapters 2 & 6.

CHAPTER 2

Previous Work

2.1 Conventional and Creep-feed Grinding

Research into creep-feed grinding, as opposed to grinding in general, is relatively limited. However, much of the understanding of the way in which a grinding wheel behaves can be applied throughout the range of grinding practice from conventional to creep-feed.

Some of the earliest quantitative work undertaken to try to understand the grinding process was carried out in 1952 by Marshall and Shaw [10]. In their paper they established many of the basic parameters which are still used today for quantifying grinding operations. They mounted workpieces on a dynamometer on a surface grinder and measured forces in the horizontal and vertical directions. Since for a conventional grinding operation the vertical force will pass virtually through the centre of the grinding wheel, they considered that the energy used in the process could be taken as the horizontal force multiplied by the wheel surface speed. This not only gives a measure of the power to be supplied and then dissipated in the process, but also, since the stock removal rate can be determined from the depth of cut and the table speed, it allows the specific grinding energy to be calculated. This is the amount of energy required to remove a unit volume of workpiece material and is an important measure of the efficiency of the process. Generally the higher the specific energy, the lower the limiting stock removal rate which can be achieved before workpiece burning occurs. Marshall and Shaw also showed the not surprising fact that forces are proportional to the width of the workpiece, and it is now common practice to normalise the forces to a unit

workpiece width.

Interestingly, Marshall and Shaw discovered that the specific energies in grinding were typically an order of magnitude bigger than those measured in metal cutting operations. In a subsequent paper [11] they explained this in terms of dislocation theory, claiming that the very small chip thickness resulted in the shear stress of the material approaching the theoretical value. They tried to confirm this with a 'micromilling' technique but found that milling with very small chip thicknesses still did not give the same high energies. They suggested that this could be due to the large negative rake angle likely to be found on the average grinding grit which could result in a large amount of plastic chip deformation and friction on the rake face. Although later work showed this to be only partly so [12,13], these papers contributed much to early grinding research.

In subsequent years, several papers were published which added to the understanding of Marshall and Shaw's original experimental results. In 1955 Hahn published a paper [14] which recognised that a grinding grit has no clearance on the wear land behing the actual cutting edge. Indeed he recognised that because the path of an individual grit is trochoidal relative to the workpiece there can be a positive contact force between this land and the workpiece which will significantly contribute to the overall grinding force. A further paper published at about the same time [15] established equations for the geometry of the undeformed chip under a variety of grinding conditions, and underlined the importance of the maximum thickness of the undeformed chip, which is basically a wedge but curved into a trochoidal shape, in influencing the magnitude of the grinding forces.

In 1966 Hahn published a paper [16] which divided the grinding action into three categories: rubbing, ploughing and cutting. He postulated that when up-grinding (in up-grinding the direction of wheel rotation is such that the cut is from the bottom of the contact arc to the top and vice versa for down-grinding), the grit initially rubs against the workpiece surface causing local elastic deflections, then it starts to plough material aside, forming a burr and then eventually, as the normal force at the leading edge becomes large enough, it forms a chip. Hahn's results were obtained predominantly on easy-to-grind materials under fine grinding conditions. He used an experimental set-up which maintained a constant normal grinding force to avoid changes in grinding conditions due to elastic deflection of the machine, and thus determined the cutting ability of the wheel purely as a function of the normal force. Hahn considered an easy-to-grind material to be one with which negligible rubbing or ploughing took place. This results in a plot of normal force against stock removal rate being a straight line through the origin. If a significant amount of rubbing and ploughing is taking place then this plot would have an intercept on the force axis, since a fraction of the measured force would not be contributing to the actual stock removal. Materials which show the latter characteristic are classed as difficult-to-grind. For easy-to-grind materials, Hahn defined a 'metal removal parameter' (Λ) which is simply the gradient of the normal force versus metal removal rate characteristic. This can be defined by

$$Z' = \Lambda F'_N$$

In another paper [17] Hahn discussed the transition from ploughing to cutting in more detail, and showed that the transition from ploughing to cutting occurs when a fracture appears in the plastic region under each grit.

The force at which this occurs will depend on the material being ground, and hence the classification of easy and difficult-to-grind materials.

Malkin subsequently published a paper [12] which took this concept much further. He correlated the grinding forces with the area of the wear flats on the grits, and showed that as a wheel wears, these flats increase in size and that the grinding forces increase proportionally. He labelled this wear mechanism as attritious wear and showed it to be fundamental in the grinding process. He divided the grinding force and hence also the specific grinding energy into two components, a cutting energy (e_c) which includes both ploughing and chip formation energies, plus a sliding energy (e_s) owing to friction on the wear flats. Hence:

$$e = e_c + e_s$$

It is the sliding energy which increases as the grit wears, hence the overall grinding energy increases. By plotting specific energy (e) against the area of the wear flats and extrapolating back to zero wear flat area, Malkin determined the value of the specific cutting energy. He also showed that at a critical wear flat area, the plot of grinding forces against wear flat area showed a sharp change in gradient, corresponding to workpiece burning. He argued that this was due to very high temperatures under the grits allowing plastic flow of the workpiece material which inhibits chip formation. Hence there is a return to a predominantly ploughing regime, which has been confirmed by observation of burrs thrown up by ploughing under these conditions [17].

In another paper [18] Malkin showed that whilst attritious wear is important in controlling the cutting ability of the wheel, it is insignificant in influencing the overall rate of wheel loss. He described a second mode of wheel

wear which is caused either by bonds between grits breaking or grits themselves fracturing. This he called fracture wear. His experiments showed that as the wear flat on a grit grows, so does the force on it until eventually it is either fractured or torn from the wheel. This mechanism is the primary cause of wheel loss under conventional shallow-cut grinding conditions.

Scientific studies of creep-feed grinding are still relatively few. One of the first was carried out by Shafto [8] who established many fundamental relationships for creep-feed. Since Shafto's work is fundamental to the investigation reported in this thesis it will be discussed in some detail.

Shafto creep-feed ground both an easy-to-grind material (AISI 01 Annealed Tool Steel) and a difficult-to-grind material (C1023 Nimonic alloy) and measured the variation of the grinding stresses (grinding force per unit area of contact) around the long arc of cut. This is important under creep-feed conditions for two reasons. Firstly, unlike conventional grinding, the point of action of the resultant grinding force will not, under surface grinding conditions, be vertically below the centre of the wheel. Hence both horizontal and vertical forces will contribute to the tangential force experienced at the wheel periphery. So to calculate the tangential force and, from this the energy used in grinding, it is necessary to know whereabouts the resultant force acts. Secondly, by knowing the stresses around the arc the relationships between the local stresses and local infeed can be determined. Shafto suggested that creep-feed, with its characteristically long arc of cut, could be thought of as a series of plunge grinding operations, varying in feed rate from a maximum at the top of the arc of cut to zero at the bottom. The stress results which he obtained confirmed this since they showed that, for an easy-to-

grind material, the local stresses were directly proportional to the local infeed rate normal to the wheel surface. His results also showed that the resultant grinding force could be considered to act at a point one third of the way from the start of the arc of cut.

It should be mentioned here that creep-feed is normally carried out in a down-grinding mode whereas conventional grinding is done in an up-grinding mode. This has been shown to give lower grinding forces, a higher limiting stock removal rate and a better surface finish [19]. In terms of chip formation this mode of grinding results in the chip thickness starting at a maximum and decreasing throughout the arc. In conventional cylindrical grinding the opposite mode is preferred for two reasons; it eliminates backlash problems in the workhead drive but also it has been found to give lower grinding energies [17]. Hahn explained this in terms of the interference between the wear flat on the grit and the workpiece. Because the grit path relative to the workpiece is trochoidal, but the wheel circular, under down or climb grinding conditions this interference will reduce the stress level at the leading edge of the grit, thus promoting an early transition from cutting to ploughing. In creep-feed however, the much lower feed rate means there is much better conformity between the wheel and the grit path which reduces this problem. Ohishi et al [20] showed that by using climb grinding under creep-feed conditions the chip formation starts at the beginning of the arc and can be maintained all the way to the bottom. This results in negligible ploughing and a lower overall grinding energy. A further advantage is that the coolant can more effectively be applied at the start of the arc where the local stock removal rate is greatest.

Shafto's finding that the local stresses could be directly related to the local normal infeed rate led to

the conclusion that the specific grinding energy and the ratio between the tangential and normal stresses (η) are constant around the arc of cut for any particular feed rate. For an easy-to-grind material he defined these stresses as

$$\sigma_n = \Lambda . V_f \ Sin\theta$$

and

$$\sigma_t = \eta . \Lambda . V_f Sin\,\theta$$

where $V_f Sin\,\theta$ is the local normal feed rate at an angle θ from the end of the arc of cut, and Λ is a grinding parameter similar to that used by Hahn [16]. By integrating these stresses around the arc of cut he derived equations for the total grinding forces which agreed well with the measured results.

The integration is effectively the area enclosed under a plot of local stress against position around the arc, starting from a maximum at the beginning of the arc to zero at the bottom. Shafto showed that the specific grinding energy is uniquely related to this maximum normal infeed rate (MNIR - the feed rate normal to the wheel surface at the start of the arc of cut) over a wide range of feed rates and depths of cut. Halving the arc length (ℓ_c) for example by reducing the depth of cut would halve the total grinding forces, provided the MNIR (V_N) was kept constant. However, the stock removal rate can be shown to be

$$Z' = \tfrac{1}{2} V_N \ell_c \qquad \text{(See Appendix 2)}$$

Hence the stock removal rate would also be halved and the specific grinding energy would remain the same. This result is significant since it suggests that grinding operations carried out with different depths of cut, wheel size or mode (cylindrical or surface

grinding) can be compared, provided they are described in terms of this maximum normal infeed rate.

2.2 Creep-feed Form Grinding

Many comparisons of creep-feed and conventional grinding have been made, and one feature which they all report is the good form holding characteristics of creep-feed [5, 21, 22, 23, 24].

Several researchers [23, 24] have suggested that the reason for this is the lack of multiple wheel-workpiece encounters as would occur in conventional surface grinding. However, the same characteristic has been observed under cylindrical grinding conditions [25] which suggests that this is not entirely so. Trmal [5] has carried out experiments using interupted grinding passes to check this hypothesis and his results further confirm that the lack of multiple impacts is relatively insignificant. He suggests that the cause has more to do with the predominant wheel wear mechanism. Malkin [12, 18] showed that there are two wheel wear mechanisms acting simultaneously, and under conventional grinding conditions fracture of the grit and bond was shown to be the predominant mechanism. However, creep-feed grinding results in considerably lower forces per active grit. The predominant undeformed chip shape is long and thin as opposed to short and fat as is the case for conventional grinding, which means that the force on a grit will be lower, but will act over a longer time [26]. The lower instantaneous force is not as effective at fracturing the bond or grit, and hence attritious wear tends to dominate. Larger wear flats will be formed before the force on a grit is sufficient to remove or fracture it. Softer wheel grades are therefore used in creep-feed to try and promote fracture wear and

avoid large wear flat areas, but the predominant wheel wear mechanism is still by attrition. Trmal argues that when a profile involves a convex curvature on the wheel, grits on the peak of the profile will be easier to remove than those on a flat face due to the smaller bonded area. Hence under conventional grinding conditions they would be relatively easily removed. However under creep-feed conditions they may still only be attritiously worn rather than plucked from the wheel and the wear would therefore be more even around a profile.

Grinding wheels used for creep-feed are usually soft coarse wheels with a large degree of porosity. The coarse open structure reduces the number of active grits and hence increases the undeformed chip thickness. This, together with the softer wheel grade, helps promote fracture wear, which allows blunted grits to be removed from the wheel. The high degree of porosity aids coolant supply as will be discussed in Section 2.4.

The form holding abilities therefore seem to stem mainly from the wear mechanism being one of attrition rather than macroscopic removal of grits. This attritious wear mechanism has been shown to be partly due to chemical reaction and is, therefore, a function of temperature [27] hence the long contact length,which allows high grit temperatures to be reached, may promote the growth of wear flats. New ultra-hard abrasives which resist this type of wear, such as CBN, are therefore proving especially beneficial for creep-feed form grinding operations [28,29].

Other work specifically on creep-feed form grinding is scarce. One recent result which is relevant is that of Saljé et al [30]. This paper reports the results of grinding tests carried out at a range of face angles. The angle between the grinding wheel face and the wheel

axis was varied from 0° to 60°. Forces in directions both perpendicular to the wheel axis and axially along it were measured. The results obtained suggest that the resultant of these two forces always acts normal to the grinding face and that its magnitude is independent of the angle for similar grinding conditions.

The use of diamond roll dressers is particularly relevant to form grinding. A thorough study of diamond roll dressing and the grinding characteristics associated with its use was carried out by Malkin and Murray [31]. They showed that for any particular type of roll the important operating conditions are the roll to wheel surface speed ratio and the infeed of the roll per revolution of the grinding wheel. Nowadays the form accuracy which can be obtained with this type of dresser has reached 2μm [32] but their use has been inhibited by their high initial cost. However, now that grinding times are improving the time taken to dress the wheel is becoming significant and diamond rolls are quicker. Furthermore diamond rolls are suitable for use in automatic cycles since they can accurately reproduce a complicated profile without the need for time consuming setting or inspection [33].

2.3 The Effect of Workpiece Material on Grindability

Clearly the properties of a workpiece material are going to influence its grindability. This can be in a number of ways. Initially it would seem that the ultimate shear stress of the material would be significant in influencing the forces necessary to form a chip; however, as Malkin and others have shown [12] the chip formation energy is only a part of the total energy expended in the process. Rubbing on the wear flats also contributes a significant proportion to the total power requirement. Yet the growth of the wear flats appears to

be partially due to abrasive wear [34] and its rate therefore is going to depend on the nature of the workpiece material. Malkin showed that once the specific cutting energy for a material had been separated from the total grinding energy this value could be more closely correlated with the melting point of the material, which he took as a measure of the strength of the atomic bonding. In another paper [35] Malkin argued that the minimum specific cutting energy should tend towards the melting energy of the material being ground. The fact that it tends towards a higher value he explained by the presence of friction on the rake face of the grits which are likely to be at a negative angle of about -60° [36]. The experimental work was carried out on a variety of materials using neat oil as a lubricant so as to minimise the effect of friction on the wear flats.

In conventional grinding then, where the rubbing energies can be small it would be expected that steels of different hardness would exhibit similar specific grinding energies since the melting temperature will be constant. This characteristic has been observed by both Marshall and Shaw [10] and Malkin [12], yet Schleich [26] does report a small difference with hardness. However, under creep-feed conditions a hardness effect may be more apparent because of the thinner chips and the predominantly attritious wear mechanism.

Salmon [9] has carried out measurements of wear flat area when creep-feed grinding a difficult-to-grind Nickel based alloy, which is known to exhibit specific energies which rapidly rise to more than 400J/mm^3 under creep-feed grinding conditions. He continuously dressed the grinding wheel whilst grinding using a diamond roll dresser and maintained different wear flat areas by varying the dresser infeed rate. In this way he plotted specific energy against wear flat area just as Malkin did.

However, because he was able to achieve very low wear flat areas he did not have to extrapolate back so far to obtain the specific cutting energy. This revealed that Malkin's extrapolation may possibly have resulted in a value of cutting energy that was too high, and that the specific chip formation energy may be closer to the melting energy than Malkin expected.

The rapid rise in wear flat area when grinding Nimonic alloy can soon lead to a state where 97% of the grinding energy is rubbing energy [9]. On the basis of these findings the 'continuous dressing' technique is now being used commercially to reduce grinding energies drastically and thus raise the stock removal rates by, in some cases, 25 times [37]. This technique however will clearly lead to rapid wheel usage and may not therefore always be economically justified [38] despite massive claims for its potential [39]. Materials which are difficult-to-grind in creep-feed are materials which give rise to rapid growth of wear flats on the grits, which may not necessarily be the same criterion as for conventional grinding where the stress needed to cause a plastic fracture at the leading edge of the grain is the controlling parameter [17].

Werner [40] has developed a semi-analytical model of the grinding process that calculates grinding forces for any grinding condition from conventional through to creep-feed. The grindability of a material is reflected in his equations by an exponent in the range 0.5 - 1, one end being a predominantly rubbing regime and the other a cutting regime. It is difficult to extract physical understanding of the grinding process from Werner's model, especially without the experimental examples needed to illustrate the parameters involved, nor, so far as it is possible to tell, does the model take into account elastic deflections of the grinding wheel which

increase the true contact arc length under shallow cut conditions [41].

2.4 Workpiece temperatures and the Burn Limitation

The fact that so much research has been carried out on temperatures in workpieces under a variety of grinding conditions reflects the importance attached to this topic. Much of this work is summarised by Snoeys et al [42] who list over 150 references on topics related to temperatures in grinding. Despite this vast amount of work there is still much disagreement about the fundamental concepts when considering the thermal aspects of grinding. The reasons for this appear to stem from the vast array of grinding conditions under which experimental work has been carried out by different researchers, and from a certain amount of confusion over what the temperatures measured actually relate to.

There can be two possible reasons for concern over workpiece temperatures - thermal damage or workpiece distortion. Thermal damage can appear in many forms [43, 44] but in steels it is usually associated with a visible oxide layer, a hard surface layer of Martensite and a soft tempered layer below it. Littman and Wulff [44] have found that a surface temperature of 840°C is necessary to cause rehardening of the surface layer by quenching from the bulk of the material, but, essentially, the surface layer has to rise above its austenising temperature for rehardening burn to occur although temper burn can be caused at lower temperatures. For conventional grinding this is accompanied by an increase in the grinding forces and an increase in wheel wear [45]. When grinding coolant is being used quenching of the hot surface can also lead to grinding cracks.

The problem of thermal distortion is related more to the bulk temperature of the workpiece than to the transient surface temperature, hence in the case of a conventional cylindrical grinding operation the total temperature rise can be thought of as a steady state bulk workpiece temperature plus a once per revolution transient. It would be the former that would cause bulk workpiece deformation and the latter thermal damage [46].

Almost all the analyses of workpiece temperatures under conventional grinding have been based on Jaeger's classic paper [47]. This is a general solution for a heat source moving over a semi-infinite plane, and it provides solutions for the transient temperature field in two dimensions. One of the more significant of the analyses based on Jaeger's work is that of Des Ruisseaux and Zerkle [48]. This extends Jaeger's original model to include surface cooling from the remainder of the workpiece surface, although other researchers have also developed models based on the same original equations [49, 50, 51].

One problem with applying this type of model is in knowing how much of the energy used in the grinding process goes directly into the workpiece. Malkin [52] studied this problem in some detail and reported that virtually all the rubbing and ploughing energy goes into the workpiece plus 55% of the chip formation energy. Since the amount of rubbing energy can vary so much depending on the wheel, the dressing and the grinding conditions, this may help explain the widely different estimates of the total percentage entering the workpiece which are discussed by Maris et al [53]. Using the partition values obtained [52] Malkin attempted two analyses [54]. The first considered each grit as a heat source and broke this down further into two sources, one at the shear plane and one under the wear flat; the second treated the whole contact arc as a heat source and

calculated a mean grinding zone temperature. To determine the instantaneous temperature local to a grit the first is superimposed upon the second. This analysis suggested that the temperature at the leading edge of a grit is indeed close to the melting point of the material as Malkin had previously postulated [12], yet burn only occured when the mean grinding zone temperature reached the austenising temperature.

It is worth mentioning here that the circumferential spacing between successive active grinding grits is very large compared to the size of the wear flats on a grit. Bhattacharyya et al [55] for example have measured the wheel profile and shown that the distance between successive grits may be in the order of 50 - 100 times the circumferential dimension of a wear flat. From this result it is not surprising that it is the mean surface temperature and not the high transient temperature under the grit that controls the burn limitation.

A typical conventional grinding arc length would be 1 - 2mm yet Bhattacharyya's measurements [55] suggested that the distance between successive active grains may be as much as 10mm. So although only one or two grits may be present in the grinding arc at any one time, the total number passing a point in the workpiece may be large. Des Ruisseaux and Zerkle [56] estimated the number of grits to pass any point in the workpiece to be in the order of 100 - 250. In view of this, most models consider the interference zone as a continuously acting uniform heat source.

The application of coolant appears to be not very effective at reducing the high local surface temperature in the grinding zone, although it is reported to reduce the bulk workpiece temperature [46]. Consequently grinding fluids with good lubricative properties are generally

preferred for reducing temperatures under conventional grinding conditions, since these reduce the amount of energy to be dissipated by reducing the sliding energy. [57].

Many experimental arrangements have been used to measure the grit contact temperature. These often rely on the formation of a thermocouple between a thermocouple wire embedded in the workpiece and the workpiece material as the grinding grit passes [51, 58, 59]. Other researchers however have used thermocouples placed at various distances below the surface [52, 8, 46]. These results confirmed that very high temperature peaks do exist but that their influence is limited to very small depths below the surface.

In creep-feed grinding Jaeger's model appears not to be generally applicable since the heat source is not moving rapidly over a plane surface which is an assumption of Jaeger's model. It is often suggested that creep-feed grinding only works because any thermal damage is in that part of the arc of cut which is subsequently ground away [61, 62]. However generally no such damage has been reported on tests stopped whilst the full arc of cut is still maintained [8, 9, 62]. The amount of heat being generated in a creep-feed grinding operation may well be as much as 1kW per mm width of workpiece, hence it would seem likely that only a small fraction of this can be going into the slow moving workpiece if the process is to work at all. If this is so then the action of the coolant in removing the heat generated must be crucial in creep-feed grinding.

One recognised feature of creep-feed grinding is thermal surging; both the forces and the workpiece temperatures can suddenly rise rapidly and then fall again. Shafto [8] explained this in terms of film boiling. He suggested that at a critical power flux, the heat transfer mechanism

from the coolant changed from nucleate to film boiling, thereby drastically reducing the heat transfer coefficient and allowing the workpiece temperature to rise. He then suggested that the high temperatures accelerated the wheel wear allowing self-sharpening and a return to stable grinding conditions to take place. If this hypothesis is correct then it would appear to be impossible to grind satisfacorily with workpiece temperatures in excess of the burnout temperature which is about 120°C [63]. Shafto found that the maximum power flux (which is at the top of the arc of cut) at which these surges occurred was between 32 and 36W/mm² and concluded that this criterion could be used for determining the limiting stock removal rate under creep-feed grinding conditions.

Further work on coolant application was carried out by Powell [64], who used an electrically heated dummy workpiece to determine the burnout power flux under various methods of coolant application. Powell's work also suggested that the maximum power which could be dissipated was in the order of 30-40W/mm². He also showed that to achieve this, it is important that the coolant be applied effectively throughout the arc of cut, and that of the various methods he tried the best way to do this was by means of a coolant 'shoe'. This 'shoe' is situated just ahead of the grinding zone (See Plate 2) and in intimate contact with the grinding wheel. Grinding fluid is applied under pressure and enters the structure of the wheel, which has induced porosity to allow this to happen. It is then expelled from the wheel under the action of centrifugal force and, provided the system is correctly designed, will provide a coolant supply throughout the arc of cut which may well be in excess of 50mm in length. Powell showed there to be a critical shoe pressure below which an adequate supply of coolant is not maintained and the power flux at burnout falls. Other methods of coolant application have been tried [65] but for research applications

the coolant shoe still provides a consistent method of achieving an adequate coolant supply.

Values of burnout power flux lower than 35W/mm² have been reported by Ohishi et al [20] for example, but it is not clear whether the grinding fluid is an oil or a water based one. Stuart [62], however, reports values of burnout power flux of approximately 24W/mm² when using a water based fluid.

One of the few models not based on Jaeger for predicting temperature under conventional grinding conditions is Werner's [60]. This model is an extension of the grinding force model already discussed [40]. Under conventional grinding conditions it is assumed that the temperatures are simply proportional to the power dissipated per unit area within the grinding arc, although Werner's paper does not offer any discussion on the actual values. Indeed in two other papers [23, 66] he shows the same characteristic but with different absolute values. For the creep-feed regime Werner claims that the temperatures are again proportional to the power flux but are inversely proportional to the time taken for the heat source to pass a point in the workpiece surface. The only correlation between this model and experimental results appears to be based on one creep-feed grinding temperature measurement at a depth of cut of 1mm, which is not a representative creep-feed condition. Even at this point on the characteristic the error between the measured value and the model is 75% which Werner suggests is due to the energy being removed with the chips, which is not included in his model. However, assuming a modest specific grinding energy of 30J/mm³ and representative material properties, this would require a chip temperature of over 5000°C.

Werner does not accept the idea of film boiling yet he does not offer any explanation of how satisfactory

cooling can be obtained in the arc of cut if the temperature there is in excess of 500°C, as he claims, [60] when film boiling is known to occur at temperatures over 160°C at best [67].

Peters' model [68] which does use Jaeger's equations but with a cooling term added in both the conventional and creep-feed regimes, claims to give good agreement with the same experimental result of Werner's, provided a chip loss of only 5% is assumed. There are, however, some useful trends reported from this model. It suggests that as the depth of cut is increased the temperature would continue to rise if no cooling were applied and that the reducing temperatures measured in the creep-feed regime are due solely to the coolant, with approximately 86% of the energy going to the coolant at a 2mm depth of cut. Peters found that in the creep-feed regime as the depth of cut increases the model tends towards a steady state condition in which the surface temperature rises until all the heat is going to the coolant, but the value of the surface temperature reached depends on the value of convective heat transfer coefficient assumed, for which Peters offers no justification. He predicts a temperature of 500°C for a 5mm depth of cut yet if a value of convective heat transfer coefficient of 0.1W/mm²/°C is used as suggested by Shafto, this would reduce the surface temperature to 100°C which falls within the possible range of stable temperatures.

One study of workpiece temperatures which relates specifically to thread grinding was undertaken by Druminski [69]. He concluded that the maximum temperatures always occur at the crests of the threads and that burn always occurs when the temperature exceeds 300°C at a point 0.6mm below the crest of the thread, independantly of the grinding or wheel conditions. Druminski's experiments were all carried out with neat oil as the

grinding fluid.

2.5 Oil versus Water as a Grinding Fluid

It is usually considered that fluids used in grinding perform two main functions, namely cooling and lubricating. Thus a water-based fluid would be chosen for its cooling ability and a neat oil for its lubricating properties.

In conventional grinding several studies [54, 57, 70, 71, 73] have concluded that the use of oil consistently results in lower specific grinding energies and longer wheel life between dressings. Mercier et al [72] concluded that the heat transfer coefficient which can be achieved in processes such as conventional grinding is not large enough to achieve a significant amount of cooling, and that the lubricative properties therefore become more significant. Lubricating the rake face of a grit will reduce the friction forces and therefore the specific cutting energy. Furthermore it is argued [57] that the use of oil attenuates the rate of growth of the wear flat, which gives longer wheel life.

A further function of the grinding fluid is to prevent the chip from adhering to the grits. This phenomenon is known as loading and is caused by the freshly ground, highly reactive surfaces present reacting with the grit material, usually Al_2O_3. Once these metallic cappings are present they will cause very high grinding energies since there is now friction between similar metals in the grinding arc. If however the new surfaces can be induced to rapidly form a stable compound on their surfaces, then this problem will be reduced or alleviated. With steels it has been shown that the presence of oxygen is important [51, 73] since this allows a thin oxide layer to form and reduce loading. Other materials,

notably Titanium [74], are well known to cause loading and to be particularly difficult to grind successfully.

Surface active additives have been shown to be very effective at increasing the rate of formation of a stable surface layer [25] and thus reducing grinding energies and wheel wear rates. These are usually sulphurated or chlorinated compounds as discussed by Duwell [75].

Precision form grinding operations traditionally use neat oil as the grinding fluid since it gives better profile retention [76]. As already discussed, profile retention is a function of the attritious wear rate of the grit, which Duwell and others [75, 27] have shown to be not only a mechanical wear process but also a chemical erosion process. Oils, with long polymeric molecules, prove to be best not only at lubricating and reducing the mechanical wear, but also at preventing reactions between the abrasive and the metal surface, thereby greatly reducing the attritious wear rate.

In creep-feed grinding it has been shown that the cooling ability of fluid is much more significant, and that the cooling properties of a water-based fluid are possibly preferable. Hassell [77] has compared oil and water-based fluids under creep-feed conditions and concluded that oil allowed a higher stock removal rate. He quotes values of mean power flux at burnout of 6W/mm^2 and 16W/mm^2 for water and oil respectively. The water value is approximately one sixth of that expected from other work [8, 64] however this may be because of the type of grinding wheel used. This was a fine grit non-induced porosity wheel similar to those used in conventional thread grinding operations which would inhibit successful through-the-wheel coolant application. Whereas oil, possibly because of its higher surface tension may adhere to the wheel surface and perform satisfacorily

when water may not. Liverton [78] has also carried out creep-feed grinding using a neat oil coolant and reports a maximum power flux of 17W/mm² (8.5W/mm² mean average around the arc). This agrees with results recently reported by Pearce and Ye [79] who quote mean burnout power flux values of 9W/mm² when creep-feed grinding a Nimonic alloy. Overall, Pearce and Ye concluded that oil gave higher normal forces, better profile retention and improved surface finish when compared with a water-based fluid but that the water-based fluid allowed significantly higher stock removal rates before the onset of burn.

CHAPTER 3

Theory

3.1 Geometry in Form Grinding

The geometry of the cutting zone under creep-feed form grinding conditions can be complicated. This section is intended to identify the ways in which feed rates are considered under plane grinding conditions, and to discuss how these may usefully be extended to form grinding operations. It is important to be clear about what is meant by plane grinding. The term plane grinding is used here to describe an operation where the ground surface is flat and parallel to both the wheel and workpiece axes when considering cylindrical grinding. In addition, if a diamond roll is being used for dressing it is intended that for plane grinding the axis of the roll should also be parallel to the ground surface.

Fig 1 shows a typical plane creep-feed cylindrical grinding operation. The length of the arc of cut depends upon the depth of cut (a) and the diameters of the wheel and workpiece (d_s, d_w) but it is usually greater than 10mm for creep-feed cylindrical grinding.

As discussed in Section 2.1 the maximum normal infeed rate (MNIR) has been shown to be a useful way of describing a creep-feed grinding operation. It was shown that for an easy-to-grind material, the local stresses have been found to be proportional to the local normal feed rate, hence the total grinding forces can be found by integrating these stresses from the maximum at the start of the arc of cut to zero at the bottom. Furthermore, the specific grinding energy, which influences how much power is to be dissipated for a given stock removal rate, was shown by Shafto to depend uniquely on the MNIR and to

be otherwise independent of the depth of cut and workpiece surface speed. Shafto showed this to be so for both an easy-to-grind and a difficult-to-grind material and it is therefore assumed to hold for the material being considered in this work. Referring again to Figure 1 the MNIR can be defined as

$$V_N = V_w.Sin(\alpha+\beta) \qquad \text{(See Appendix II)}$$

for cylindrical creep-feed grinding.

Since the grinding forces can apparently be determined in terms of the local normal feed rates, then it should be possible to extend the idea to form grinding. Consider the angle grinding operation shown in Figure 2; in this case the MNIR will be given by

$$V_N = V_w.Sin(\alpha+\beta).Cos\,\gamma$$

Again V_N is the feed rate normal to the wheel surface at the start of the arc of cut. It is assumed that the workpiece is narow relative to its diameter so that the geometry and the workpiece surface speed can be assumed to be constant across the width. The path traversed by an individual grit will still be in a plane perpendicular to the wheel axis, but the direction of the resultant grinding force will be normal to the ground face as has been shown by Saljé et al [30]. Provided the wheel properties are isotropic there is no reason why this should affect the grinding characteristics, so the same relationship between the local normal feed rate and the local stresses as in plane grinding should still apply. This in turn should result in the same relationship between specific energy and MNIR for all values of face angle (γ), for similarly dressed wheels.

The wheel dressing conditions can be treated in a similar fashion. The important operating conditions in wheel dressing, when using diamond rolls, have been shown to be the surface speed of the roll relative to the wheel surface speed and the depth of cut of the diamond roll into the wheel as discussed in Section 2.2. In Figure 2 the diamond roll is being fed into the wheel at a radial infeed rate V_D yet the effective infeed normal to the active surface of the wheel is V_d such that

$$V_d = V_D.\text{Cos}\gamma$$

The surface speed ratio will vary across the width, but again the assumption is made that the change in diameters across the active face is small. The effective dressing parameter is then V_d, and to maintain constant dressing conditions as the face angle increases, the radial infeed (V_D) will have to be significantly increased.

The derivation of equations for the stock removal rate and other relevant quantities under plane and angle grinding conditions are described in Appendix II.

Experimental work to test the effect of dressing and grinding at a range of face angles was carried out and is described fully in Section 4.1.4.

For a compound form, such as the one in Figure 3, the geometry becomes more complicated. The semi-circular form shown is an example of a typical ballscrew track profile, but there is no reason why the approach about to be described could not be adopted for any form. In this case it can be seen that the depth of cut and the angle of the ground face varies around the form. The depth of cut will be a maximum on the centreline and will decrease to zero at the sides of the form. However, by taking any particular perpendicular plane through the form (AA),

the problem can be brought back to a simple angle face problem. To calculate the grinding forces, the form can be divided into a finite number of angle grinding problems as shown in Figure 3. Each one can then be considered as an individual cut and the total grinding energy found by summation. Taking the i^{th} segment.

$$V_{n_i} = V_w.\mathrm{Sin}(\alpha_i+\beta_i).\mathrm{Cos}\gamma_i$$

and also

$$V_{d_i} = V_D.\mathrm{Cos}\gamma_i$$

for the wheel dressing cycle.

Each of the factors in these equations will vary from segment to segment.

If the specific grinding energy depends only on the dressing conditions V_d and the maximum normal infeed V_N in any particular plane, and is otherwise independent of the depth of cut and the angle of the face, then the power requirement in each segment can be calculated from results of tests carried out under plane grinding conditions. Hence the total distribution of power generation, both around the form and around the arc of cut for each segment, can be fully defined. The larger the number of segments considered the greater will be the accuracy of the method. However since ultimately this accuracy will depend on the reliability of the experimental results obtained under plane grinding conditions, there is little point in taking the formulation to a limit and deriving integral equations. Points to be considered when choosing the segment width (Δz) are the change in angle across the segment due to the curvature of the form and the change in depth of cut. As illustrated in Figure 3 these considerations lead to the choice of a decreasing segment

width towards the sides of the form.

Once the power generation profile is known, and if the fraction of the grinding energy entering the workpiece can be determined, then, using a finite element analysis it should be possible to calculate the temperature field in the workpiece. This enables not only the limiting stock removal rate before the onset of burn to be determined, but also any thermal distortions.

3.2 One-dimensional Heat Flow Analysis

The problem of determining how much of the grinding energy actually goes into the workpiece has been discussed and shown to be fundamental to this piece of work. Previous attempts to determine this factor have relied on surface grinding a workpiece and measuring temperatures either in the bulk of the workpiece [52] or at the grit contact [51]. There are a number of problems with each of these approaches. In conventional grinding the heat source is passing relatively quickly and the transient response time of the thermocouple and recording equipment is all-important if the true peak temperature is to be detected. In creep-feed grinding, because of the slower feed rate this problem is not so critical but any analysis of the heat flow is sensitive to the heat losses from faces of the workpiece other than the ground surface. If, however, a workpiece could be ground which is thermally insulated on all except the ground face, then a much more accurate result should be possible.

As already discussed, creep-feed grinding can be thought of as a series of plunge grinding operations varying in plunge feed rate from a maximum at the start of the arc to zero at the bottom. Using this concept, it is possible to model the process by plunge grinding an

insulated pin-type workpiece and monitoring the temperature within it. This leaves only the ground face exposed for heat transfer yet should reasonably model the creep-feed grinding process.

The resulting problem is a straightforward one-dimensional transient heat flow problem but with a moving boundary as illustrated in Figure 4.

Mathematically the problem is similar to the abrasive cut off operation discussed by Eshgy [80].

The heat flow within the pin is governed by the Fourier equation

$$\frac{\delta^2 T}{\delta x^2} = \frac{1}{\alpha} \cdot \frac{\delta T}{\delta \tau}$$

Two possible boundary conditions were considered at the bottom face in the modelling, firstly an adiabatic boundary

$$\left[\frac{d T}{d x}\right]_L = 0$$

which represents the proposed experimental condition, and secondly a Dirichlet or fixed temperature boundary

$$T_L = \text{Constant}$$

This was incorporated so that the effect on the burn out flux of varying workpiece temperature fields could be seen; this would reveal whether burn out occurs at a fixed value of heat flux, as has previously been suggested in creep-feed grinding, or whether it depends more on the mean surface temperature.

The boundary conditions at the wheel workpiece interface

were less easy to define.

Three different options were incorporated into the modelling:

1) $$eV_p = -k\left[\frac{dT}{dx}\right]_b + h(T_b - T_c) + \rho C_p V_p (T_b - T_a)$$

This is a complete energy balance approach. The term on the left represents the power being generated per unit area, and the three on the right represent conduction into the workpiece, convection to the coolant and heat lost with the chips respectively.

2) $$-k\left[\frac{dT}{dx}\right]_b = q_w.e.V_p$$

This condition, referred to as 'fixed partitioning', allows a constant fraction (q_w) of the grinding energy to go into the workpiece independently of the workpiece surface temperature.

3) $$-k\left[\frac{dT}{dx}\right]_b = [q_w - q_v(T_b - T_c)]e.V_p$$

This is a model between the previous two. The partitioning value falls as the workpiece surface temperature T_b rises, but only by an amount q_v which can be varied. It is not a fully convective boundary as in case 1.

In all three cases the power input was assumed to be uniform over the ground surface of the workpiece.

Initially the problem appears to be a straightforward one-dimensional transient heat flow, but it was subsequently found when calibrating the experimental equipment that there was a small heat loss into the insulating material,

a resin bonded cement compound known as Sindanyo. The rate of heat loss depended on the cross-sectional area of the workpiece: the larger the workpiece the closer the approximation is to the theoretical one-dimensional case. To allow for this loss, a term was incorporated in the modelling representing a heat loss proportional to the local temperature. The determination of this loss term is fully described in Section 4.3.2.

The equations could be solved analytically as discussed in Reference [81]. However, it was decided to use a finite difference technique because of the greater flexibility offered. Using this method a computer routine was developed that could quickly solve the model for a wide range of boundary conditions. One advantage of the finite difference technique is that the moving boundary condition can be easily accommodated by interpolation between a dummy node outside the workpiece and the first node within it. The use of the technique in this application is discussed in Reference [82] and a full description of the formulation is given in Appendix III.

The computer program was designed to accept a wide range of conditions. Material properties could be specified, so as to allow a comparison between material of low or high thermal conductivity such as Nimonic alloy or steels. Grinding feed rates and specific grinding energies can be specified as can the initial workpiece temperature and the coolant temperature. Also specified are a term for the loss to the insulation, the type of boundaries at both the top and bottom face, and, for a fixed partition type of boundary, the values of q_w and q_v. The program then checks for stability according to criteria discussed in Appendix III and produces the output either as a temperature -time listing for each node in the workpiece or as a temperature profile through the workpiece for each time increment.

The use of a high-speed computer allowed a very fine mesh to be used. As a check on the accuracy, the program was run several times, but each time doubling the size of the steps. It was found that a relatively coarse mesh could be used before the result changed significantly and that the largest error arose in calculating the surface temperature, which involved interpolating over an increasing range. The Fourier number was determined by the program as the largest that would maintain stability, and from this the time interval calculated.

3.1 Finite Element Analysis

To extend the findings from the work on energy partitioning to a realistic grinding case, a more sophisticated model was needed. Furthermore, if temperatures under form grinding conditions were to be investigated, then a three-dimensional model would be necessary. With this in mind, a finite element package, which was shortly to become available at the South Western Universities Computer Centre (SWURCC) was selected. The package, called LUSAS, should have been capable of modelling 3D field problems under transient and steady state conditions, according to its original specification. However, it was only implemented in stages, and the 3D capability did not become available until there was insufficient time remaining to develop a 3D model. A 2D plane grinding operation however was successfully modelled and some useful results obtained.

Shafto [8] produced a finite element modelling of a similar problem. He used a convective boundary condition similar to condition 1 in Section 3.2, and developed both a steady state and a transient model, which he compared with experimental measurements of the workpiece temperatures. The results of his analysis are shown in

Figure 5. As can be seen the results for the steady state analysis are at least as close to the measured ones as for the transient analysis. By the stage illustrated in the test, the temperature field around the arc has reached a quasi-static state, and moves along with the arc of cut. Points in the workpiece remote from this heat affected zone are unaffected and are at or near ambient temperature. On this basis it is reasonable to treat the problem as steady state if mid-test conditions are being considered; only at the beginning and end of the test will transient effects be significant. The mesh used for the analysis is shown in Figure 6. It is a 2D triangular mesh which is designed to allow for easy changes in both the depth of cut and the wheel diameter, both of which will affect the arc length. A surface grinding operation was chosen, since this will allow comparison with the wide range of results already available from other work. The thermal properties of the workpiece could also be varied. As will be discussed in Section 5.5 the partition was found to be nearly constant over a wide range of workpiece temperatures, hence Shafto's original method can be simplified and the heat input within the arc of cut considered as a constant fraction of the local power flux. Furthermore, if tests are considered as steady state at a point about halfway along a specimen as shown in Figure 5 then it is reasonable to fix the temperatures on the sides, end and bottom faces at ambient temperature; this is substantiated by Shafto's finding that varying the convective heat transfer coefficient on these faces had very little effect, since the temperatures on the surface are very close to that of the coolant anyway. The convective heat transfer coefficient on the top face outside the arc of cut could be varied, but a value of $0.1 W/mm^2/^{\circ}C$ was found to give the best agreement with experimental results.

As already discussed, the heat generated around the arc

of cut was considered to be proportional to the local normal feed rate, and the percentage of this heat going into the workpiece at any particular feed rate was taken from the results of the 1D plunge tests.

Had it been possible to extend the model to a 3D case, then the power flux generation profile around the form as well as around the arc would have been incorporated. From this the maximum workpiece temperatures and any thermal distortion could be calculated. However, useful results have been obtained from the 2D model and these are described in Section 5.7.

CHAPTER 4

Experimental Equipment and Test Procedures

This chapter is divided up according to the three different experimental set-ups used. Basic cylindrical grinding tests using both oil and water-based fluids and the insulated pin tests were carried out on a creep-feed plunge cylindrical grinder. Tests to investigate the effect of workpiece material and hardness were carried out on a creep-feed surface grinder. The pin tests are detailed under a separate heading to the cylindrical tests since they require a rather different technique.

4.1 Cylindrical Grinding Tests

4.1.1 The Grinding Machine

The machine used for these tests was a purpose-built creep-feed plunge cylindrical grinder. (Plate 1). This had been designed and built primarily as a research tool to investigate the process of creep-feed grinding in a cylindrical mode [78].

The machine was built on a reinforced concrete base with the main spindle motor mounted remotely on a second concrete base. The wheel spindle was mounted statically on the base and the workpiece slideway moved radially towards the wheel. Wheel dressing was by means of a diamond roll which was mounted on its own slideway diametrically opposite the workpiece station and was driven by its own motor. All the spindle and slideways bearings were hydrostatic in order to achieve high static and dynamic stiffnesses. Workpieces were mounted on a mandrel which located between centres. The tailstock centre was hydraulically loaded to 7000N to ensure that high static stiffness was maintained.

Both the dresser and the workpiece slideways were driven by pre-loaded ballscrews and directly coupled DC servomotors which were controlled by pulse width modulated transistor servodrivers. Resolvers on the motors provided feedback to the servodrivers for both speed and position. The control system allowed up to three different feed points to be specified at which the workpiece plunge feed rate could be stopped or changed. These feed points and the feed rate required were set by means of edge switches on the control console. The dresser infeed rate was specified as a percentage of the workpiece feed rate; hence if it was set at 100% then both slideways would be moving into the wheel at the same rate. This allowed the wheel to be 'continuously dressed' whilst still producing a round component. The control system also enabled either slideway to be jogged in or out under manual control for setting-up.

The wheel and working zone were enclosed in a steel housing to retain the coolant and to provide protection for the operator in the event of a wheel breakage. When the workpiece moved into the grinding position the centres were accomodated through two slots in the housing and a sliding gate was closed over the aperture through which the workpiece moved. The control system recognised a 'home' position outside the wheel guard, where easy access for loading and unloading was possible. As the slideway moved away from the wheel it made a limit switch as it approached the 'home' position. Once the servodriver received this signal it stopped the motor at the next zero position on the resolver which occurred once per revolution. In this way the 'home' position was always repeatable. In this position an offset value was manually entered into the controller which was nominally the radius of a component which would be just touching the wheel if it were between the centres. The feed points were then specified as absolute radii. The dresser slideway operated in a similar fashion but as the slideway

moved in the workpiece radius counter increased in value since this represented a decreasing wheel size.

A third servomotor and driver controlled the workpiece rotation. This system also used a closed loop feedback system to maintain the workpiece speed. A 10-turn potentiometer on the control panel set a reference voltage to the servodriver which it then compared with the output from the tacho-generator on the back end of the motor. The servodriver then controlled the current in order to keep this voltage difference at zero. The motor drove the workhead through a toothed belt and a worm drive gearbox which provided a reduction of 10:1.

Two problems were encountered with this design. Firstly the workpiece rotation motor tended to 'creep' even when the reference signal was at zero volts, which made plunging into a stationary workpiece difficult. Although there was an offset potentiometer within the servodriver the effect was found to be temperature dependent and the creep could not be totally eliminated. On studying the servodriver specification it became apparent that there were two disable terminals which, when grounded, prevent the servodriver from driving the motor in either direction. By incorporating an on/off switch into the control circuitry which grounded these pins, the motor could be disabled and the workpiece creep stopped.

The second problem arose due to wear in the worm drive gearbox. A torsionally stiff workpiece drive is essential if creep-feed climb grinding is to be carried out, since the grinding force tends to pull the workpiece into the wheel. The backlash which appeared was allowing the workpiece to advance in a series of jerks giving a workpiece surface of alternate burnt and unburnt lines. The worm and wheel in this gearbox, which was supplied by T I Matrix, consisted of a dual lead worm with a

varying tooth width along its length. Hence by moving the worm axially relative to the worm gear it was possible to eliminate this backlash.

Grinding fluid was supplied from either a tank containing soluble type oil or from a separate system containing neat oil. Both systems incorporated filtering devices. The flow to the machine was via an orifice plate and a gate valve for monitoring and regulating the flow rate respectively. Coolant application was by means of a coolant shoe (Plate 2) which could be adjusted to maintain intimate contact with the wheel.

4.1.2 Instrumentation and Calibration

i) Forces

On this machine the forces acting were measured at the grinding wheel spindle. The bearings on this spindle consisted of two hydrostatic journal bearings each with six pockets. By measuring the differential pressure across the three pairs of diametrically opposed pockets of the front spindle bearing, the load being exerted on the bearing could be determined. To do this it was necessary to know the area over which the pressure being measured was acting, which was taken to be the projected area of the bearing pocket plus some portion of the land between the pockets and the drain, which was at atmospheric pressure. By assuming a linear pressure distribution across the lands then the effective area could be taken as half the geometrical land area plus the projected pocket area. (See Appendix IV).

The three forces measured were resolved vertically and horizontally and moments taken about the rear bearing in order to determine the forces acting in the plane of the

workpiece. When grinding on an angle face the line of action of the force normal to the wheel surface depends on the wheel diameter, which had to be taken into account. If the line of action of this force passed close to the centre of the rear bearing then no load would be exerted on the front bearing since the moment about the rear bearing would be zero, and the force could not be measured (See Appendix IV). This would occur for a face angle of approximately 60°, therefore face angles significantly greater or less than this value were chosen. Appendix IV gives further details of the geometry of the machine relevant to the force measuring system and the necessary equations.

The differential pressures were measured with variable reluctance pressure transducers which give a 0 to 1 volt output for differential pressures in the range 0-7 bar. The output from these passed through 5 Hz low-pass filters to eliminate any once per wheel revolution frequency content which was caused by out of roundness of the bearing journal. Originally the outputs from the filters were directly coupled to a U-V recorder. However, since galvanometers are essentially current measuring devices, significant power was being drawn from the filters, which was causing a non-linearity in the calibration. Furthermore it was not possible with this set-up to vary the sensitivity of the force measuring system. To overcome these problems a 3 channel DC voltage and current amplifier was interposed between the filters and the galvanometers. This had a high input resistance and the gain was variable by discrete steps which allowed different ranges to be selected without the need for recalibration.

The galvanometers used had a sensitivity of 1.6mA/mm, a natural frequency of 1000 Hz and were viscous damped.

The system was calibrated as a complete unit and thereafter care was taken not to vary the matching of components. It was decided to calibrate the system both statically and dynamically, ie with the wheel running at full speed, since it was thought possible that hydrodynamic effects might have been acting at the bearing lands, which would result in the measured forces being too low. A loading system was designed which allowed forces to be applied to the rotating spindle by means of calibrated weights. The forces could be applied in either a horizontal or a vertical direction. Loads up to 600N were applied in 100N steps and then removed, again in 100N steps, to check for repeatability. This was done with the load acting in both horizontal and vertical directions and with the spindle stationary and rotating at 500 and 1000 rpm.

No hydrodynamic effect was apparent and the system proved to be both linear and repeatable.

ii) Workpiece Rotational Speed

The 10-turn potentiometer controlling the workpiece speed was calibrated for speeds in the range 0.1 to 130 rpm. A stopwatch was used for the slow speeds and a hand held tachometer for the higher ones. The speed holding under load proved to be better than 1% throughout the speed range.

iii) Wheel and Dresser Speeds

These were measured for each test with a hand held tachometer. The speed holding of the two motors was claimed by their manufacturers to be better than 0.25% for a 50% change in load. Originally the dresser was driven via a flat belt and pulleys but these were found to slip when contaminated with grinding fluid. To avoid this, the belt and pulleys were replaced with a toothed belt and pulley

set.

iv) Wheel and Workpiece Dimensions and Surface Finish

The wheel diameter was determined by measuring, with a vernier caliper, the gap between the wheel periphery and a reference plate fixed to the wheel guard which was a known distance from the wheel spindle centreline. The workpiece diameter and width were measured with a micrometer. Two methods of measuring the depth of the wear scar, which is produced where the wheel has been grinding, were attempted, firstly by grinding a shim mounted in a special holder between the workpiece centres and then inspecting this shim under a shadowgraph. This method however was unsuitable when the grinding face was at an angle to the wheel axis, so a jig for traversing an LVDT across the surface of the slowly revolving wheel was designed. A tungsten carbide follower was used to protect the LVDT.

Neither of these methods proved particularly satisfactory since the depth of wheel wear was so small, typically less than 10μm. The first method allowed a confidence of ±3μm but the second method proved even less accurate due mainly to the roughness of the wheel being of the same order as the step to be measured and a lack of adequate stiffness in the slideway for the LVDT.

The workpiece surface roughness was measured with a Talysurf remote from the grinding machine.

v) Dresser and Workpiece Plunge Feed Rates

The infeed rates were determined by the accuracy of the servodrive system. This was checked using a dial gauge and a stopwatch to time the movement over a certain distance. The feed rates were found to be inaccurate

between the first and second feed points due to a fault in the edge switch used to select the feed rate in this range. To avoid this error whenever plunge feed rate was important, such as when dressing the wheel, feed rates after the second feed point were used.

vi) Grinding Fluid Application

The pressure in the coolant shoe was shown by Powell [64] to be the parameter which controls the flow of coolant through the wheel. This was monitored with a 0-4 bar Bourdon gauge which was connected directly to the shoe chamber.

Powell's work showed that there is a minimum shoe pressure which will achieve a full supply of coolant throughout the arc of cut and therefore allow the maximum possible power flux at burnout to be reached. To check that this pressure was being exceeded, a workpiece was ground at a feed rate just below the burn limit and the forces noted. A second workpiece was then ground under identical conditions but with the coolant supply pressure reduced by 25%. Provided there was no significant difference in the forces and no burn evident on the second test, then the original pressure was considered to be adequate. This resulted in the use of a shoe pressure of 0.5 bar for the water-based fluid and 1 bar for the neat oil.

vii) Grinding Wheel Balancing

If the out-of-balance forces became excessive, the force measurement traces on the U-V recorder showed considerable 'fuzz' despite the 5 Hz low-pass filters. This out-of-balance was monitored by connecting an oscilloscope across the unfiltered output from one of the differential pressure transducers. The amplitude of the out-of-balance force could be measured directly from the oscilloscope.

Balancing was carried out by adding weights to a groove in the loose wheel flange. The procedure used was to run the wheel at a known speed without any weights added and to record the amplitude of the out-of-balance force. One weight was then added, the wheel run at the same speed and the resultant out-of-balance recorded. This weight was then moved to a point 180° from the first position and the resultant measured again. From these results equations could be set up and solved (See Appendix V) that identified where the two balancing weights should be situated to balance the wheel. This procedure was carried out whenever the amplitude of the out-of-balance force exceeded 50N at 1000 rpm which corresponded to a peak to peak voltage of 35mV on the oscilloscope.

4.1.3 Experimental Procedures

Tests were carried out with both plane and angle faced workpieces over a range of dresser and workpiece feed rates. The general procedure was similar for all the tests and the conditions used are summarised in Table 1.

i) Workpiece Preparation

The workpiece material was BS 708A42 (EN19C) which is a typical material used for ballscrews. The full composition is given in Appendix VI. Initially workpieces were manufactured from case hardened 100mm bar supplied by PGM Ballscrews. However, later specimens were produced from stock bar and subsequently through hardened. The depth of cut which could be obtained was limited by the depth of the case hardening, and a nominal value of 3mm was used throughout the testing. The hardness was checked and maintained in the range 650-700 VPN.

The specimens which were in the form of a ring (Plate 3) were pressed onto the mandrel and locked with a C-ring.

Wheel Grade	: Universal Grinding Wheel Co WA100K26V
Nominal Diameter (d_s)	: 600mm
Surface Speed (V_s)	: 30m/s
Dressers	: 160 stones/carrat Sintered Bonding
Face Angles	: 0° 40° 80° Plus one with a 4mm radius semi-circular form
Overall diameter	: 150mm
Dresser to Wheel surface speed ratio	: +0.8
Approximate depth of wheel removed at each dressing	: 0.3mm (on radius)
Dresser infeed rate (V_d)	: 0.2-3μm/rev (normal to wheel surface)
Workpiece material	: BS 708 A42
hardness	: 600-700 VPN
Nominal Diameter	: 100mm
Depth of cut	: 3mm (unless stated otherwise)
Workpiece Feed Rate MNIR (V_N)	: 10-50mm/min
Grinding Fluid	: Either: Castrol Clearedge EP284 (Soluble) Dilution 60:1
	Or: Duckhams Adformal EP7 (Neat Oil)
Supply Pressure	: Soluble Oil 0.5 bar Neat Oil 1 bar

TABLE 1 TEST CONDITIONS FOR THE CYLINDRICAL GRINDING TESTS

The specimens were then conventionally ground to achieve concentricity with the centres and to remove any scale on the surface. The hardness was checked at various points around the surface and the workpiece diameter and width measured and recorded.

ii) Grinding Wheel Specification

The wheel used for this work was designated WA100K26VMRNC. This was a vitrified bond aluminium oxide wheel with a 100 mesh grit size, a K hardness designation, and a high degree of induced porosity which is achieved by adding Naphthalene pellets to the mix before curing, whereupon it evaporates and leaves a porous structure. This is a harder wheel than has been used for previous plane form studies in creep-feed grinding [8, 9, 62], but it was felt to be more representative of the type of wheel used for form grinding work.

iii) Machine Settings

Because of the many variables involved in the process, a system for ensuring that all the relevant parameters had been recorded was developed. This consisted of a printed sheet on which all initial conditions were recorded (Figure 7), together with the desired dressing and grinding conditions. These values were then entered into a computer program which stored these values by test number and produced an output of the required wheel and dresser speeds etc (Figure 8).

A second sheet was used to record the results of the test and the deflection of the U-V recorder traces (Figure 9) and these could then be fed into the same program at a later date and a full set of results produced (Figure 10) for printing and storage.

The use of this system ensured that no mistakes were made in the computation of the results and that full results for all tests were stored on the computer.

iv) Test Procedures

Having obtained the required speeds and feeds from the computer program, the stationary workpiece was plunged into the wheel to the required depth of cut. It was then retracted and the dresser jogged in until it was 30μm from the wheel surface. All dressing was carried out with a dresser to workpiece surface speed ratio of +0.8. The wheel was dressed at the required infeed rate until approximately 0.3mm had been dressed off the radius of the wheel before the dresser was returned to its home position without allowing any dwell time. The new wheel diameter was measured and recorded, and the workpiece was advanced so that the wheel was once more in the previously ground arc, having made due allowance for the amount of wheel dressed off. The wheel shutter was closed behind the workpiece and the coolant flow set. The appropriate gain on the force measuring amplifier was selected and the individual traces adjusted as necessary. The U-V paper was allowed to run for a few seconds in order to establish a datum, since the measuring system detected all forces acting on the wheel including coolant or dressing forces. The desired workpiece rotational speed was set on the 10-turn potentiometer and the workpiece drive motor turned on. The test was allowed to continue for a predetermined time which ensured that at least 200mm^3 of material per mm width of workpiece had been removed. The workpiece was then retracted from the wheel before stopping the rotation. The U-V trace was allowed to run for a further few seconds to give a second measure of the coolant forces acting, before the coolant was stopped. The wheel was left running for 30 seconds to expel any coolant in it.

The workpiece was retracted before stopping the rotation so that any surface damage in the grinding arc would not be ground away as the elastic deflections in the structure relaxed.

When using the neat oil grinding fluid it was found that the coolant forces exerted on the wheel were influenced by the proximity of the workpiece to the wheel and by whether the arc was single or double as it would be before the rotation is started. So to obtain a true value of the coolant forces present during grinding,the workpiece rotation was stopped briefly during the test. The grinding forces were found to be unaffected by this pause.

After grinding, the workpiece diameter was measured and recorded and a visual examination of the workpiece surface made. The surface finish was measured at certain points around the specimen corresponding to the required grinding times from the start of the cut. When using a water-based coolant, burn was easily identifiable by the presence of tempering colours and subsequent hardness checks confirmed that specimens which looked unburnt had suffered no change in hardness. With oil-based fluids however it was not always so clear. To ensure that the true limitation had been found these specimens were washed in acetone and then etched in a 5% Nital solution and then in 3% Hydrochloric acid in Methylated Spirits, before being thoroughly rinsed off with acetone and then distilled water. This procedure showed unburnt areas as light grey, softened areas as dark grey and rehardened areas as white. Rehardening would occur if the surface had been above the austenising temperature (730°C) before being quenched to give a hard layer of Martensite.

v) Results Analysis

The U-V traces were inspected and the duration of the test

measured and recorded. The deflections of the traces corresponding to the grinding forces were measured and recorded at approximately 8 to 10 points throughout the test. Using a computer digitising table or similar for this operation was considered, but it was felt that a careful manual examination of the traces was more useful and any unusual surges or changes could be noted and reflected in the points chosen for measuring. All the values measured were recorded on the results sheet (Figure 9) which was laid out for easy transfer of the data into the computer. The results produced by the program are shown in Figure 10. The grinding forces are first calculated in horizontal and vertical directions and then rotated to give the forces normal and tangential to the wheel surface at a point one third of the way from the start of the arc of cut, since Shafto [8] showed this to be the point through which the resultant grinding force acts. (See Appendix IV). The specific grinding energy was calculated from

$$e = \frac{V_s . F'_T}{Z'}$$

and the power flux was defined as

$$H = \frac{V_s . F'_T}{\ell_c}$$

The forces and values of stock removed are normalised per unit width of ground face. Values of stock removal rate and MNIR are calculated as described in Appendix II.

Another computer program was then written to plot the graphs for each test using the Gino-f package of subroutines. Plots of tangential and normal forces, force ratio, specific grinding energy and power flux against stock removed were produced (Figures 11-14). From these plots, values of specific grinding energy after various amounts of material had been removed could be determined

by interpolation. A third computer program was then used to plot graphs of specific energy against MNIR for each dresser feed rate and specific energy against dresser feed rate and specific energy against dresser feed rate for each value of MNIR. The program would search for tests carried out with the same dressing conditions or at the same MNIR. If it found three or more it plotted the graph (Figures 15 & 16).

4.1.4 Angle Face Tests

The procedure for the angle face tests was essentially very similar to that of the plane tests but there are several additional points to be considered.

i) Specimen Preparation

The specimens used were pre-cut with the required face angle prior to heat treatment so that a constant radial depth of cut could be maintained across the ground face. Because of the varying effective radius of the wheel and workpiece across these specimens, there was a change in such parameters as the dresser speed ratio and the MNIR. With this in mind the specimens were dimensioned so that the variation across the width was never more than ±7%. Examples of these specimens are shown in Plate 3.

ii) Diamond Roll Dressers

In addition to the plane diamond roll dresser already fitted to the machine, new dressers were supplied with face angles of 40° and 80°. These rolls were supplied by J K Smit and were to the same specification as the original roll, namely 160 stones/carat handset. (See Table 1). All three rolls are shown in Plate 4.

iii) Hydrostatic Thrust Bearings

Dressing and grinding on angle faces imposes a significant axial load on the spindle, dresser and workhead bearings. Problems had previously been encountered with the hydrostatic thrust bearings in the workhead, which are subject to the static load from the hydraulic tailstock. These had touched down at a load well below their ultimate design load and had subsequently been replaced with needle roller bearings. All the other thrust bearings use a similar design which consists of a single annular pocket supplied by oil leaking from the journal pockets. The design relies on the thrust face being perfectly flat and perpendicular to the axis of the bearing, so that the axial clearance is constant all around the bearing. Since these conditions can never be achieved, the true stiffness of these bearings is considerably lower than their design stiffness. Calculations suggested that the maximum end thrust which could be encountered on the wheel spindle was 11kN based on the maximum motor power and on 80° face angle. The maximum theoretical load that the spindle thrust bearing could withstand is 73kN which should allow an adequate safety margin, especially since the motor is unlikely to reach full load conditions. The dresser thrust bearings were also found to be adequate on the basis of maximum motor power.

iv) Test Procedure and Results Analysis for Angle Face Tests

Wheel dressing conditions were calculated by the computer program described in Section 4.1.3 to give the specified infeed per revolution in a direction normal to the wheel surface in the plane of the centreline of the workpiece. The maximum and minimum values of the roll speed ratio were also printed out as a check that this ratio never came too close to unity, which is known to cause rapid dresser wear. For the 80° roll (See Plate 4) it was not possible to

achieve normal infeeds greater than 1μm/rev on account of the very high radial infeed rates needed.

The program also calculated the workpiece rotational speed necessary to achieve the required MNIR at the workpiece centreline, and printed out the maximum and minimum values away from the centreline.

The only additional measurement required was the axial position of the workpiece relative to the grinding wheel, since this would affect not only the line of action of the normal force component, but also the effective diameter of the grinding wheel.

4.1.5 Form Grinding Tests

A range of tests were undertaken using a profiled diamond roll dresser. This dresser is shown in position in the machine in Plate 5. The form was semi-circular with a 4mm radius, and is representative of a ballscrew track. The dresser was produced by J K Smit & Sons to the same specification as each of the other dressers used in this work, and is as specified in Table 1. It was used to produce the form on the wheel, and hardened steel workpieces (BS 708A42) were then ground to a depth of 3mm. The procedure used was essentially the same as that for the plane cylindrical tests described in Section 4.1.3 and the forces were measured at the wheel spindle in the usual manner.

A computer program was used which divided the form into 19 segments and calculated the dresser infeed rate, the MNIR and the stock removal rate for each segment as described in Section 3.1 so as to calculate the predicted overall power.

4.2 Surface Grinding Tests

4.2.1 The Grinding Machine

The surface grinding machine (Plate 6 and Figure 17) used was of an earlier design [62] than the cylindrical grinder described previously, but it did share some similar features. Again the wheel spindle and slideway bearings were hydrostatic and dressing was by means of a diamond roller. The slideway was driven from the main spindle motor via a series of gearboxes which allowed a range of feed rates to be selected. This drive chain then drove a ballscrew which provided the table motion via an electromagnetic clutch. Limit switches at either end of the table travel disengaged the clutch and thereby stopped the table motion.

The dresser infeed was provided by a wedge on one end of the table which, by means of a cranked lever arm, fed the dresser into the grinding wheel (Figure 18). Although the motion of the dresser is in an arc the component of the infeed radially towards the centre of the wheel could be considered constant over small distances. Appendix VII details the calculations necessary to relate the slideway speed to the radial dresser infeed rate.

The workpiece was mounted on a strain gauge dynamometer (Plate 7) which was bolted onto the table. This dynamometer was designed by Salmon[9] and consisted of three I-beams fitted with temperature compensated strain gauges in a bridge network. Two of these beams supported the components of the grinding force in a vertical direction and the third the horizontal component. Each of the strain gauge bridges was supplied by a 10v DC stabilised power supply via an offset potentiometer which allowed the bridge to be balanced. This ensured that when no load was acting there was no current flowing through the external measuring system. The output from each bridge went through a voltage

amplifier, a 10 Hz filter and a current amplifier and was then recorded on a 3-channel U-V recorder.

The system was calibrated with the dynamometer mounted on a materials testing machine. Loads were applied in the plane of each I-beam in turn via a calibrated proving ring. The two vertical beams were loaded in compression, but the horizontal one was loaded in tension since this was the mode it worked in under grinding conditions. Considerable cross coupling was found between the beams, despite them being necked to reduce bending effects. Loads up to 600N were applied in 100N steps and the deflections of the U-V traces noted both on loading and unloading. Having produced a matrix of sensitivities for applied loads, this was inverted so that any applied load could be calculated from the trace deflections.

The wheel spindle and dresser rotational speeds were determined from tacho-generators on each shaft which were connected to a digital voltmeter and calibrated against a hand held tachometer.

Specimen and wheel dimensions were measured in a similar fashion to that described for the cylindrical tests in Section 4.1.2.

Soluble oil grinding fluid was used, which was supplied from the same system as that described in Section 4.1.1. This was applied by means of a coolant shoe and the pressure monitored by a Bourdon gauge.

The grinding wheel used throughout this series of tests was designated WA60/80FP2V, which is a coarser, softer grade wheel than that used for the cylindrical tests, but with similar induced porosity.

4.2.2 Workpiece Materials

Three different steels were ground in this series of tests. Their full compositions are given in Appendix VI. The first is the steel described in Section 4.1.3, namely BS 708A42 (EN19C). This is a 1% chromium 0.2% Molybdenum steel. It was ground in both its soft and its fully hardened states. The second steel was a plain carbon steel BS 070M55 (EN9), but of otherwise similar composition to the first. This steel was chosen since, unlike the first one, it contained no hard carbides in an otherwise homogenous matrix. It was also ground in both its soft and fully hardened condition. It was anticipated that these tests would provide an indication of the relative importance of hardness and carbide presence on the grinding forces and on their rate of increase as the wheel wore. The third steel used was a low carbon non-heat-treatable steel BS 080A32 (EN3) chosen to represent a truly homogenous structure, containing mainly pro-eutectoid and eutectoid ferrite and very little cementite (Iron Carbide); furthermore this material was similar to one of the steels which Schleich was grinding when he reported an effect due to hardness. [26]

All specimens were prepared as rectangular blocks (Plate 8) suitable for mounting into the dynamometer, before heat treatment where necessary. The 1% chromium steel was oil quenched but for the plain carbon steel water quenching was necessary to achieve full hardness. Hardness in the range 650-700 VPN was considered satisfactory.

4.2.3 Test Procedures and Results Analysis

The test conditions used are summarised in Table 2. For each of the five workpiece/hardness combinations, a

Wheel	:	Universal Grinding Wheel Co
Grade	:	WA60/80FP2V
Nominal Diameter (d_s)	:	600mm
Surface Speed (V_s)	:	30m/s
Dresser	:	160 stones/carat
Diameter	:	100mm
Dresser to Wheel Surface Speed Ratio	:	+0.8
Approximate depth of wheel removed after each dressing	:	1mm (on radius)
Dresser infeed rate (V_d)	:	1.85µm/rev
Workpiece materials	:	BS708A42 680/180 VPN
		BS070M55 700/200 VPN
		BS080A22 180 VPN
Depth of cut	:	3mm
Workpiece Feed Rates MNIR (V_N)	:	8.5 and 34mm/min
Grinding Fluid	:	Castrol Clearedge EP284
		Dilution 60:1
Supply Pressure	:	0.7 bar

TABLE 2 TEST CONDITIONS FOR THE SURFACE GRINDING TESTS

similar procedure was adopted. The grinding wheel was dressed at a feed rate of 1.85μm/rev and the dresser withdrawn without allowing any dwell time.

For each test the specimen's height and the gap between the grinding wheel and the dynamometer base were measured. Packing was then placed underneath the specimen to achieve the depth of cut of 3mm. After grinding the specimen was measured again and the true depth of cut calculated.

Five specimens of each type were ground between dressing at two feed rates; only after five specimens had been ground was the wheel redressed. The feed rates used were 60mm/min and 240mm/min, corresponding to stock removal rates of $3mm^3/mm/s$ and $12mm^3/mm/s$ respectively. The surface finish of each specimen was measured after grinding using a Talysurf.

In addition to the five conventional tests carried out for each feed rate and workpiece type, one test was carried out using continuous dressing. By selecting the appropriate wedge angle for the dresser feed mechanism, the same dresser infeed rate of 1.85μm/rev could be maintained throughout a grinding test. This effectively provided a measure of the grinding forces for a freshly dressed wheel with nearly zero wear flat area, and allowed the specific cutting energy to be determined directly, since there should be very little rubbing energy.

For each specimen ground the force traces were measured at a point just before the end of the grinding pass which stopped whilst still making a full arc of cut. A simple computer program was used to calculate the grinding forces from the calibration matrix described in 4.2.1. These were resolved in directions normal and tangential to the wheel surface at a point one third of the way from the start of the arc of cut, and the specific energy

calculated as described in Section 4.1.3.

4.3 Energy Partitioning Tests

4.3.1 Design of the Test

As discussed in Section 3.2 it was decided that the energy partitioning to the workpiece could be determined by measuring the bulk temperature rise of an insulated workpiece. In order that heat should only enter or leave the workpiece within the arc of contact with the grinding wheel, these tests were carried out by plunge grinding a pin type workpiece which was thermally insulated. The machine chosen for carrying out these tests was the creep-feed plunge cylindrical grinding machine described in 4.1.1 since it had the facility for plunging a stationary workpiece directly into the wheel whilst measuring the grinding forces at the wheel spindle.

The experimental arrangement used consisted of an expendible workpiece holder (Plate 9) into which small pin type workpieces could be set (Figure 19). The holders were made of Sindaanyo which is a resin bonded cement compound now widely used as a substitute for asbestos. It has the advantages of low thermal conductivity (0.92W/m/°C)and very low grinding energies. The latter advantage was necessary since the workholder would be ground away at the same time as the pin. Preliminary tests indicated grinding energies for the Sindanyo were in the order of 5-10J/mm^3 which would result in the pin grinding forces being measurably large relative to the total energy.

The workholders were machined in the form of rings which would fit on the mandrel used for the cylindrical grinding test. The maximum dimensions of the ring were fixed by

the aperture in the wheel-guard at a diameter of 100mm and a width of 30mm.

It was considered that the pins should have as large a cross-sectional area as possible if the heat flow was to be considered as one-dimensional on the centreline. Conversely however, it was desirable that the total amount of material removed should be small so that the wheel wear and consequent change in grinding energy would be negligible throughout a test. These considerations together with the constraint on the overall size lead to a circular cross section pin 20mm long by 10mm diameter. The bores in the workholder were made 18mm deep so that the pin initially protruded. This was so that the grinding forces could be measured before grinding of the Sindanyo commenced, and the effective heat flux acting on the pin determined.

The pins and the workholders were tightly toleranced so that the pins were always a tight fit in the bores. This was to ensure that no coolant could come into contact with the side faces of the pin. Each workholder had six pins in it, which allowed six tests to be carried out by indexing the workhead around to each pin in turn.

The pins were mostly manufactured from BS708A42(EN19C), although a few pins were produced in a Nimonic alloy (MARM002) so that a comparison with the results of Shafto [8] was possible. The full specification of these materials is given in Appendix VI.

A 1mm diameter hole was drilled from the bottom of each pin to a depth of 9mm from the bottom face (Figure 19). This allowed a thermocouple to be inserted into a position halfway down the insulated portion of the pin. The hole was kept as small as possible and perpendicular to the expected isotherms so as not to disturb the temperature

field unduly. After machining, the hole was cleaned out by injecting acetone with a syringe to force out any machining debris.

Since only low temperatures were to be measured (0-300°C) a base metal thermocouple with a high thermopower was required [83]. The thermocouple selected was a Nickel-Chromium/Nickel-Aluminium junction (Type K). This combination has a moderately high thermopower of approximately 40μV/°C in the range of interest, and was available in 0.2mm diameter wire with plastic insulation. This enabled the thermocouple junction to be accommodated in a hole of only 1mm diameter. Furthermore the small thermal inertia of the thermocouple leads was also considered to be significant if transient temperatures were to be measured. One reported problem with this type of thermocouple [83] is its tendency to oxidise at high temperatures; however, the temperature and duration of these tests were below those conditions at which this problem arises.

The junctions were formed by fusion welding the wires in an oxygen-free atmosphere. The welding was achieved by briefly striking an arc between the touching ends of the wires and a graphite electrode. This was carried out in a stream of natural gas to displace any oxygen and prevent oxidation of the bead that forms. Care was taken to maintain the plastic insulation right up to the thermocouple bead. A thin layer of 'Rapid Araldite' was then applied to the insulation from a point approximately 2-3mm from the bead for a length of approximately 10mm. This was then inserted into the cleaned hole in the pin in one go and held firmly against the bottom of the hole until the Araldite had set. Pulling the thermocouple out of the hole again could result in Araldite being transferred onto the bead which would impair the heat transfer to it, and was therefore avoided.

Each pin and thermocouple was then pressed into the workholder; the leads being first lead along a groove in the bottom of the pin and fed through a small hole in the side of the workholder (Figure 19).

Each thermocouple had a corresponding reference junction which was held at 0°C in a thermos flask containing crushed ice. All the cold junctions being used at any one time were taped together in such a way that the beads could not touch each other, and then inserted down a glass tube through the bung of the thermos flask.

No problems with earthing were envisaged because each pin was electrically insulated by the Sindanyo workholder.

The thermocouple circuit was completed by a Y-t recorder with a high input impedance (7.5M) and a rapid response to transient inputs (0.25 seconds for a full scale deflection on the Y axis). On the scale normally used, a full scale deflection corresponded to a temperature of 150°C, hence unless temperature changes greater than 600°C/s were encountered, which would require a heat input greater than the total possible grinding energy, then the recorder could be relied upon to keep up with transients in the bulk temperature.

4.3.2 Calibration

The calibration of the tests was carried out in several stages.

The first step was to calibrate a thermocouple formed by the above method, but not inserted into a pin. This was done by placing the thermocouple in a beaker of boiling water and then leaving it to cool. The thermocouple output was compared with measurements of the water

temperature made with a glass/mercury thermometer. The calibration obtained agreed well with the standard calibration given in thermocouple tables [84]. Thereafter the standard calibration was used throughout. This procedure was then repeated with a thermocouple and pin assembled, and the same calibration obtained.

As a next step, a pin and thermocouple were assembled in a workholder and the protruding 2mm ground off so that the top face was flush with Sindanyo. This face was then heated with saturated steam and the thermocouple response noted. It was found that the thermocouple reading rose asymptotically to a value of only approximately 85°C. This was repeated for three pins and the same transient response obtained to within 6% each time, which was taken as an indication of the consistency of the thermocouple mounting. It was unclear whether the fact that the temperature reached was only 85°C instead of 100°C as expected, was due to the surface not reaching 100°C or whether it was due to heat losses through the insulation. To check this a dummy workholder was produced with three bores of the same depth (18mm) but with different diameters, namely 6mm, 10mm and 16mm. Three suitable pins were produced with thermocouples fitted in the usual place and manner to fit into each of the bores. In addition to the thermocouple at the centre, a further one was spot-welded onto the centre of the exposed surface. Each pin in turn was then heated using steam and the response of both thermocouples plotted simultaneously by using a multiplexer. The surface thermocouple rose to a temperature of very nearly 100°C within 8 seconds and then stayed constant (Figure 20). The other thermocouple rose slowly to steady state values of approximately 73°, 84° and 90°C for the 6mm, 10mm and 16mm pins respectively. These results suggested that it was heat losses to the insulation that were significant and that the one-dimensional assumption became less valid

as the pin size decreased. In an attempt to overcome this, another dummy workholder was produced with a 2mm air gap around the pin, except at the top and bottom corners where some location was necessary (Figure 21). This proved marginally better, but under grinding conditions it was envisaged that the ingress of grinding fluid into the air gap would negate any advantage.

At this stage it was decided therefore to modify the one-dimensional heat flow model (see Section 3.2) to incorporate a loss term that was proportional to the local pin temperature. The model was still considered as one-dimensional but in each step of the finite difference calculation a quantity of heat was rejected, which was proportional to the temperature above ambient at that point and time.

The computer program was modified so that the constant of proportionality (C_L) for this loss could be specified in the input to each program run. The program was then used to model the responses obtained for each of the three different size pins. The program was run several times and the loss term varied by trial and error until the theoretical heating curve matched the experimental curve. An example of the results obtained and the matching theoretical curve are shown in Figure 22. It was expected that the loss term for each pin would be proportional to the reciprocal of the pin diameter since the area of the pin, which was directly related to the heat input, was proportional to the square of the dimensions, whereas the surface area per unit depth, which was directly related to the heat loss, was proportional to the dimensions. A plot of the empirically determined loss terms against the reciprocal of the pin diameter is shown in Figure 23 and as can be seen, this proved to be so.

From this calibration the value of the loss term (C_L) was

taken as $\hat{3}00W/m^2/^{\circ}C$ which is the gradient of the plot in Figure 23.

A full explanation of this term is given in Appendix III.

This model assumes that there is no temperature gradient between the axis of the pin where the temperature is recorded, and the outside face where the losses are taken as proportional to the surface area.

Considering an element of a pin diameter d and thickness Δx at a temperature t above ambient then the heat loss from this element would be

$$\pi d \Delta x t C_L$$

which equals the radial conduction rate at the periphery of the pin

$$-\pi d \Delta x k \left[\frac{dt}{dr}\right]_R$$

where $\left[\frac{dt}{dr}\right]_R$ is the radial temperature gradient at the edge of the pin.

Hence for an element of the pin at 80°C above ambient and a workpiece conductivity of 41W/m/°C (steel pins) then this temperature gradient would be 585°C/m. If this gradient is extrapolated back to the axis of the pin the temperature difference between the axis and the periphery would be 2.9°C. This gives an error of 3% in the loss term which can be considered as negligible.

When using Nimonic pins the corresponding theoretical error is 10% due to the lower thermal conductivity. However calibration of these pins using steam suggested that the same value of C_L was valid. The true error is likely to be smaller than the values quoted above since

the actual temperature gradient will decrease towards the centre of the pin. Furthermore the loss term itself is small relative to the total heat input, hence it is not surprising that the overall error cannot be measured in calibration tests.

The calibration also assumed that the temperature of the Sindanyo around the pin did not rise very significantly above ambient temperature. This assumption appears justifiable since the theoretical curve shown in Figure 22, which was derived using this assumption agrees well with the experimental result. Indeed in this case the Sindanyo was being externally heated by the steam in addition to the heat loss from the pin, whereas in real grinding tests it would be cooled by the action of the coolant. The low thermal conductivity of the Sindanyo (0.92W/m/°C compared with 41W/m/°C for the steel pins and 9.6W/m/°C for the Nimonic pins) and the relatively short duration of the tests (<90s) further justified this assumption.

Having calibrated the set up, each pin to be used in the grinding tests was heated using steam after assembly and the transient response compared with that obtained for the calibration pins. Any that were not within 10% of the mean of the original three calibration pins were rejected.

4.3.3 Experimental Procedure

Having assembled and calibrated the workholder assembly, it was mounted on the mandrel and located between the workpiece centres. The thermocouple leads, which were sheathed in rubber pipe to protect them from mechanical damage, were carefully lead away to the recording equipment. For each test the wheel was first dressed at the required dresser infeed rate as described in 4.1.3 and then the workholder moved in to the first feed point, which was

set so that the pin was approximately 25μm from the wheel surface. The coolant flow was set and the force measuring and temperature recorders started. The coolant and force measuring system were both as described in Section 4.1, but an amplifier gain of x5 was used on account of the low forces. The pin was plunge ground for 2mm at the required infeed rate (V_p) and then stopped. At this point the temperature trace was checked to ensure that no heat had entered the pin during the operation, and if it had, the infeed was stopped long enough for the temperatures to reach a steady state again. The plunge feed was then continued until the thermocouple was destroyed. The workslide was sent to its home position and the coolant and force recording equipment stopped. From the force trace the forces were measured during the initial plunge, and the specific grinding energy calculated. The force trace during the grinding of the insulated portion of the pin was also examined and any unusual features noted. As the plunge grinding proceeds the arc length in the Sindanyo increases and, for small subtended angles, the stock removal rate of the Sindanyo increases linearly with time. Hence the total grinding force would also be expected to increase linearly at a rate determined by the specific grinding energy for the Sindanyo. Any deviation from this trend may indicate a change in the specific energy as the wheel wears, which would invalidate the assumptions made in the theory. Only when grinding the Nimonic pins was any change seen. To overcome this these tests were repeated with continuous dressing which enabled a constant specific energy to be maintained. Some steel pin tests were also repeated with continuous dressing to investigate the effect of continuous dressing on energy partitioning.

The conditions varied were the wheel dressing conditions, the plunge feed rate and the type of grinding fluid - oil or water-based. In addition tests were done on a wheel

Wheel	:	Universal
Grade	:	WA100K26V
Nominal Diameter (d_s)	:	600mm
Surface Speed (V_s)	:	30m/s
Dresser	:	160 stones/carat
Diameter	:	150mm
Dresser to wheel surface speed rates	:	+0.8
Dresser infeed rate	:	0.2-3μm/rev
Workpiece materials	:	BS708A42 (Steel)
		MARM002 (Nimonic) (Supplied by Rolls Royce 1971 Ltd)
Pin Diameter	:	10mm
Length	:	20mm
Plunge feed rates (V_p)	:	Steel 6-18mm/min
		Nimonic (without continuous dressing) 3-6mm/min
		Nimonic (with continuous dressing) 6-15mm/min
Grinding Fluid	:	Castrol Clearedge EP284 (Soluble) Dilution 60:1
		Duckhams Adformal EP7 (Neat Oil)

TABLE 3 TEST CONDITIONS FOR THE PIN GRINDING TESTS (ENERGY PARTITIONING TESTS)

which had previously been used to cylindrically grind a hardened steel specimen and was therefore no longer in its 'as dressed' condition. The full range of conditions investigated is summarised in Table 3.

Having obtained a value for the specific grinding energy and the temperature history for the pin, the computer program was then used to model the experimental result by varying the boundary conditions.

Workpiece material properties were obtained from standard references for the steels and from Rolls Royce Ltd for the Nimonic alloy and are as stated in Appendix VI.

CHAPTER 5

RESULTS

5.1 Plane Cylindrical Grinding Tests

A first series of tests was carried out to establish a datum from which to compare the results of further testing. The large number of variables in any grinding process make it very difficult to draw conclusions from comparisons of results arrived at under different conditions. The machine used, the grinding wheel type and the workpiece material all affect the measured forces.

The tests were carried out as straightforward creep-feed cylindrical grinding tests, as described in Section 4.1, using the water-based coolant and the BS708A42(EN19C) steel.

In each of the subsequent series of cylindrical grinding tests the same experimental conditions were used but with only one variable changed at any one time. For example, in the angle face tests the only change was the angle of the ground face and in the grinding fluid tests the only change was the type of fluid being used.

One specific requirement of the tests described in this section was to produce a matrix of results from which the power flux distribution for compound forms could be calculated. As discussed in Section 3.1 the variables which are likely to influence the grinding energy are the dresser infeed rate (V_d) and the MNIR (V_N) provided that all the other conditions remain the same. Hence if it can be shown that the angle of the face being ground has no effect on the grinding process, so long as the above parameters are measured normal to the ground surface, then it should be possible to calculate the power flux distribution purely from the results obtained under plane

grinding conditions. With this aim in mind the plane grinding tests were carried out with a wide range of workpiece rotational speeds and with a variety of dresser infeed rates, so as to produce a complete range of results.

The slowest workpiece speed that could be achieved was 660s/rev which for a 3mm depth of cut corresponded to an MNIR of approximately 10mm/min. (The MNIR has been used to describe the workpiece feed rate throughout these results because of its direct relationship to the kinematics of the process as discussed in Section 2.1). Tests were carried out at increasing rotational speeds until workpiece burning occurred.

The initial dressing conditions were varied by changing the dresser infeed rate (V_d). The slowest infeed which could be achieved was determined by the resolution of the Servodrive system and corresponded to an infeed of approximately 0.18μm per revolution of the grinding wheel. Increasing values were then used up to 3μm/rev beyond which no further change in the measured forces was seen.

A selection of the computer printed results are shown in Figures 11 and 12. All these figures are plotted against the volume of material removed, hence zero stock removed corresponds to the initial grinding conditions with a freshly dressed wheel and the stock removed figure is proportional to the time from the start of the test. Figure 11 shows the variation in normal and tangential forces with stock removed for a test carried out with a high dresser feed rate (3μm/rev) and a high MNIR (40mm/min). The points corresponding to zero stock removed initially appeared to be higher than would be expected. However this appeared to be either a transient effect in the force measuring system or a function of the dynamic response of the machine. This was confirmed by applying a static load

to the stationary grinding wheel. When this load was suddenly applied the same effect could be seen. In subsequent results these initial points have been omitted since they do not reflect true grinding effects.

The result shown in Figure 11 shows that even after removing nearly 800mm^3/mm of material, which corresponds to grinding 3mm off nearly all the way round a 100mm diameter specimen, the forces had only risen by approximately 30%.

The rise in specific energy over this same period is shown in Figure 12.

Figures 24 and 25 however show the corresponding results for a test carried out with the same initial dressing conditions but at a lower MNIR (V_N= 10mm/min). Here the forces and the specific grinding energy can be seen to be rising much faster. The specific energy has risen by approximately 40% after only 250mm^3/mm of material has been removed.

As a further comparison Figures 26 and 27 show the same characteristic for a test carried out at the same slow feed rate (V_N = 10mm/min) but with a finely dressed wheel (V_d = 0.2μm/rev). This test shows much higher initial forces and specific energy than that shown in Figures 24 and 25, but the specific energy does not increase so rapidly as the test proceeds. Interestingly though, the normal force does increase rapidly during the course of this test.

To summarise the results from the large numbers of individual tests is not easy. Figure 28 shows the dependence of specific energy on the initial dressing conditions at various times from the start of each test. All the tests

shown here were carried out at the same MNIR of 10mm/min. Reading vertically up the graph at any one dresser feed rate corresponds to the specific energies for just one test, but after increasing amounts of stock had been removed. These values would be taken directly from results such as those shown in Figures 25 and 27. The values after 10mm³/mm were as near to initial values as could reliably be measured due to the transient effect in the bearings as described above. The results show clearly how at this feed rate the specific energy increases more rapidly for a coarsely dressed wheel than for a finely dressed wheel. For the test at the lowest dresser feed rate the condition of the freshly dressed wheel was apparently very different than that for the feed rates above 1μm/rev. A similar result is reported by Salmon [9] who measured specific grinding energies whilst continuously dressing the grinding wheel at various feed rates. Furthermore the wheel wear mechanism for the finely dressed wheel appears to be different since not only is the initial specific energy higher, but it also does not increase as rapidly as for the more coarsely dressed wheel conditions. This is further illustrated by the G-ratios for the same series of tests shown in Figure 29. (The G-ratio is the ratio of the volume of workpiece material removed to the volume of wheel worn away). Even allowing for the errors in the measurement of the depth of wheel wear which were discussed in Section 4.1.2 there is clearly a considerably lower rate of wheel loss for the finely dressed wheel.

Figure 30 shows the dependence of the specific energy on the workpiece feed rate after various amounts of material had been ground off. These tests were all carried out with a dresser feed rate of 3μm/rev and are represented in a similar way to those shown in Figure 28. Interestingly this figure shows that the initial specific grinding energy is nearly independent of the workpiece feed rate, but it increases more rapidly for the low feed rates than

for the faster ones. A further indication of what is happening in these tests is given by Figure 31. This figure shows the variation of the normal force for the same tests as in Figure 30. Under the initial conditions the normal force appears to be directly proportional to the feed rate, which suggests that the amount of rubbing occuring is very small. However as the amount of stock removed increases so does the normal force, especially at the low feed rates, which suggests an increase in the amount of rubbing which is taking place as the wear flat area on the grits grows.

As a final summary of these tests Figure 32 shows the variation of specific energy with dresser infeed rate at a range of workpiece feed rates. This figure only shows the values after 200mm^3/mm of stock had been removed; hence to represent the full range of results, similar figures were prepared for each value of stock removed. From these results a complete matrix of values of specific energy as a function of the three variables of interest (dresser feed rate, MNIR and stock removed) has been established for this combination of wheel grade, workpiece material and grinding fluid.

5.2 Angled Face Grinding Tests

To determine whether the same relationships between the specific energy and the dressing and grinding conditions held when grinding at an angle to the wheel and workpiece centrelines, tests were carried out at angles of 40° and 80°. In both cases the dresser feed rate was defined as the feed rate normal to the wheel surface and the MNIR as the feed rate normal to the surface at the start of the arc of cut as described in Section 3.1. The radial depth of cut was constant for all the face angles at 3mm.

The increase of the normal and tangential grinding forces for each of the three face angles with time are shown in Figure 33. Before each of these three tests, the grinding wheel was dressed such that the dresser infeed normal to the wheel surface (V_d) was the same in each case; likewise the MNIR of the workpiece (V_N) was maintained. As can be seen, within the limits of experimental error, the resulting grinding forces clearly show the same trend in each case. The stock removed figures are per mm width of ground face.

A selection of results for the variation of specific energy against MNIR are presented in Figures 34 and 35. All the values shown are after the same amount of stock had been removed. With the 80° dresser the total amount of material that could be removed for one revolution of the workpiece was less than 100mm³/mm hence it was only possible to compare results up to this point. In addition it was not possible to achieve normal dresser infeed rates higher than 1μm/rev for the 80° dresser due to the high radial infeed rate needed. However very low infeed rates could be achieved with greater reliability than for the plane dresser. From these results it again appears that there is reasonable agreement across the range of face angles tested, and that there is no obvious dependence on the angle of the ground face.

Figure 36 shows the relationship between specific grinding energy and normal dresser feed rate (V_d) whilst keeping the MNIR constant. Here there is very good agreement for all face angles tested. This figure also further demonstrates the typical dependence of specific grinding energy on dresser infeed rate at low feed rates as described in the previous section. The corresponding improvement in surface finish with decreasing dresser infeed rate is shown in Figure 37, and again the relationship holds independently of the face angle.

From these results it is evident that there is no kinematic difference between a plane grinding operation where the ground face is parallel to the wheel and workpiece axes and one where it is inclined to them, provided that the workpiece feed rate and the dresser feed rates are equated in a direction normal to the ground surface. Not only are the wheel properties imparted by the dressing process dependent solely on this normal infeed, but the resulting specific cutting energy and the way the wheel properties change with time have all been shown to depend on the MNIR and to be independent of face angle.

5.3 Form Grinding Tests

Having shown in the previous section that the grinding conditions depend solely on the feed rates of the dresser and the workpiece normal to the wheel surface, it should be possible to calculate the total power requirement for a form.

Tests were carried out using the form dresser described in Section 4.1.5 at a range of workpiece speeds and under a variety of wheel dressing conditions. The grinding forces were measured and the total grinding power calculated from these. The results obtained are shown in Figures 38 and 39, and an example of a ground workpiece is shown in Plate 10.

Using the method of splitting the form into a series of segments, as described in Section 3.1, a computer program calculated the local dresser infeed rate (V_d), the local MNIR (V_n) and the local stock removal rate for each segment. From the range of plane tests described in Section 5.1 the specific grinding energy in each segment could be read off from graphs such as that in Figure 32, and the total power requirement calculated by summing the

power required for each segment. These calculated values are also shown in Figures 38 and 39. The results show very good agreement between the measured and the calculated values; the largest error being approximately 17% for the test carried out at a low radial dresser infeed rate. Under this condition the local dresser infeed rates were all less than or equal to 0.5, hence as can be seen from Figure 36, the specific energy values taken from such figures are subject to the greatest error in this range.

These results substantiate the findings using the angle face dressers and verify that any grinding operation can be considered solely in terms of the local feed rates. This result allows the total grinding power and the distribution of the power generation around the form to be calculated for any shape of form.

5.4 The Grinding of Hard and Soft Steels

The tests to establish the effect of steel type and hardness were carried out on a creep-feed surface grinder as described in Section 4.2. Each of the steels were ground in both their hard and soft states, where appropriate, and both a high and a low workpiece feed rate were used.

Figure 40 shows the results for the low feed rate tests (V_N = 8.5mm/min) and Figure 41 the results for the high feed rate (V_N = 34mm/min). These figures show the increase in specific energy with stock removed for each of the workpiece types. The total amount of stock removed in each case before redressing the wheel is nearly 900mm^3/mm, which was achieved by grinding 5 workpieces of each type.

The point at zero stock removed was obtained by carrying out a test whilst continuously dressing the grinding wheel. This ensured that the wheel was permanently in its 'as

dressed' condition, hence the same grinding performance was obtained as at the first moment of a conventional test. The dresser infeed rate was the same as for the conventional tests (V_d = 1.85μm/mm).

Before looking at the effect of the workpiece material there are some general points to note from these results. Firstly for all the material types the rate of increase of the specific energy is lower for the high feed rate tests than for the low feed rate ones. This agrees with the results described in the previous section for the cylindrical grinding tests. Secondly these results provide a basis for assessing the relative advantage of continuous dressing when grinding these materials. Figure 40 shows that, at worst, the specific energy rose to a value of four times that which was attained by using continuous dressing even after removing 800mm³/mm. It is therefore unlikely that continuous dressing would prove advantageous solely for increasing the stock removal rate, although it may still be beneficial in maintaining form accuracy.

With regard to the variation between different materials, it is clear that the hardened materials not only result in higher initial specific energies but that the rate of increase of the specific energy as the wheel wears is greater for both feed rates. This effect is more evident than any due to the presence or otherwise of various carbides in the material. Indeed in Figure 40 the soft 1% CrMo steel which would contain both Chromium and Molybdenum carbides shows exactly the same result as for the 0.15% Carbon steel which would contain only a very small amount of cementite (iron carbide).

Figure 42 shows the variation in surface finish for the 0.55% carbon specimens throughout each series of tests. Not surprisingly, the continuous dressing tests exhibit

the same surface finish for both feed rates, since the wheel condition is being controlled by the dresser infeed rate which was the same in all cases. The clear trend here is the much better surface finish obtained on the hard specimens than on the soft ones at both feed rates.

5.5 Energy Partitioning Tests

The tests to determine how much of the energy used in the grinding process actually enters the workpiece were carried out by plunge grinding insulated pin-type workpieces as described in Section 4.3. An example of the results obtained is shown in Figure 43. The experimental curve in this figure shows the increase in the temperature recorded by the thermocouple as the grinding proceeded, up to the point where the thermocouple was ground away. The finite difference technique described in Section 3.2 was then used to model this result. Two of the possible boundary condition options are shown. The convective boundary option suggested that if the boundary condition was of this type then the temperature recorded by the thermocouple would initially rise rapidly and then more slowly. The value for the convective heat transfer coefficient of 80000 $W/m^2/°C$ was chosen so that the model would coincide with the experimental result at the point where the thermocouple was destroyed. However a much closer fit to the experimental result was achieved by using the second type of boundary condition and assuming that a fixed percentage of the grinding power was going into the workpiece irrespective of the workpiece surface temperature. In this case a value of 1.8% for the partitioning (q_w) gave the closest fit.

The 'fixed partition' model implies that a fixed amount of heat is going into a decreasing mass of material. This would tend to make the gradient of the experimental curve

increase as the test proceeds. However the situation is complicated by the fact that the heat loss to the insulating material is increasing as the temperatures rises and by the fact that the thermocouple is effectively moving closer to the heat source. The fact that the model does not exactly reproduce the experimentally measured result is likely to be due to a number of causes; one possible reason is that the model assumes that the heat loss is always to a fixed temperature sink, whereas the temperature of the insulation will actually increase. This means that the loss term in the model is too large, especially at high temperatures. A further possible cause is that the grinding energy may not stay constant throughout the test. If the wheel condition is changing significantly as the test proceeds and the amount of power being generated at the surface is increasing then this would also tend to make the gradient of the temperature-time curve increase, assuming the fraction of that power entering the workpiece stays the same. However it is quite conceivable that the partitioning value is changing also and that these two variations are partially cancelling each other out.

To investigate this possibility a test was carried out whilst simultaneously dressing the grinding wheel at a constant rate. This ensured that the wheel condition, and hence the power being generated, could not change. The result obtained is shown in Figure 44. In this case the experimental curve does show a decrease in the percentage of the grinding energy entering the workpiece as the boundary temperature increases. To model this result the third type of boundary condition discussed in Section 3.2 was used. It was found that a reasonably close fit could be obtained by using an initial partitioning value of 2.5% but which reduced by 0.015%/°C as the boundary temperature increased. Hence by the time the boundary temperature reached 100°C the percentage of the

heat generated which is entering the workpiece has fallen to 1%. In all the other tests carried out with steel specimens continuous dressing was not used and the constant partitioning value model could be used with acceptable accuracy. However it must be borne in mind that this is likely to be because the increase in the grinding energy and the fall in the partitioning value cancel each other out. This approach will not affect the calculated value of the workpiece surface temperature, but the value of the partitioning factor used can only be considered as an average value across the range of temperatures encountered.

Figure 44 also shows the mean surface temperature as calculated by the finite difference program. In this case it can be seen to have reached a value of 90°C by the time the thermocouple was ground away.

The result from a test carried out without continuous dressing is shown in Figure 45. In this case the wheel was dressed only before the test. The experimental result shows a near linear increase in the temperature recorded by the thermocouple up to a point approximately 33 seconds from the start of the test. At this point the temperature rose rapidly to a value in excess of that which could be recorded, which was 300°C. At the same time the traces from the force recording system showed a similar sharp change in gradient and an audible change in the grinding was noted. On subsequently inspecting the workpiece it showed heavy oxidation on the surface, indicating grinding burn (Plate 9). Subsequent hardness checks confirmed that thermal softening had taken place. This occurrence was observed for several tests with similar characteristics in each case.

On applying the model to this result it was found that a constant partitioning value of 1.85% closely reproduced

it. The mean workpiece surface temperature calculated by the program shows that at the point where burn apparently initiated, the workpiece surface temperature was approximately 132°C. All the tests where burn occurred showed a similar result, namely that when burn did occur the workpiece surface was always between 120°C and 140°C.

Another test where burn occurred is shown in Figure 46. In this case the wheel was not freshly dressed before the test, but had already been used to remove 900mm³/mm of material from a 100mm diameter hardened steel specimen. This had been cylindrically ground at a depth of cut of 3mm. The result obtained and the modelling of it show two things, firstly that the partitioning value of 1.9% is not significantly greater than that obtained for a freshly dressed wheel at the same plunge feed rate which was 1.7% (Figure 47). The specific grinding energy however had increased from 38J/mm³ for the freshly dressed wheel test to 63J/mm³ for the test shown in Figure 46. Hence the temperatures measured were significantly higher.

The second significant point is that the surface temperature at burn was again in the 120-140°C band.

Figure 48 shows a result for a Nickel alloy specimen. This material was included in the test program so as to provide a comparison with the work of Shafto [8] and others [9, 62] who have produced results from work carried out with it. In this case the temperature recorded rose steadily as it did with the steel specimens. However, the onset of burn did not appear as a sudden increase in the temperature but instead it appeared as a gradual increase in the gradient of the curve with a number of peaks or surges. At the same time the force traces showed an erratic behaviour with many rapid surges.

The modelling of this result suggested that approximately

1.4% of the power generated was entering the workpiece and that the surface temperature when burn started was approximately 112°C.

Figure 49 shows a similar result but at a higher plunge feed rate, again the surging behaviour in both the force and temperature traces was seen. The partitioning value was 1.1% and the burnout temperature 108°C.

Nimonic alloys are known to produce rapidly increasing specific grinding energies as grinding proceeds [62]. For this reason it was decided that to ensure there was no change in the grinding energy throughout the tests these ought to be repeated using continuous dressing. A result from one such test is shown in Figure 50. Here the modelling gives very good agreement with the experimental result with a partitioning value of only 0.42%. This very low value is less than half that obtained without continuous dressing, which allowed very much higher feed rates to be used; not only is the specific grinding energy much reduced by continuous dressing but also the fraction of this energy entering the workpiece is lower.

Figure 51 shows a result for a test using neat oil grinding fluid. This shows the same linear increase in the recorded temperature as was seen for the tests using soluble oil type grinding fluid. However the percentage of the grinding energy which enters the workpiece is apparently very much higher. In this test approximately 13% of the grinding energy went into the specimen. It can also be seen from the figures that the temperature at which burn occurs is much higher. In this case the burnout temperature was approximately 295°C. This particular result can be considered especially reliable since the thermocouple was very close to the surface at the point where burn occurred.

Figure 52 shows the result from another test using neat oil.

In this case a constant partitioning value of 15% provides a close fit to the experimental results, and the burnout temperature is again very similar to the previous result at 290°C.

The relationship between the partitioning value and the plunge feed rate is summarised in Figure 53. This figure shows the results of tests carried out with identically dressed wheel surfaces for each material but at a range of feed rates. It appears that there is a tendency for the partitioning to decrease as the feed rate increases for both materials by approximately 25% in the range of feed values tested. The results of the tests carried out on the Nimonic specimens with continuous dressing are also shown.

Figure 54 shows the dependence of the partitioning on the dressing conditions. Generally it appears that the partitioning value is lower for a coarsely dressed wheel than for a finely dressed one, and that this trend is more marked for the oil based fluid than for the water-based one.

5.6 Oil versus Water as a Grinding Fluid

In order to compare oil and water-based grinding fluids a series of tests similar to those described in Section 5.1 was carried out but using a neat oil type grinding fluid.

The first important observation was that with oil it is not always obvious when grinding burn has occurred. In extreme cases the oil produced smoke and a black carbon residue was present on the ground surface, although this could be easily removed with acetone. In less obvious cases however, the workpiece would look completely undamaged and only subsequent etching or hardness checks would reveal any damage. As a result of this uncertainty,

all the specimens were etched as a matter of course. With water-based fluids however, burn was clearly shown by a range of tempering colours up to 10mm down the sides of the workpiece and a black oxide layer on the surface. An example of a burnt specimen ground with each type of fluid is shown in Plate 11.

In addition it was not obvious from the force traces when burn had started to occur with the oil-based fluid. Figure 55 shows the increase in the power flux for a test with the oil-based fluid. The point where it suddenly increases corresponds to where burning started to occur on the workpiece. Figure 56 shows the forces for the same test and, as can be seen, it is the tangential force which increases whilst the normal force stays nearly constant. Yet in another test (Figures 57 and 58) the power flux rises sharply as before and then falls again. The specimen started to burn at the onset of the sharp rise in the power flux and continued to burn until the end of the test, despite the subsequent fall in the power flux. Figure 58 shows that not only did the tangential force rise during this surge but also that the normal forces fell momentarily. In yet another test (Figures 59 and 60) the forces and the power flux fell at the onset of burn and continued at this lower level whilst the workpiece still showed evidence of thermal damage until the end of the test. The only consistent feature of these tests was that the mean power flux at the onset of thermal damage was in all cases approximately 8 - 11W/mm^2.

For the tests carried out with the water-based fluid however, burn was readily identifiable from the force traces. As soon as the workpiece started to burn the forces rose rapidly and never subsequently decreased. The value of mean power flux at which this occurred was in the range 16-20W/mm^2 for a 3mm depth of cut.

The limiting power flux value however, was found to depend upon the depth of cut and Figure 61 shows this relationship for the water-based fluid.

Figure 62 shows results for two tests carried out under similar conditions but each with one of the two different grinding fluid types. This figure illustrates how the specific grinding energy increases with the amount of stock removed and is a reflection of the increase in the amount of rubbing taking place as the wheel wears. Clearly the initial specific grinding energy is much lower for the test using the oil-based fluid than for the water-based one. However, the increase in the specific energy as the wheel wears was more rapid for the oil test than for the water one. This trend is even more apparent in Figure 63 which again shows results for two tests, but these tests were carried out with a more finely dressed wheel and at a lower feed rate than those shown in Figure 62. Here the specific energy for the test with the oil-based fluid actually exceeds that for the water-based one. The surge in the specific energy trace occurred when workpiece burning started as discussed previously.

Figure 64 illustrates the relationship between specific energy and feed rate for both the oil and water tests. These values are all taken after 100mm^3/mm of material had been removed. However, as the previous two figures illustrate, the specific energy for the oil-based tests increases fairly rapidly and the values would be significantly different at a later stage through each of the tests.

This also applies to Figure 65 which shows the relationship between the specific grinding energy and the dressing conditions. As shown in Figure 63 the values of specific energy for the tests carried out with a finely dressed wheel actually changed rapidly with time so that the value for the oil test could have been higher than the

water one if the same figures were plotted after, say, 400mm^3/mm of material had been removed.

Attempts to measure the depth of wheel wear were not very successful since the depth of the wear scar was less than could reliably be resolved on the Shadowgraph. It was in all cases however less than for the corresponding tests with a water-based fluid.

Figure 66 is especially interesting since it shows that a better surface finish was obtained with the water-based fluid than with the oil based one throughout the range of dressing conditions. This result is unexpected since other researchers [79] have reported better surface finishes with oil than with water.

5.7 Finite Element Analysis

A finite element model of a workpiece being ground under creep-feed surface grinding conditions was developed as discussed in Section 3.3. By using the values of specific energy determined in the plane grinding tests and the partitioning values obtained from the pin tests, the maximum workpiece temperature for any grinding conditions could be determined.

Figure 67 shows the maximum temperature in the workpiece for a range of depths of cut and wheel diameters. This result is for a constant stock removal rate. Increasing the depth of cut or the wheel diameter increases the length of the contact arc, and therefore spreads the power dissipation over a larger area. So although the total power input to the workpiece is nearly the same in all cases, the peak temperatures reached, under steady state conditions, is lower.

Since it appears from the pin tests that there is a maximum surface temperature above which burn will occur, it was possible with this finite element model to determine at what value of power flux burn would occur for a range of grinding conditions. This was done by running the program several times and finding a value of mean power flux that would just cause the burnout temperature to be reached at the hottest point. This was done for various depths of cut, and for both oil and water-based coolants. A partition value of 1.7% was used and burnout was assumed to occur when the maximum temperature exceeded 130°C for the water-based coolant; for the oil, values of 13% and 290°C were used respectively.

A Nimonic workpiece was also modelled by using appropriate material properties as listed in Appendix VI. In this case a partition value of 1.1% and a burnout temperature of 110°C were used as deduced from the pin tests with the water-based coolant.

The results from these analyses are shown in Figure 68. The result for the water-based fluid on the steel workpiece suggests a mean burnout power flux of approximately 15W/mm² for a 3mm depth of cut. The experimental result in Figure 61 however, suggests a value of approximately 19W/mm². These two results are not directly comparable however, since one represents a surface grinding operation and the other a cylindrical operation which will result in a shorter arc length; however the fact that they are of the same order largely substantiates the findings from the pin tests and their application in this manner. These results and their significance will be discussed in more detail in the next chapter.

CHAPTER 6

Discussion

This chapter is intended to focus on the significant results and to relate them to previous understanding of the creep-feed grinding process. It also underlines the important findings and discusses how these can be applied to improve understanding and control of the process.

For the purposes of this chapter it is convenient to discuss the results according to their significance rather than to their method, and therefore the format of the discussion is slightly different from that previously adopted.

6.1 Creep-feed Grinding

From the results a number of interesting features relating to creep-feed grinding in general terms are apparent and these will be discussed in this section.

The results of the plane cylindrical grinding tests showed that the specific energies rose faster at lower feed rates (Figure 30) and that this increase was accompanied by a corresponding increase in the normal force component (Figure 31). Malkin [12] suggested the following form for the force components:

$$F_N = F_{NC} + F_{NS}$$

$$F_T = F_{TC} + \mu F_{NS}$$

The results discussed in Section 5.1 suggested that the initial ratio of tangential to normal force (ie when $F_{NS} = 0$) was approximately 0.5 but that it steadily

decreased and tended to a value of around 0.3.

If the cutting components of the forces (F_{NC} and F_{TC}) are assumed to stay constant then this change in the force ratio reflects the increase in F_{NS} as the wear flat area grows and suggests that the value of μ, which is effectively a coefficient of friction, is approximately 0.3 for this particular combination of workpiece, wheel grade and grinding fluid.

It is the rate of growth of this rubbing component that controls how rapidly the specific grinding energy increases. Salmon [9] showed that for a Nickel alloy the forces increased rapidly until as much as 97% of the total grinding energy could be used in overcoming this rubbing component of the tangential force.

From the results presented in Figure 30 it appears that the rate of growth of this rubbing component depends on the feed rate, however if the results presented in Figure 30 are replotted as a function of the number of wheel revolutions, an interesting result is obtained (Figure 69). This figure shows the increase in the specific energy as a function of the length of time that each grit has been active. Hence if the feed rate is increased by a factor of 3 the number of wheel revolutions until the same amount of stock has been removed will be reduced by one third. Figure 69 suggests that the specific energies are more a function of the time each grit has been active than of the grinding forces for the range of conditions under which these tests were carried out. If this is so, it suggests that the wear mechanism is one of attritious wear, and that very little fracture wear, which would depend on the forces acting, is taking place. Furthermore since this wear process seems to depend predominantly on time rather than force it would appear that Duwell's [75] suggestion that the wearing of the grits is

predominantly by chemical action may be correct under these conditions. Further evidence of this comes from tests to compare the relative merits of oil and water as grinding fluids. Figures 62 and 63 show that the rate of increase of the specific energy was greater for the tests carried out with oil than for those carried out with water, which suggests a more rapid growth of the wear flats on the grits. Yet if the wear mechanism were one of mechanical wear it would be expected that the rate of wear would be reduced by the use of a fluid with good lubricating properties, such as oil. It was also found from the pin tests that when using oil the grinding zone temperature is likely to be over twice that occuring when using a water-based fluid. It is possible that the increased temperature is influencing the rate of growth of the wear flats. This, too, suggests that it is a chemical erosion process, depending on time and temperature rather than a mechanical wear process which would depend more on load and lubrication.

Looking more closely at Figure 62 it appears that the initial specific grinding energy is lower with oil than it is with water, which suggests a lower cutting energy for oil than for water. However it is known that the specific grinding energies rise very rapidly during the early stages of a creep-feed grinding test when using a water-based fluid and then more slowly. This is illustrated in Figures 40 and 41 which show a 'continuous dressing' test which represents the conditions at the first moment of grinding before any wheel wear can occur. Taking values of initial specific energy from these figures suggests that the values for oil and water shown in Figures 62 and 63 may not be very different at the start of a test, but that the values for the water test increased very rapidly during the first few seconds of the test, which were impossible to record due to the transient effect in the force measuring system as described in

Section 5.1. It may be that with a freshly dressed wheel, which should have virtually no wear flats, the local stresses on each asperity in contact with the workpiece will be relatively large. This may cause rapid mechanical wear when using a water-based coolant until the local stresses have fallen to a level which allows the erosion wear process to become predominant and the subsequent growth of the wear flats to proceed at a much slower rate. With oil however, it may be that this phase of the wear process is less evident since the lubricative properties of the oil prevent it. Hence the growth of the specific energy appears to start off at a lower level but to increase more rapidly due, possibly, to the lack of the initial rapid wear regime and to the more rapid progress of the subsequent wear.

It is interesting that a better surface finish was obtained with the water-based fluid than with the oil-based one as shown in Figure 66. A better surface finish implies more active grits and a larger wear flat area. More grits result in a smaller chip thickness and therefore smaller but more numerous grooves in the ground surface which gives a smaller 'peak to valley' height. Whilst a larger wear flat area results in more rubbing which effectively burnishes the surface behind each cutting edge. If the initial rapid wear mechanism suggested above does take place when using a water-based coolant then this would cause an increase in the number of active grits since the effective surface of the wheel would move to a deeper level (Figure 70). Furthermore the initial rapid growth in the wear flat area may result in it being larger after any particular amount of stock has been removed.

The results shown were obtained with a moderately hard wheel (K grade) which would suppress any fracture wear. Ye and Pearce [79] for example who reported a better

surface finish with oil than with water were using a softer (G grade) wheel and were grinding a 'difficult to grind' Nickel alloy. It may well be that under these conditions more grit fracture or pullout would occur and that the number of active grits would not increase. Ye and Pearce do, however, report similar results to those in Figures 62 and 63, with oil giving lower initial grinding energies but a more rapid increase.

Results obtained under creep-feed conditions may not be directly comparable with those obtained under conventional grinding conditions. In conventional grinding the contact time for an individual grit is very much shorter due to the shorter arc length and therefore the temperatures reached by the grits are likely to be lower. Furthermore the force per active grit is several times higher than in creep-feed grinding.

One test described in Section 5.1, results of which are shown in Figures 26 and 27, showed a very low wheel wear rate. This test was carried out with a very finely dressed wheel and it was found that the initial specific energies were high and did not change very rapidly with time as shown in Figure 27.

The results suggested that the wheel surface condition after dressing was different from that produced by higher dresser infeed rates. Murray and Malkin [31] explained the mechanism of rotary dressing in terms of the interference angle between the diamonds on the roller and the wheel. This is a function of the diameter of the wheel and roller and of the surface speed ratio and the dresser infeed rate. Murray and Malkin suggested that at low interference angles the diamonds do not actually break the grits but simply scratch across the surface, thereby generating flats. At larger interference angles more of the grits would be broken or removed to produce a

random surface structure. These mechanisms explain the form of the curves in Figure 28. At low dresser feed rates some of the grits already have flats on them before grinding and therefore the initial specific grinding energy is high. However, the rapid wheel wear was not evident and the wheel apparently immediately started to wear by the slower erosion on the flats that were already present.

It is interesting at this stage to consider Hahn's description of chip formation [17]. He described how, when up-grinding, a grit initially rubs as it moves up the grinding arc then ploughs and finally, when the stress under the leading edge is great enough, a fracture is formed in the plastic area under the grit and a true chip is formed. Materials which form a chip easily he described as 'easy-to-grind' and those for which a significant amount of ploughing and rubbing takes place as 'difficult-to-grind'. Malkin [12] extended this idea and concluded that as the wear flat on a grit grows, a point is eventually reached where the stress under the flat is no longer high enough to fracture the plastic surface and the grit continues to plough. This is shown by a sharp increase in the specific grinding energy and the onset of workpiece burning. All these ideas however, only apply when up-grinding. When down-grinding, as is the case in creep-feed, the stages are the other way around. The chip formation is started as soon as the grit contacts the workpiece and continues all the way to the bottom of the arc as shown by Shiozaki et al [19]. However, because of the nature of the interference zone, there will be a negative clearance between the wear flat and the workpiece, hence the significant amount of rubbing takes place concurrently with the chip formation. Under these conditions it is not the ease with which a fracture is formed in the plastic surface which influences how difficult a material is to grind but it is the rate of growth of the wear flats which seems to be influenced by

the temperature in the grinding zone, and by time.

6.2 The Effect of Material Hardness

The results presented in Figures 40 and 41 show that the specific grinding energy does depend on the bulk material hardness. The points plotted at zero stock removed represent the specific cutting energies since these tests were carried out with continuous dressing and there can therefore be very little rubbing energy. These results show that even the specific cutting energies vary with hardness, which is a different finding from that of Malkin [12] who showed that the specific cutting energies were independent of hardness for a range of steels. He postulated that the chip formation process could be considered as an adiabatic shear process and that the minimum grinding energy tends towards the melting energy. He claimed that because the temperature in the shear plane tends towards the melting point of the material then any previous heat treatment would be irrelevant.

However, the results obtained in this work suggest that under creep-feed grinding conditions there is a variation in the specific cutting energy with hardness. It is possible that the adiabatic assumption does not hold under creep-feed conditions since the instantaneous stock removal rate per grit is lower than for a conventional grinding operation. For the same stock removal rate and the same number of active grits on the wheel surface the volume of the chips produced would be the same for a creep-feed as for a conventional operation. However the creep-feed chip would be long and thin whereas the conventional chip would be short and fat. Hence the energy needed to form a chip in creep-feed would be released more slowly as the grit travels the full length of the grinding arc, whereas for conventional grinding the

energy would be released very rapidly. This may result in the instantaneous temperature in the shear plane being lower for creep-feed than for conventional and not high enough to allow thermal softening to take place. Although the temperature is still likely to be above the austenizing temperature, the time period is unlikely to be long enough to allow softening to take place, and therefore the shear stress of the material will be reflected in the specific cutting energy.

Figures 40 and 41 show that there is a slight difference between the rates at which specific energies increase as the wear flat area grows for the hard and soft specimens, but not by a significantly different amount. This is not surprising since whether the material is in a hard or a soft state it is still considerably softer than the aluminium oxide grits which have a Vickers hardness of approximately 1800. Neither is there any reason why any chemical action in the grinding zone should be affected by the hardness of the material. There does however appear to be a much larger difference in the increase in the specific energy during the initial wheel wear phase. The hard specimens showed an approximately 50% greater increase during the initial wheel wear phase than the soft specimens. This is evident at both feed rates.

One possible explanation for this, based on the idea of an initial abrasive wear phase followed by a chemical erosion type of wear (called 'solubility wear' by Hahn), is as follows:

During the initial grinding phase the grits are being rapidly worn by abrasive wear; the contact force between the flats on the grits and the material being determined by the degree of interference behind the leading edge of the grit. For a soft material this interference will be partially accommodated by elastic deflections of the workpiece material and therefore the contact force will

be lower and the stress level below which abrasive wear ceases to predominate will be reached at a smaller wear flat area. For the hard materials however, the workpiece material will deflect less for a given contact force and larger wear flats will be formed before this wear mechanism ceases to predominate.

Further evidence for this theory can be found in Figure 42. The surface finish for the hard specimens is consistently better than for the soft specimens. As discussed in the previous section this implies a larger wear flat area and more active grits which would arise if the above hypothesis were true. As the wear flats on the individual grits grow, the degree of overlap between grits whose centrelines are not in exactly the same plane across the wheel increases. Hence the number of grits crossing any point on the workpiece surface increases giving a better surface finish.

There was no obvious effect on the specific grinding energy due to the carbides present in the various materials ground. However, the carbides encountered, principally chromium and molybdenum, are less hard than the aluminium oxide grits [85]. A different result may well be obtained when grinding materials containing carbides that are harder than the wheel grits, such as tungsten or titanium. Nimonic contains titanium and tungsten carbides.

6.3 Creep-feed Form Grinding

From the results of the tests carried out with the angle face dressers it is evident that there is no fundamental difference in the grinding process no matter what the angle between the ground face and the wheel axis. Furthermore the results of the tests carried out with the form dresser confirm that the method described in Section 3.1

for calculating the total grinding power is justified.

These findings enable a number of useful general points regarding form grinding to be identified. Firstly, when dressing the semi-circular form illustrated in Figure 3 using a diamond roll dresser the local normal infeed rate of the dresser into the wheel is going to decrease towards the sides of the form. This may result in very high specific grinding energies being encountered due to the characteristics shown in Figure 36. For the semi-circular shape considered throughout this work, this is unlikely to be a problem since the depth of cut, and hence the local stock removal rate, is also decreasing towards the sides of the form. This means that the local power flux is still likely to be smaller at the sides of the form than at the centreline. Figure 71 shows this variation in local power flux as a function of angle around the semi-circular profile, from 0° at the centre to 90° where the ground surface is perpendicular to the workpiece axis. This figure has been derived by calculating the local normal dresser infeed and the local MNIR around the form and using values of specific energy from the plane cylindrical grinding tests. Two results are shown, one for a high radial dresser infeed rate and one for a low one. The radial dresser infeed rate is equivalent to the normal dresser infeed rate at the centreline of the form and the local infeed rate decreases towards the sides. For the high radial dresser infeed rate the local normal infeed rates will be relatively high until well around the form; the specific energy values will all be from the flat portion of the characteristic shown in Figure 36. However with the low radial infeed rate the specific energy will rise rapidly as the normal dresser infeed rate falls; all the values are from the steep portion of the curve shown in Figure 36. Hence if the specific energy value increases more rapidly than the stock removal rate is falling, then the power flux may

well be at a maximum at a point away from the centreline of the form. This is illustrated by curve B in Figure 71 which shows that with a low radial dresser infeed rate of 0.4μm/rev the maximum power flux would occur at approximately 20° from the centreline.

Knowing the distribution of power generation around the profile is necessary if the temperatures in the workpiece are to be calculated. This information, together with a knowledge of how much of this power goes into the bulk of the workpiece, enables the temperature distribution in the workpiece to be calculated. This in turn allows the limiting stock removal rate to be determined, since it is known from the pin tests that workpiece burning will be triggered as the workpiece surface exceeds the burnout temperature. In addition, knowing the temperature field within the workpiece allows the distortion caused by thermal expansion to be calculated. This is particularly useful in the ballscrew grinding application since it enables the errors resulting from grinding to be calculated in advance and to be taken into account, thereby bringing the process under more accurate control.

A further example of how the understanding generated by this work could be applied is shown in Figure 72. This diagram shows a creep-feed cylindrical grinding operation with an angle approach so as to grind a face and a diameter simultaneously. The configuration shown by the solid lines would result in identical wheel conditions being generated on both faces by the dressing cycle. However, if a better surface finish were required on the face than on the diameter, then this could be achieved by using the configuration shown by the dotted lines. Furthermore the surface finish that would be obtained could be determined in advance by carrying out plane tests with the appropriate wheel and workpiece combination and the necessary angle of approach calculated.

Further discussion on the applications of this work is included in Reference [86].

6.4 Energy Partitioning and the Burn Limitations

The method for measuring how much of the grinding energy entered the workpiece as heat proved to be especially informative. Not only did the results obtained show good consistency within themselves but they also provided an explanation for some of the findings of other researchers.

The finding that a nearly fixed proportion of the grinding energy enters the workpiece irrespective of the mean temperature is especially interesting. If the heat input across the ground face of the pin were uniform this would not be possible; initially all the heat would enter the workpiece, and then, as the surface temperature rose, a steady state condition would be reached at which point all the heat would be transferred to the coolant.

From the tests carried out it seems that, at worst, only 2.5% of the grinding energy enters the workpiece (Figure 44), and that when the workpiece surface has reached nearly 100°C 1% of the energy is still going into the workpiece.

An explanation for this may be found in the theoretical work of Clements [87]. He modelled the grinding process by considering each grit as a heat source; the heat input being uniformly distributed across the wear flat on each grit. He then set up and solved the equations for the temperature distribution in the workpiece due to the passage of such a grit. However, in the region between one grit and the following one he introduced a cooling term such that if the workpiece surface temperature were above 160°C the coolant would be film boiling and no heat transfer to the coolant would be taking place, but once

the surface temperature had fallen to below 160°C then effective forced convective heat transfer would be occuring. The resulting surface temperature profile is shown in Figure 73. This result shows temperature against circumferential grit spaces; the abcissa being the number of grit diameters from the leading edge of one grit. Reading from left to right the temperature rises very rapidly and reaches an instantaneous maximum of nearly 700°C before falling after the grit has passed. In the next region the only heat loss from the surface is by conduction into the bulk of the workpiece and then, once the surface temperature falls below 160°C, convection to the coolant becomes effective and the surface temperature falls more rapidly. The inset figures show the temperature profile into the workpiece at each stage and show that in the initial stages all the heat is being conducted into the workpiece and then, once the film boiling region is passed, there is a positive temperature gradient at the workpiece surface indicating that heat is being drawn out. If this mechanism does apply then it is not surprising that the mean workpiece surface temperature has little effect on the partitioning since during the time when heat is actually entering the workpiece no convective cooling is taking place and the surface temperatures are significantly higher than the mean workpiece temperature, thereby making its effect relatively small.

Clements' work was based on a material of relatively low thermal conductivity, similar to that of the Nimonic alloy used in this work. For steels, which have a thermal conductivity approximately 4 times greater, a different result would be obtained. It should be stressed that Clements' work is largely qualitative, and although values have been assigned to the various parameters these are not necessarily based on detailed experimental work. However the trends and concepts highlighted in the analysis are in agreement with the experimental results presented

in this thesis, and further development of the model is warranted. It would be informative, for example, to integrate the temperature gradients normal to the ground surface (as shown in Figure 73) across a cycle, and hence arrive at a theoretical value for the net heat conducted into the workpiece for comparison with the experimental values presented.

Clements' model includes a stability criterion which suggests that once a critical temperature at the start of a cycle (the leading edge of a grit) is exceeded, then for a certain grit/space ratio there is insufficient time for the heat generated to be dissipated before the next grit arrives. This leads to an unstable temperature rise. Figure 74 illustrates this stability criterion. This shows the workpiece surface temperature at the start of a cycle against the space/grit ratio. Hence for a space to grit ratio of, say, 70 and a heat input of 1.75E9W/m² over the area of the wear flat, stable conditions would be reached with a temperature at the start of the cycle of approximately 43°C. (Clements' calculations assumed an infinite heat sink below the workpiece surface). However as the grinding wheel wears and the wear flat size increases then the space/grit ratio falls and the temperature necessary to obtain stable conditions rises, until eventually the limit of stability is reached and the temperature rises rapidly. This figure suggests that this occurs when the mean workpiece surface temperature at the start of the cycle exceeds approximately 83°C. This compares with an experimental value for the mean temperature throughout the cycle of 112°C. A direct comparison could only be made by determining the mean value of the curve in Figure 73, but, given the unknown factors involved, these values are of sufficiently close order to justify further investigation.

The pin tests with the steel workpieces, however, burnt

unstably at a higher mean surface temperature in the range 120 - 140°C, which is very likely a consequence of the higher thermal conductivity of the material. This is also reflected in the partitioning values. For the steel pins approximately 1.8% of the heat entered the workpiece whereas for the Nimonic pins the value was only approximately 1.1% under similar conditions.

Continuously dressing the grinding wheel had little effect on the partitioning value when grinding the steel workpiece, however with the Nimonic workpieces the value fell from 1.1% to approximately 0.42%. This may account for Salmon's finding that higher power fluxes could be maintained without workpiece burning occuring when continuously dressing. Salmon's work was carried out with a similar Nickel alloy and he found that the power flux at burnout was as much as two to three times higher when continuously dressing than when creep-feed grinding conventionally. If, as the results of this work suggest, the partitioning value more than halves when continuously dressing and when grinding this particular material, then it is reasonable that the power flux value should double to produce the same thermal field in the workpiece.

The mean surface temperature at which burn occurs need not necessarily be the same as the temperature at which film boiling starts. From Figure 73 it is evident that there is no reason why the mean temperature throughout the time period of this cycle should coincide with the temperature at which film boiling occurs. The mean surface temperature is likely to depend on the grit spacing and, most importantly, on the thermal conductivity of the workpiece. Hence the different values found for the two workpiece materials. Figure 54 shows that the partitioning value falls for more coarsely dressed wheels. This may be because a coarsely dressed wheel is likely to have a greater space/grit ratio, and there will therefore be a longer period

after the transition back to effective convective heat transfer before the next grit passes.

When burning occurred with the Nimonic workpieces, the temperature and force recordings were seen to rise in a series of surges. This has been observed by other researchers when creep-feed grinding this material [8]. Shafto's explanation was that the rise in temperature caused any loading on the grits to be removed and the grinding forces to temporarily fall before rising again.

With the steel specimens this was never observed, neither with the pin tests nor the surface or cylindrical creep-feed tests. In these cases, once burn occurred the forces and temperature rose rapidly and steadily to much higher values. On examining the wheel surface after grinding the Nickel alloy material, evidence of metallic debris adhering to the grits was found in cases where burning had not occurred. However, after grinding a steel specimen, no loading was visible unless burning had occurred, in which case very heavy loading of the grinding wheel was clearly visible. It is possible that the nature of the bond between the grinding chips and the wheel grits is such that for the steel specimens this loading only occurred once the temperature rose, thereby increasing the grinding energies even further and producing an unstable situation. Whereas for the Nimonic specimens the sudden rise in temperature caused the loading to be removed. Further work on the chemical nature of loading is necessary if this hypothesis is to be substantiated.

When using the neat oil grinding fluid the same rapid increase in temperature was observed when burning occurred, but at a much higher surface temperature. This occurrence was accompanied by the production of much acrid vapour suggesting that at least one of the components of the oil was boiling off. Since the pin tests with the oil-based

fluid are also reliably modelled by the fixed partition model, it is reasonable to suppose that a similar mechanism to that modelled by Clements is taking place, but that the transition to film boiling occurs at a higher temperature.

It is clear from the results of the pin tests that under creep-feed grinding conditions oil can result in much higher workpiece temperatures being sustained without burning occuring than is the case with a water-based fluid. However, because a considerably greater fraction of the power used goes into the workpiece the power flux at burnout is smaller than is the case for a water-based fluid. The limiting stock removal rate is consequently hard to establish since with the oil-based fluid the specific energy rises so fast. Figure 64 however, suggests that there is no clear advantage of either type of fluid in terms of stock removal rate.

The occurrence of burn when using the oil-based fluid was seen to cause very different effects on the forces and hence the specific grinding energy. Figures 56, 58 and 60 show that these can either rise, fall or surge and return to their original value. No explanation is evident for this, but it is worth noting that Furukawa et al [88] report similar characteristics when creep-feed grinding. Their observations relate to work carried out with a soluble type fluid, however they do offer an explanation in terms of thermal expansion which will cause an increased infeed and thermal softening which may reduce the chip formation energy, but quantitative analysis is needed if this explanation is to be substantiated.

A paper recently published by Yasui and Tsukuda [59] on the effect of fluid type under conventional grinding conditions suggests that the film boiling mechanism also applies in conventional grinding. Their results, some of

which are reproduced in Figure 75, show that as the depth of cut is increased the workpiece temperature when using soluble oil suddenly increases and thereafter follows the same trend as dry grinding. This discontinuity occurs at a temperature of approximately 80° above room temperature, which is in the same region as was found for the pin tests. Yasui and Tsukuda also found a similar occurrence with neat oil fluid but at a surface temperature of approximately 290°C above room temperature, which again is in reasonable agreement with the results of this work. These results may account for why researchers such as Osman and Malkin [57] have found little or no advantage in using a soluble coolant for conventional grinding, since so called 'wet' grinding may in fact be dry due to the film boiling of the coolant. Conventional grinding can still be carried out without coolant due to the rapid passage of the heat source over the workpiece, whereas in creep-feed the rate of conduction of heat away through the slow moving workpiece is so slow that unless effective surface cooling is taking place in the arc of cut, then the temperature will rapidly rise and cause burning.

It is evident then that Malkin's partitioning values of approximately 60% obtained under conventional grinding conditions are extremely unlikely to be applicable in creep-feed where the action of the coolant is paramount if satisfactory grinding is to be achieved.

In order to put the partitioning values obtained into a form which can be used to compare them with results from other work, a finite element analysis was used. Figure 68 shows the burnout power flux limitation obtained from this analysis for different depths of cut. Care must be taken when comparing these values which are for a surface ground workpiece with those obtained under cylindrical grinding conditions, since the arc length for any depth of cut would be significantly different. The values of

power flux are mean values around the arc. If the power generation is assumed to be proportional to the local infeed rate as shown by Shafto then the distribution with distance from the start of the arc would be triangular and therefore the maximum power flux as quoted by Shafto is twice the mean value.

Figure 68 suggests that the mean power flux at burn would be approximately 10W/mm² when making a 3mm cut in a Nimonic workpiece using a water-based fluid. This is rather lower than the values quoted by Shafto and Salmon, who reported values of approximately 16-20W/mm² (mean values). However, taking into account the possible errors in the method, these values are not unreasonable. That the experimental burnout heat fluxes are higher than the theoretical ones suggests that the partitioning value is, if it is in error, lower than measured. One possible reason for this may be that the normal infeed rates in surface grinding are likely to be up to 40-50mm/min, however in the pin tests it was only possible to go up to values of 15mm/min without burning occuring instantly. As Figure 53 shows, the partitioning value does fall with increasing infeed rates, possibly due to more heat being removed with the thicker chips. Therefore partitioning values obtained at these higher feed rates may be even lower than those measured. Similarly when applied to steel workpieces, the model predicts mean burnout power flux values of 14-18W/mm² whereas the experimental results in Figure 61 suggest values of approximately 18-28W/mm². Likewise the modelling using an oil-based fluid predicts a mean burnout flux of 4.5W/mm² whereas the experimental results suggest a value approximately twice this. Overall though, the modelling appears to validate the results obtained and to indicate that the true partitioning values are likely to be less than those measured from the pin tests.

Further agreement with the findings of this work can be

found in the results of work by Druminski [69] who investigated creep-feed thread grinding using an oil-based coolant. He reported that burn always initiated at the crests of the threads and that the temperature measured near the surface at this point was always approximately 300°C. Given the restricted heat path from the crests of the threads it is quite possible that this is where the maximum temperature will be reached and, as in the work reported in this thesis, the critical temperature appears to be around 290-300°C for oil.

It is still difficult to account for the claims by Werner [60] that workpiece temperatures in the order of 500°C are possible in creep-feed grinding. The trend of decreasing temperatures with increasing depth of cut shown in Reference [60] is supported by the results of this work (Figure 67), but the absolute values reported by Werner are in the order of four times higher than those in Figure 67, even for a stock removal rate that is only one quarter of that used to obtain the results in Figure 67. It is not clear from Werner's paper how he determines the various constants in his empirical equations and it is these that probably lead to the confusion.

6.5 Creep-feed Ballscrew Grinding

It was originally stated that one of the aims of this work was to assess the feasibility of creep-feed grinding ballscrew tracks. From the research carried out the following points are evident:

1 It is possible to creep-feed grind a ballscrew form. The limiting stock removal rate, the total power required for any form and the resulting surface finish can all be determined from the result of tests carried out under plane grinding

conditions with the same wheel grade and workpiece material.

2 A water-based coolant gives a lower rate of increase of the specific energy, a better surface finish and lower workpiece temperatures under the conditions tested. The lower workpiece temperatures are especially advantageous in avoiding thermal distortion. Furthermore the bulk temperatures in the workpiece can be calculated for any grinding conditions from a suitable proprietary finite element package.

3 With a water-based coolant there may be an initial rapid wear region with a coarsely dressed wheel. To achieve minimum wheel wear and therefore maximum accuracy, a low dresser infeed rate should be used.

Further work on ballscrew grinding needs to be done on a suitable machine. Since the machine used for this work is a plunge grinding machine it was only possible to grind one revolution of a workpiece. A ballscrew would require significantly longer grinding times than could be achieved in this way. A complete grinding operation for this application may eventually involve a creep-feed rough grinding pass for which wheel wear and surface finish would not be significant, followed by a conventional shallow cut pass to achieve the required accuracy and surface finish.

To compare a creep-feed method with the existing method on a time basis, it would be necessary to take into account the rewinding time between passes and the handling times on transferring from the pre-cutting operation to the heat treatment and on to the grinding operation. Since most of this work could be eliminated it is likely that the creep-feed method would have an advantage.

From the results of this work it is now possible to make an informed comparison of the two methods for a specific case.

CHAPTER 7

Conclusions

The program of research described in this thesis was structured so as to produce further understanding of the creep-feed grinding process. This in turn would enable its application to the grinding of forms, particularly in steel components, to be more fully quantified and controlled. The main conclusions from the work are summarised below.

7.1 The Extension of Previous Creep-feed Research to Form Grinding Applications

By grinding on a range of angled faces up to 80° it has been shown that when grinding hardened steels there is no difference in the grinding mechanism provided that the infeed rate is defined normal to the face being ground. Shafto [8] showed that for plane grinding the infeed rate normal to the ground surface at the start of the arc of cut was a meaningful way of describing the creep-feed grinding process, and that the specific grinding energy was directly related to this parameter, which he called the maximum normal infeed rate. The angle face tests carried out as part of this work confirm that the same relationship holds throughout the range of face angles tested.

Furthermore, when diamond rolls are being used for dressing, the relationship between the condition of the wheel surface after dressing and the dresser infeed rate normal to the wheel surface is independent of the face angle.

It has been shown how these results can be applied to a form and how the total power requirement and the distribution

of power around the face can be calculated from data acquired under plane grinding conditions.

7.2 The Relationship between Specific Grinding Energy, Workpiece Hardness and Type of Grinding Fluid

The specific grinding energy was found to depend on the bulk hardness of the workpiece material. This result is contrary to results published by Malkin [12] who suggested that the chip formation happens so rapidly that it can be considered as an adiabatic process, and that the temperature reached is close to the melting energy of the material. It is possible that under creep-feed grinding conditions, when the chip is formed over a time period in the order of 20 times longer than for conventional grinding, that the temperature is not so high and that the shear stress of the material is reflected in the specific grinding energy.

The use of oil as a grinding fluid was found to result in lower initial specific grinding energies but in a more rapid rate of growth of the specific energy which implies a more rapid rate of wear of the grits than is the case for the water-based fluid.

The predominant wear mechanism in creep-feed grinding has already been shown to be one of attrition of the grits rather than of fracture of the grits and bonds as would occur in conventional grinding [5]. There is further evidence, in addition to that of Duwell [75] and others, from this work to suggest that this attritious wear process is predominantly one of chemical erosion, since the rate of growth of the wear flats on the grits appears to depend on time and temperature rather than on the cutting force and the degree of lubrication.

7.3 Energy Partitioning and Workpiece Burn

By grinding insulated workpieces it was established that, at most, only 2.5% of the power used in the grinding process actually enters the bulk of the workpiece when creep-feed grinding a hardened steel with an effective supply of water-based coolant. It was also established that the criterion by which the onset of grinding burn can be predicted is one of workpiece surface temperature and not power flux, as was originally suggested by Shafto. The critical surface temperature was found to be approximately 120 - 140°C for a water-based fluid. It was shown that this temperature would be reached, for a workpiece with geometry such as those used by Shafto, with a power flux of approximately 30W/mm². However with different depths of cut,and particularly when grinding forms, different power flux values may cause the critical temperature to be reached. A 3-dimensional finite element method would enable the maximum temperatures to be calculated for any power flux distribution.

When using an oil grinding fluid to grind hardened steel workpieces the fraction of the heat entering the workpiece is much higher. Values in the range 11-15% were recorded and the critical surface temperature was found to be approximately 290°C.

CHAPTER 8

Recommendations for Further Work

8.1 Further Comparison of Oil and Water-based Grinding Fluids

By comparing the specific grinding energies for tests carried out with continuous dressing but with both oil and water-based grinding fluids, it would be possible to establish whether the grinding fluid does actually affect the specific cutting energy. If not then this would lend further evidence to the idea that the specific energy rises very rapidly in the initial moments of a conventional creep-feed grinding test with a water-based fluid.

A further useful piece of work in this area would be to investigate the growth of the wear flats as a function of stock removed for both oil and water-based fluids. If, as the work reported in this thesis suggests, the wear flats grow rapidly and then more slowly for water, but at a steady rate for oil this would reinforce the possibility that attritious wear is influenced by temperature and time, and is therefore at least partially due to chemical erosion.

It would also be worthwhile to develop a technique of measuring grit temperature in process during creep-feed grinding. With some information on the temperatures involved it may be possible to do more meaningful research into the chemical nature of the wheel wear mechanism and to determine what features of the coolant are desirable to control it.

8.2 The Extension of Clements' Theoretical Model

Now that the pin test method of measuring both the fraction of the grinding energy entering the workpiece and the surface temperature has been established, it should be possible to develop Clements' theoretical model and to make direct comparisons with experimental results. The effect of various workpiece thermal conductivities and convective cooling times should be analysed and the model should be extended so as to give a theoretical value for the energy partitioning. The range of experiment covered by the pin tests also needs to be widened. Tests carried out at very low plunge feed rates, where grit ploughing would be significant should be carried out and a wider range of materials should be included. Also the effect of wheel speed should be investigated. To check the validity of the fixed partitioning assumption across a wide range of surface temperatures it would be interesting to arrange to subcool a pin type workpiece and measure the partitioning under these conditions.

If Clements' model is found to be justified under a wider range of conditions then it would be a useful way of determining the effect of grit spacing and wheel speed for workpiece materials of different thermal conductivity. It may also be possible to explain why continuous dressing, which will result in a large space/grit ratio, is effective at reducing the fraction of the grinding energy which enters the workpiece when grinding materials of low thermal conductivity.

References

1 Financial Times, "Science Council claims £1m a year Rolls-Royce saving", 29 April 1981.

2 Metalworking Production, "Creep-feed shapes the way to success", pp 101-106, February 1981.

3 American Machinist, "Creep-feed grinding makes gains", pp 100-103, May 1983.

4 Machining and Production Engineering, "Creep-feed - the precise way to shift more metal", pp 14-19, February 1981.

5 Trmal G J, "Comparison of creep-feed and conventional grinding", proc of the 21st MTDR Conference, Swansea, pp 323-328, September 1980.

6 Otsuka J, Fukada S & Obuchi N, " A study of Thermal Expansion of Ball Screw", Bull Jap Soc of Precision Engineering, Vol 17 No 4, pp 273-274, December 1983.

7 Machinery and Production Engineering, "Large order for Ballscrews", p 11, September 1981.

8 Shafto G R, "Creep-feed Grinding", PhD Thesis, University of Bristol, 1975.

9 Salmon S C, "Creep-feed Surface Grinding", PhD Thesis, University of Bristol, 1979.

10 Marshall E R & Shaw M C, "Forces in Dry Surface Grinding", Trans ASME, Vol 74, pp 51-59, January 1952.

11 Backer W R, Marshall E R & Shaw M C, "The Size Effect in Metal Cutting", Trans ASME, Vol 74, pp 61-72, January 1952.

12 Malkin S & Cook N H, "The Wear of Grinding Wheels. Part 1 - Attritious Wear", Trans ASME Series B, Vol 93, pp 1120-1128, November 1971.

13 Yoshikawa H, "Criterion of Grinding Wheel Tool Life", Bull Jap Soc of Precision Engineering, Vol 3 No 1, pp 29-32, 1963.

14 Hahn R S, "The Effect of Wheel-work Conformity in Precision Grinding", Trans ASME, Vol 77, pp 1325-1329, November 1955.

15 Reichenbach G S, Mayer J E, Kalpakcioglu S & Shaw M C, "The Role of Chip Thickness in Grinding", Trans ASME, Vol 78, pp 847-859, May 1956.

16 Hahn R S, "On the Mechanics of the Grinding Process under Plunge Cut Conditions", Trans ASME, Series B, Vol 88, pp 72-80, February 1966.

17 Hahn R S, "On the Nature of the Grinding Process", proc of 3rd MTDR Conf, Birmingham, pp 129-154, September 1962.

18 Malkin S, "The Wear of Grinding Wheels. Part 2 - Fracture Wear", Trans ASME, Series B, Vol 93, pp 1129-1133, November 1971.

19 Shiozaki S, Furukawa Y & Ohishi S, "Experimental Study on Grinding Forces under Up and Down-cut Process by Creep-feed Grinding", Bull Jap Soc of Precision Engineering, Vol 11, No 2, June 1977.

20 Ohishi S, Furukawa Y, Shiozaki S & Okada S, "The Design and Development of Creep-feed Grinding Machine and Wheel and their Optimal Utilization in view of Workpiece Burning", Proc of 20th MTDR Conf, Birmingham, pp 375-382, September 1979.

21 Saljé E & Brandin H, "Vergleichende Untersuchungen beim Pendelschleifen und Tiefschleifen von Profilen", Maschinenmarkt 85 (1979), pp 1309-1312.

22 Shibata J, Inasaki J, Yonetsu S, "On Characteristics of Wheel Wear in Creep-feed Grinding", Bull Jap Soc of Precision Engineering, Vol 15, No 3, pp 193-194, September 1981.

23 Werner P G, "Application and Technological Fundamentals of Deep and Creep-feed Grinding", SME Paper, No MR79-319, 1979.

24 Konig W & Lauer-Schmaltz H, "Tiefschleifen - eine moderne Verfahrensvariante des Flachschleifenprozesses", Trennkompendium, Bd 1, Edition Technischer Fachinformation, Bergisch Gladbach, pp 352-358, 1978.

25 Zhou Q Z & Shaw M C, "Cylindrical Creep-feed Grinding", Proc of 9th NAMR Conference, 1981.

26 Schliech Von H, "Flachschleifen mit hohen Leistungen unter Vermeidung thermischer Randzonenschadigung", Technische Mitteilungen, Vol 11/12, November/December 1980.

27 Kirk J A & Syniota W D, "Scanning Electron Microscopy and Microprobe Investigation of High Speed Sliding Wear of Aluminium Oxide", Wear Vol 27, pp 367-381, 1974.

28 Shafto G R, "Creep-feed Profile Grinding with ABN 300", Industrial Diamond Review, April 1979.

29 Konig W & Schleich H, "Deep Grinding of High Speed Tool Steel with CBN", Industrial Diamond Review, October 1980.

30 Saljé E & Damlos H, "Creep-feed Grinding, Profile Grinding", Proc of 9th NAMR Conf, 1981.

31 Murray T & Malkin S, "Effects of Rotary Dressing on Grinding Wheel Performance", Trans ASME, Journal of Engineering for Industry, Vol 100, pp 297-302, August 1978.

32 Meyer H R & Wiemann H, "Diamond Roller Dressers, their Design and Application Considerations in Europe", Proc Diamond-Partner in Productivity, 1974.

33 Malkin S & Murray T, "Comparison of Single Point and Rotary Dressing of Grinding Wheels", Proc of 5th NAMR Conf, pp 278-283, May 1977.

34 Lal G K, Matsuo T & Shaw M C, "An Investigation of the Wear of Abrasive Grains by Rubbing on Ferrous and Non-ferrous Surfaces", Wear, Vol 24, pp 279-293, 1973.

35 Malkin S & Joseph N, "Minimum Energy in Abrasive Processes", Wear, Vol 32, pp 15-23, 1975.

36 Samuels L E, "Abrasive Surface Finishing", Proc Int Grinding Conf, Carnegie Mellon University, Pittsburgh, Pennsylvania, USA, p 283, April 1971.

37 Howes T D, "The Technique of Dressing during Grinding", Proc Int Conf on Creep-feed Grinding, p 184, 1979.

38 Pearce T R A & Howes T D, "Applications of Continuous Dressing in Grinding", Proc of 23rd MTDR Conference, Manchester, pp 203-209, September 1982.

39 "Taking the Creep out of Creep-feed Grinding", Modern Machine Shop, pp 80-87, November 1982.

40 Werner G, "Influence of Work Material on Grinding Forces", Annals of CIRP, Vol 27/1, pp 243-248, 1978.

41 Verkerk J, "The Real Contact Length in Cylindrical Plunge Grinding", Annals of CIRP, Vol 34/1, pp 259-264, 1975.

42 Snoeys R, Maris M & Peters J, "Thermally induced Damage in Grinding", Annals of CIRP, Vol 27/2, pp 571-581, 1978.

43 Tarasov L P, "Some Metallurgical Aspects of Grinding", Machinery - Theory and Practice, ASM, pp 409-464, 1950.

44 Littman W E & Wulff J, "The Influence of the Grinding Process on the Structure of Hardened Steel", Trans ASM, Vol 47, pp 692-714, 1955.

45 Malkin S, "Burning Limit for Surface and Cylindrical Grinding of Steels", Annals of CIRP, Vol 27/1, pp 233-236, 1978.

46 Lee D G, Zerkle R D & Des Ruisseaux N R, "An Experimental Study of Thermal Aspects of Cylindrical Plunge Grinding", Trans ASME, Series B, Vol 94, pp 1206-1214, November 1972.

47 Jaeger J C, "Moving Sources of Heat and the Temperature at Sliding Contacts", Proc of the Royal Soc of NSW, Vol 76, pp 203-224, 1942.

48 Des Ruisseaux N R & Zerkle R D, "Temperatures in Semi-Infinite and Cylindrical Bodies Subjected to Moving Heat Sources and Surface Cooling", Trans ASME, Series C, Vol 92, pp 456-464, August 1970.

49 Sato K, "Grinding Temperatures", Bull Jap Soc Grinding Engineers, Vol 1, pp 31-33, 1961.

50 Takasawa K, "Thermal Aspects of the Grinding Operation", Ind Diamond Review, pp 143-149, April 1972.

51 Outwater J O & Shaw M C, "Surface Temperatures in Grinding", Trans ASME, Vol 74, pp 73-86, January 1952.

52 Malkin S & Anderson R B, "Thermal Aspects of Grinding. Part 1 - Energy Partition", Trans ASME, Series B, Vol 96, pp 1177-1183, November 1974.

53 Maris M & Snoeys R, "Heat Affected Zone in Grinding Operations", Proc of 14th MTDR Conference, Manchester, pp 659-669, September 1973.

54 Malkin S, "Thermal Aspects of Grinding. Part 2 - Surface Temperatures and Workpiece Burn", Trans ASME, Series B, Vol 96, pp 1184-1191, November 1974.

55 Bhattacharyya S K & Hill C G, "Characterisation of Grinding Wheel Topography and Wear", Proc of 17th MTDR Conference, Birmingham, pp 171-180, September 1976.

56 Des Ruisseaux N R & Zerkle R D, "Thermal Analysis of the Grinding Process", Trans ASME, Series B, Vol 92, pp 428-434, May 1970.

57 Osman M & Malkin S, "Lubrication by Grinding Fluids at Normal and High Wheel Speeds", Trans ASLE, Vol 15, pp 261-268, May 1972.

58 Karaim I P, "Grinding Temperature Measurement using a Thermal Electrode", Russian Engineering Journal, Vol 50, No 5, pp 89-90, 1970.

59 Yasui H, Tsukuda S, "Influence of Fluid Type on Wet Grinding Temperature", Bull Jap Soc Precision Engineering, Vol 17, No 2, pp 133-134, 1983.

60 Werner G & Schlingensiepen R, "Creep-feed - an Effective Method to Reduce Work Surface Temperatures in High Efficiency Grinding Process", Proc of 8th NAMR Conf, pp 312-319, May 1980.

61 Geisweid G & Gartner W, "Deep and Oscillation Grinding - Temperature and Power Requirements", Ind Diamond Review, pp 285-288, August 1978.

62 Stuart T V, "High Speed Creep-feed Grinding", PhD Thesis, University of Bristol, 1977.

63 Collier J G, "Forced Convective Boiling and Condensation", Pubd McGraw & Hill, 1972.

64 Powell J W, "The Application of Grinding Fluid in Creep-feed Grinding", PhD Thesis, University of Bristol, 1979.

65 Graham W & Whitson M G, "Some Observations of Through-Wheel Coolant Application in Grinding", Int Journal of Machine Tool Design and Research, Vol 18, pp 9-18, 1978.

66 Werner G, "Technologische und konstruktive Voraussetzungen fur das Tiefschleifen", Zeitschrift fur industrielle Fertigung, pp 613-620, 1979.

67 Farber E A & Scorah R L, "Heat Transfer to Water Boiling under Pressure", Trans ASME, Vol 70, p 369, 1948.

68 Peters J & Vansevenant E, "A Thermal Model covering Pendulum Grinding and Creep-feed Grinding", Annals of CIRP, Vol 32/1, pp 491-494, 1983.

69 Druminski R, "Einfluss der Werkstuckgeschwindigkeit auf die Temperaturen beim Tiefschleifen", Werkstatt und Betrieb, Vol 111, pp 733-739, 1978.

70 Wagner H W, "Grinding Fluids - Characteristics and Applications", Mech Eng, Vol 73, No 2, pp 128-132, February 1951.

71 Shaw M C, "Grinding Fluids", Manufacturing Engineering Transactions, Vol 1, pp 16-22, 1972.

72 Mercier R J, Malkin S & Mollendorf J C, "Thermal Stresses from a Moving Band Source of Heat on the Surface of a Semi-infinite Solid", Trans ASME, Series B, Vol 100, No 1, pp 43-48, February 1978.

73 Duwell E J, Hong I S & Macdonald W J, "The Effect of Oxygen and Water on the Dynamics of Chip Formation during Grinding", Trans ASLE, Vol 12, pp 86-93, 1969.

74 Shapiro A M, "Fluorides and Silico-fluorides as Extreme Pressure Additives in Lubricating Fluids for Titanium", Trans ASLE, Vol 12, pp 80-85, 1969.

75 Duwell E J, Hong I S Y Macdonald W J, "The Role of Chemical Reactions in the Preparation of Metal Surfaces by Abrasion", Wear, Vol 9, pp 417-424, 1966.

76 Palmer R J, "Matrix's Approach to High Speed Form-Profile Grinding", Technical Report, T I Matrix.

77 Hassell B, "A Grinding Fluid Comparison", MAI Thesis, Trinity College, Dublin, 1979.

78 Liverton J, "Creep Rotation Plunge Cylindrical Grinding", PhD Thesis, University of Bristol, 1980.

79 Ye N E & Pearce T R A, "A Comparison of Oil and Water as Grinding Fluids in the Creep-feed Grinding Process", Submitted to the I Mech E for publication.

80 Eshgy S, "Thermal Aspects of the Abrasive Cut-Off Operation. Part 1", Trans ASME, Series B, Vol 89, pp 356-360, 1967.

81 Adams J A & Rogers D F, "Computer-aided Heat Transfer Analysis", Pubd by McGraw-Hill, 1973.

82 Croft D R & Lilley D G, "Heat Transfer Calculations using Finite Difference Equations", Pubd by Applied Science Publications, 1977.

83 Benedict R P, "Fundamentals of Temperature, Pressure and Flow Measurements", Pubd by T Wiley & Sons, 2nd Edition, 1976.

84 Kaye G W C & Laby T H, "Tables of Physical and Chemical Constants", 14th Edition, Pubd by Longman, 1973.

85 Morgan J M & Salter N D, "The Creep-feed Grinding of Hard and Soft Steels", Accepted for publication by ASME.

86 Salter N D & Howes T D, "A Study of Creep-feed Cylindrical Form Grinding", Proc of 24th MTDR Conf, Manchester, pp 285-293, September 1983.

87 Clements R R, Theoretical work on temperatures generated in Creep-feed grinding, University of Bristol, To be published.

88 Furukawa Y, Ohishi S & Shiozaki S, "Selection of Creep-feed Grinding Conditions in view of Workpiece Burning", Annals of CIRP, Vol 28, pp 213-218, 1979.

89 Rogers G F C & Mayhew Y R, "Engineering Thermodynamics Work and Heat Transfer", Pubd by Longman, 1967.

APPENDIX I

Industrial companies which supplied information or materials.

T I Matrix

Sponsorship and information on thread and ballscrew grinding.

J K Smit & Sons

Diamond Roll Dressers

Universal Grinding Wheel Company

Grinding wheels and information on grinding wheel properties and manufacturing methods.

PGM Ballscrews

Information on ballscrew grinding methods and some case-hardened material for test specimens.

IBL Ballscrews, Barnstaple

Information on ballscrew grinding methods.

APPENDIX II

Geometrical Relationships in Plane and Angle Grinding

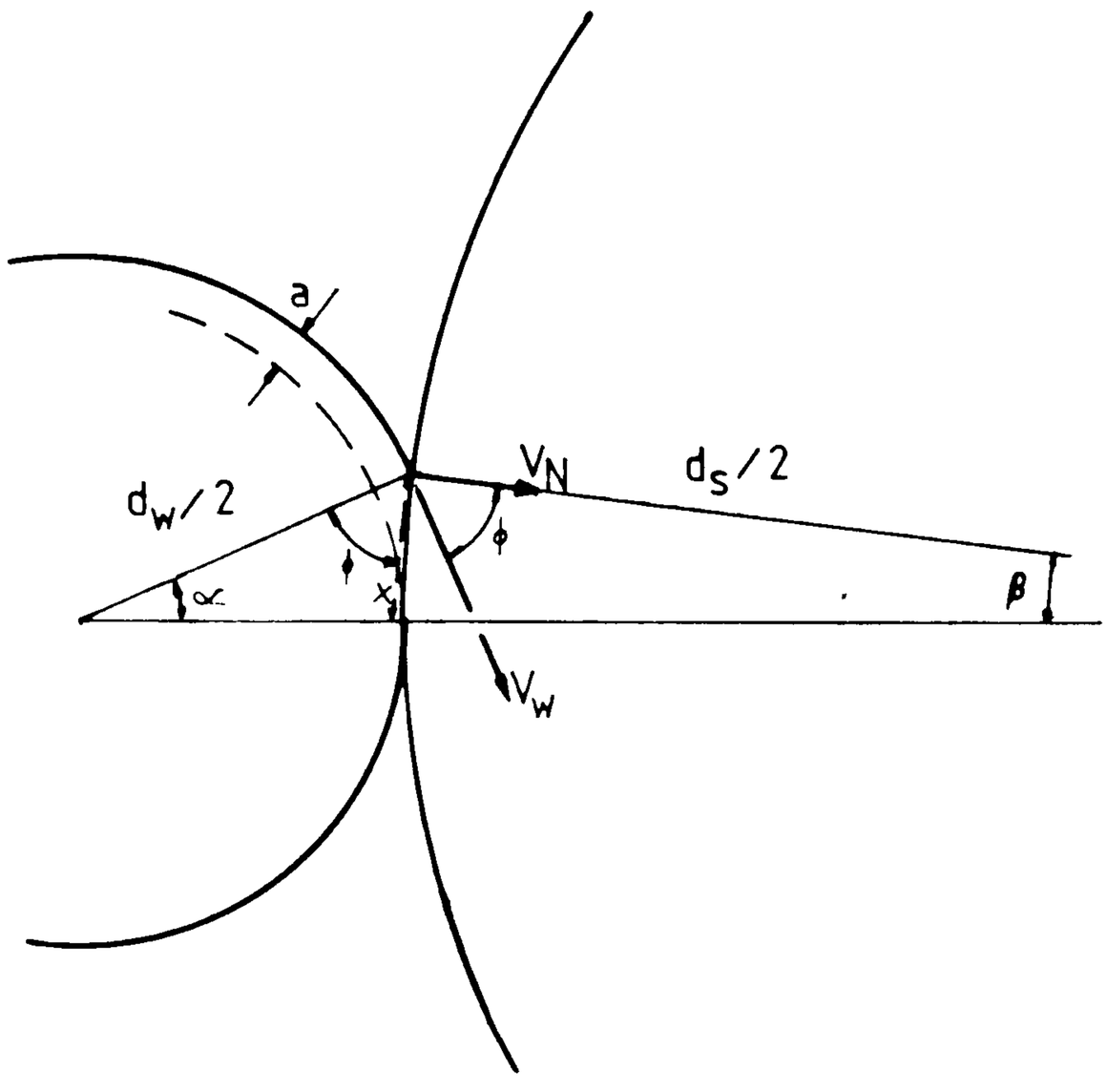

FIG A2.1

Maximum Normal Infeed Rate (V_N)

$$V_N = V_w \cos\phi \qquad (2.1)$$

$$= V_w \sin(\alpha + \beta)$$

Arc Length (ℓ_c)

$$\ell_c = \frac{d_s}{2} \cdot \beta \qquad (2.2)$$

Stock Removal Rate (Z')

Stock removed in one revolution of workpiece

$$= \frac{\pi d_w^2}{4} - \frac{\pi (d_w - 2a)^2}{4}$$

$$= \pi a (d_w - a)$$

Time taken for one revolution

$$= \frac{\pi d_w}{V_w}$$

$$\therefore \quad \underline{Z' = (a - a^2/d_w) V_w} \qquad (2.3)$$

Furthermore from Fig A2.1

$$\text{Cos}\phi = \frac{(d_w/2)^2 + X^2 - (d_w/2 - a)^2}{2.X.d_w/2} \qquad (2.4)$$

Where

$$X = \frac{d_s}{2} \text{Tan}\beta$$

But for small β $\text{Tan}\beta \rightarrow \beta$

$$\therefore \quad X = \frac{d_s \beta}{2} = \ell_c \qquad \text{From Eqn 2.2}$$

Substituting $X = \ell_c$ into Eqn 2.4 and simplifying gives

$$\text{Cos}\,\phi = \frac{\ell_c}{d_w} + \frac{a}{\ell_c} - \frac{a^2}{d_w \ell_c}$$

From Eqn 2.1

$$V_N = \frac{V_w}{\ell_c} (\ell_c^2/d_w + a - a^2/d_w) \qquad (2.5)$$

From Fig A2.1

$$\ell_c^2 = X^2 = (d_w/2)^2 - (d_w/2 - a)^2$$

$$= ad_w - a^2$$

Substituting into Eqn 2.5 gives

$$V_N = \frac{2V_w}{\ell_c} (a - a^2/d_w)$$

Comparing with Eqn 2.3 gives

$$Z' = \frac{V_N \ell_c}{2} \qquad (2.6)$$

* * * * * *

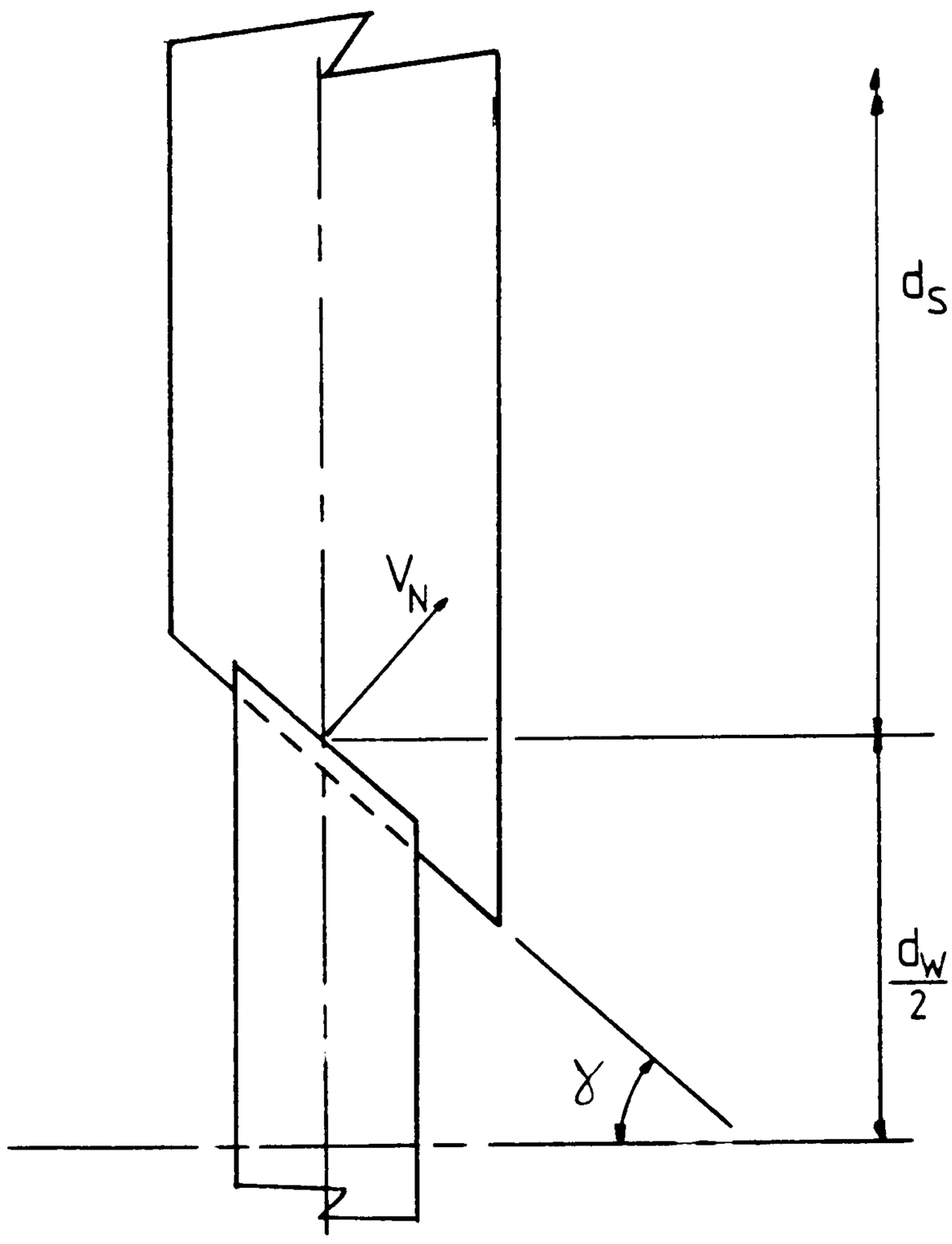

Fig A2.2

From Fig A2.2 it can be shown that the same geometrical relationships apply at the centreline of the workpiece, when grinding at an angle. The width of the workpieces used is kept small so that the variation in feed rate across the ground face was never more than ±7%.

The stock removal rate per unit width of ground face can be shown to be

$$Z' = V_w.\cos\gamma(a - a^2/d_w)$$

And

$$V_N = V_w.\sin(\alpha + \beta).\cos\gamma$$

where V_w, α and β are all measured in the plane of the workpiece centreline.

APPENDIX III

One Dimensional Transient Heat Flow Using the Finite Difference Method

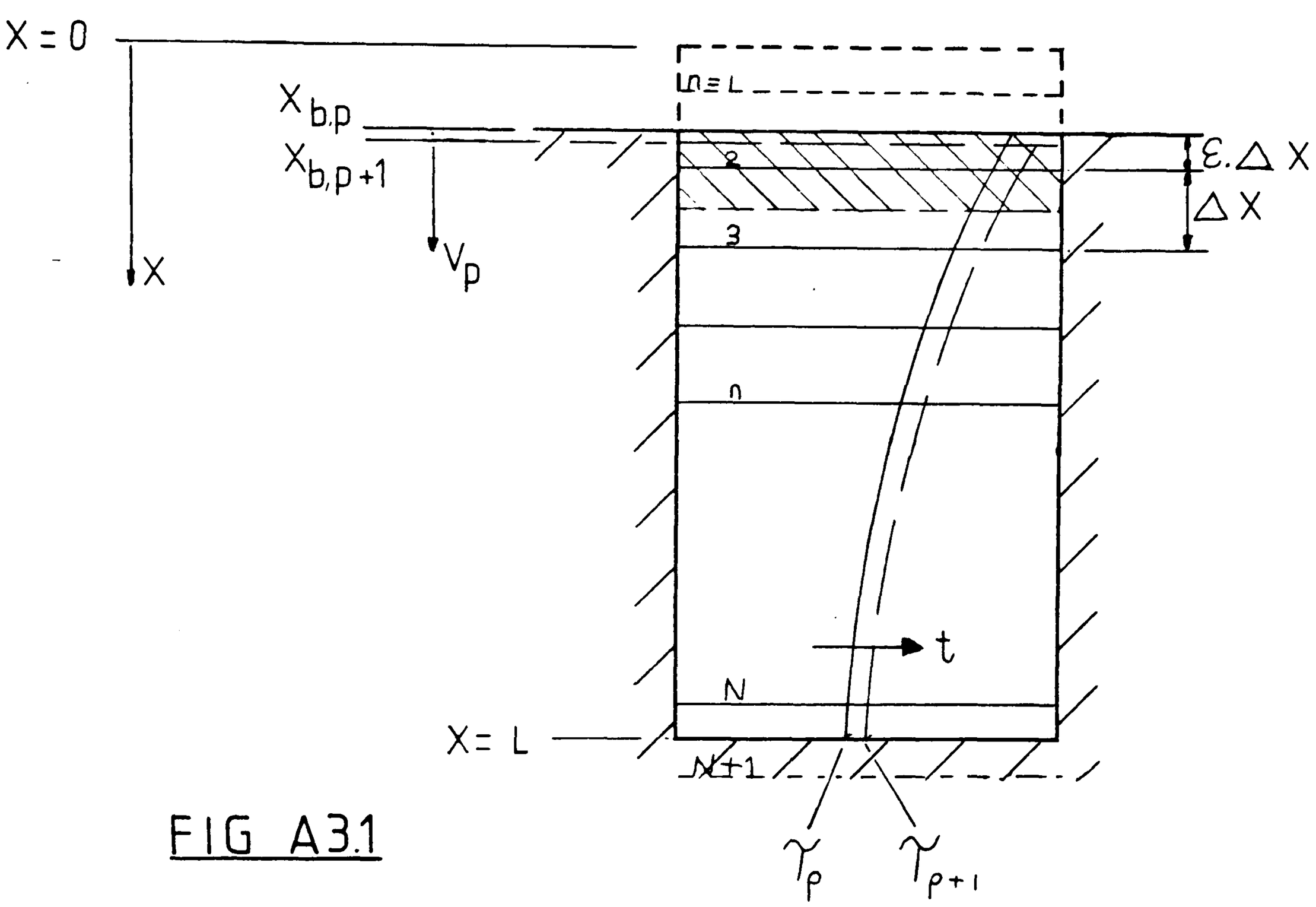

FIG A3.1

Notes

1 See also references 81, 82, 89 and Fig 4.

2 't' refers to the temperature rise above ambient. Where heat loss terms to either the coolant or the surroundings are included, these have been assumed to be at ambient temperature.

3 Suffixes:

n $(o<n<N)$ Refers to the node numbers. Node positions are fixed relative to the original top face of the pin. Hence

$$x_n - x_{n+1} = \Delta x = \frac{L}{N}$$

p $o<p<\frac{L}{2V_p\Delta\tau}$ Refers to the number of time intervals from the initial conditions

$$\tau_p - \tau_{p+1} = \Delta\tau$$

b Refers to the current boundary between the pin and the grinding wheel. Hence

$$x_{b,p} = \tau_p V_p \qquad (1)$$

One Dimensional Heat Flow Equation

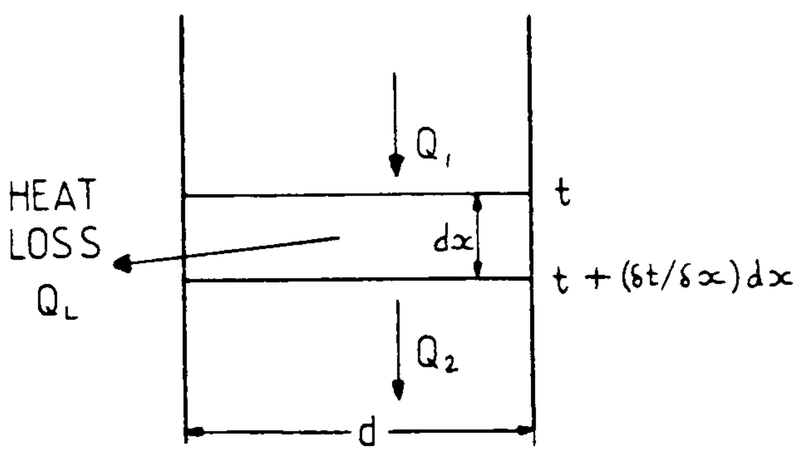

Consider the element dx in Fig A3.2

Heat flow in time $d\tau$

$$Q_{in} = -kA\frac{\partial t}{\partial x}d\tau$$

$A = \pi.d^2/4$

FIG A3.2

Heat Flow Out

$$Q_{out} = -kA\frac{\partial}{\partial x}\left[t + \frac{\partial t}{\partial x}dx\right] d\tau$$

Heat Loss

$$Q_L = \pi dC_L dx \left[t + \frac{\partial t}{\partial x}\frac{dx}{2}\right]d\tau$$

Increase in Energy contained in element

$$Q_{in} - Q_{out} - Q_L = \rho C_p A dx\frac{\partial t}{\partial \tau}\, d\tau$$

Substituting $A = \pi\frac{d^2}{4}$ and simplifying gives

$$k\frac{\partial^2 t}{\partial x^2} - 2\frac{C_L}{d}\left[2t + \frac{\partial t}{\partial x}\, dx\right] = \rho C_p\frac{\partial t}{\partial \tau} \qquad (2)$$

Finite Difference Equations

The following finite difference equations were used.

$$\left|\frac{\partial^2 t}{\partial x^2}\right|_{n,p} = \frac{t_{n+1,p} + t_{n-1,p} - 2t_{n,p}}{\Delta x^2}$$

$$\left|\frac{\partial t}{\partial \tau}\right|_{n,p} = \frac{t_{n,p+1} - t_{n,p}}{\Delta \tau}$$

$$\left|\frac{\partial t}{\partial x}\right|_{n,p} = \frac{t_{n+1,p} - t_{n,p}}{\Delta x}$$

Forward centered finite difference equations.

Substituting these equations in Equation 2 and rearranging gives

$$t_{n,p+1} = Fo.t_{n-1,p} + (Fo - W).t_{n+1,p} + (1 - W - 2Fo).t_{n,p} \qquad (3)$$

Where Fo is the Fourier Number

$$Fo = \frac{k.\Delta\tau}{\rho.C_p.\Delta x^2}$$

W is a non-dimensional term for the heat loss

$$W = \frac{2.C_L.\Delta\tau}{\rho.C_p.d}$$

Boundary Conditions

Bottom Face - two types of boundary are described in Section 3.2.

a) Adiabatic Boundary

$$\left|\frac{\partial t}{\partial x}\right|_{x=L} = 0$$

This is expressed in finite difference equations by arranging for the bottom face to lie halfway between two nodes (see Fig A3.1).

Then

$$\frac{t_{N,p} - t_{N+1,p}}{\Delta x} = 0$$

ie

$$t_{N,p} = t_{N+1,p}$$

This is then substituted in equation 3 for the last element.

b) Dirichlet Boundary

$$t_L = \text{const}$$

so that the same mesh generation routine can be used for both boundary conditions; this is expressed by

$$\frac{t_{N+1,p} + T_{N,p}}{2} = \text{const}$$

which can also be substituted in equation 3 for the last element.

Top Face - three boundary conditions were specified in Section 3.2

i) Convective Boundary

$$eV_p = -k\left|\frac{\partial t}{\partial x}\right|_b + h.t_b + \rho.C_p.V_p.t_b \qquad (4)$$

These boundary conditions can be expressed in terms of the temperature at the first node in the pin and at the node before it.

With reference to Fig A3.1: $\varepsilon_p = \frac{x_2 - x_{b,p}}{\Delta x}$

(The computer program first calculates the value of $x_{b,p}$ as in Equation 1 and then checks to see which two nodes it lies between).

By interpolation

$$t_{b,p} = (1 - \varepsilon_p).t_{2,p} + \varepsilon.t_{1,p} \qquad (5)$$

and

$$\left|\frac{\partial t}{\partial x}\right|_{b,p} = \frac{t_{2,p} - t_{1,p}}{\Delta x} \qquad (6)$$

Substituting Equations 5 and 6 into Equation 4 gives

$$t_{1,p} = \frac{(t_{2,p}.(1 - Bi.(1 - \varepsilon_p) - (Z/Fo).(1 - \varepsilon_p)) + Q/Fo)}{(1 + Bi.\varepsilon_p + (Z/Fo).\varepsilon_p)}$$

where Bi is the Biot Number

$$Bi = \frac{h.\Delta x}{k}$$

Q is a heat generation term

$$Q = \frac{e.V_p.\Delta\tau}{\rho.C_p.\Delta x}$$

and Z is a non-dimensional chip loss term

$$Z = \frac{V_p \Delta\tau}{\Delta x}$$

This boundary condition cannot however be directly substituted into equation 3 since the physical size of the segment will be varying with time. A physical argument can be used however. Consider the hatched volume below the boundary shown in Fig A3.1. If the same finite difference relationships are applied to this volume then it can be shown that:

$$t'_{2,p+1} = Fo'.t_{1,p} + (Fo-W)'.t_{3,p} - (2Fo+W-1)'.t_{2,p} \quad (8)$$

where

$$Fo' = Fo/(\varepsilon + 0.5)$$

for the first element.

The boundary temperature can then be found by using Equation 5.

ii) Fixed Partition Boundary

$$-k\left|\frac{\partial t}{\partial x}\right|_b = (q_w - q_v t_b).e.V_p$$

(Condition 2 in Section 3.2 is equivalent to putting $q_v = 0$ in the above expression).

Using the same non-dimensional parameters and Equation 5 this reduces to

$$t_{1,p} = \frac{[(Fo - Q.q_v(1 - \bar{\varepsilon}_p))t_{2,p} + Q.q_w]}{[Fo + q_v.Q.\varepsilon_p]}$$

This value of $t_{1,p}$ can then be substituted in Equation 8 for the first step of the solution and Equation 3 used thereafter. Equation 5 provides the boundary temperature.

Stability

As discussed in Reference [89] the criterion for stability of the solution can be argued physically to be that none of the coefficients in Equation 3 may be negative, which leads to

$$Fo < \frac{1 - W}{2}$$

and

$$Fo > W$$

Furthermore these stability criteria are more stringent when applied to the first element (Equation 8). Hence

$$Fo' < \frac{1 - W}{2}$$

For the boundary conditions this same condition can be applied. Hence

$$B_i + (Z/Fo) < \frac{1}{1 - \varepsilon_p} \qquad \text{from Equation 7}$$

and

$$Fo > Q.q_v(1 - \varepsilon_p) \qquad \text{from Equation 9}$$

The computer program is essentially straightforward and works systematically through the solution procedure. The step size (Δx) and the initial Fourier number are specified in the input data and the program calculates the time interval ($\Delta\tau$). It checks that all the stability criteria are met and automatically changes the Fourier number and step size if required to satisfy them. A summary of the grinding and material conditions is printed out as are the analysis parameters used. The output can be either as a temperature distribution through the pin at each time interval or as a time-temperature listing for each node. In the latter case the output can be shortened to just the boundary and the node corresponding to the thermocouple position. An example of the output is included in this appendix.

The computer program includes a further degree of complexity in that both the grinding energy (e) and q_v can vary with the amount of material removed to simulate the grinding wheel wearing.

Material properties

Density 7800.kg/m.cub
Specific heat 490.J/kg/K
Thermal Conductivity 41.0w/m/K

Grinding data

Infeed rate 15.1mm/min
Initial Specific energy 48.1J/mm.cub
+ 0.0 J/mm.cub/mm
Power flux 12.1w/mm.sq + 0.0w/mm.sq/mm

Initial specimen size 18.0mm

Analysis data
Fourier no. 0.25
Loss term 0.0015
Step size 0.0020m
Time interval 0.0932secs
No. of time steps 383
Duration of test 35.7031secs
Depth of specimen ground 8.99mm

Internal nodes

Node position relative to original top face 9.0mm

Boundary type-fixed partition
Workpiece partition= 2.500percent- 0.015percent/degC

Boundary profile

Time secs	Position mm	Temperature DegC
0.0	0.0	27.1
1.9	0.5	50.1
3.7	0.9	58.6
5.6	1.4	64.6
7.5	1.9	68.4
9.3	2.3	71.7
11.2	2.8	74.6
13.1	3.3	78.0
14.9	3.8	80.4
16.8	4.2	82.7
18.6	4.7	85.1
20.5	5.2	88.1
22.4	5.6	90.1
24.2	6.1	92.2
26.1	6.6	94.3
28.0	7.0	97.2
29.8	7.5	99.1
31.7	8.0	101.0
33.6	8.4	103.1
35.4	8.9	105.3

Time secs	Temperature DegC
0.0	20.0
1.9	22.9
3.7	29.2
5.6	35.3
7.5	40.9
9.3	46.2
11.2	51.2
13.1	56.0
14.9	60.5
16.8	65.0
18.6	69.3
20.5	73.4
22.4	77.5
24.2	81.5
26.1	85.5
28.0	89.4
29.8	93.3
31.7	97.2
33.6	101.0
35.4	105.0

APPENDIX IV

Force measurement on the Creep-feed cylindrical grinding machine

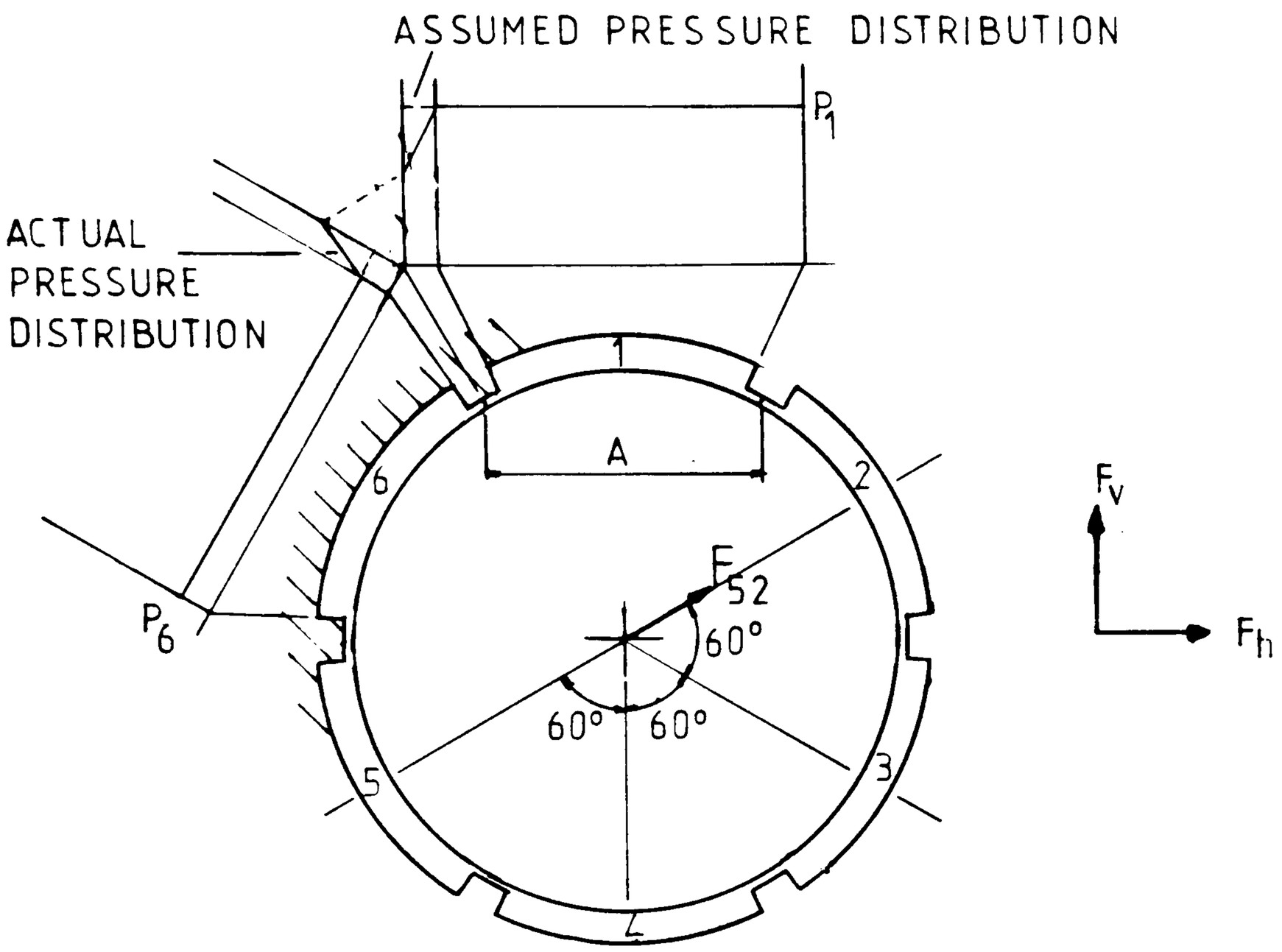

FIG A4.1

A = Projected Pocket Area

$$F_{52} = (P_5 - P_2)A \quad \text{etc}$$

$$F_h = F_{52}\text{Cos}30° + F_{63}\text{Cos}30°$$

$$F_v = F_{41} + F_{52}\text{Sin}30° - F_{63}\text{Sin}30°$$

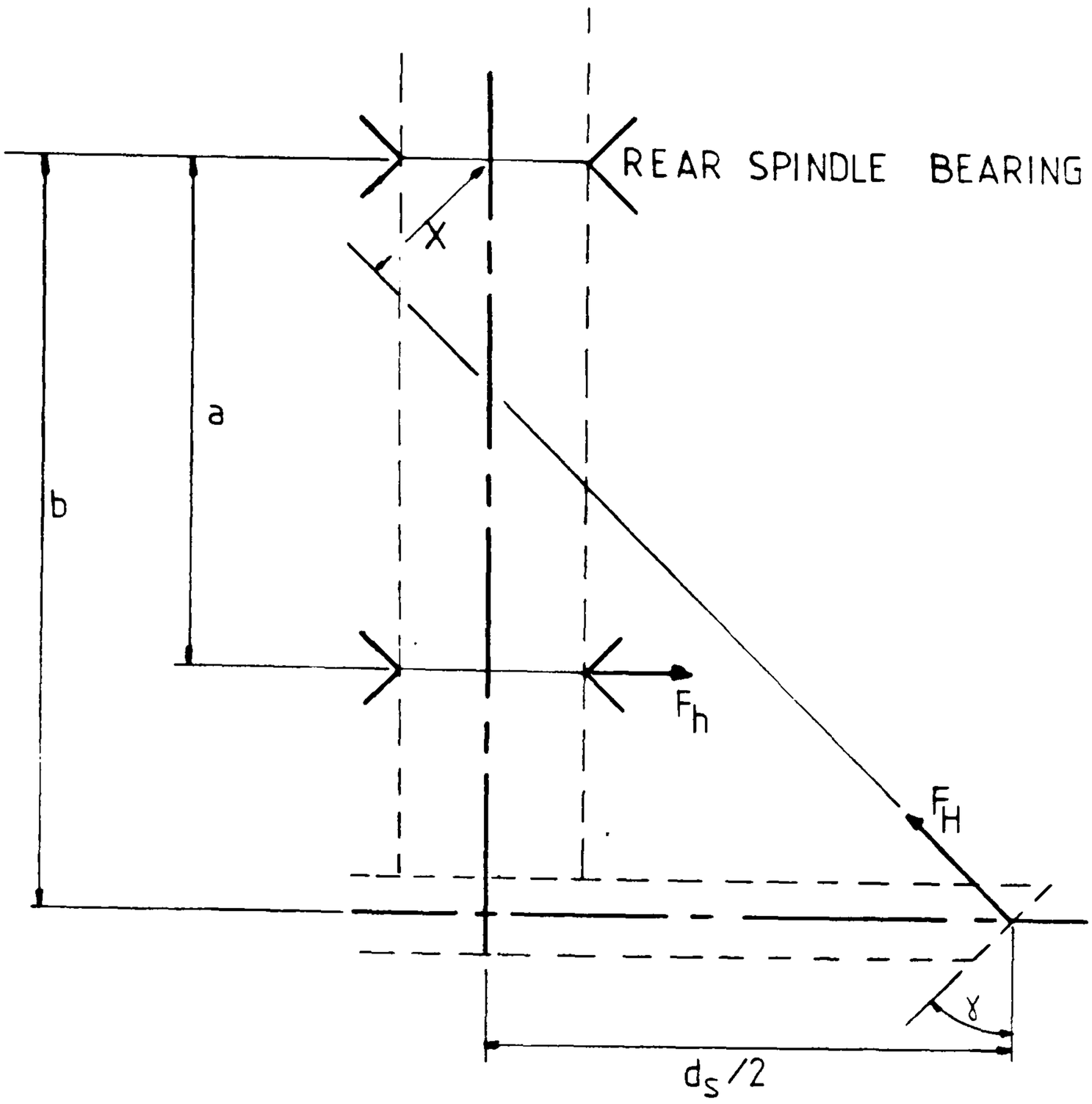

FIG A4.2

F_V = Vertical component of grinding force

$= F_v.a/b$

F_H = Horizontal component of grinding force

$= F_h.a/x$

where $x = b.\cos\gamma - (d_s/2)\sin\gamma$

Shafto (Ref 8) showed that the resultant grinding force acts at a point 2/3 of the arc length from the bottom of the arc of cut (See Fig A4.3).

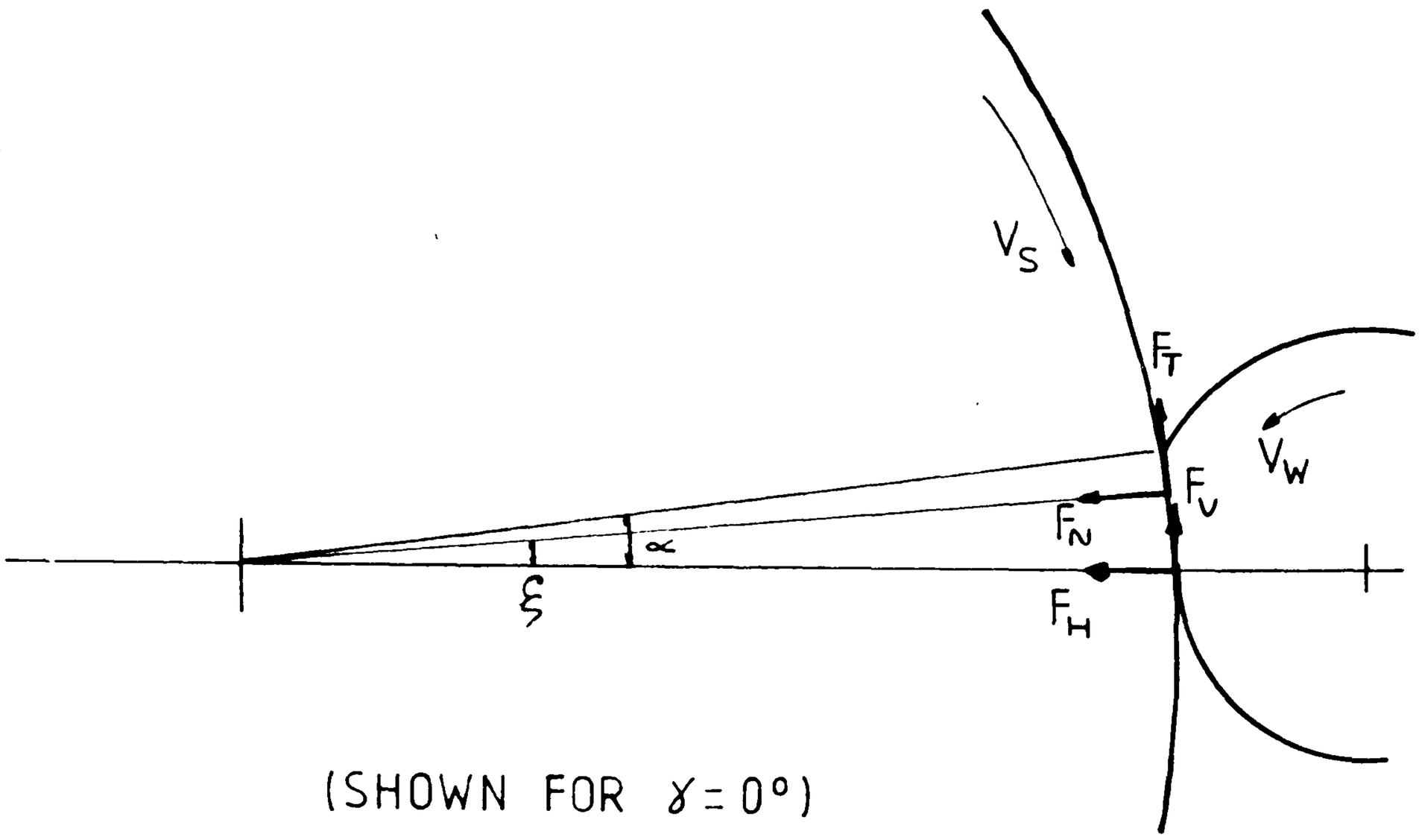

(SHOWN FOR $\gamma = 0°$)

FIG A4.3

Hence

$$F_N = F_H.\cos\xi - F_V.\sin\xi$$

$$F_T = F_V.\cos\xi + F_H.\sin\xi$$

where $\xi = 2/3\alpha.\cos\gamma$

APPENDIX V

Wheel balancing on the Creep-feed cylindrical grinding machine

On this machine wheel balancing was achieved by means of two identical balancing weights fitted at a pre-set radius to the loose wheel mounting flange.

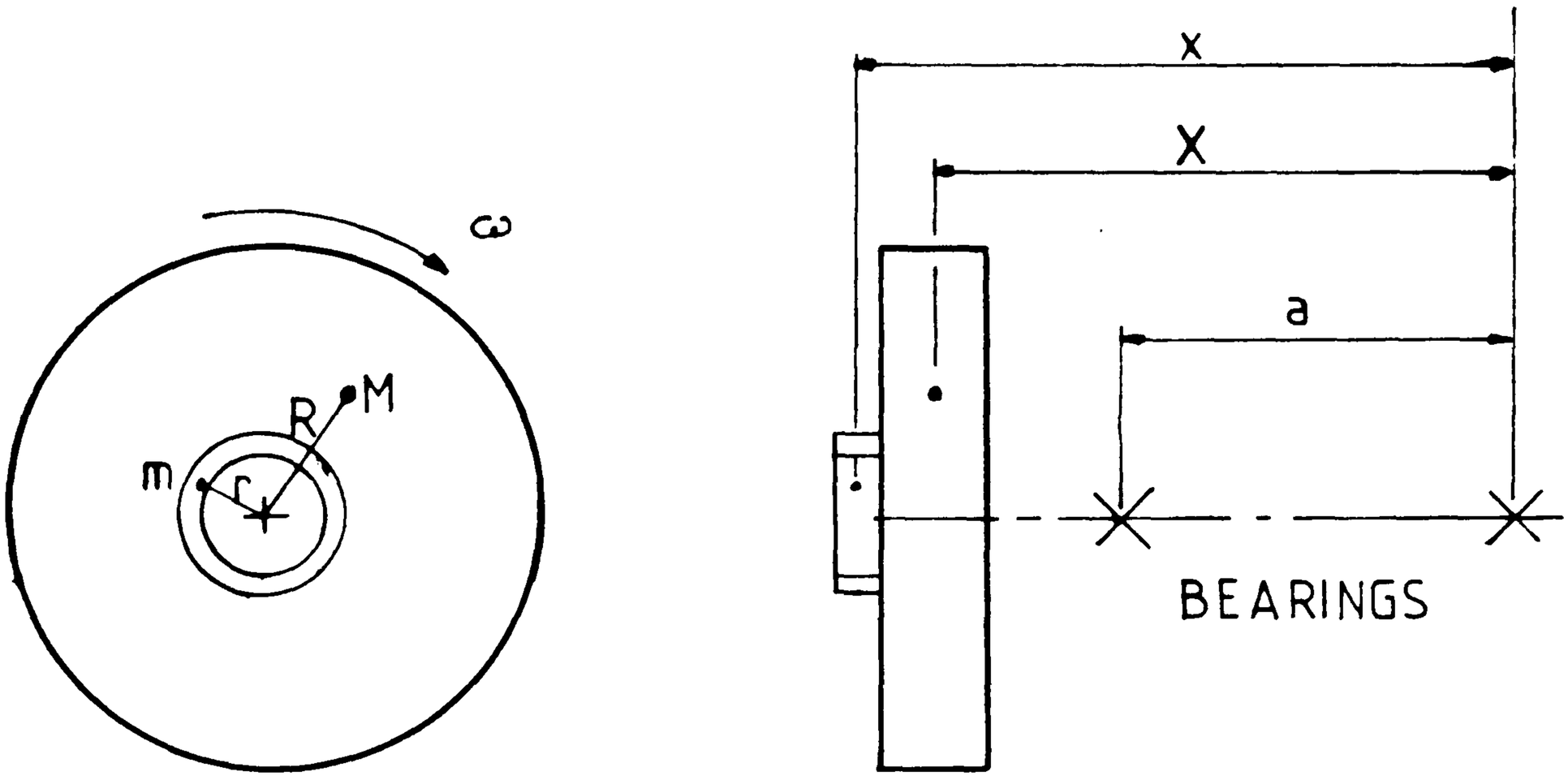

FIG A5.1

M = Out of balance mass

m = balance mass

Any out of balance forces could be detected by the force measuring system, at the front spindle bearing (See Appendix IV).

The output from one of the differential pressure transducers was displayed on an oscilloscope from which the amplitude of any out of balance force could be measured as a voltage.

Force due to out of balance mass = $MR\omega^2X/a$

= B

Force due to each balance mass = $mr\omega^2x/a$

= b

Procedure

1 Run wheel at any angular speed with no balance weights fitted.

Measure B (as a voltage).

2 Fit one balance weight at any known position and run wheel at same angular speed ω.

Measure R_1.

3 Move weight 180° around flange and repeat.

Measure R_2.

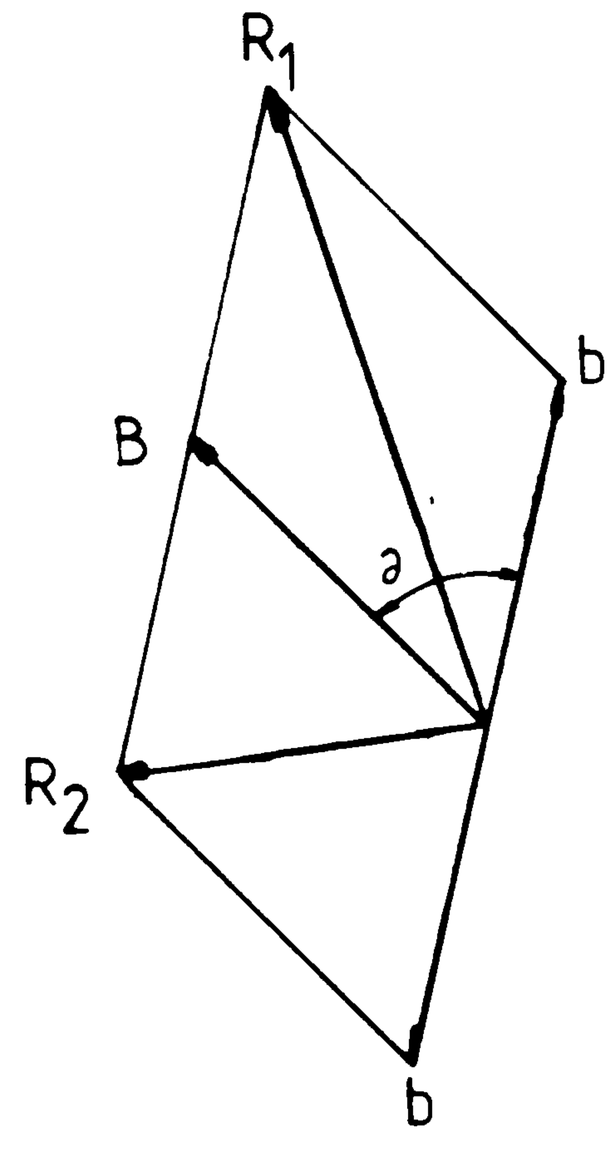

FIG A5.2

$$R_1^2 = b^2 + B^2 - 2bB\cos(180 - \partial)$$

but $$\cos(180 - \partial) = -\cos\partial$$

$$\therefore \quad R_1^2 = b^2 + B^2 + 2bB\cos\partial \qquad (1)$$

$$R_2^2 = b^2 + B^2 - 2bB\cos\partial \qquad (2)$$

Adding and rearranging gives

$$b = \sqrt{\frac{R_1^2 + R_2^2 - B^2}{2bB}}$$

Substituting in (1) gives

$$\cos\partial = \frac{R_1^2 - b^2 - B^2}{2bB}$$

Hence the angular position of the out of balance mass is determined.

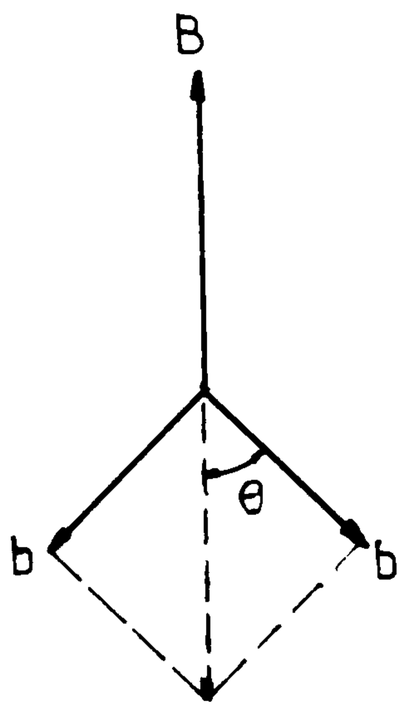

FIG A5.3

The two identical balance weights can then be positioned as in Fig A5.3 such that

$$\cos\theta = \frac{B}{2b}$$

No absolute values are required, merely three voltage readings.

APPENDIX VI

Compositions and Thermal properties of the workpiece materials

Chemical Compositions %

	C	Mn	Cr	Mo
BS 708A42	0.39-0.46	0.65-1.05	0.8-1.25	0.15-0.25
BS 070M55	0.5 -0.6	0.5 -0.9		
BS 080A22	0.16-0.24	0.5 -0.9		

Remainder Iron

MARM002	Aluminium	5.5%
	Cobalt	10.0%
	Chromium	9.0%
	Hafnium	1.5%
	Tantalum	2.5%
	Titanium	1.5%
	Tungsten	10.0%
	Nickel	Remainder

Mean Thermal Properties (at 50°C)

	Density ρ[kg/m^3]	Thermal Conductivity K[W/m/°C]	Specific Heat Cp[J/kg/°C]
BS 708A42	7800	41.0	490
MARM002*	8560	9.6	422

* Thermal properties supplied by Rolls Royce (1971) Ltd

APPENDIX VII

The dresser infeed mechanism on the Creep-feed surface grinder

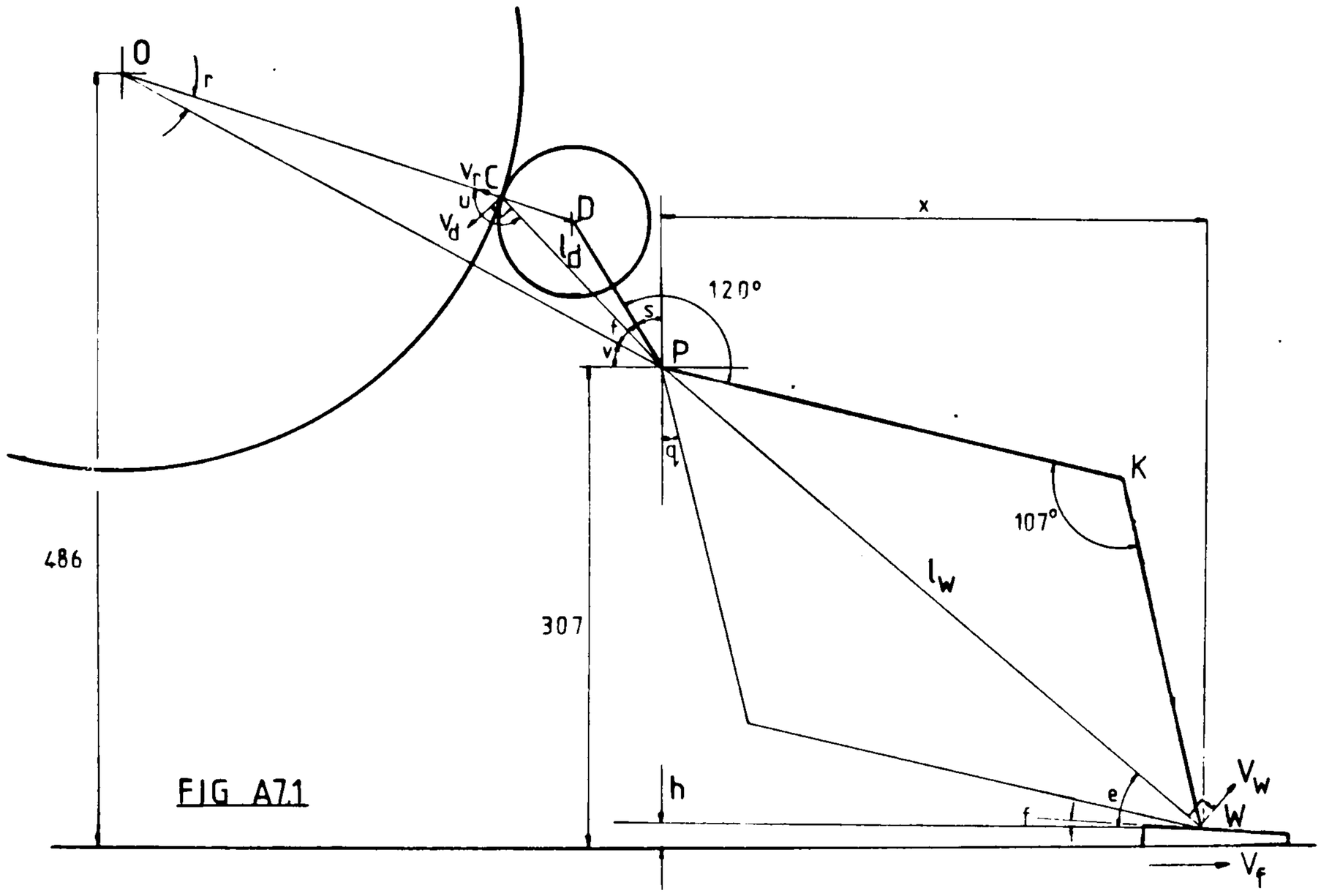

FIG A7.1

The following dimensions are fixed:

CD = 50
DP = 105
PK = 305
OP = 386

The following are variable:

OC = $d_s/2$
KW - adjustable (see Fig 18)
h - variable
f = feed wedge angle
v_f = slideway speed

Radial dresser infeed rate

$$V_r = V_d \mathrm{Cos}(u - 90)$$

$$= V_d . \mathrm{Sin}u$$

$$V_d = V_w \frac{\ell_d}{\ell_w}$$

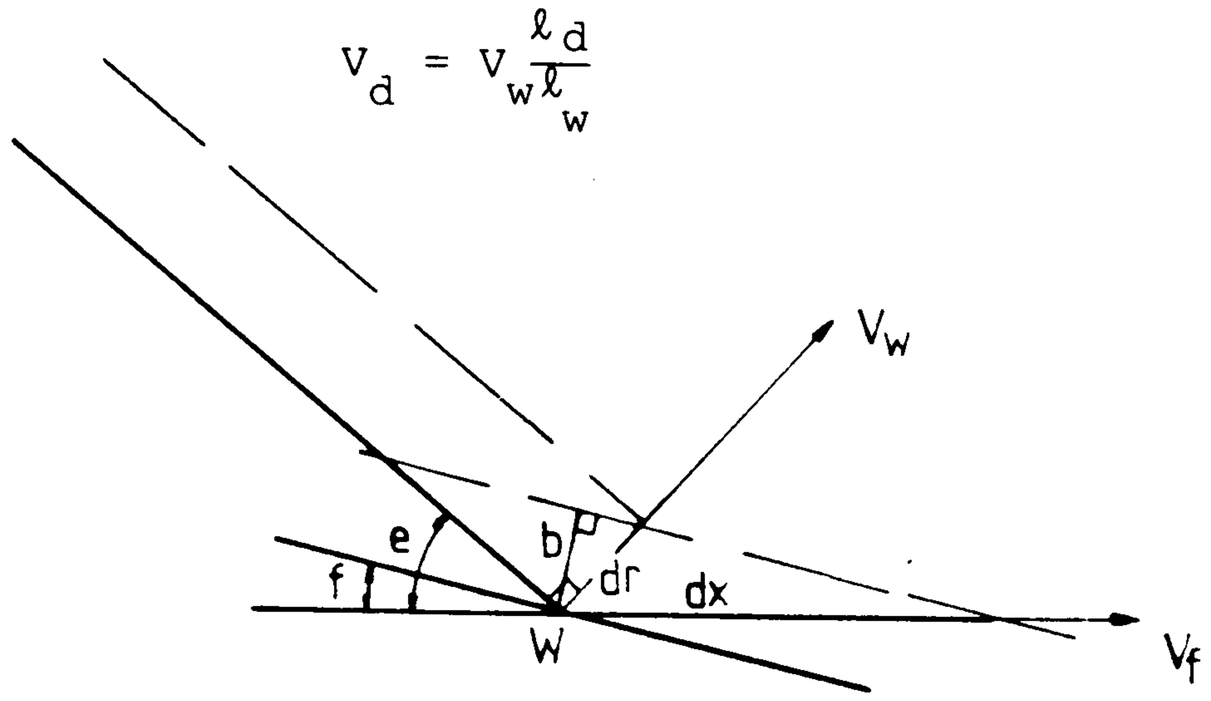

FIG A7.2

Fig A7.2 shows the wedge contact in more detail.

For a small movement of the wedge dx.

$$b = dx\mathrm{Sin}f$$

$$dr = \frac{b}{\mathrm{Cos}(e - f)}$$

$$\therefore \quad dr = \frac{dx\mathrm{Sin}f}{\mathrm{Cos}(e - f)}$$

$$= \frac{dx\mathrm{Sin}f}{\mathrm{CoseCos}f + \mathrm{SineSin}f}$$

$$\therefore \quad \frac{dr}{dx} = \mathrm{Tan}f/(\mathrm{Cos}e + \mathrm{SineTan}f)$$

$$= \frac{V_w}{V_f} \qquad \text{for small changes in e}$$

ℓ_d, ℓ_w, v and e can all be found from the geometry as follows:

$$Cosr = \frac{OD^2 + OP^2 - DP^2}{2.OD.OP}$$

$$\ell_d = \sqrt{OC^2 + OP^2 - 2.OC.OP.Cosr}$$

$$Sinu = \frac{Sinr.OP}{DP}$$

$$Sint = \frac{Sinr.OD}{DP}$$

$$v = Sin^{-1}((486 - 307)/386)$$

$$= 27.6°$$

$$s = 90 - 27.6 - t$$

$$q = s - (120 - 107)$$

$$x = PKCos(120 - 90 - s) + (307 - h - 305.Sin(120 - 90 - s)).Tanq$$

$$Tane = (307 - h)/x$$

Hence e

$$\ell_w = x/Cose$$

A micro-computer program was used to perform these calculations.

THE PLATES

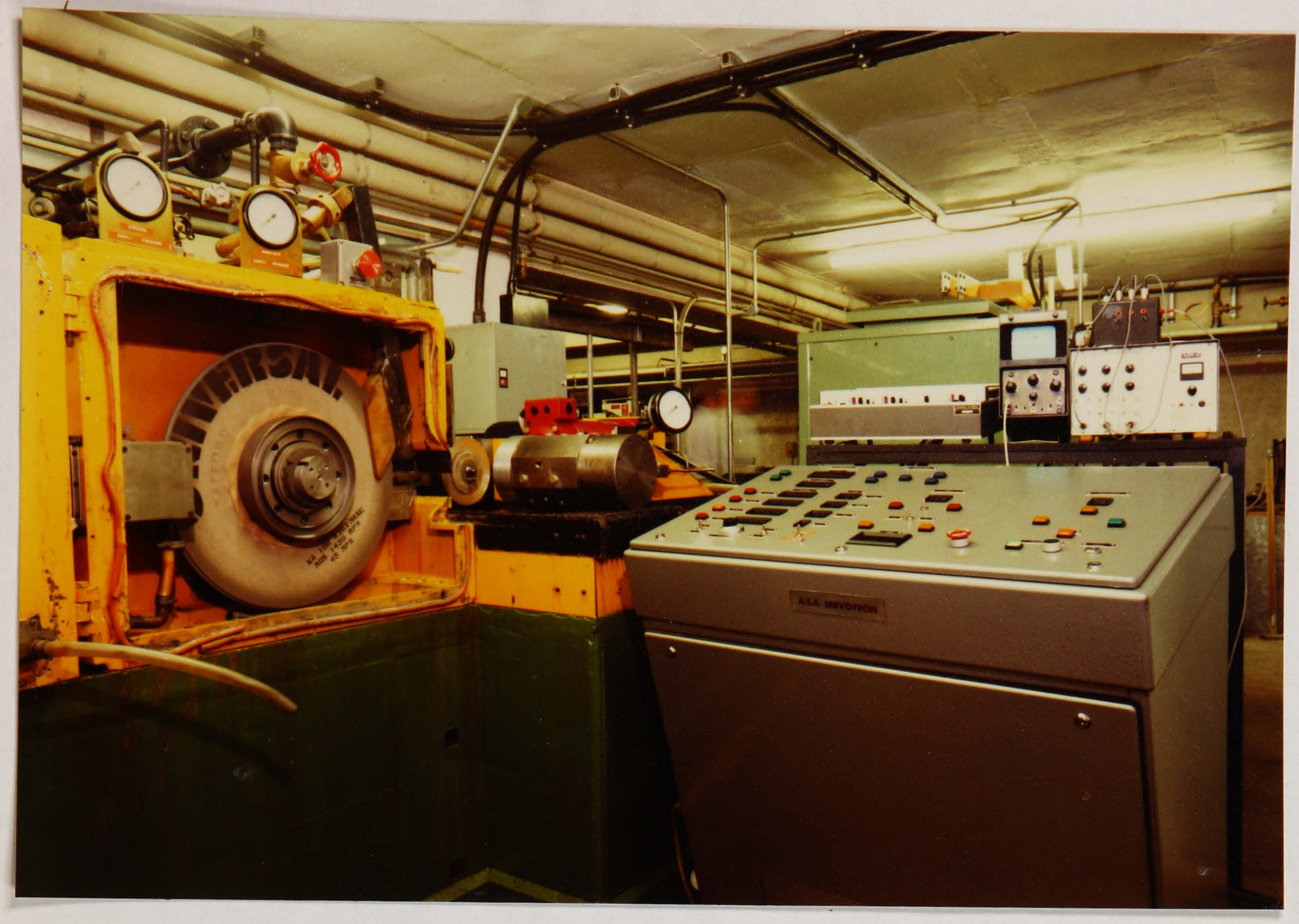

PLATE 1 GENERAL VIEW OF THE CREEP-FEED CYLINDRICAL GRINDING MACHINE

PLATE 2 THE COOLANT 'SHOE' AND A WORKPIECE IN POSITION BETWEEN CENTRES

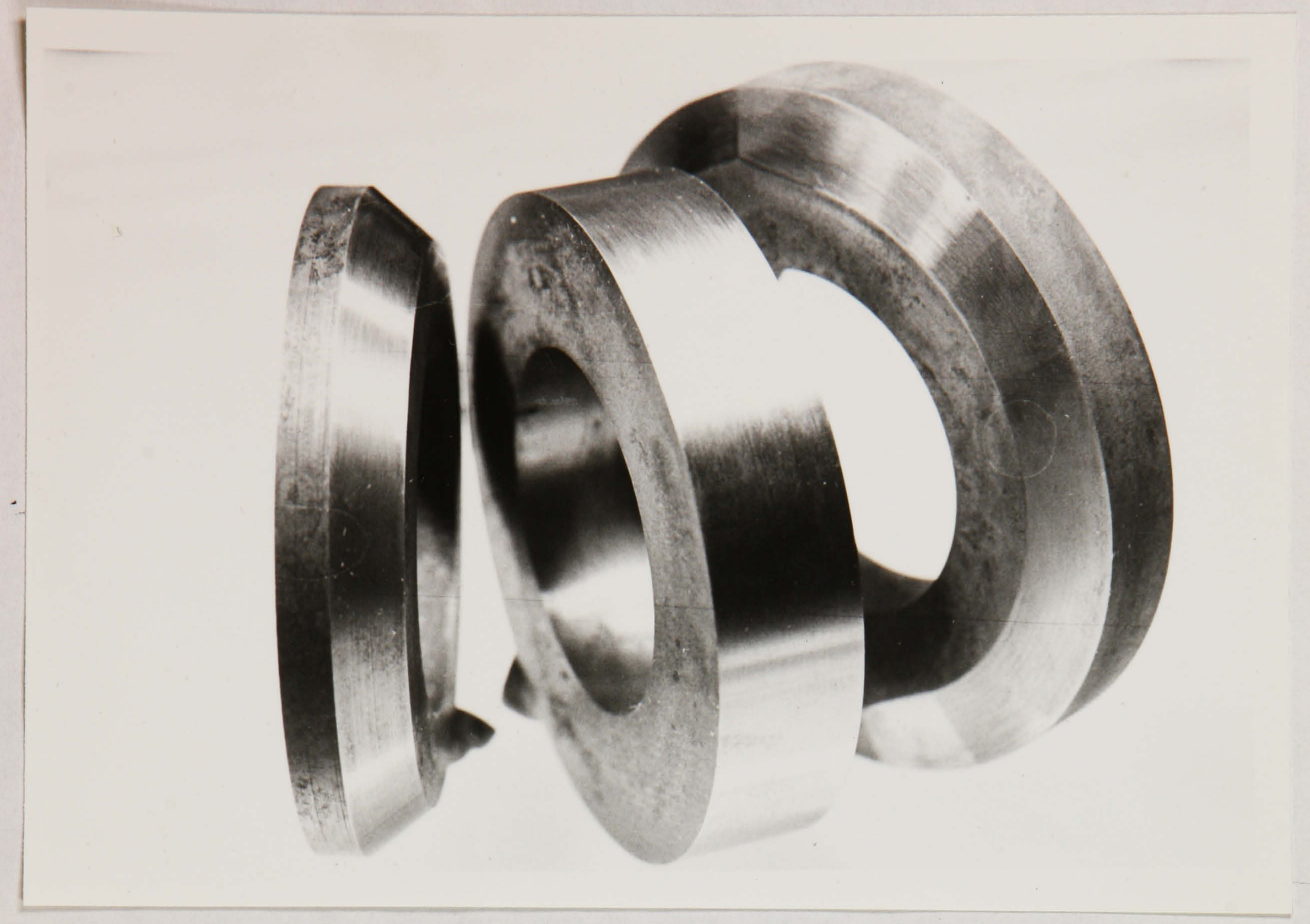

PLATE 3 CYLINDRICAL GRINDING SPECIMENS WITH FACE ANGLES OF 0°, 40° and 80°

PLATE 4 DIAMOND ROLL DRESSERS WITH FACE ANGLES OF 0°, 40° and 80°

PLATE 5 THE SEMI-CIRCULAR FORM DRESSER IN POSITION IN THE MACHINE

PLATE 6 GENERAL VIEW OF THE CREEP-FEED SURFACE GRINDING MACHINE

PLATE 7 THE STRAIN GAUGE DYNAMOMETER WITH A SPECIMEN IN POSITION

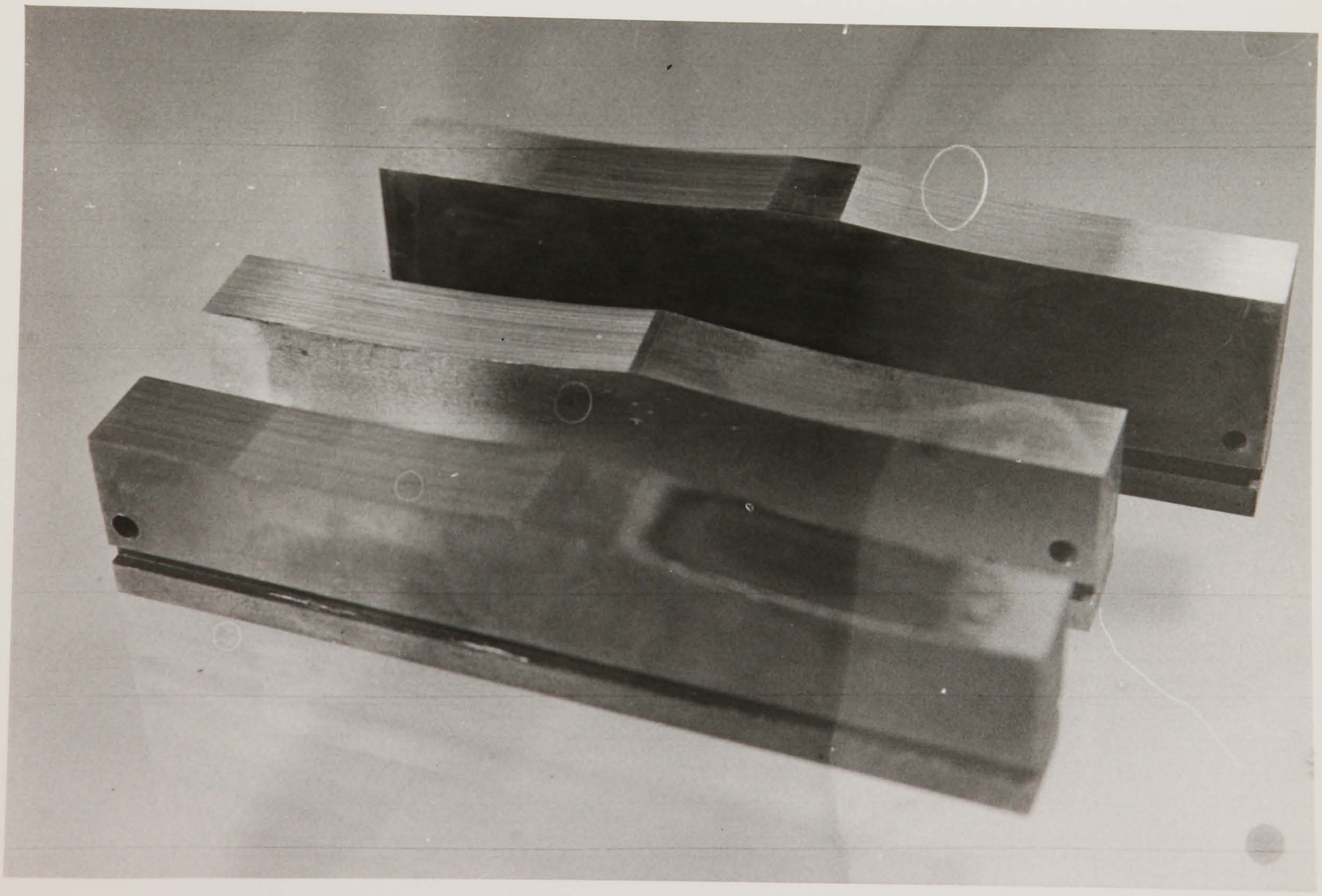

PLATE 8 SURFACE GRINDING SPECIMENS (THE ONE IN THE FOREGROUND SHOWING GRINDING BURN)

PLATE 9 PIN-TYPE WORKPIECES IN POSITION IN THE SINDANYO WORKHOLDER (THE ONE ON THE LEFT HAS NOT YET BEEN GROUND AND THE ONE ON THE RIGHT HAS BEEN GROUND AND IS BURNT)

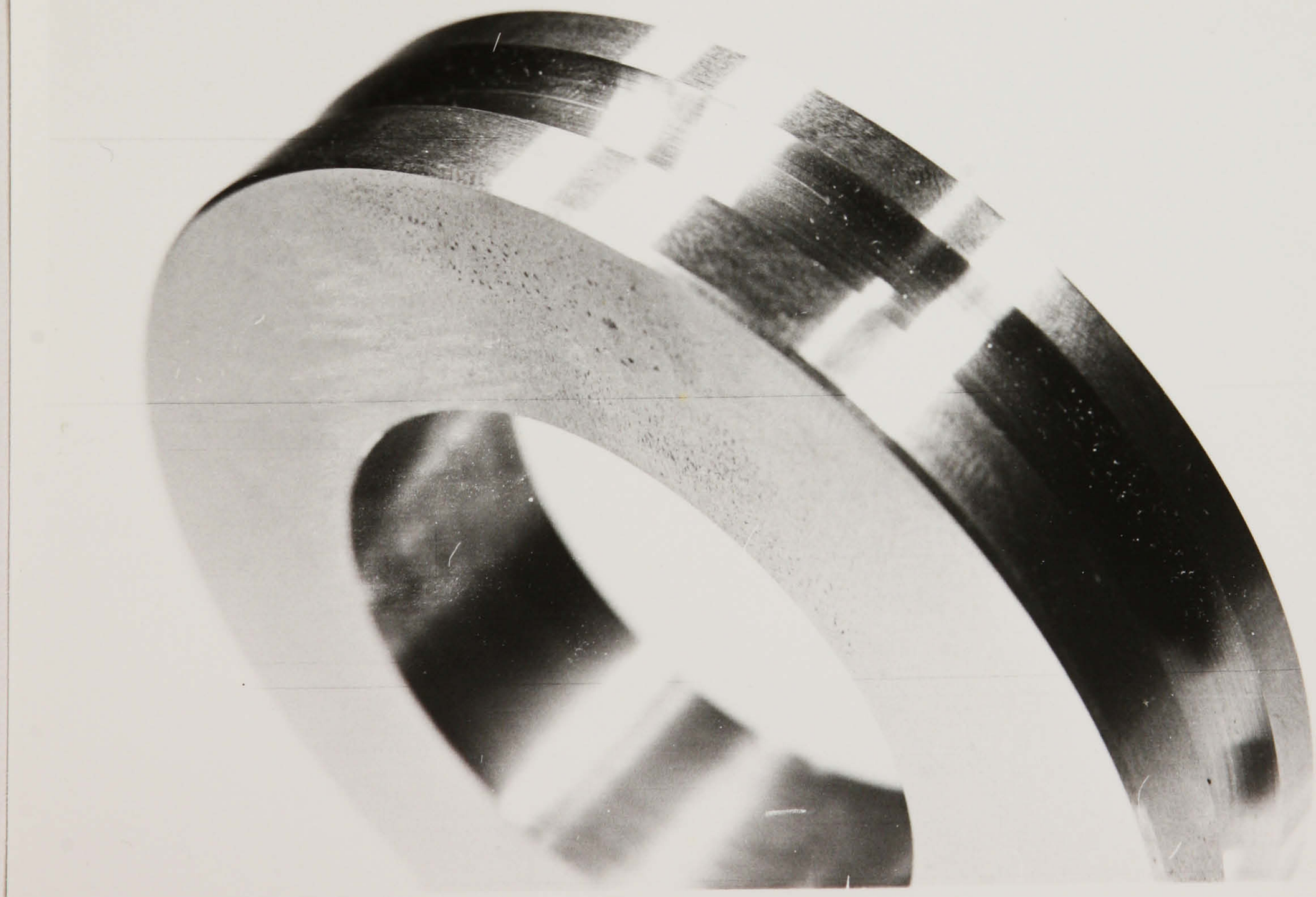

PLATE 10 A SPECIMEN WITH THE SEMI-CIRCULAR FORM

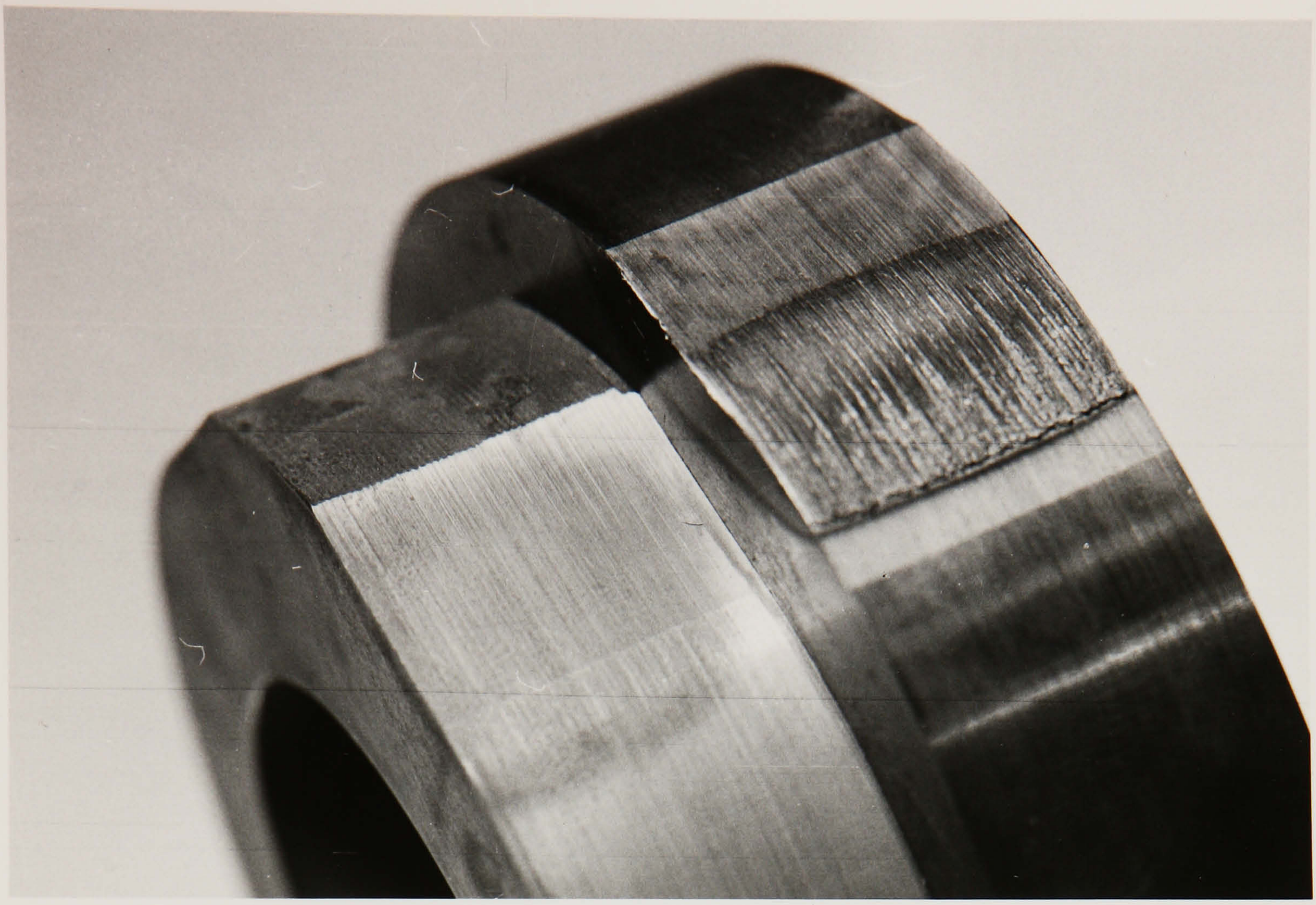

PLATE 11 TWO SPECIMENS SHOWING GRINDING BURN (THE ONE ON THE LEFT HAS BEEN GROUND WITH NEAT OIL GRINDING FLUID AND SUBSEQUENTLY ETCHED. THE ONE ON THE RIGHT HAS BEEN GROUND WITH THE SOLUBLE TYPE GRINDING FLUID)

THE FIGURES

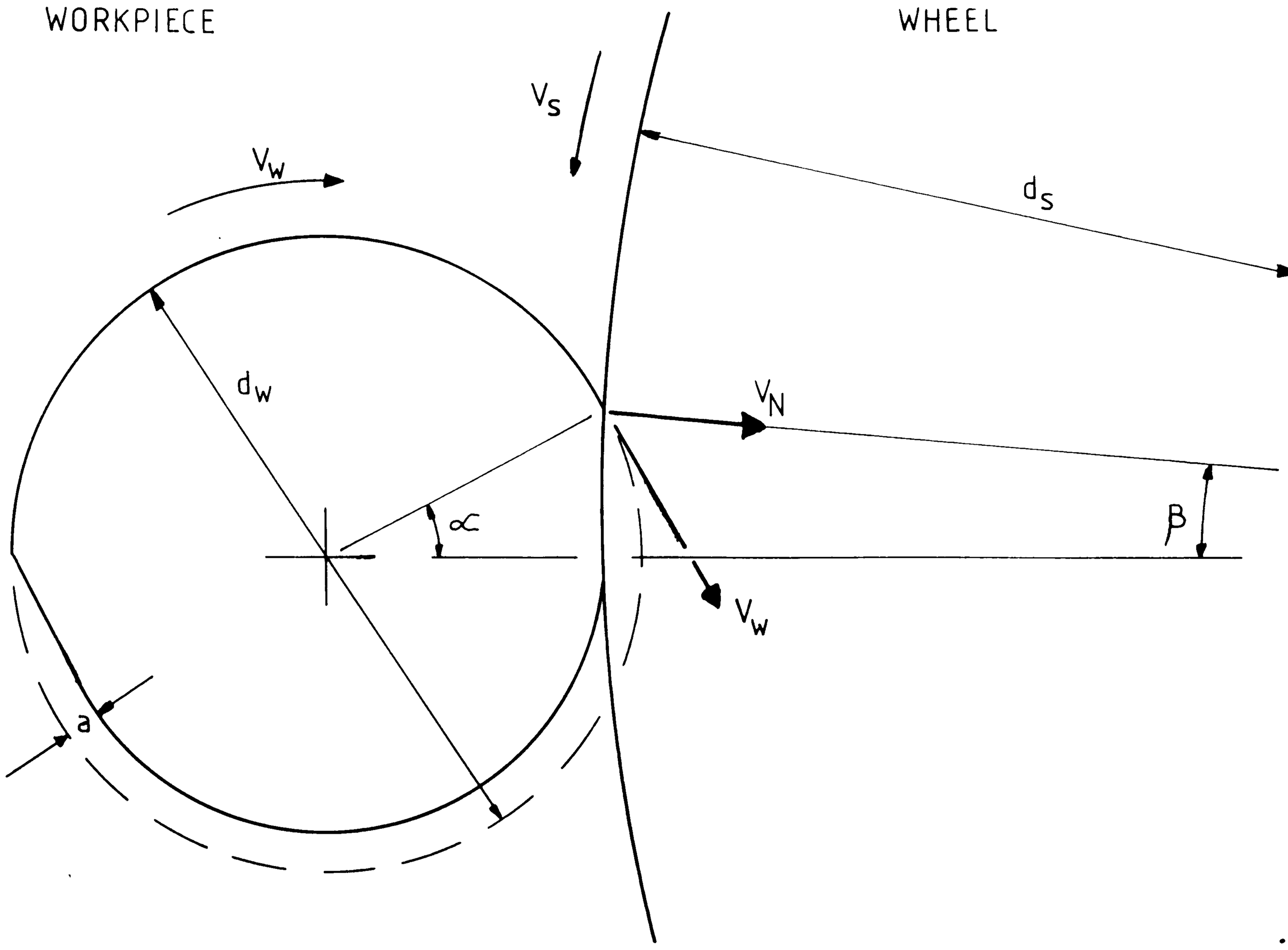

FIG 1 CREEP-FEED CYLINDRICAL GRINDING

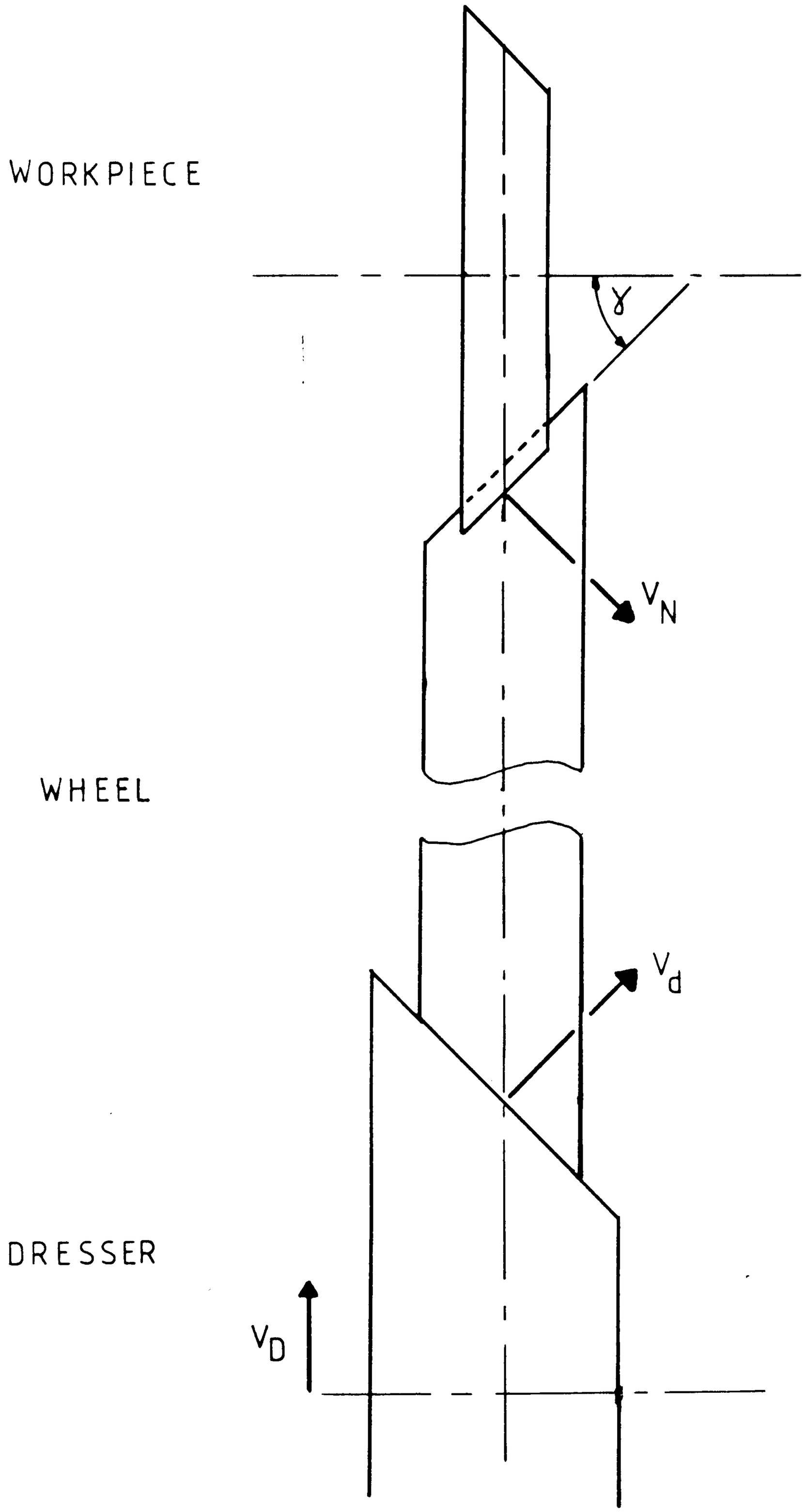

FIG 2 CREEP-FEED GRINDING ON ANGLED FACES

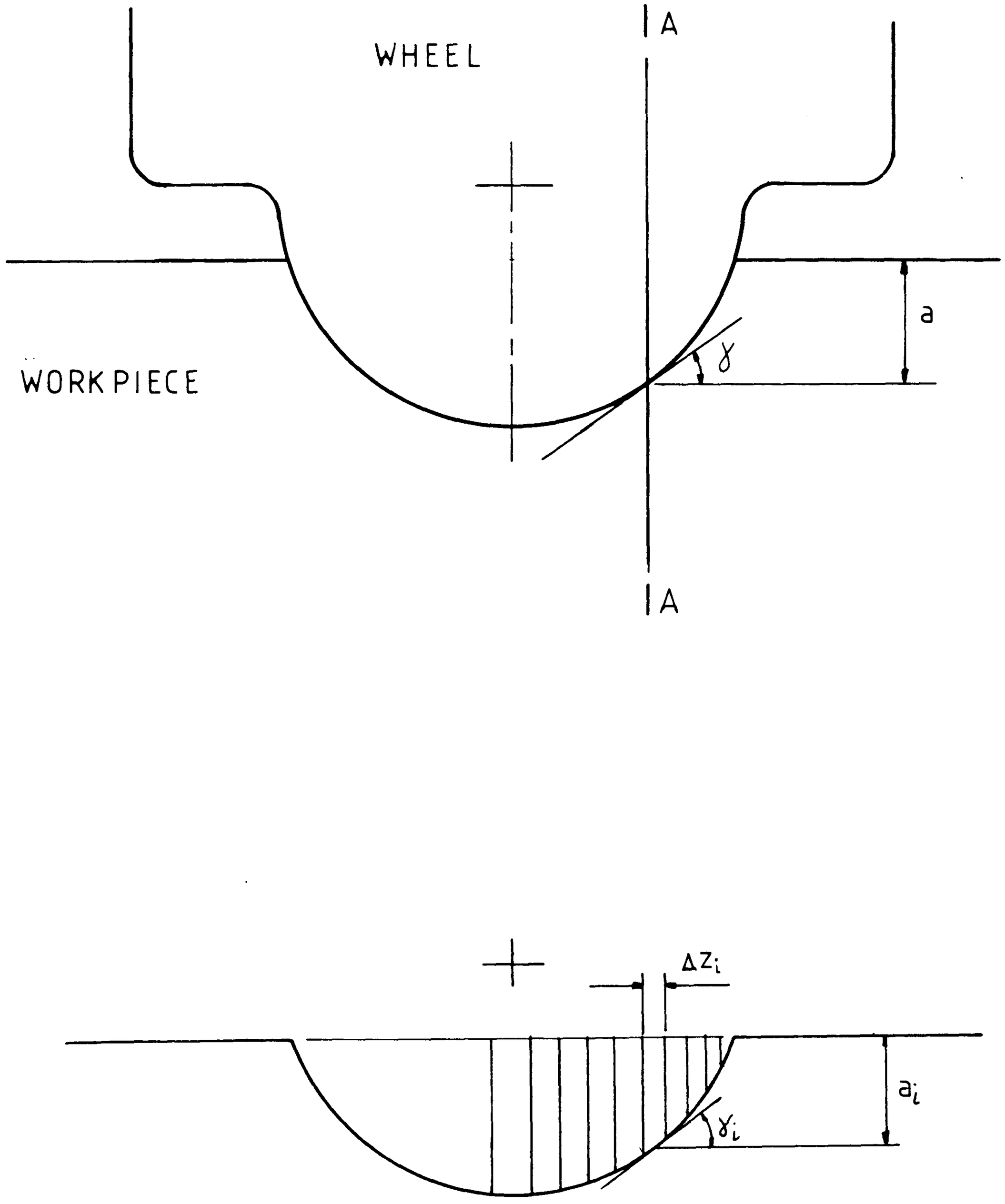

FIG 3 CREEP-FEED FORM GRINDING

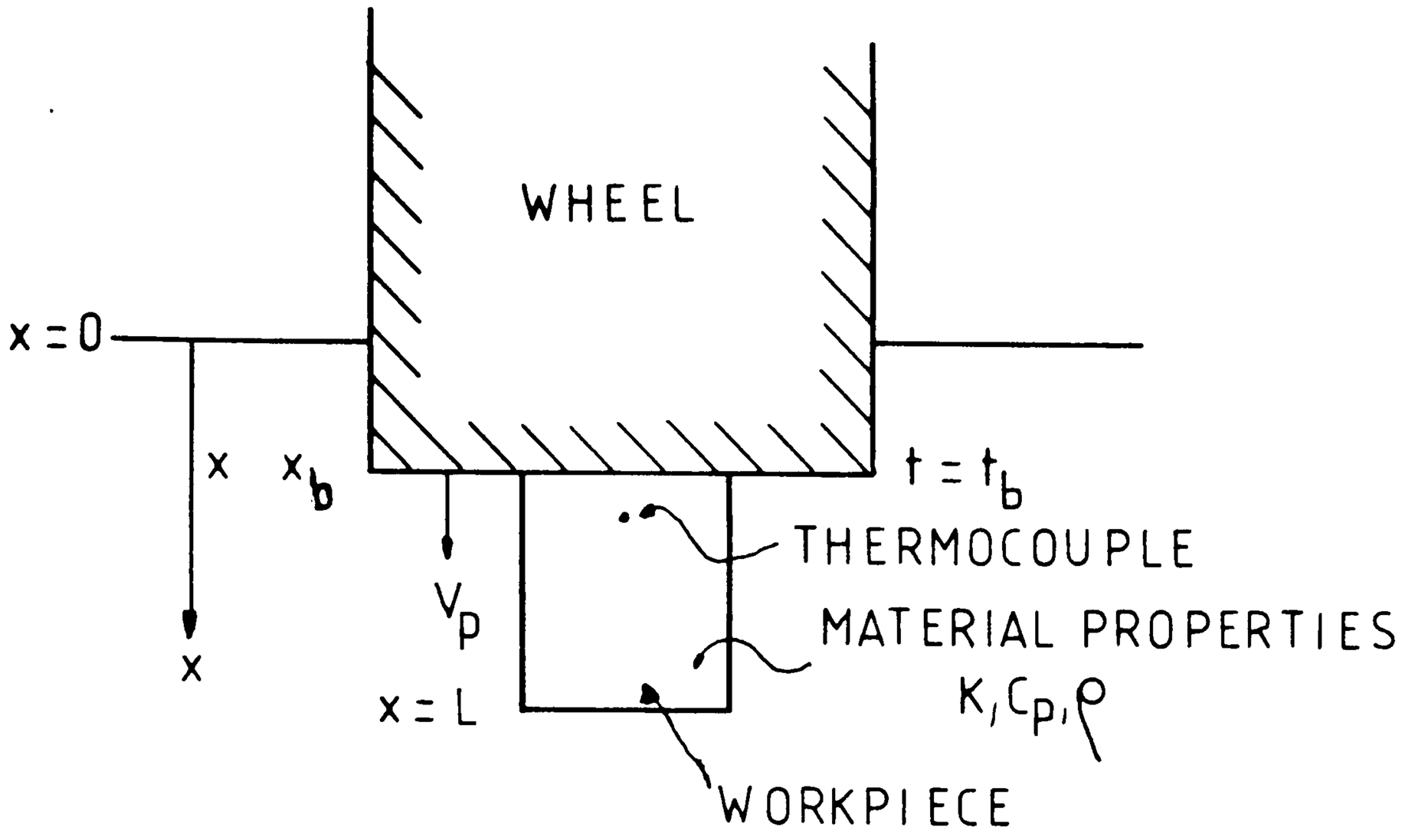

INITIAL CONDITIONS: $t = 0 \qquad 0 < x < L$

1D CONDUCTION EQUATION:

$$\rho C_p \frac{\delta t}{\delta \tau} = k \frac{\delta^2 t}{\delta x^2}$$

BOUNDARY CONDITIONS

BOTTOM FACE - $\left[\frac{dt}{dx}\right]_L = 0$

TOP FACE — i) CONVECTIVE BOUNDARY

$$eV_p = h(t_b - t_c) - k\left[\frac{dt}{dx}\right]_b + \rho C_p V_p t_b$$

ii) FIXED PARTITION

$$[q_w - q_v t_b]\, eV_p = -k\left[\frac{dt}{dx}\right]_b$$

FIG 4 1-DIMENSIONAL HEAT FLOW MODEL

BOUNDARY CONDITIONS:

COOLANT TEMPERATURE 20°C
HEAT TRANSFER COEFFICIENT AT ALL WORKPIECE SURFACES IS 0·1 WATTS/MM²°C
TANGENTIAL STRESS BETWEEN WHEEL AND WORKPIECE IS 0·16 + 8·8×U N/MM²
(WHERE U IS THE COMPONENT OF FEED RATE NORMAL TO THE WHEEL IN MM/S)
HEAT INPUT TO WORKPIECE IS 0·6 WORK DONE BY TANGENTIAL STRESS

GRINDING PARAMETERS:

DEPTH OF CUT 6·0 MM
FEED RATE 0·187 MM/S
WHEEL SPEED 30 M/S
MATERIAL IS NIMONIC C1023

SCALE:

0 10 MM

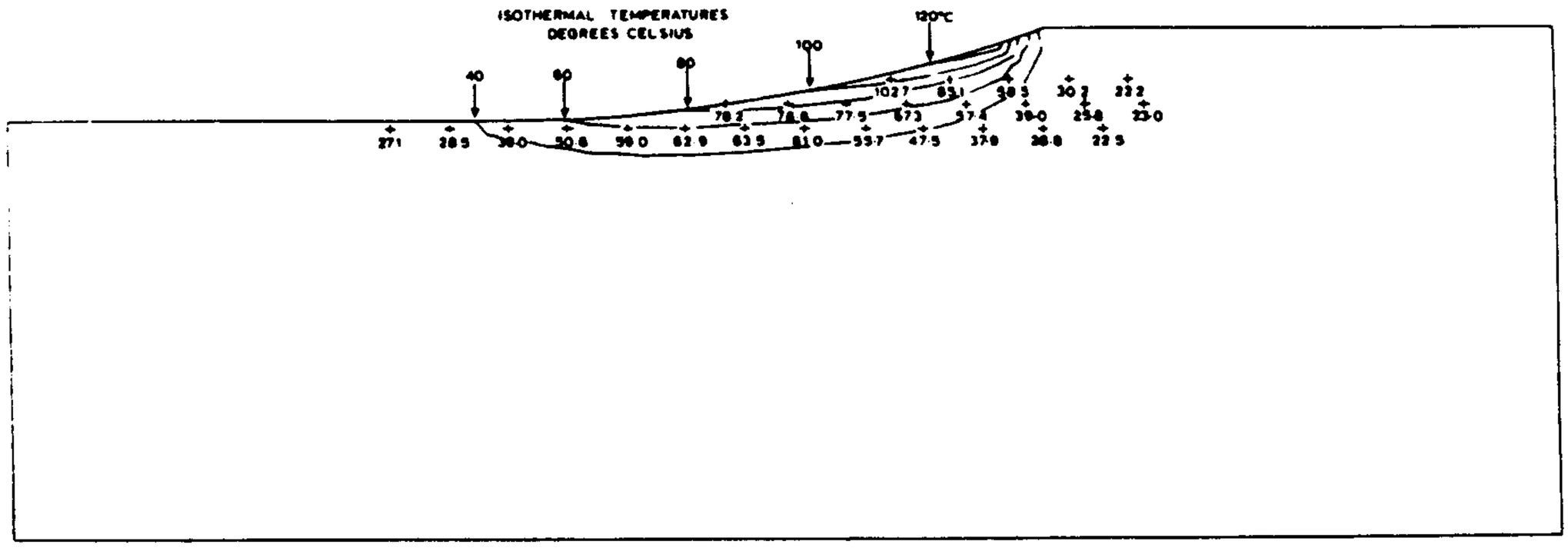

COMPARISON OF TEMPERATURES MEASURED BY THERMOCOUPLES WITH ISOTHERMALS PREDICTED BY TRANSIENT HEAT FLOW FINITE ELEMENT ANALYSIS

BOUNDARY CONDITIONS:

COOLANT TEMPERATURE 20°C
HEAT TRANSFER COEFFICIENT AT ALL WORKPIECE SURFACES IS 0·1 WATTS/MM²°C
TANGENTIAL STRESS BETWEEN WHEEL AND WORKPIECE IS 0·16 + 8·8×U N/MM²
(WHERE U IS THE COMPONENT OF FEED RATE NORMAL TO THE WHEEL IN MM/S)
HEAT INPUT TO WORKPIECE IS 0·6 × WORK DONE BY TANGENTIAL STRESS

GRINDING PARAMETERS:

DEPTH OF CUT 6·0 MM
FEED RATE 0·187 MM/S
WHEEL SPEED 30 M/S
MATERIAL IS NIMONIC C1023

SCALE:

0 10 MM

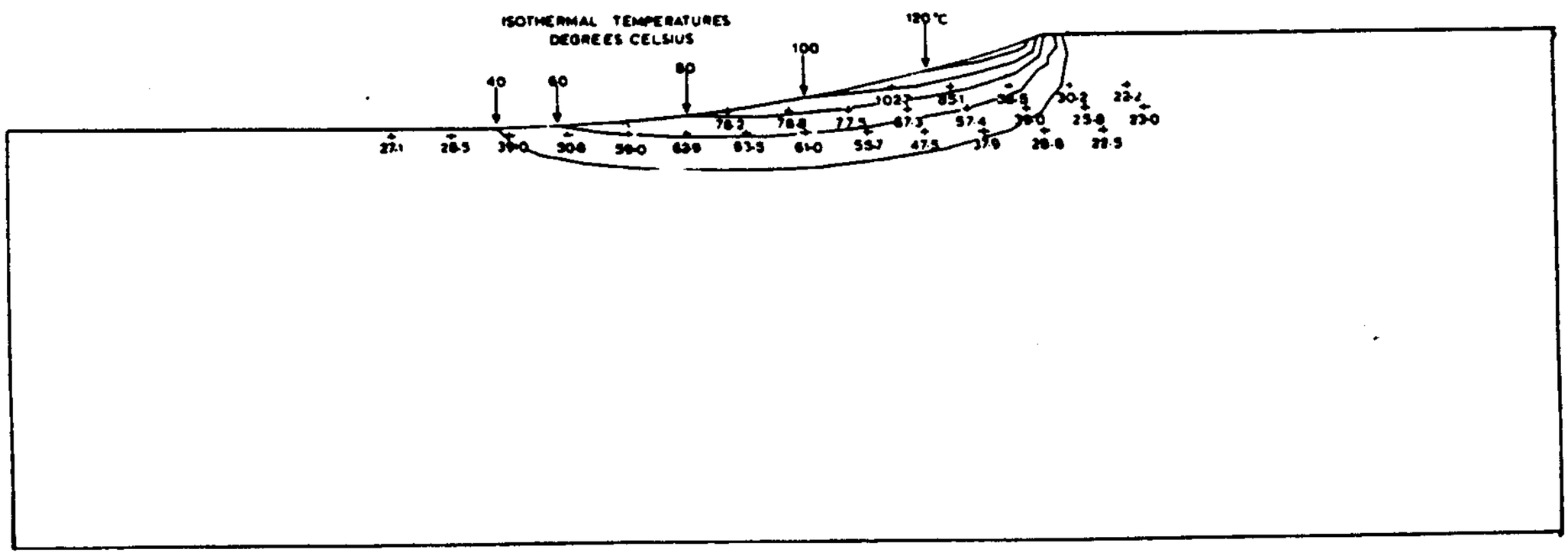

COMPARISON OF TEMPERATURES MEASURED BY THERMOCOUPLES WITH ISOTHERMALS PREDICTED BY STEADY STATE FINITE ELEMENT ANALYSIS

FIG 5 EXPERIMENTAL AND THEORETICAL TEMPERATURE DISTRIBUTIONS [AFTER SHAFTO (ref 8)]

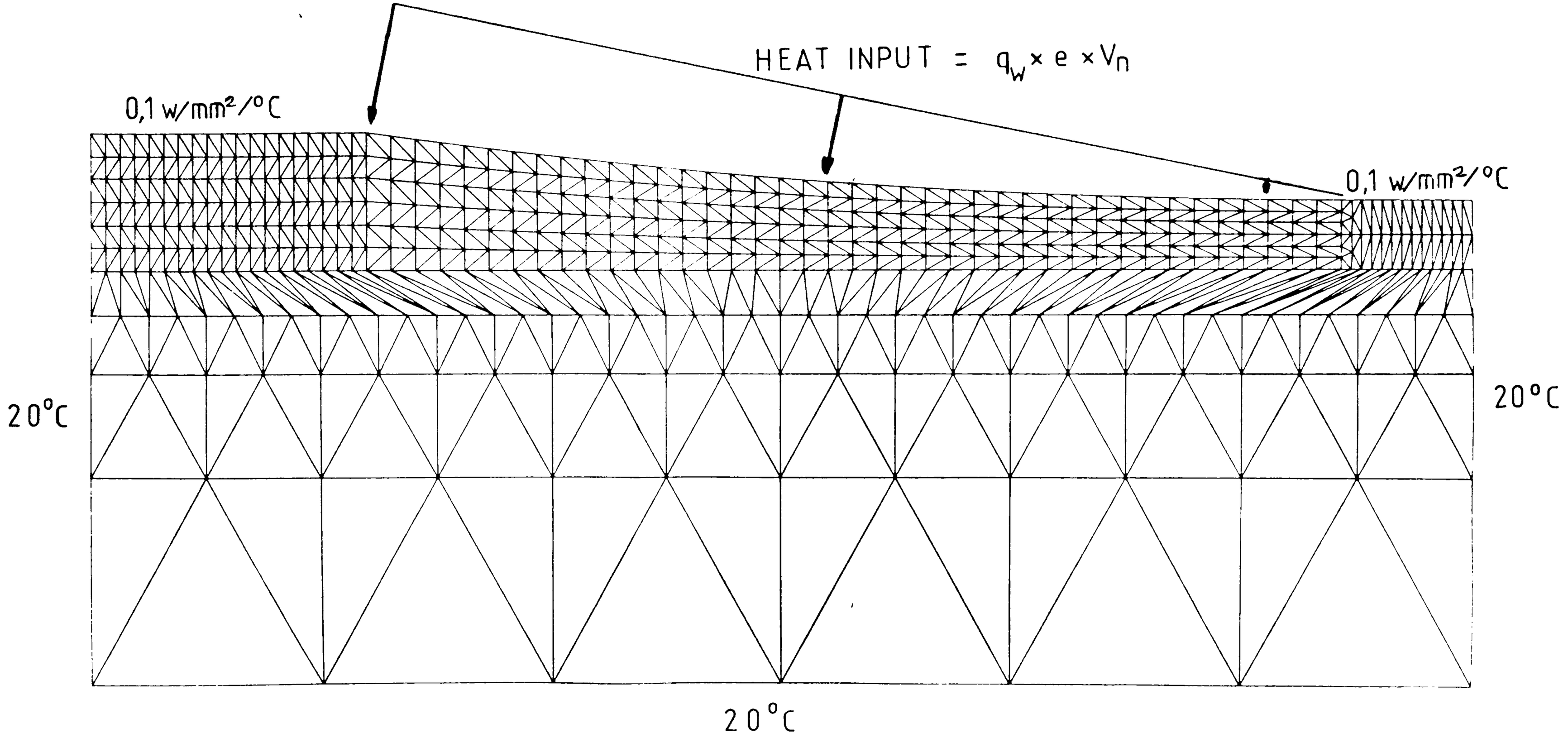

FIG 6 FINITE ELEMENT ANALYSIS MESH AND BOUNDARY CONDITIONS

TEST SHEET DATE

Test No.: 101 Material: EN19C Wheel Grade: WA100K26V

Dressing: Conventional/~~continuous~~ Neat oil coolant.

Initial Conditions

Wheel dia.:	599,6	mm
Workpiece dia.:	89,47	mm
Workpiece width:	21,20	mm
Offset:	323	
Dresser clearance:	20	µm
Contact point:	51·497	

Settings

Depth of cut:	3	mm
MNIR:	20	mm/min
Wheel speed - dressing:	30	m/s
- grinding:	30	m/s
Roll speed ratio:	+0,8	
Depth of dress:	0,3	mm
Dresser feed rate	2	µm/rev
Coolant - pressure	0,5	bar
- flow rate		v

FIG 7 INITIAL CONDITIONS FOR INPUT TO COMPUTER PROGRAM

```
Do you want to obtain initial rig settings?
yes
Please give the following information as shown:-


Test no.,Initial workpiece dia.(m.m.),Workpiece width(m.m.),
Wheel grade
101,89.47,21.2,WA100K26V/oil
Is this a continuous dressing test?
no
Input the following values as shown for the dressing cycle:-

Initial wheel dia.(m.m.),Wheel surface speed(m/s),Roll speed ratio
Depth of wheel to be dressed on radius(m.m.),Dresser feed rate(microns/rev.
599.6,30,.8,.3,2
The conditions you require are as follows:-

Wheel rotationalspeed= 956. r.p.m.

Dresser rotational speed=3056. r.p.m

Feed rate setting= 32. microns/sec

Assuming an initial dresser clearance of  30. microns, dressing should tak
place for  10.4secs.


Do not forget to set required coolant pressure and turn on u.v.recorder if
required.


Grinding condition calculations will assume that the intended
amount of wheel was dressed away. The true value of wheel diameter
after dressing should be entered under results, and corrected
values of wheel speed etc. will be given by the program.


Enter required conditions as shown:-

Depth of cut(m.m.),MNIR(mm/min),Digital readout at wheel/workpiece
contact(Before dressing),Wheel surface speed(m/s)
3,20,51.497,30
The grinding parameters required are as follows:-


Wheel speed=  957. r.p.m.

Workpiece speed= 0.135 r.p.m. OR 1 rev takes 324.0 secs

Feed point 1=  51.297

Final feed point=  51.197


These conditions will give an arc length of 15.09 m.m.
Do not forget to set required coolant flows and turn on the u.v.recorder.
```

FIG 8 COMPUTER PRINTOUT OF MACHINE SETTINGS

RESULTS SHEET

Wheel speed - dressing:	950	rpm
" grinding:	950	rpm
Dresser speed:	3060	rpm
Dresser feed rate:	32	µm/sec
Wheel dia. after dressing:	549,1	mm
Workpiece speed:	280	sec/rev
Workpiece final dia.:	83,97	mm
Depth of wheel wear:	10	µm
Duration of test:	76	sec
Sample interval:	19	sec
Surface finish:	1,5	µm

Trace deflections

Time	Δ14	Δ25	Δ36
19	3	6	8,5
38	2,5	7	10
57	3	7,5	10,5
75	3,5	8	11

FIG 9 RESULTS FOR COMPUTER ANALYSIS PROGRAM

Test no.101 Mode: conventional Wheel grade:WA100K26V/oil

Dressing conditions

Wheel surface speed=29.83 m/s

Dresser roll ratio=0.81

Dresser feed rate= 2.0 microns/rev

Depth of dress on radius=0.25 m.m.

Grinding conditions

Wheel surface speed=29.80 m/s

Depth of cut=2.75 m.m.

MNIR=22.20 mm/min

Stock removal rate= 2.68mm.cb/mm/sec

Total stock removed= 203.36mm.cub/mm

G-ratio= 10.806

Arc length=14.5m.m.

Stock removed mm.cub	Normal force N/mm	Tangential force N/mm	Force ratio
50.84	6.91	2.68	.39
101.68	8.11	2.62	.32
152.52	8.56	2.91	.34
203.36	9.05	3.20	.35

Stock removed mm.cub	Specific energy J/mm.cub	Power flux w/mm.sq
50.84	29.80	5.5
101.68	29.17	5.4
152.52	32.42	6.0
203.36	35.66	6.6

FIG 10 COMPUTER SUMMARY OF RESULTS

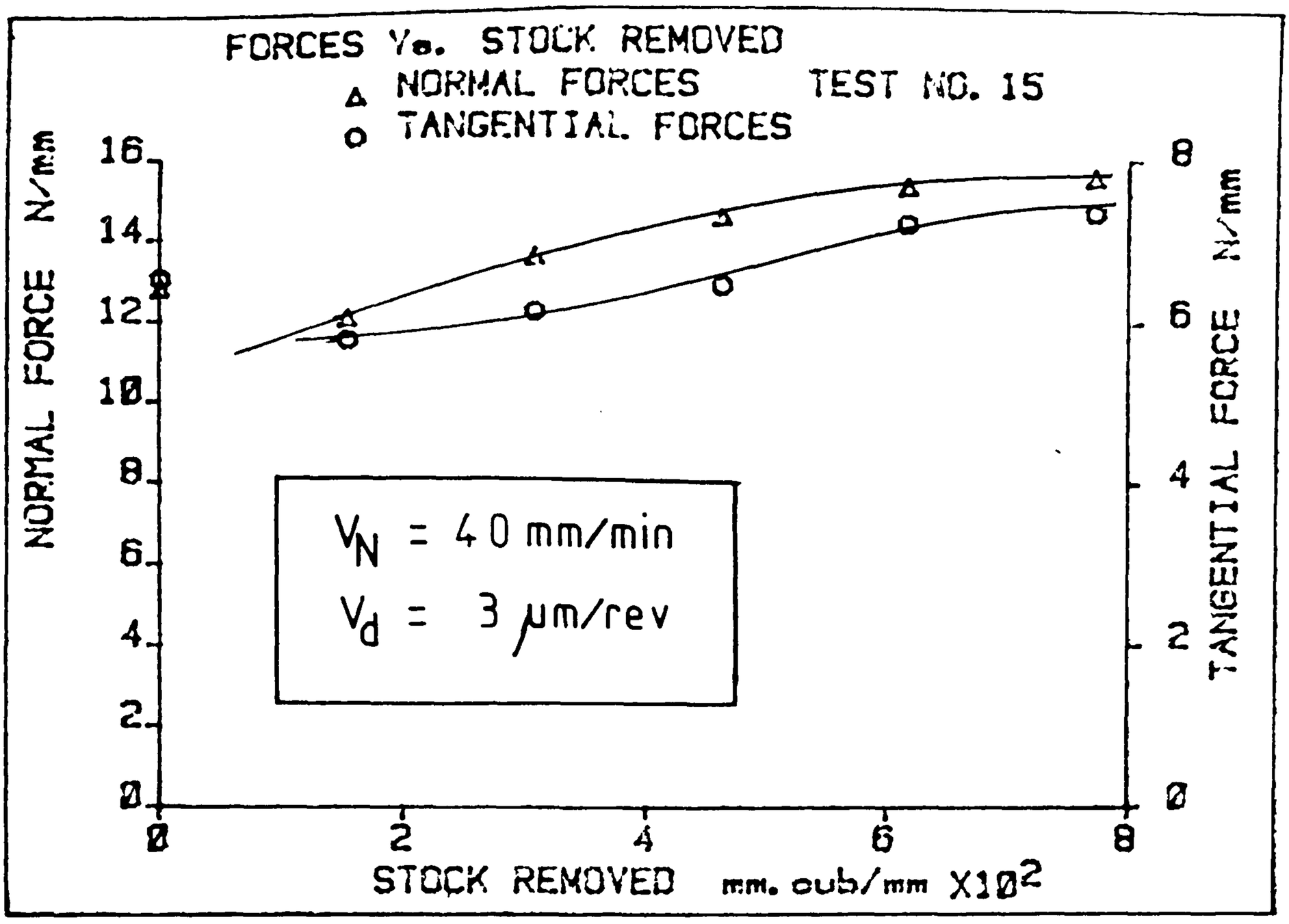

FIG 11 CHANGE IN GRINDING FORCES WITH STOCK REMOVED

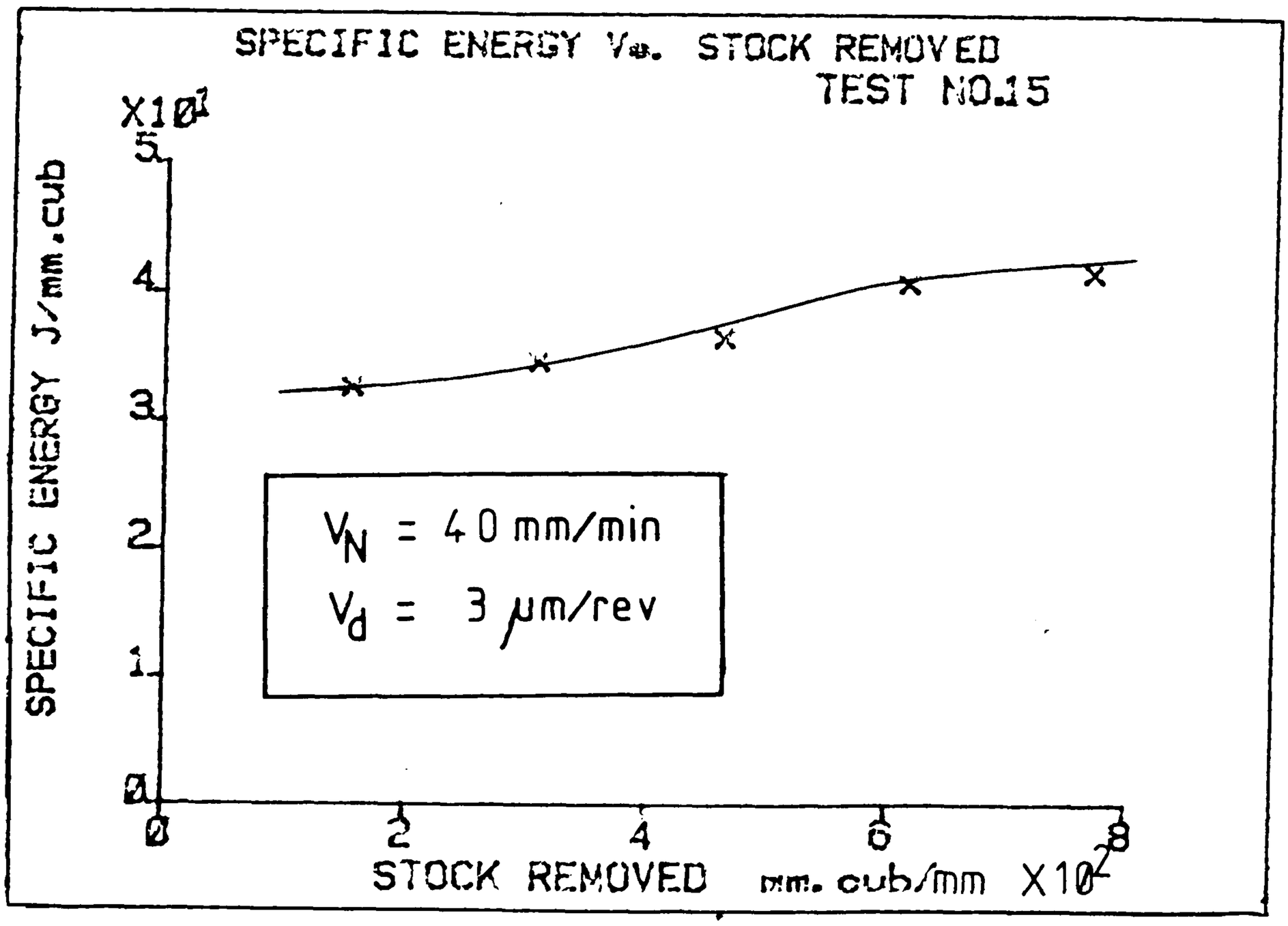

FIG 12 CHANGE IN SPECIFIC GRINDING ENERGY WITH STOCK REMOVED

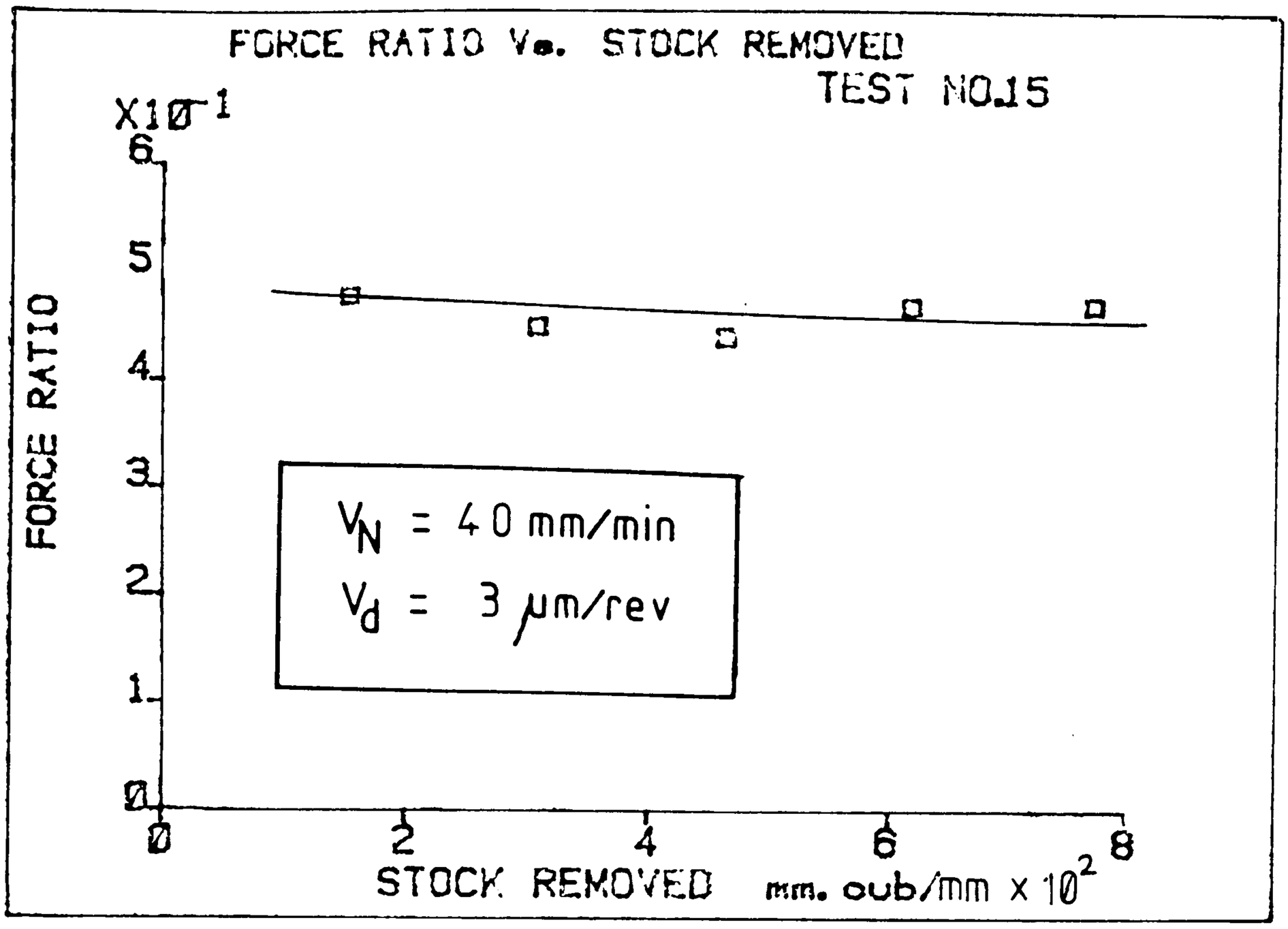

FIG 13

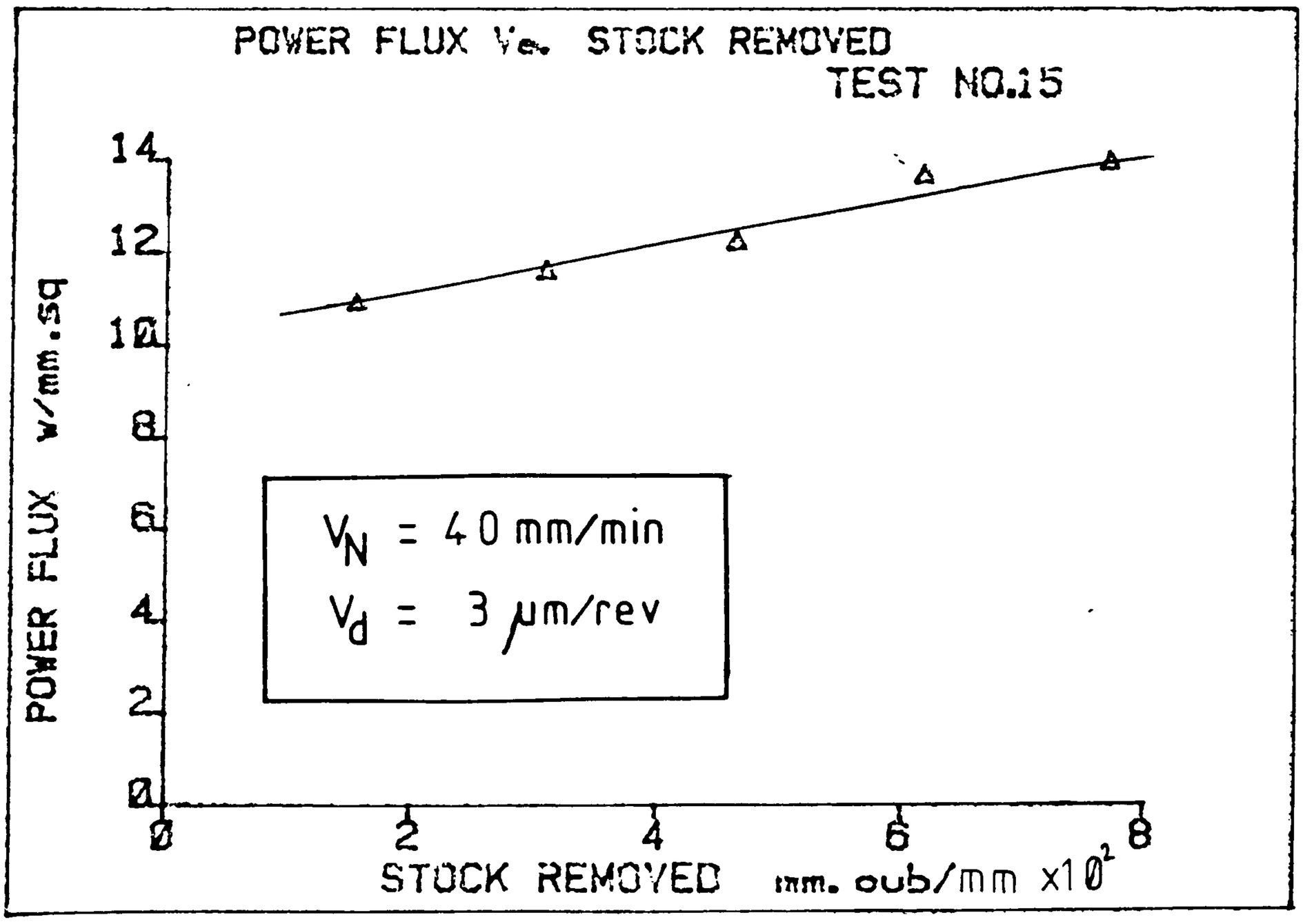

FIG 14 EXAMPLES OF COMPUTER PLOTTED RESULTS

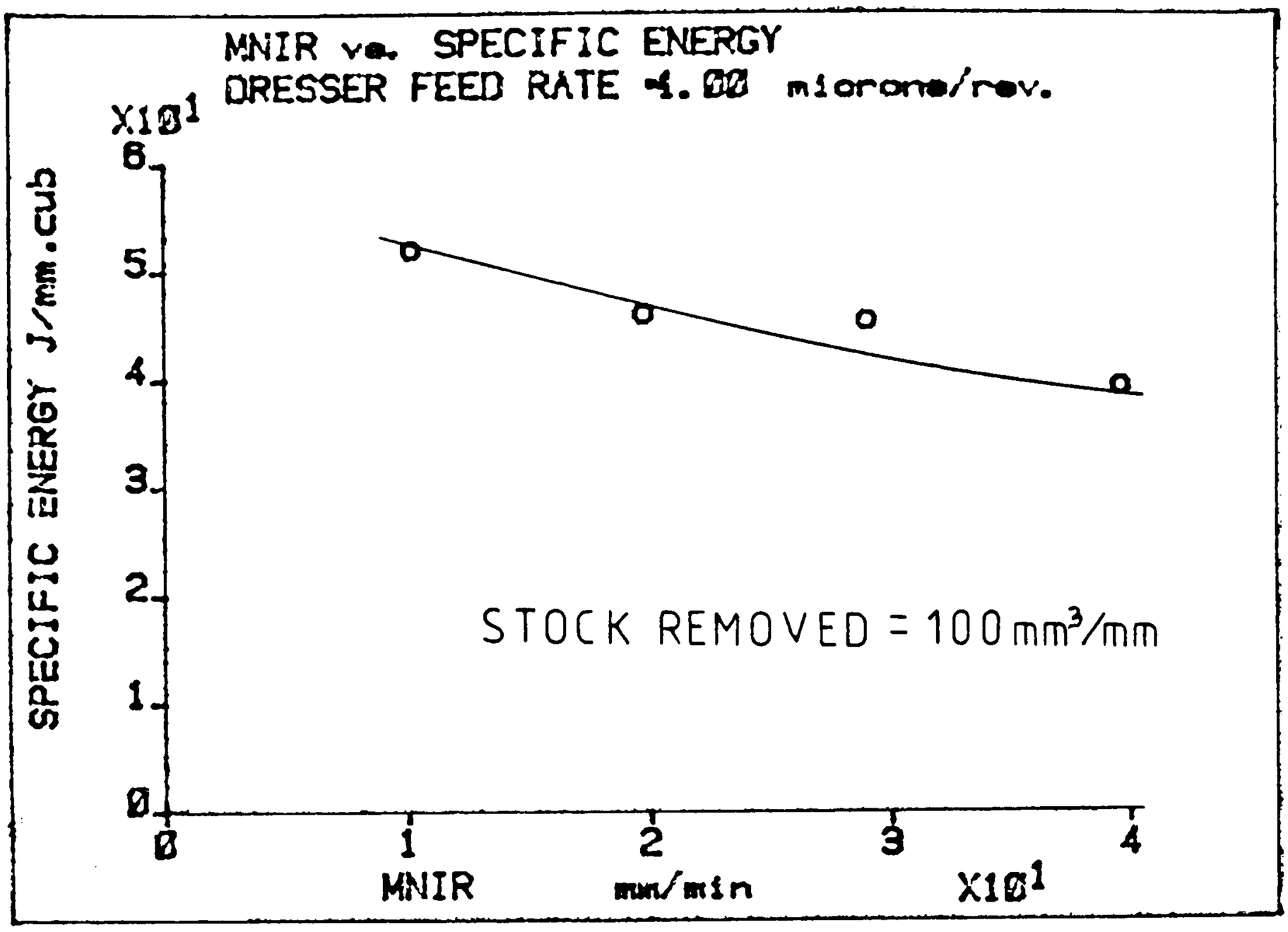

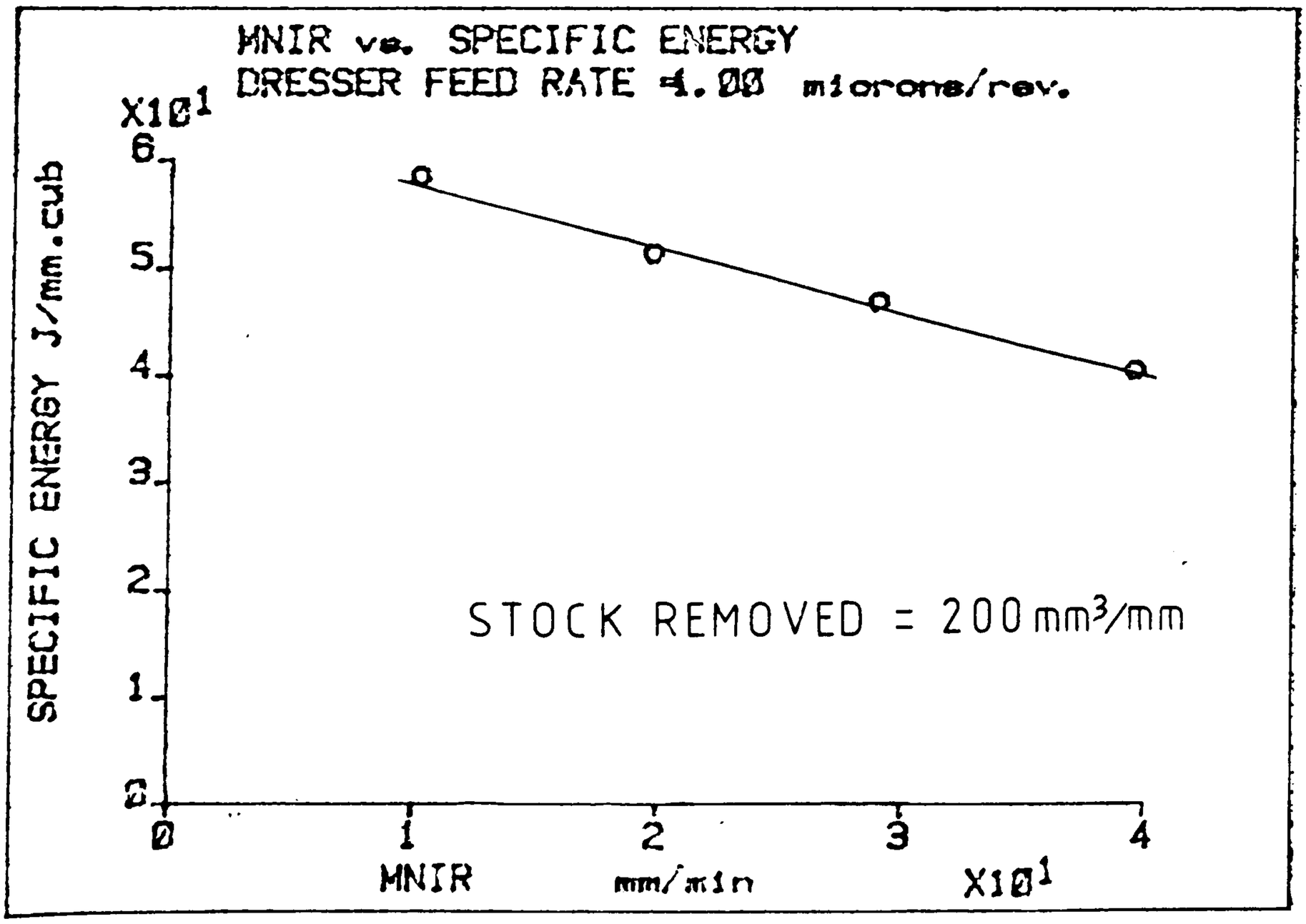

FIG 15 SPECIFIC ENERGY AGAINST MNIR AFTER DIFFERENT AMOUNTS OF STOCK HAVE BEEN REMOVED

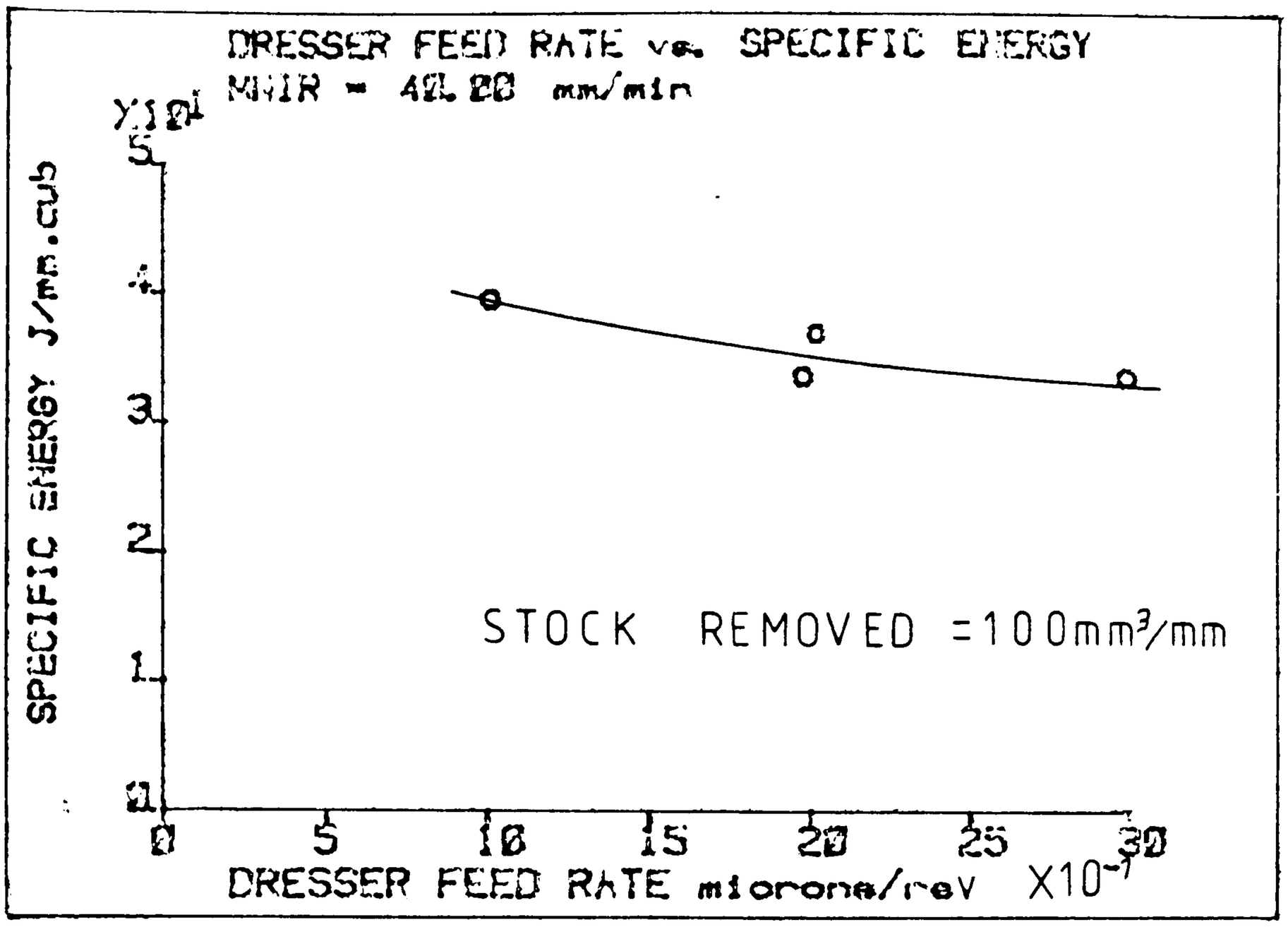

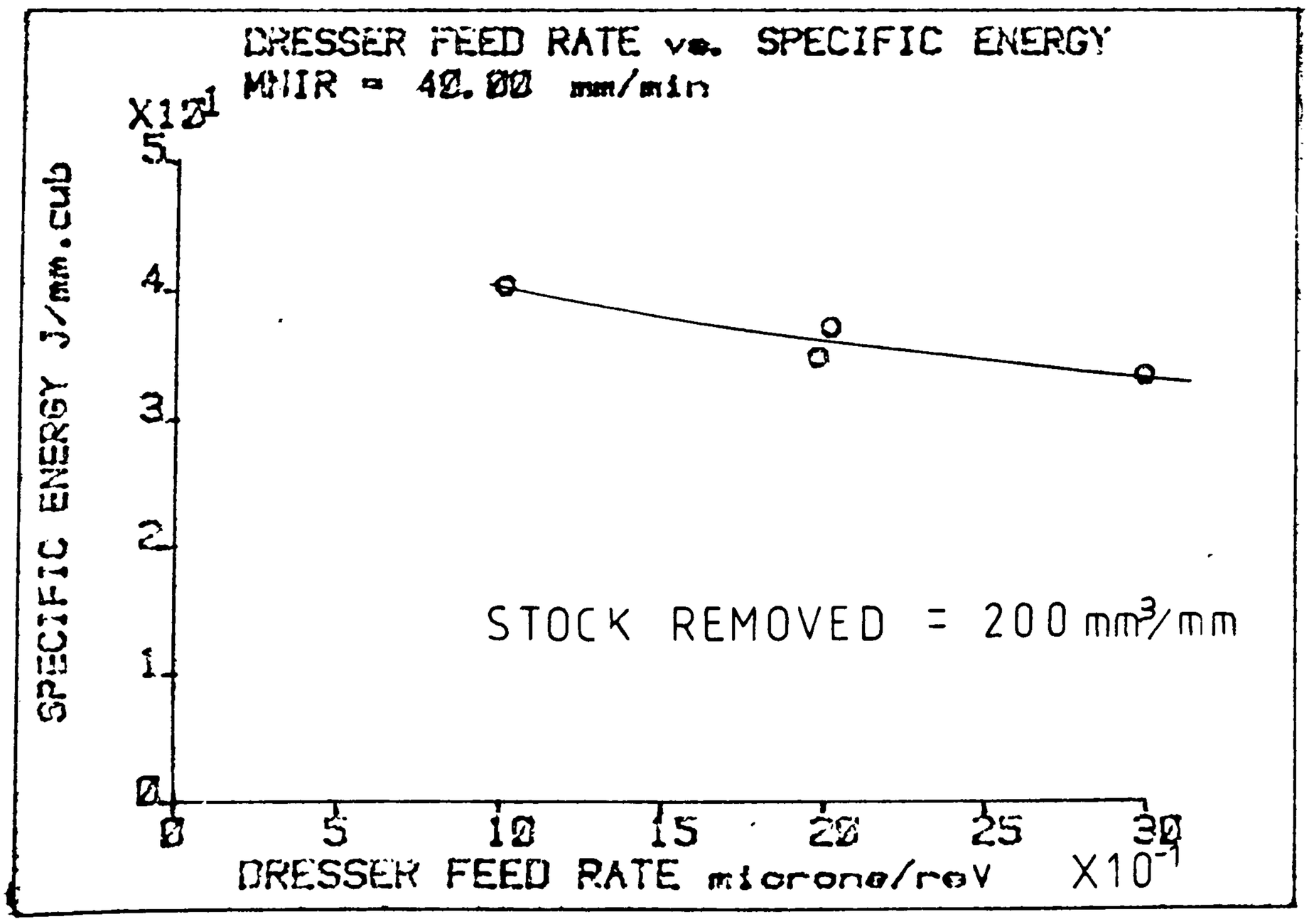

FIG 16 SPECIFIC ENERGY AGAINST DRESSER FEED RATE AFTER DIFFERENT AMOUNTS OF STOCK REMOVED

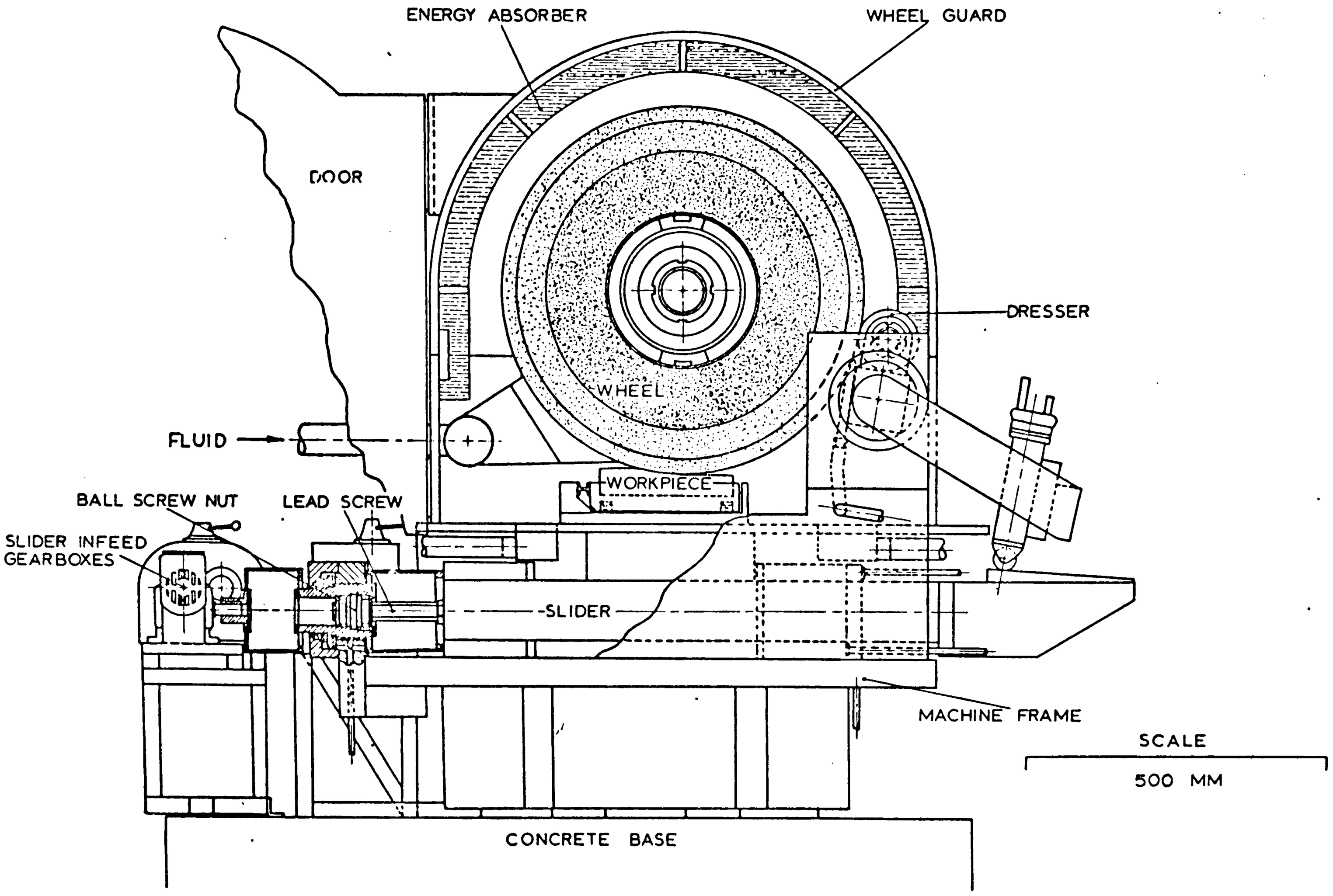

FIG 17 GENERAL ARRANGEMENT OF THE CREEP-FEED SURFACE GRINDING MACHINE [AFTER STUART ref 62]

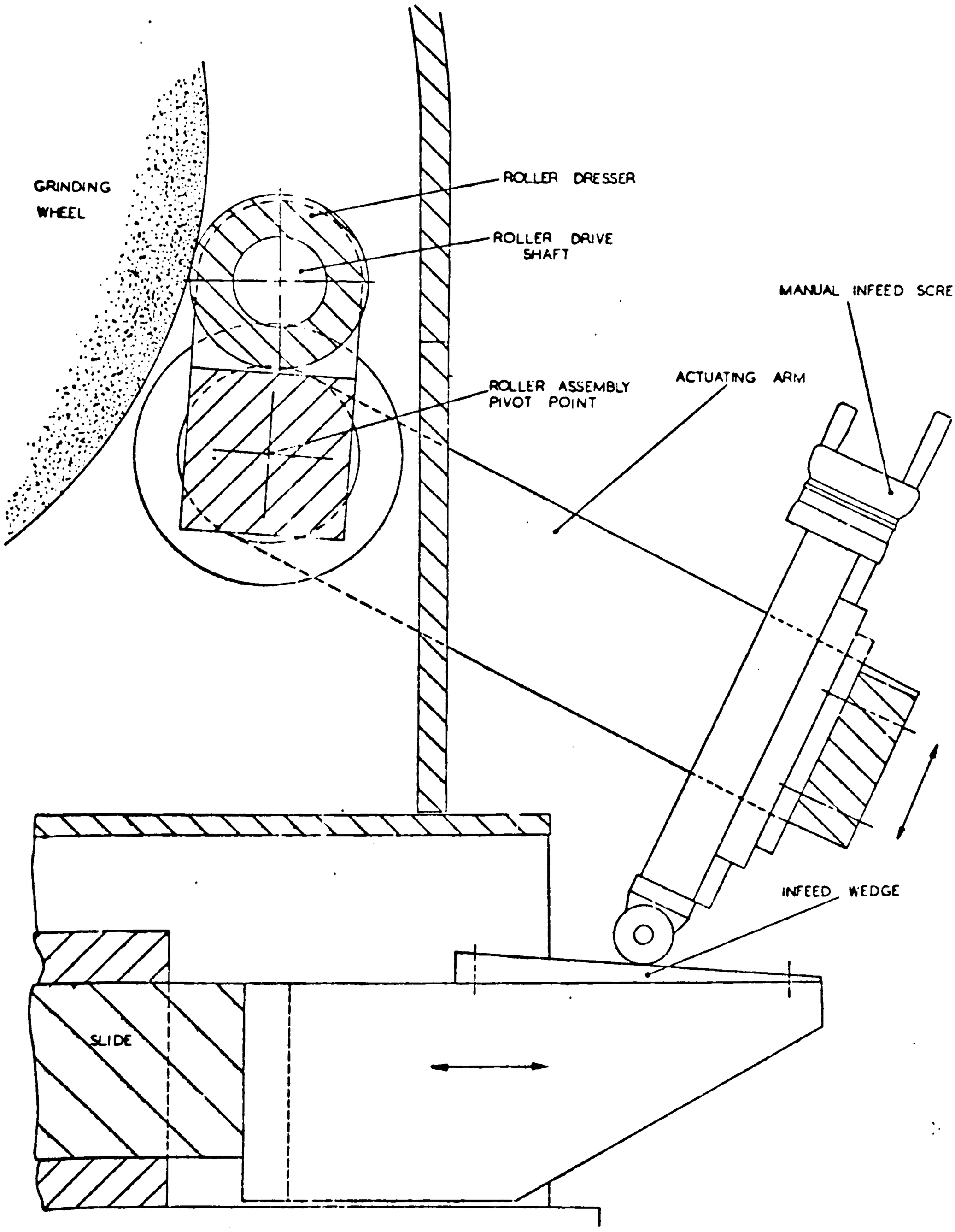

FIG 18 DRESSER INFEED MECHANISM ON THE SURFACE GRINDING MACHINE

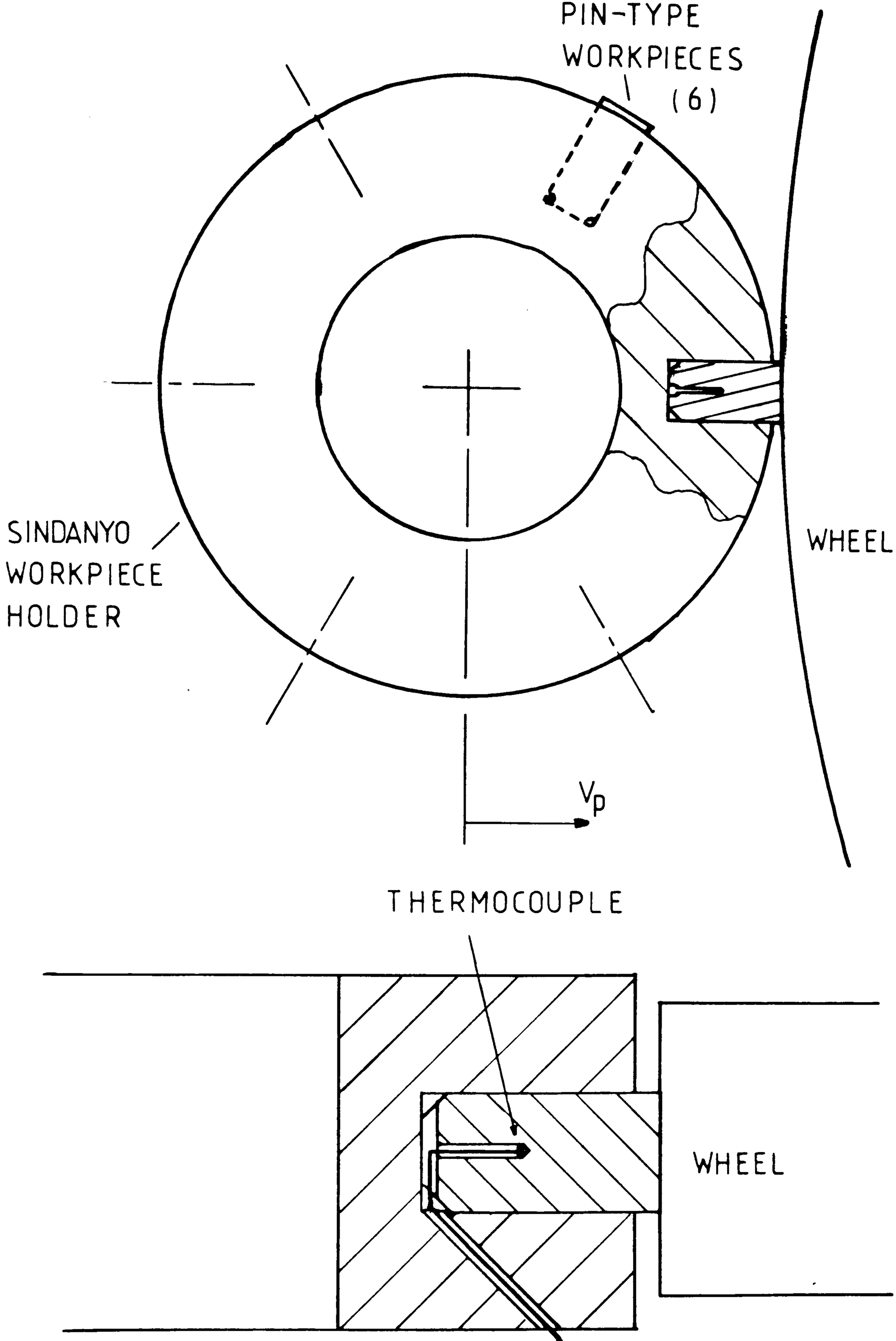

SECTION THROUGH A PIN SHOWING
THERMOCOUPLE LOCATION (2 x ACTUAL SIZE)

FIG 19 EXPERIMENTAL ARRANGEMENT FOR PLUNGE GRINDING INSULATED WORKPIECES

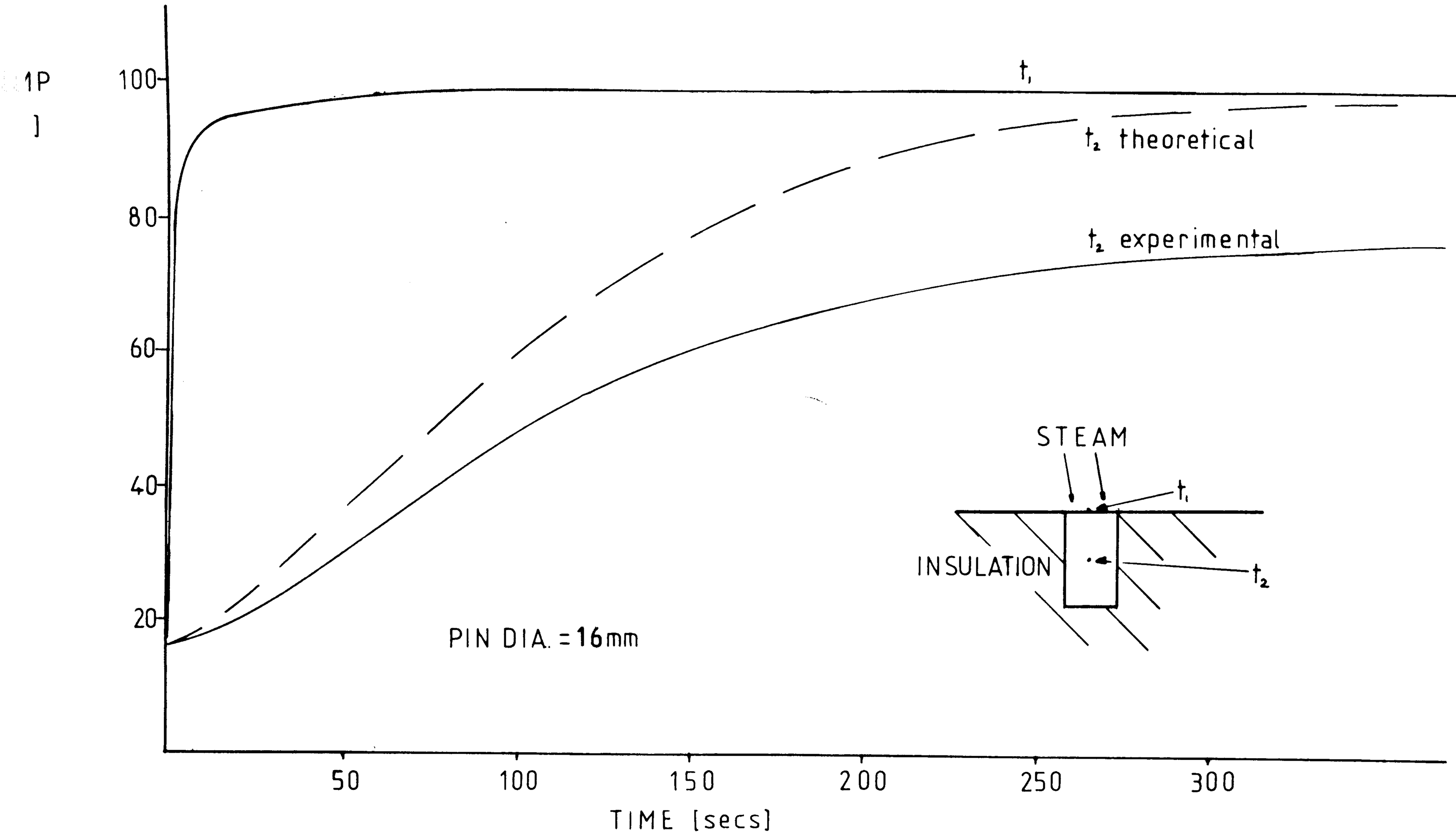

FIG 20 TRANSIENT CALIBRATION OF AN INSULATED WORKPIECE

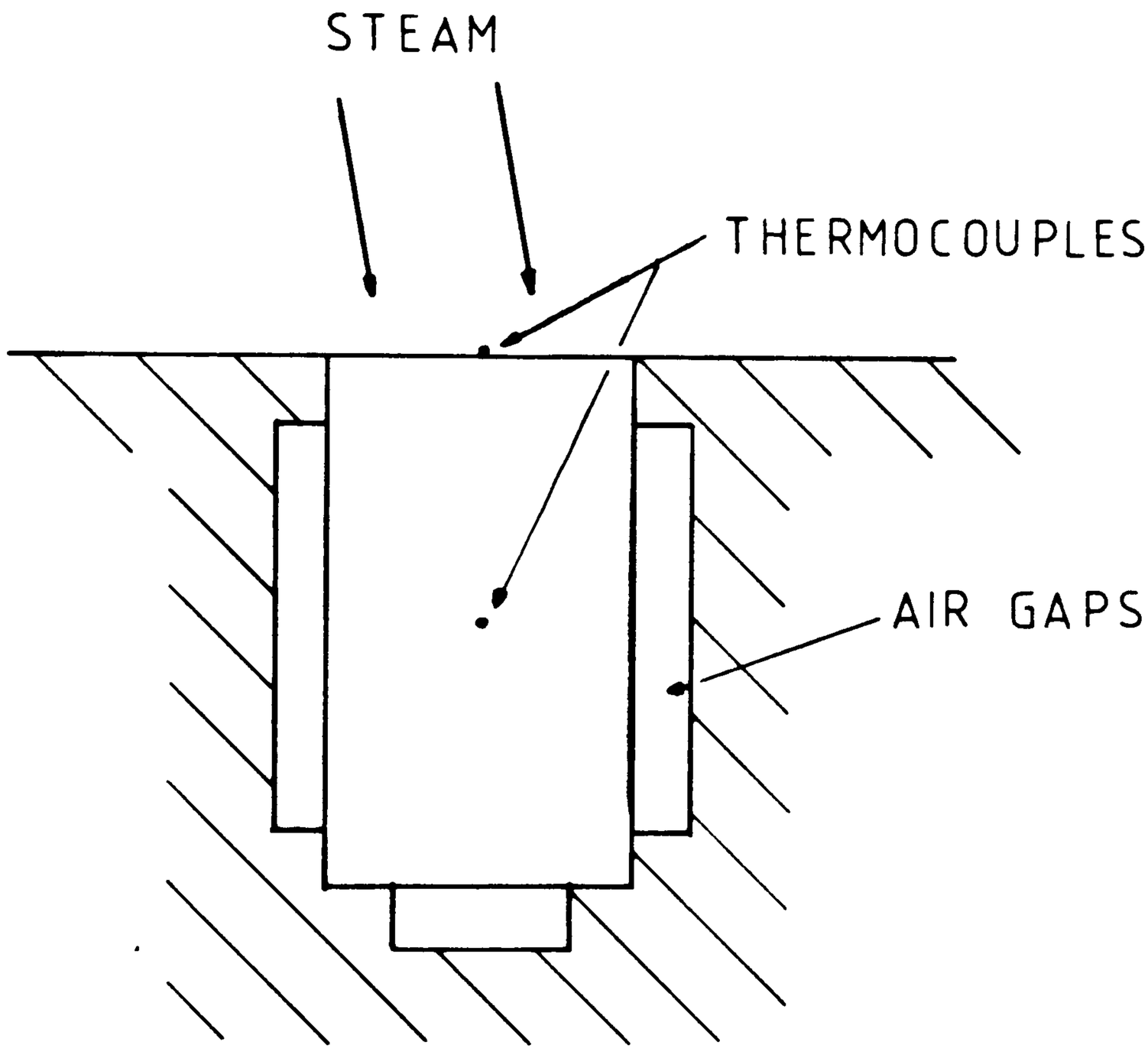

FIG 21 CALIBRATION PIN WITH AIR GAPS

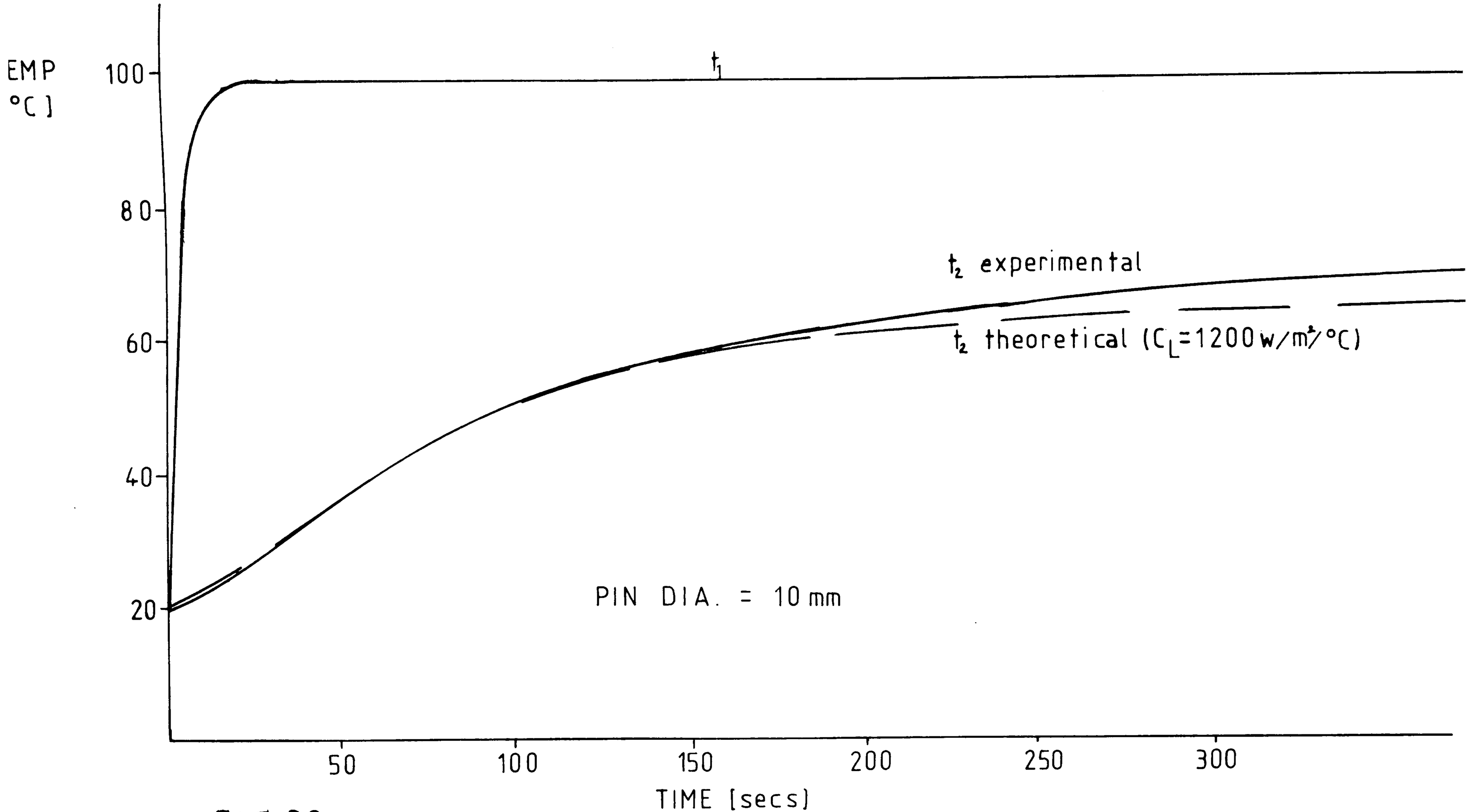

FIG 22 TRANSIENT CALIBRATION WITH MODIFIED THEORETICAL MODEL

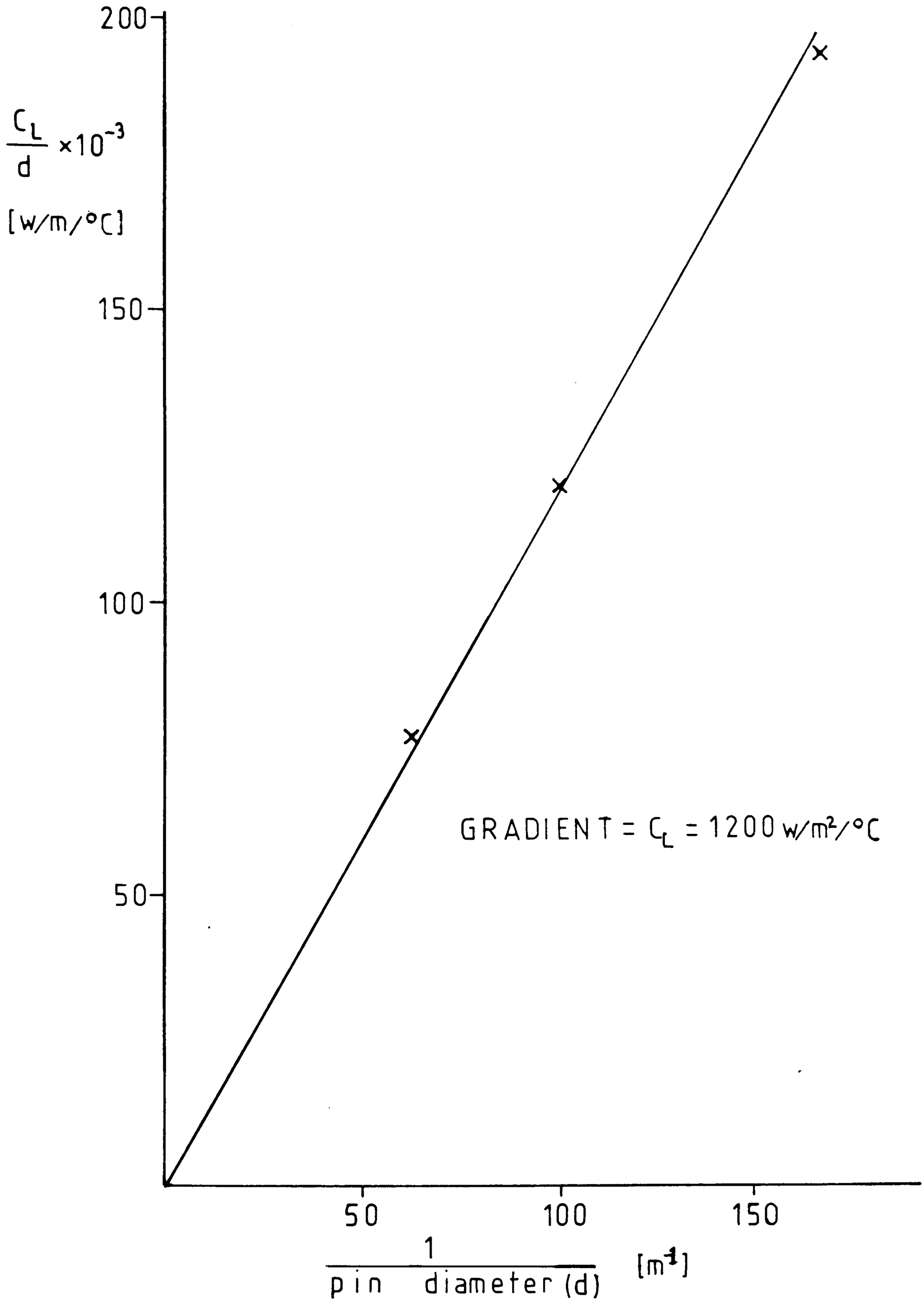

FIG 23 DETERMINATION OF LOSS TERM (C_L) USING CALIBRATION PINS OF VARIOUS DIAMETERS

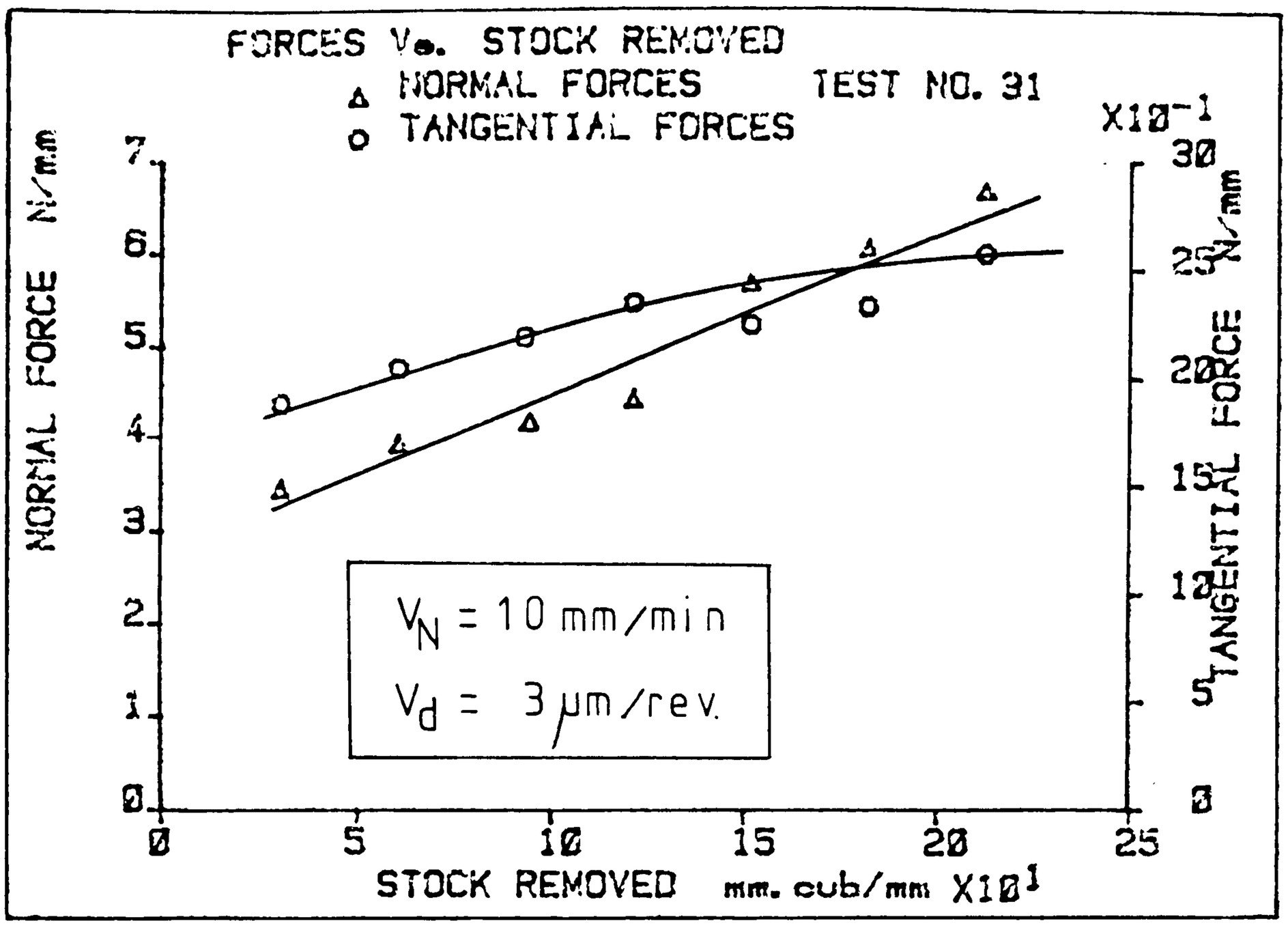
FORCES Vs. STOCK REMOVED
NORMAL FORCES
TANGENTIAL FORCES
TEST NO. 31
NORMAL FORCE N/mm
TANGENTIAL FORCE N/mm
X10⁻¹
V_N = 10 mm/min
V_d = 3 μm/rev.
STOCK REMOVED mm. cub/mm X10¹

FIG 24

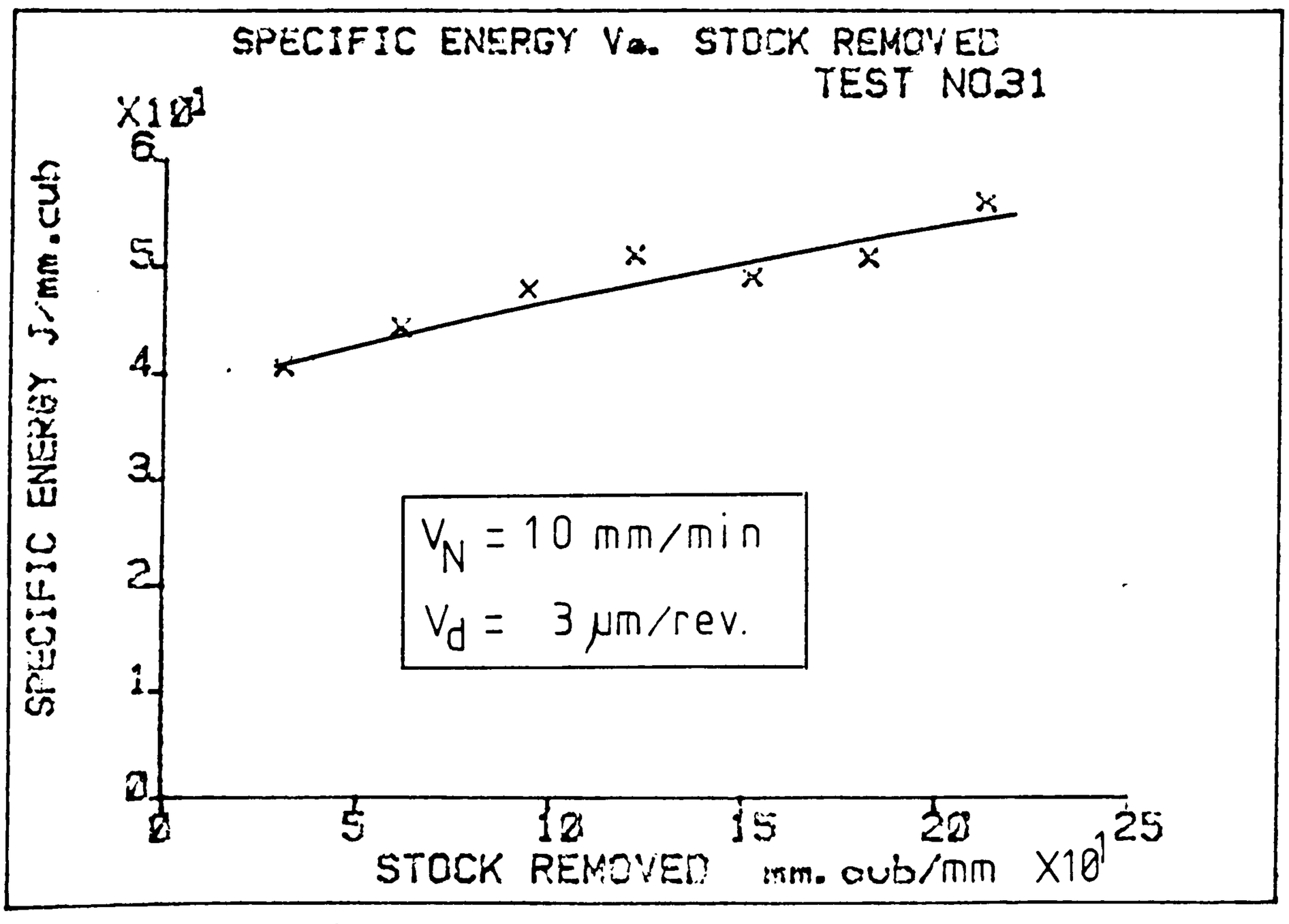
SPECIFIC ENERGY Vs. STOCK REMOVED
TEST NO31
X10¹
SPECIFIC ENERGY J/mm.cub
V_N = 10 mm/min
V_d = 3 μm/rev.
STOCK REMOVED mm. cub/mm X10¹

FIG 25

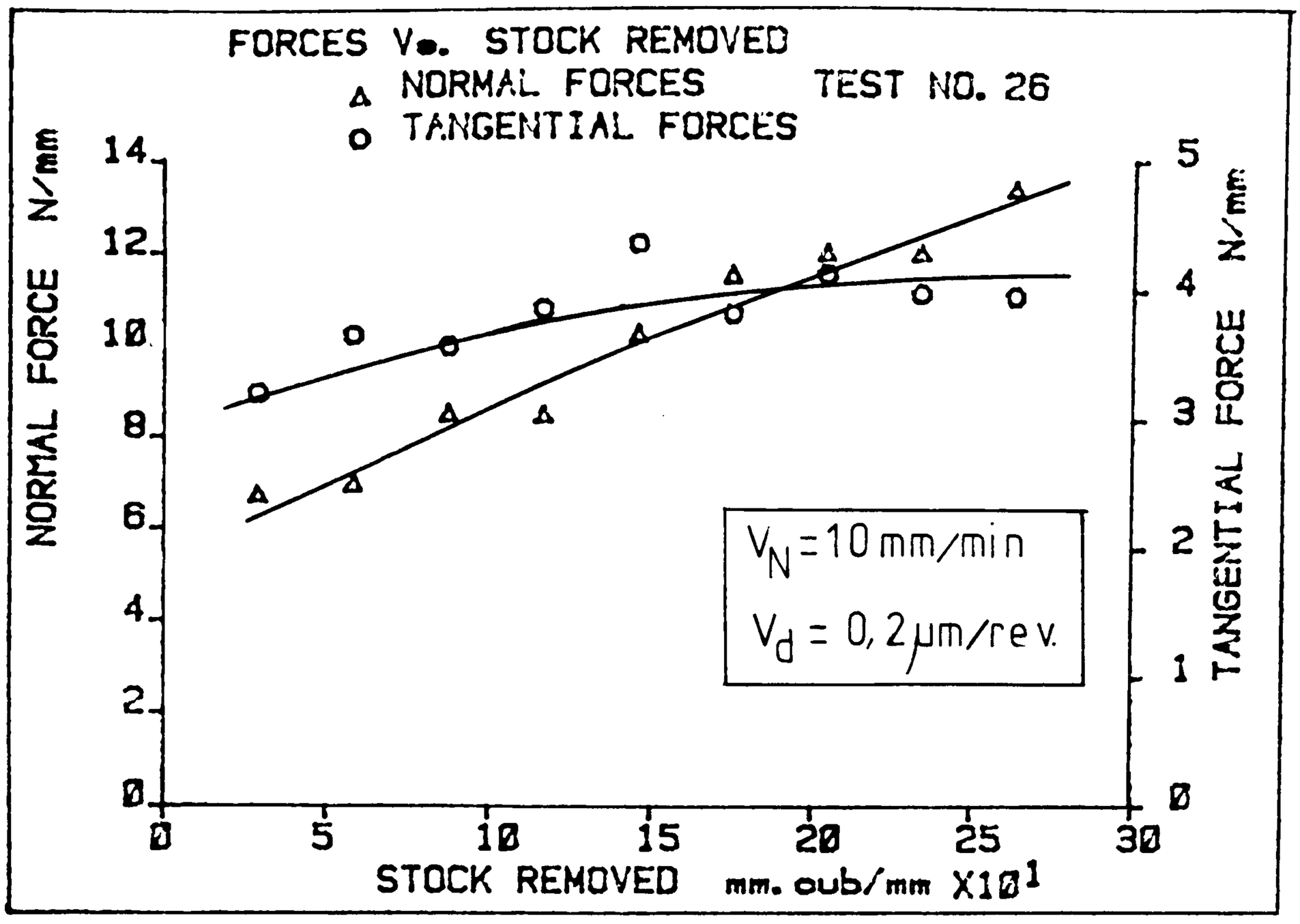
FORCES Vs. STOCK REMOVED
NORMAL FORCES
TANGENTIAL FORCES
TEST NO. 26
NORMAL FORCE N/mm
TANGENTIAL FORCE N/mm
14
12
10
8
6
4
2
0
5
4
3
2
1
0
V_N = 10 mm/min
V_d = 0,2 µm/rev.
0
5
10
15
20
25
30
STOCK REMOVED mm. cub/mm X10¹

FIG 26

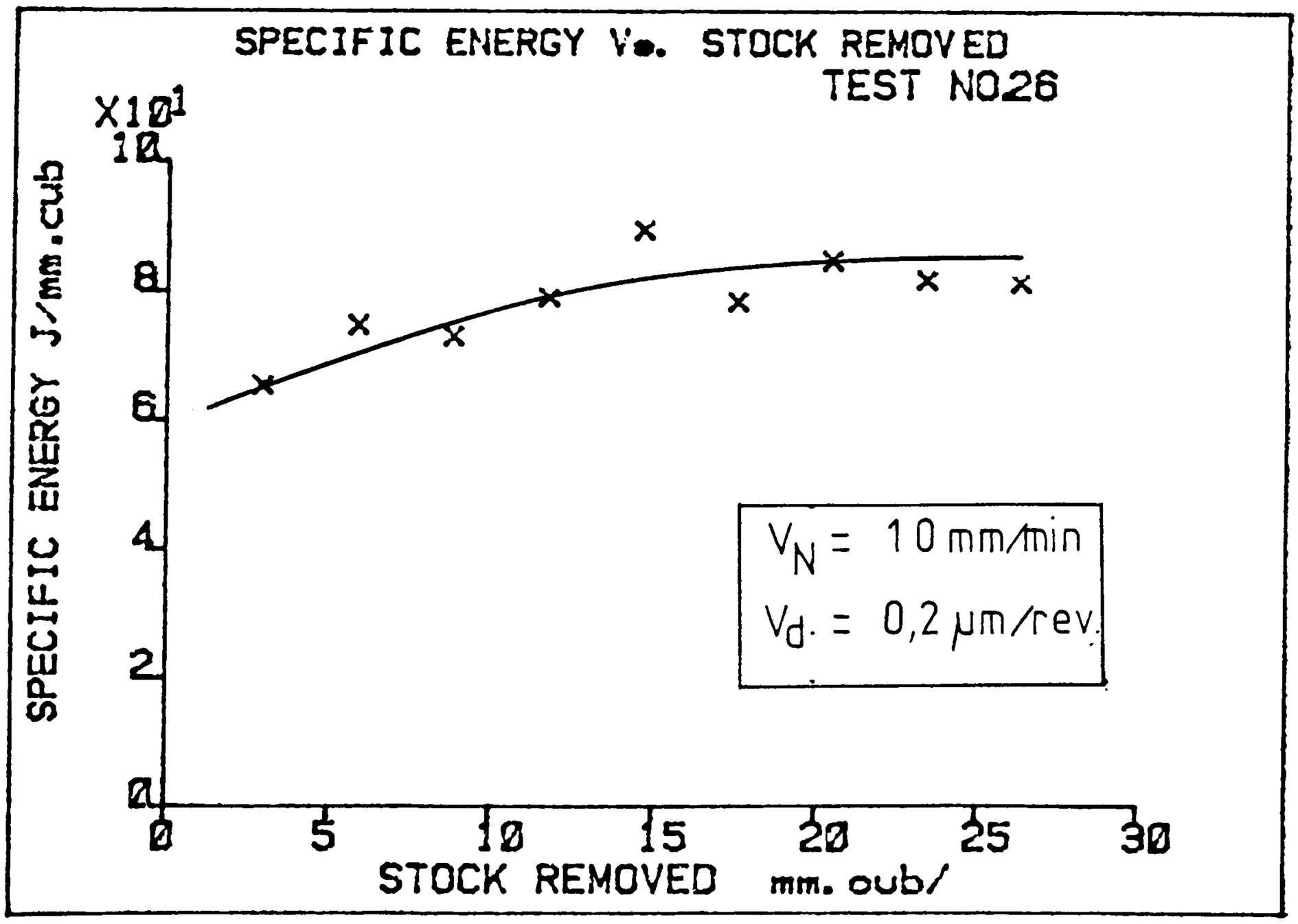
SPECIFIC ENERGY Vs. STOCK REMOVED
TEST NO26
X10¹
SPECIFIC ENERGY J/mm.cub
10
8
6
4
2
0
V_N = 10 mm/min
V_d = 0,2 µm/rev.
0
5
10
15
20
25
30
STOCK REMOVED mm. cub/

FIG 27

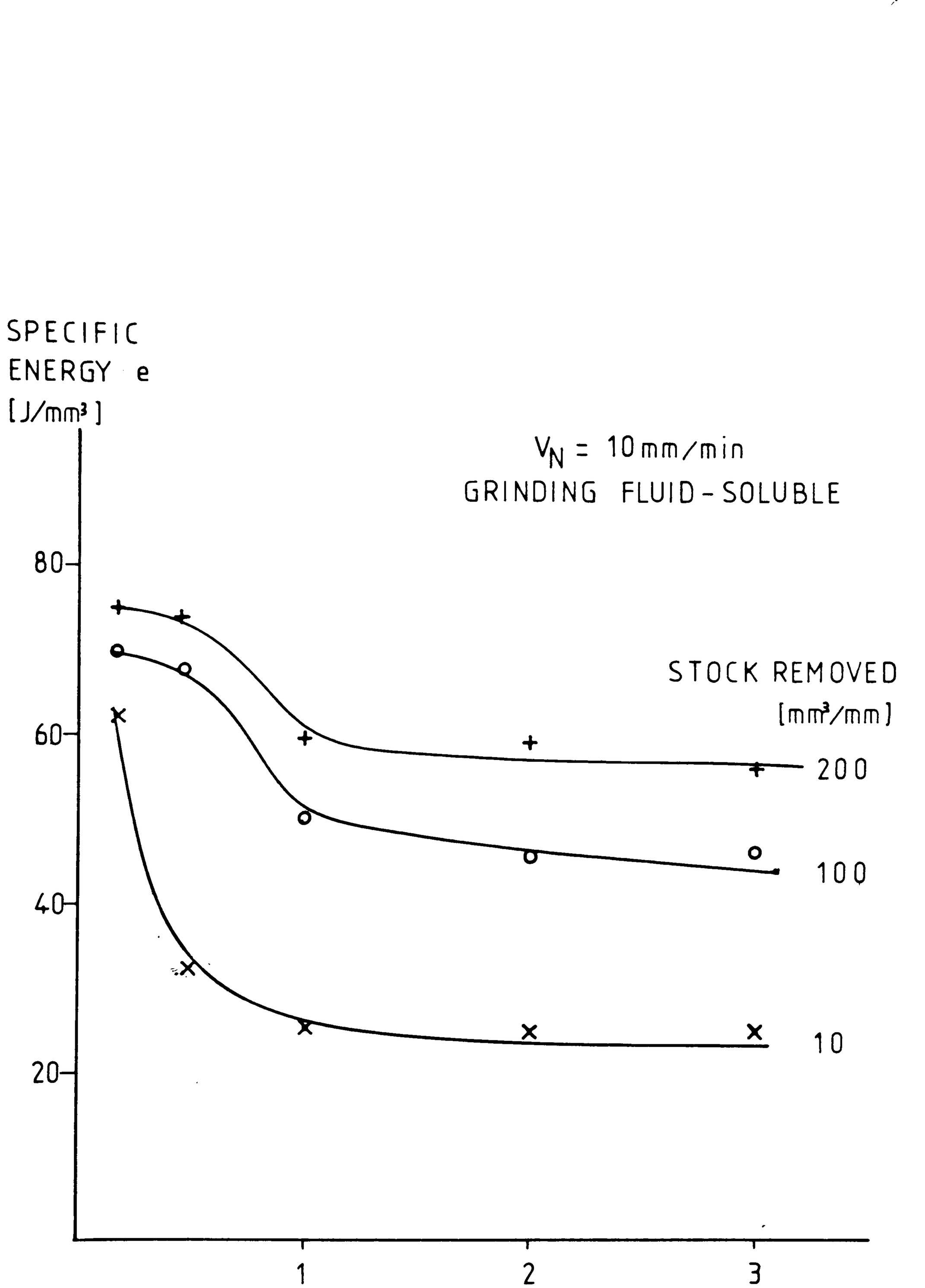

FIG 28 SPECIFIC ENERGY Vs. DRESSER INFEED RATE AFTER VARIOUS AMOUNTS OF STOCK REMOVED

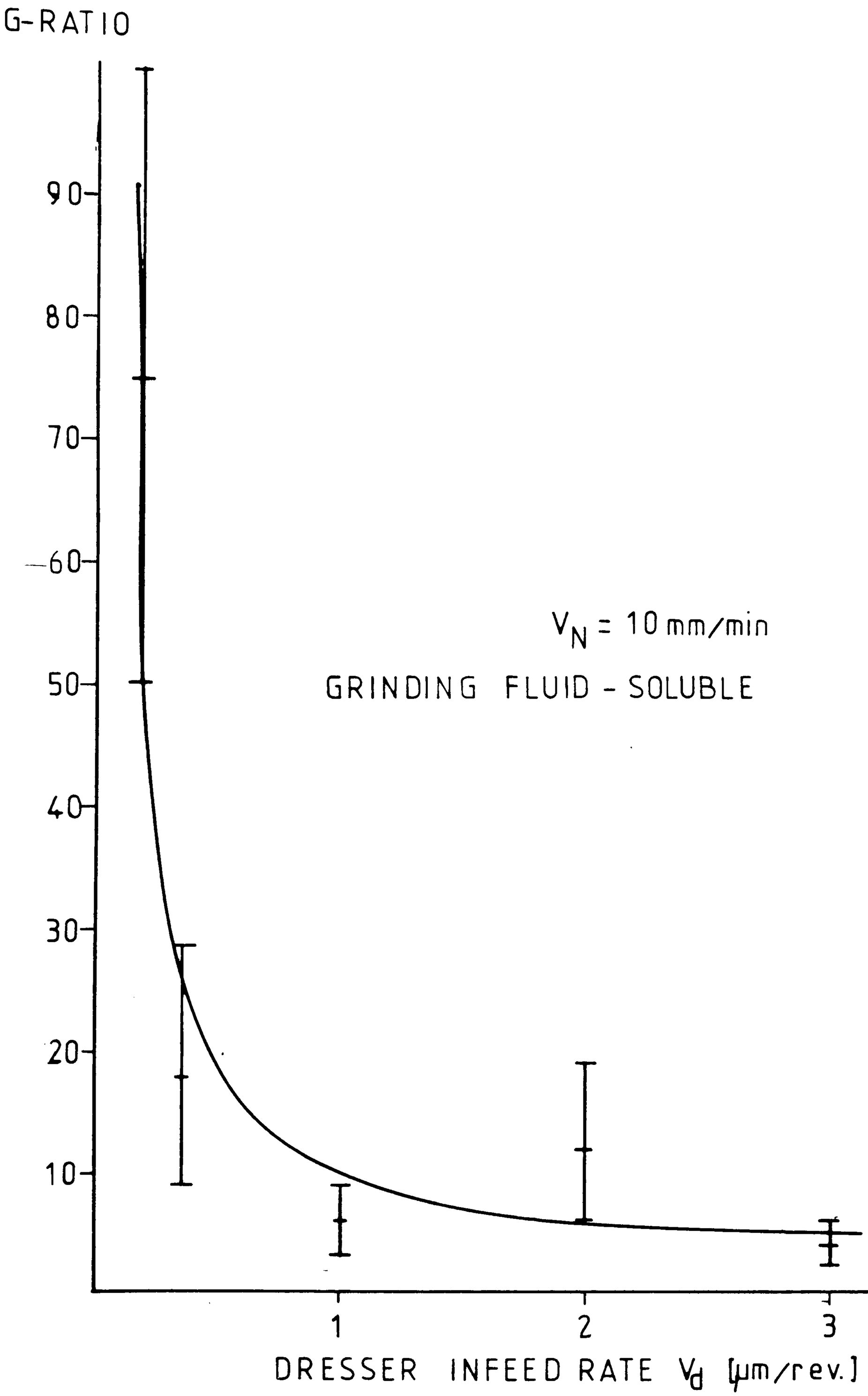

FIG 29 G RATIO Vs. DRESSER INFEED RATE

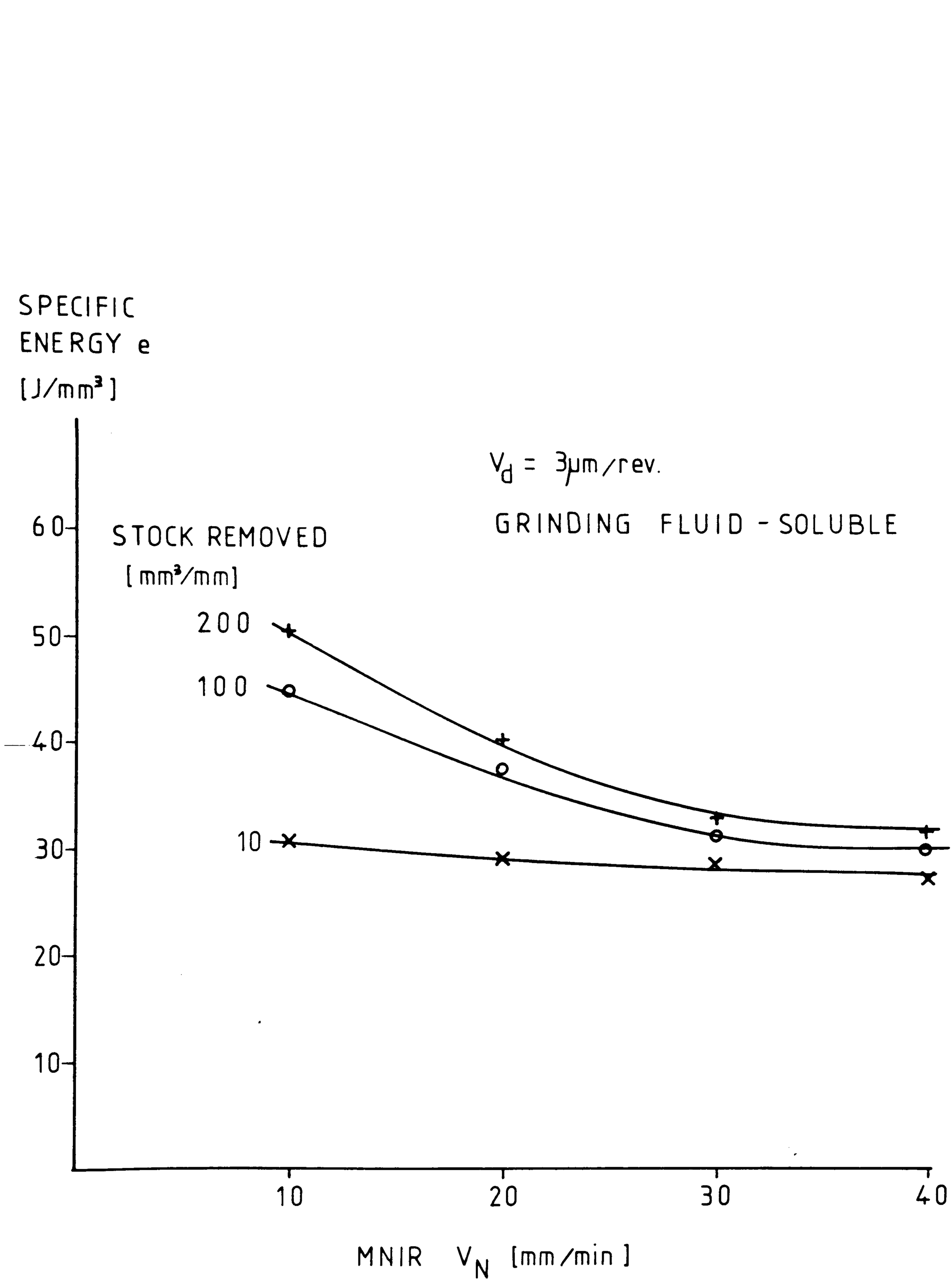

FIG 30 SPECIFIC ENERGY Vs. MNIR FOR VARIOUS AMOUNTS OF STOCK REMOVED

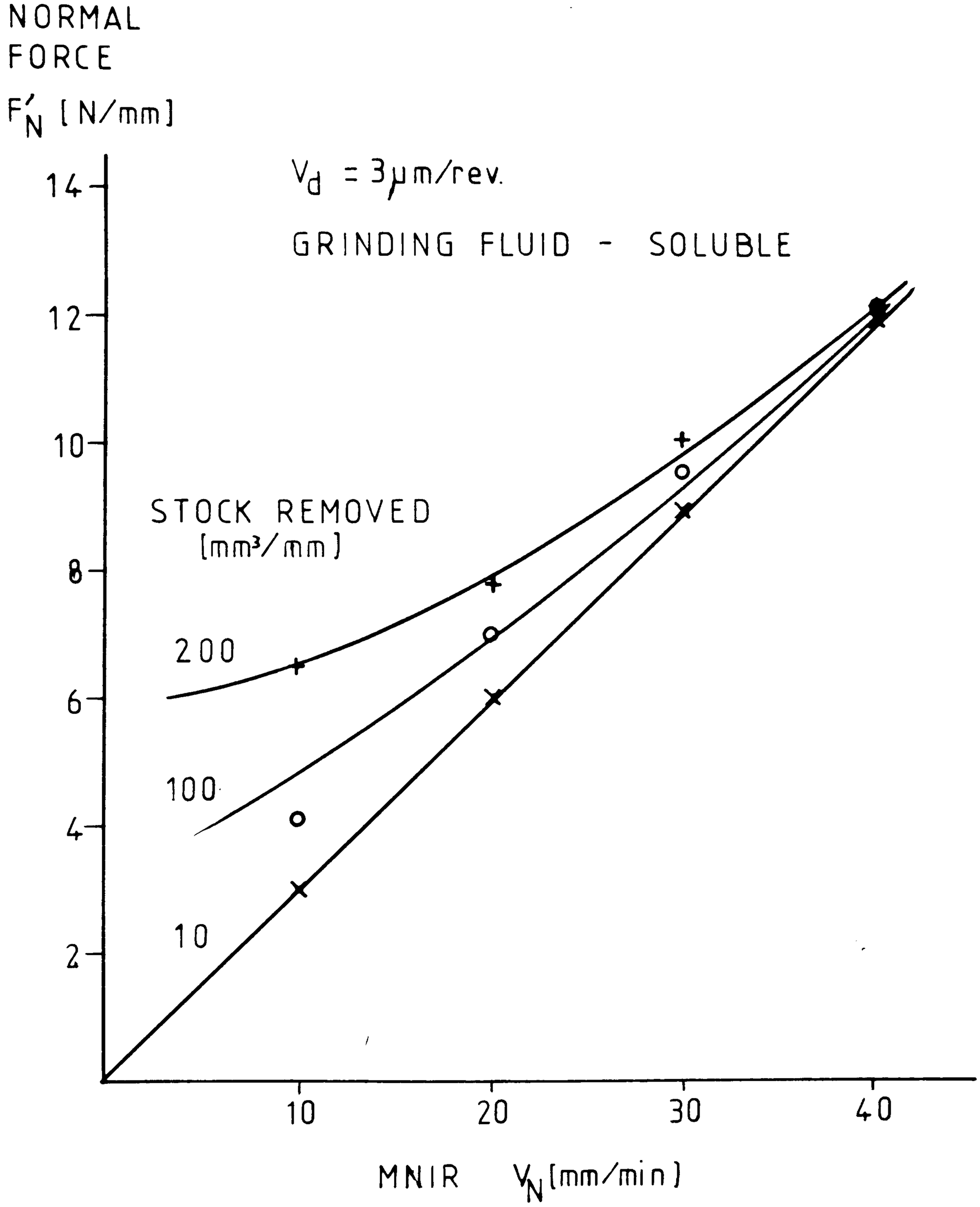

FIG 31 NORMAL FORCE Vs. MNIR AFTER VARIOUS AMOUNTS OF STOCK REMOVED

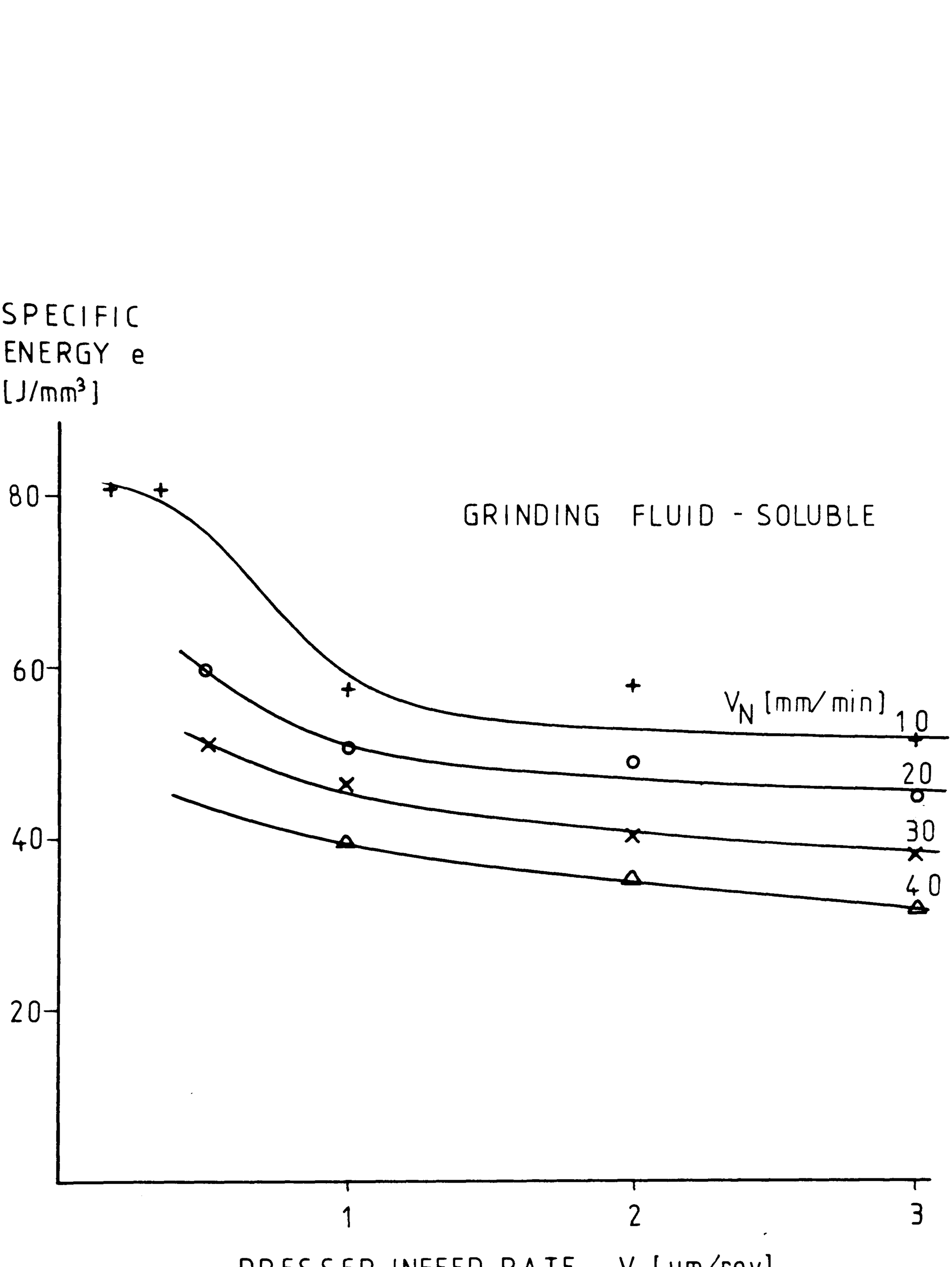

FIG 32 SUMMARY OF RESULTS AFTER 200 mm³/mm OF STOCK REMOVED

FACE ANGLE γ	SYMBOL	
	F'_N	F'_T
0°	×	+
40°	▲	△
80°	●	○

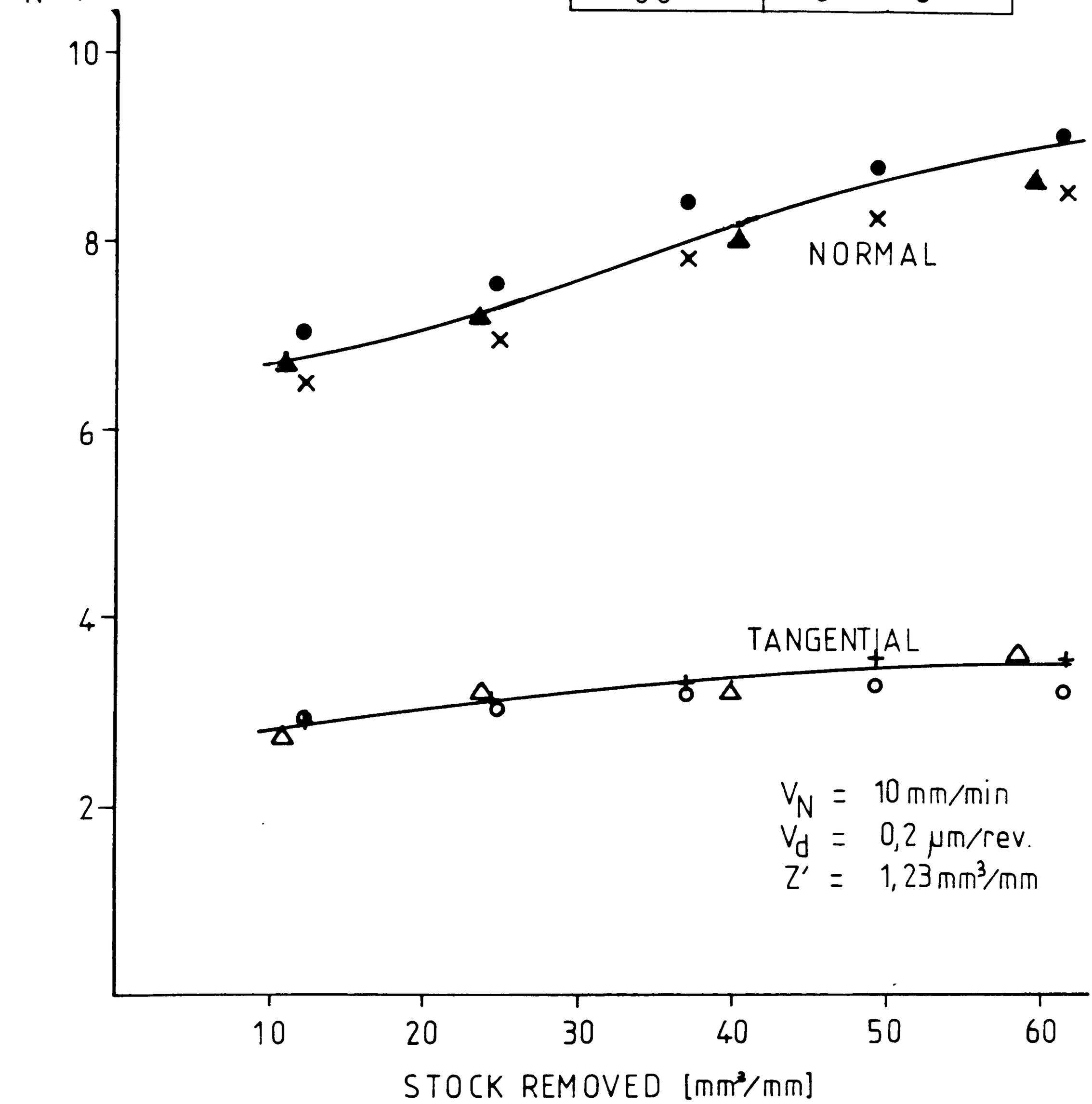

FIG 33 GRINDING FORCES Vs. STOCK REMOVED FOR TESTS CARRIED OUT AT DIFFERENT FACE ANGLES

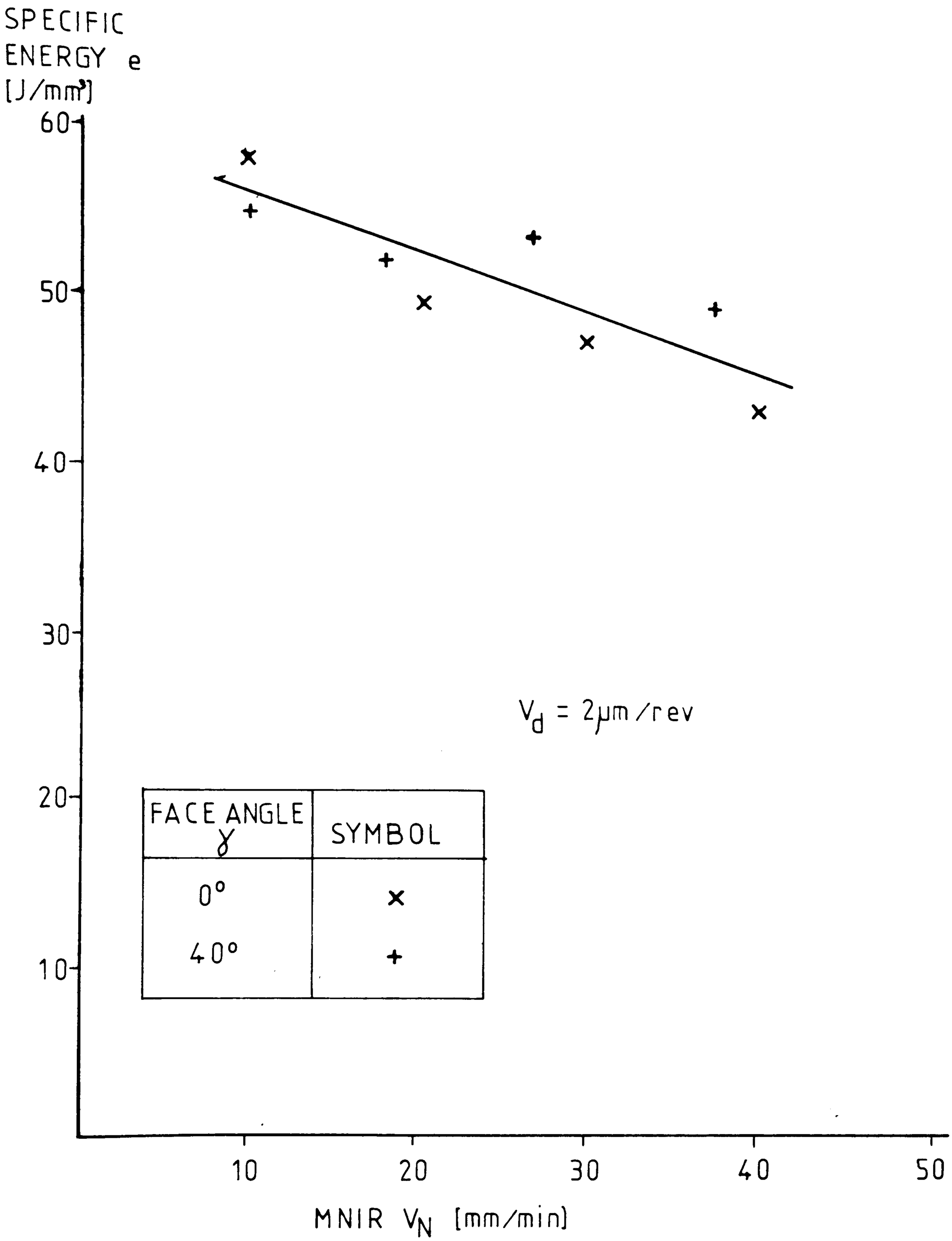

FIG 34 SPECIFIC GRINDING ENERY Vs. MNIR FOR DIFFERENT FACE ANGLES

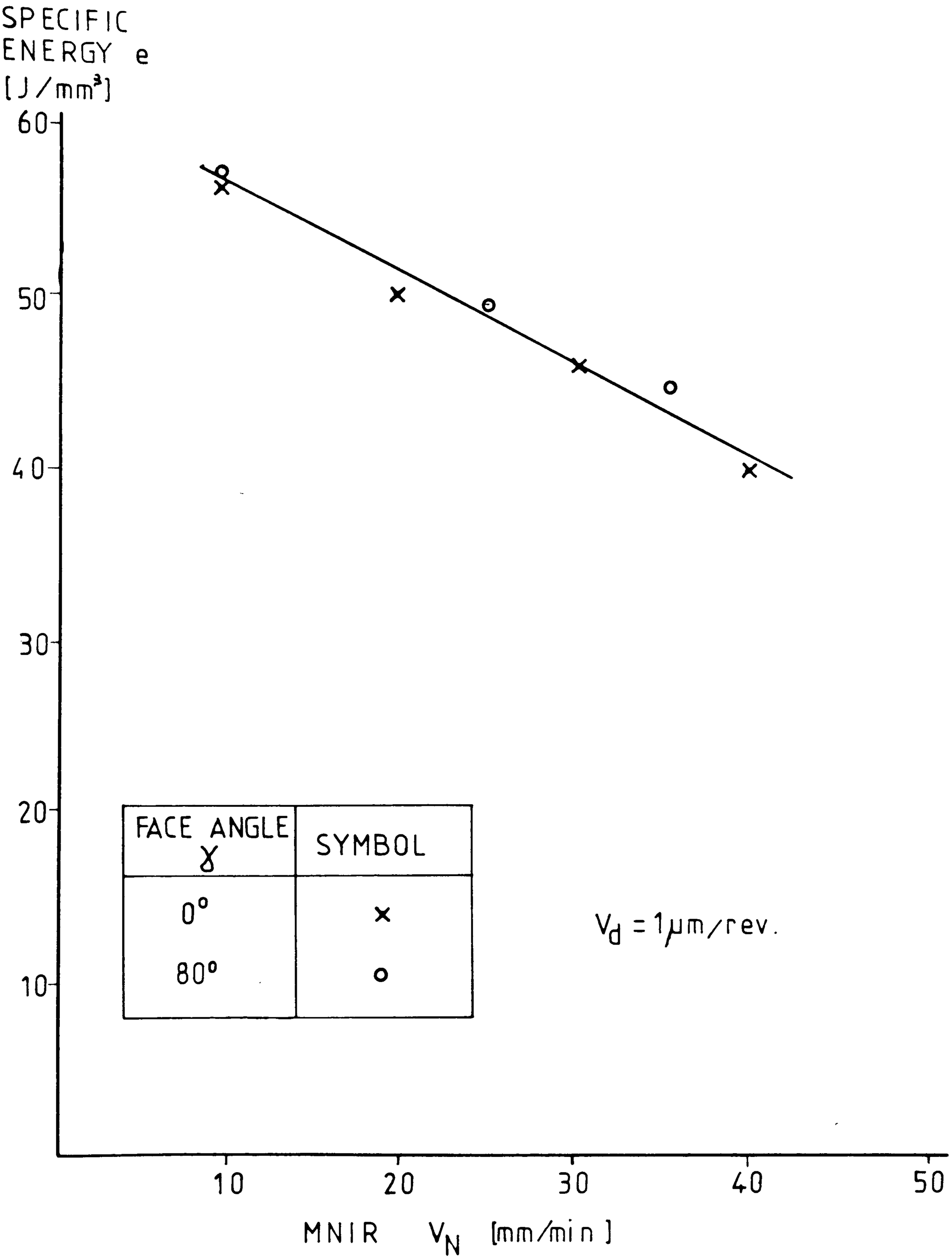

FIG 35 SPECIFIC ENERGY Vs. MNIR FOR DIFFERENT FACE ANGLES

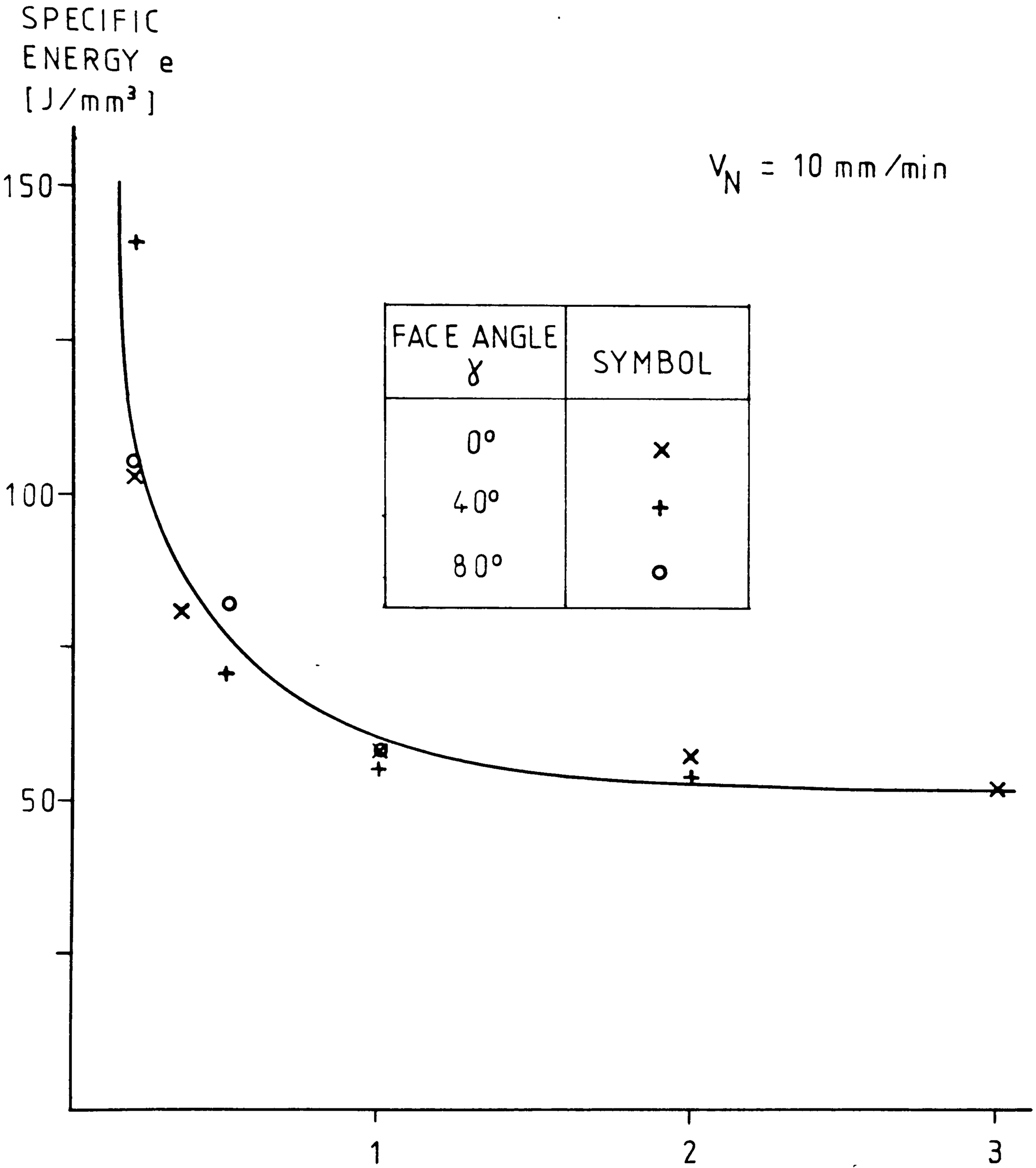

FIG 36 SPECIFIC ENERGY Vs. NORMAL DRESSER INFEED RATE FOR VARIOUS FACE ANGLES

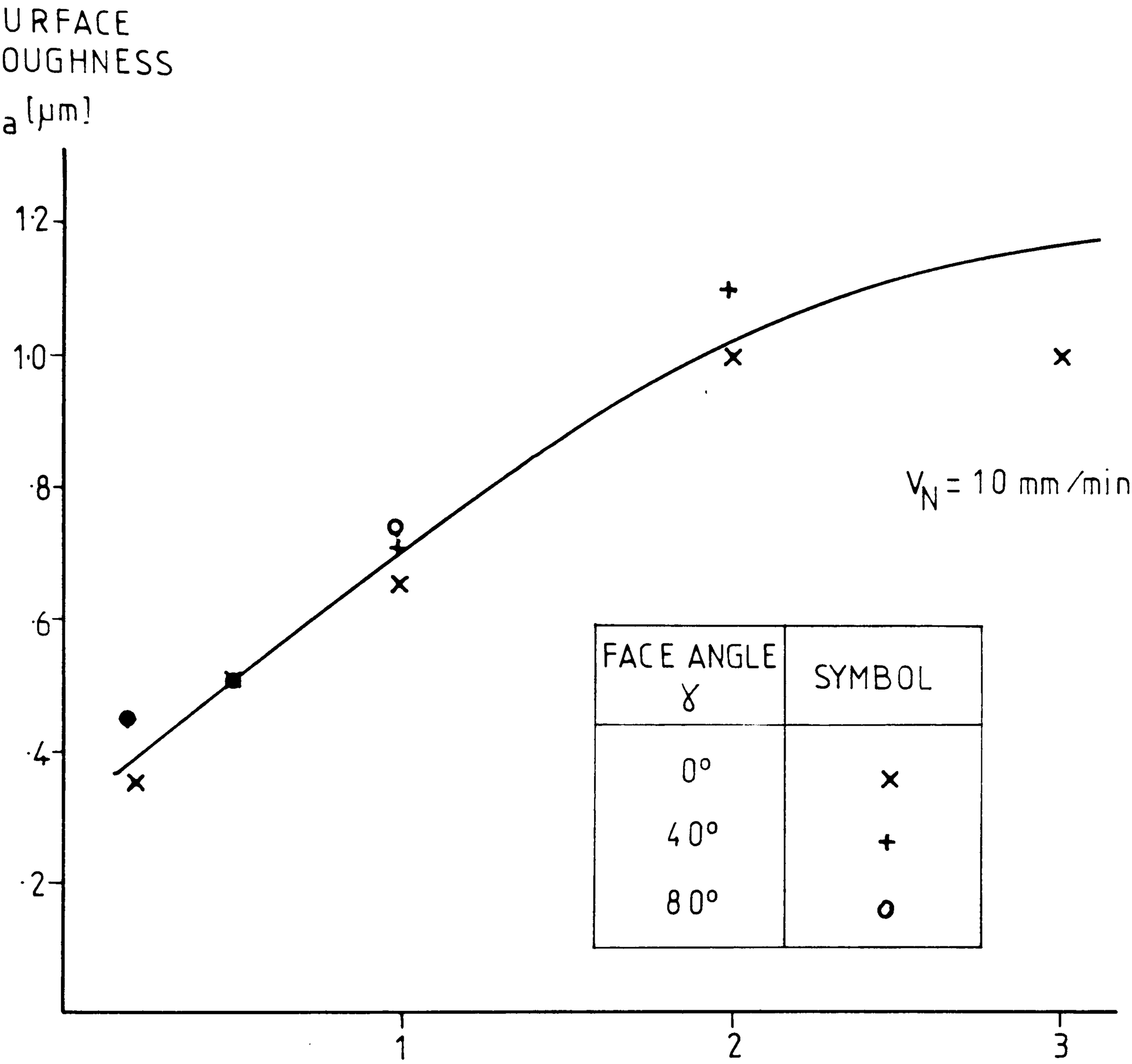

FIG 37 SURFACE FINISH Vs. NORMAL DRESSER INFEED RATE FOR VARIOUS FACE ANGLES

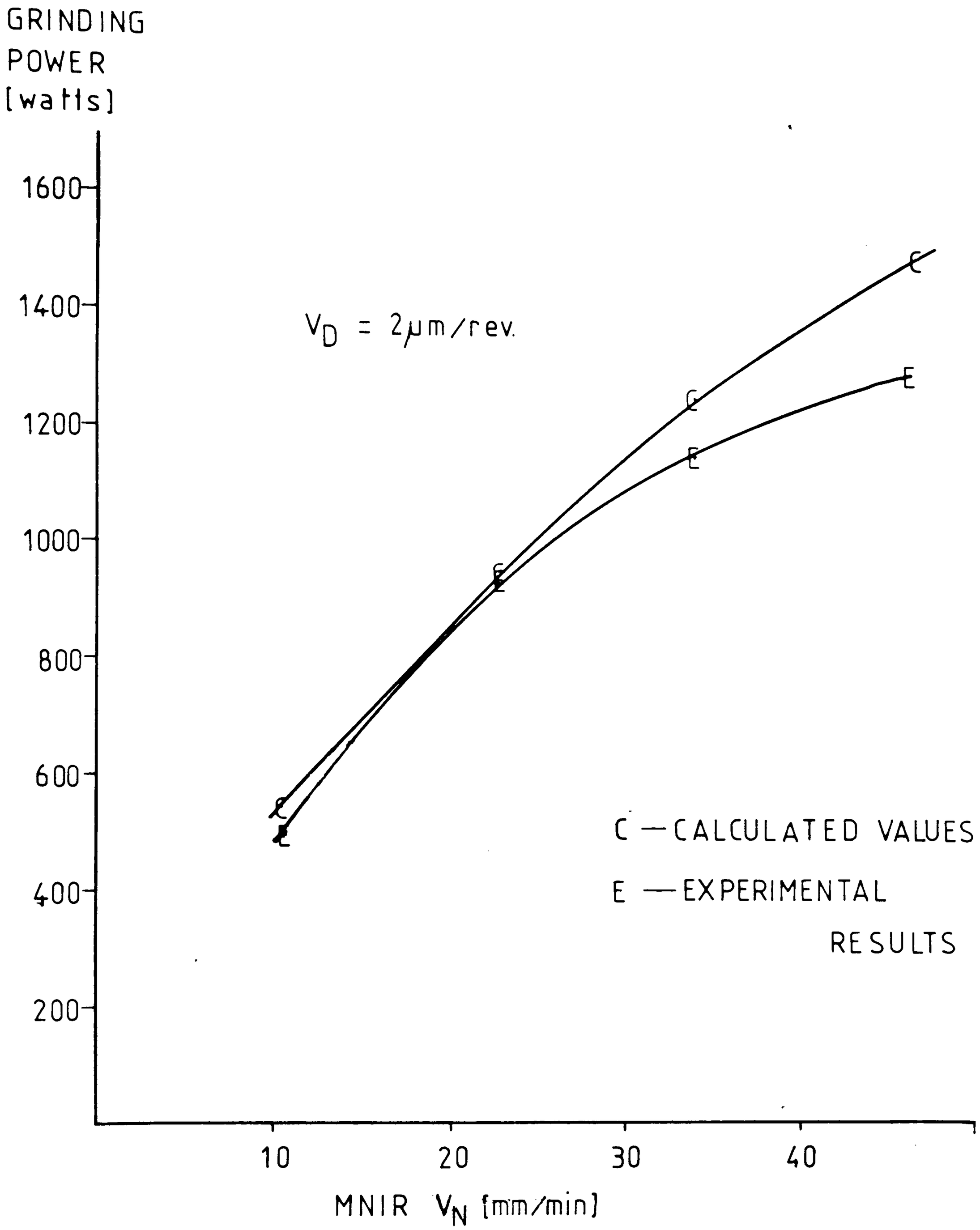

FIG 38 DERIVED AND EXPERIMENTAL VALUES OF GRINDING POWER Vs. MNIR FOR A FORM GRINDING OPERATION

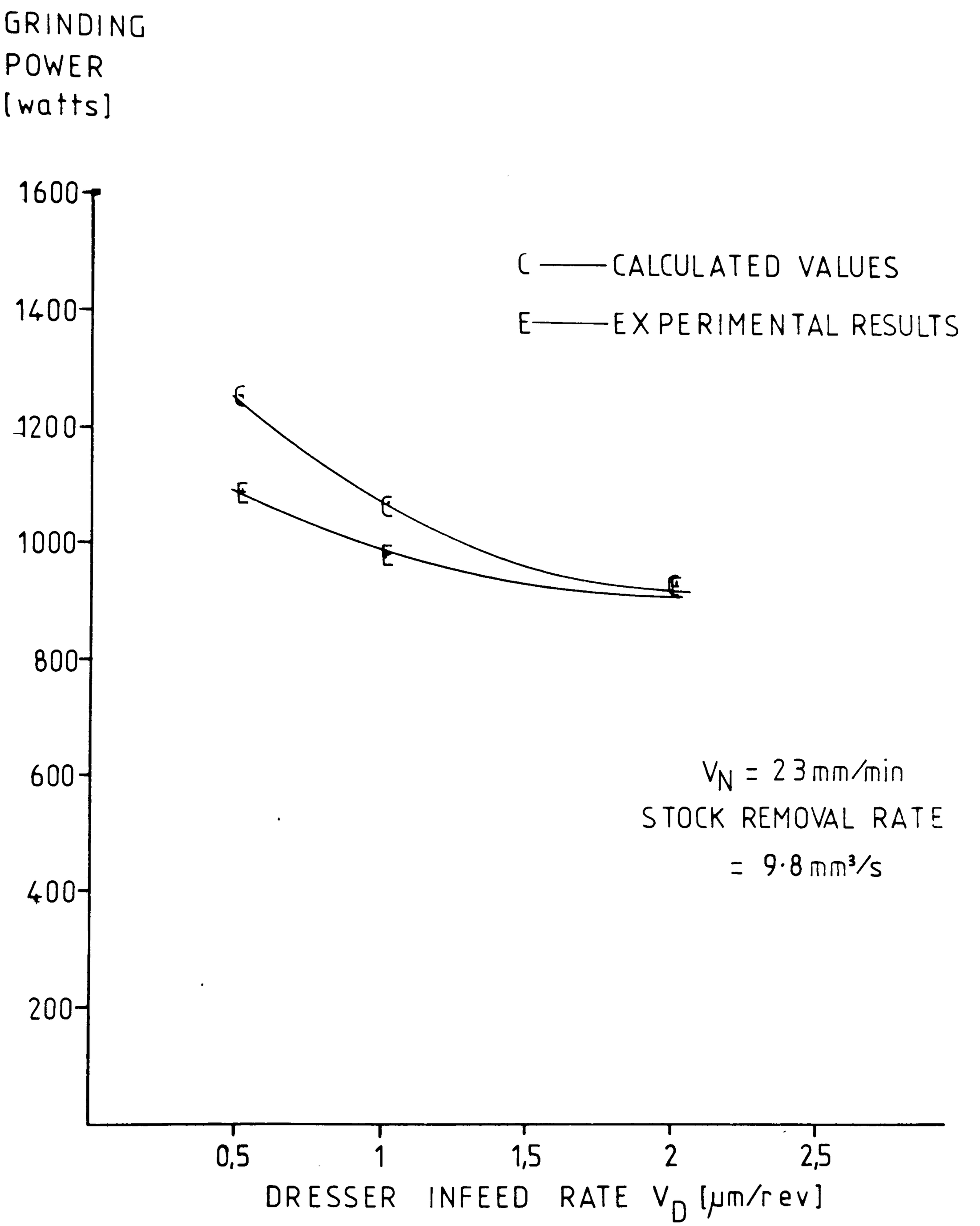

FIG 39 DERIVED AND EXPERIMENTAL VALUES OF GRINDING POWER Vs. DRESSER INFEED RATE FOR A FORM GRINDING OPERATION

	STEEL TYPE	HARDNESS V.P.N.
■	BS708A42 (EN19)	680
●	BS070M55 (EN9)	700
□	BS708A42	180
○	BS070M55	200
△	BS080A22 (EN3)	180

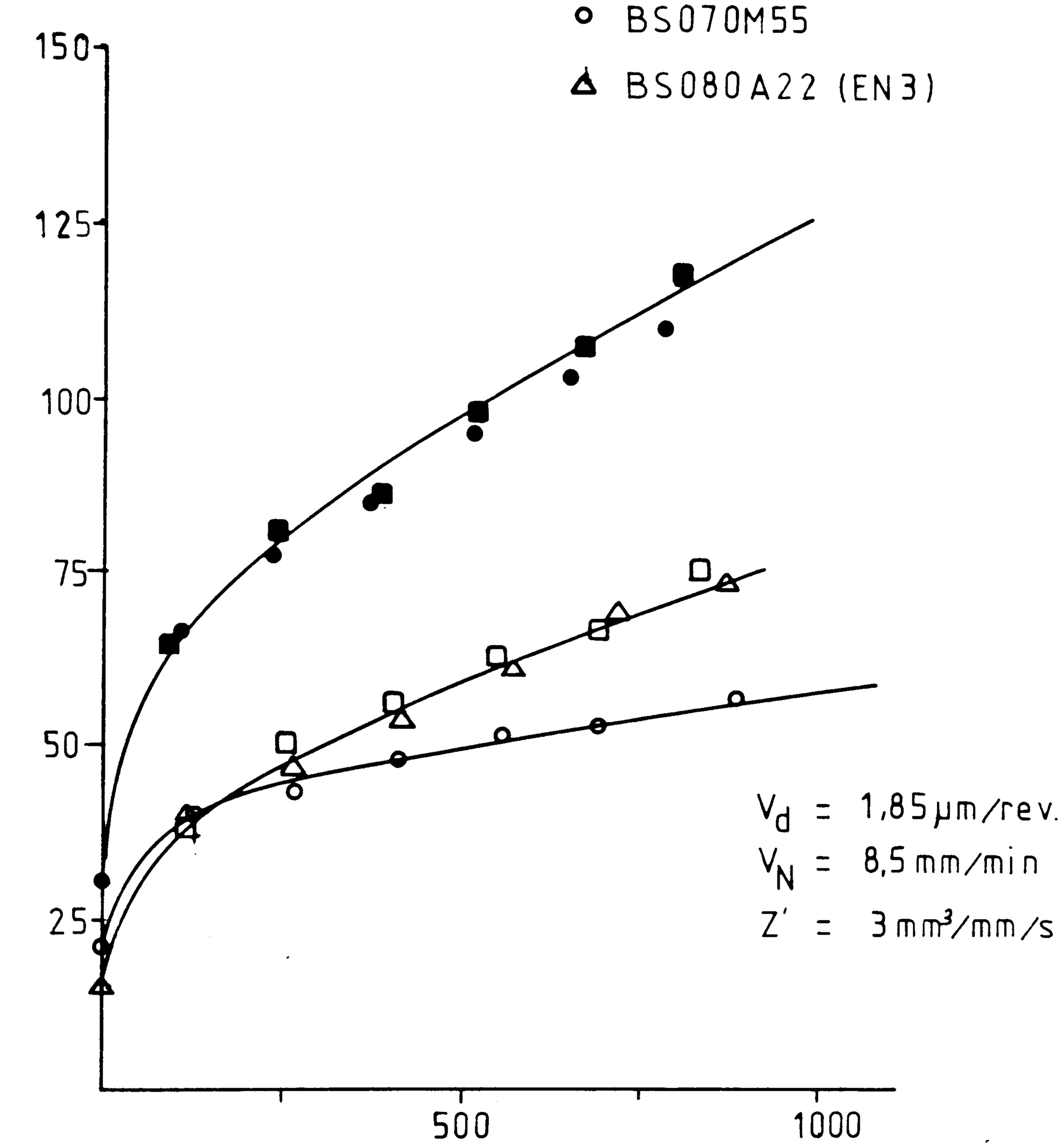

FIG 40 SPECIFIC ENERGY Vs. STOCK REMOVED FOR VARIOUS MATERIAL SPECIFICATIONS

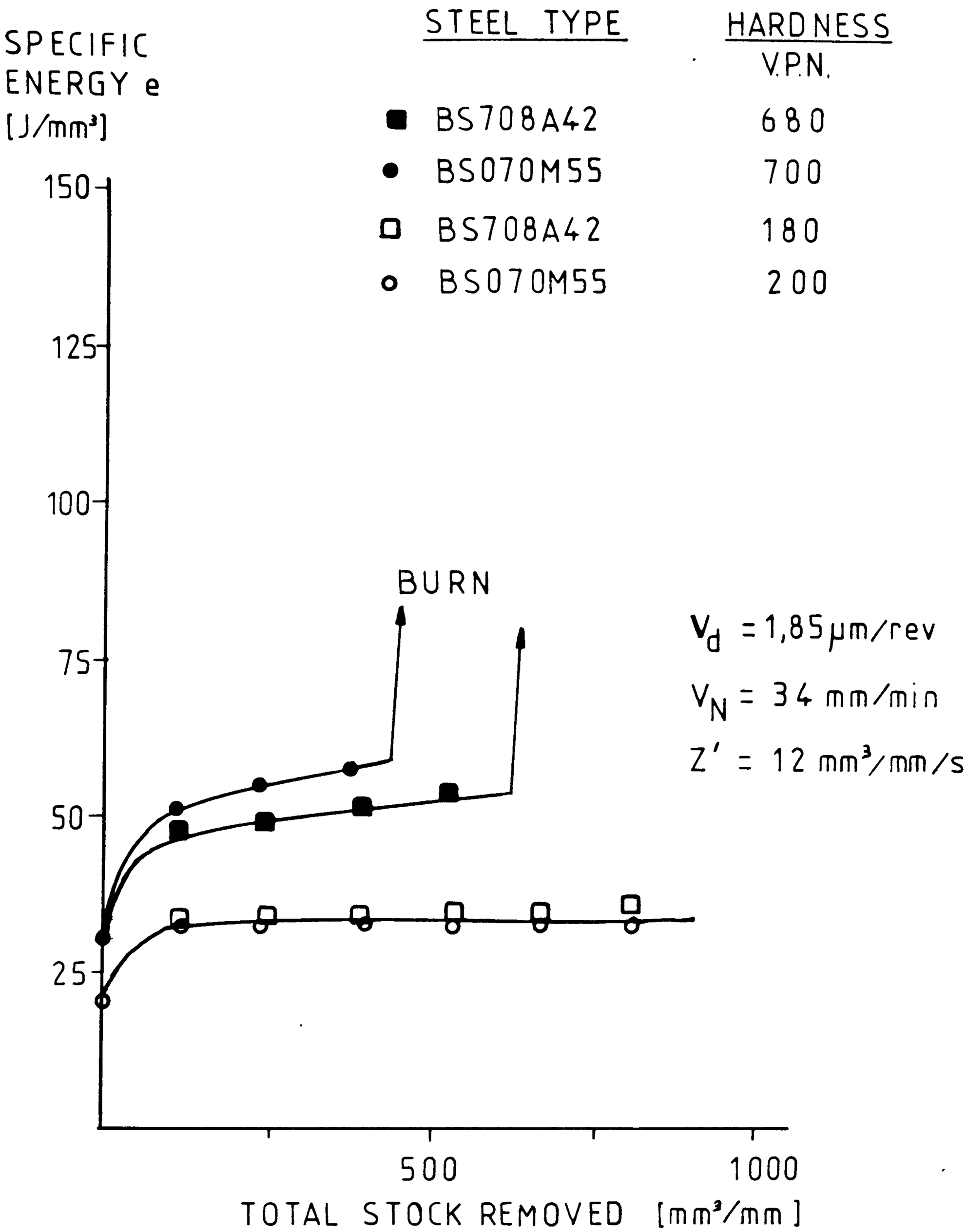

FIG 41 SPECIFIC ENERGY Vs. STOCK REMOVED FOR VARIOUS MATERIAL SPECIFICATIONS

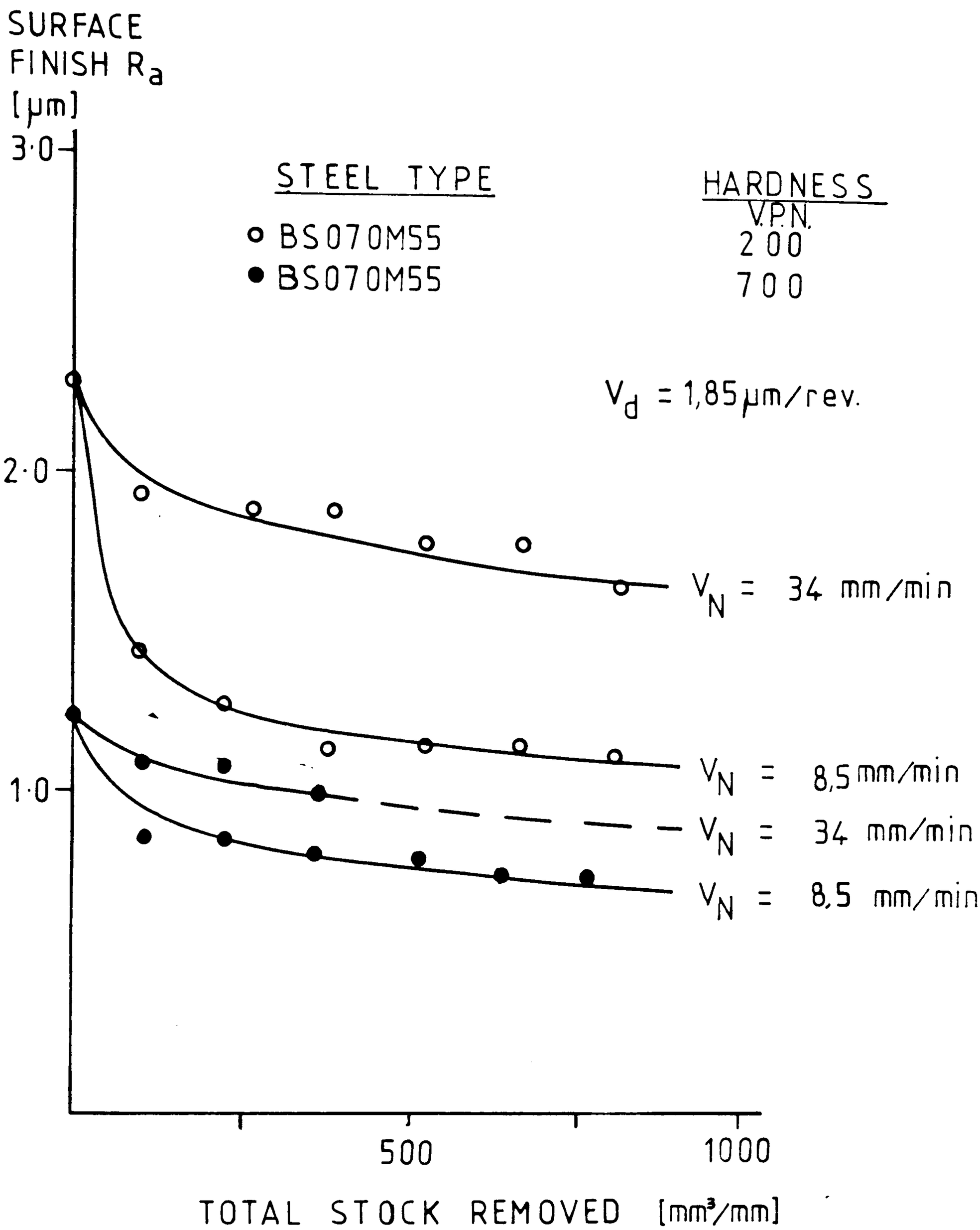

FIG 42 SURFACE FINISH Vs. STOCK REMOVED FOR A STEEL IN BOTH SOFT AND HARD CONDITIONS

Text cut off in original

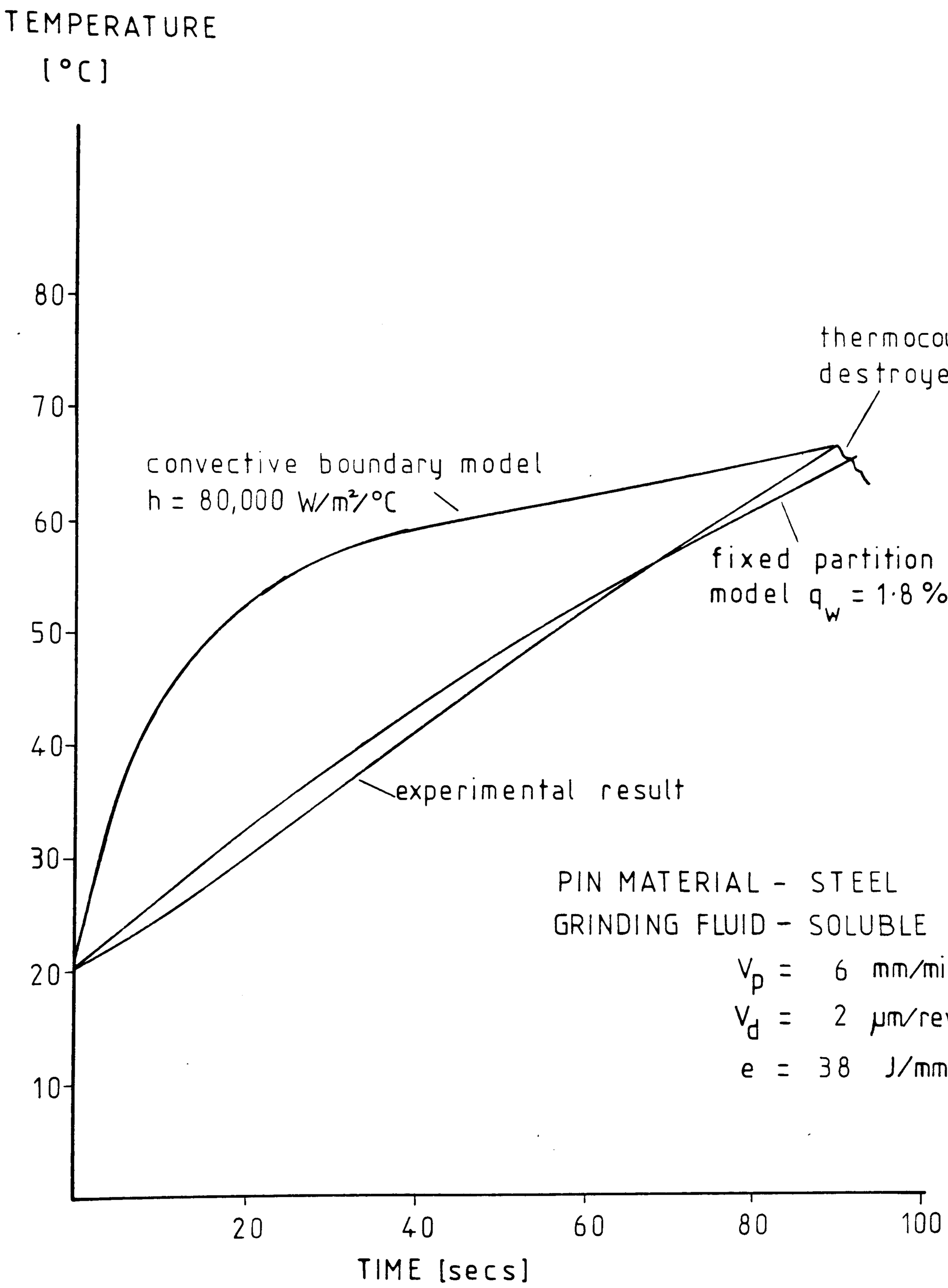

FIG 43 TEMPERATURE Vs TIME FOR AN INSULATED PIN GRINDING TEST

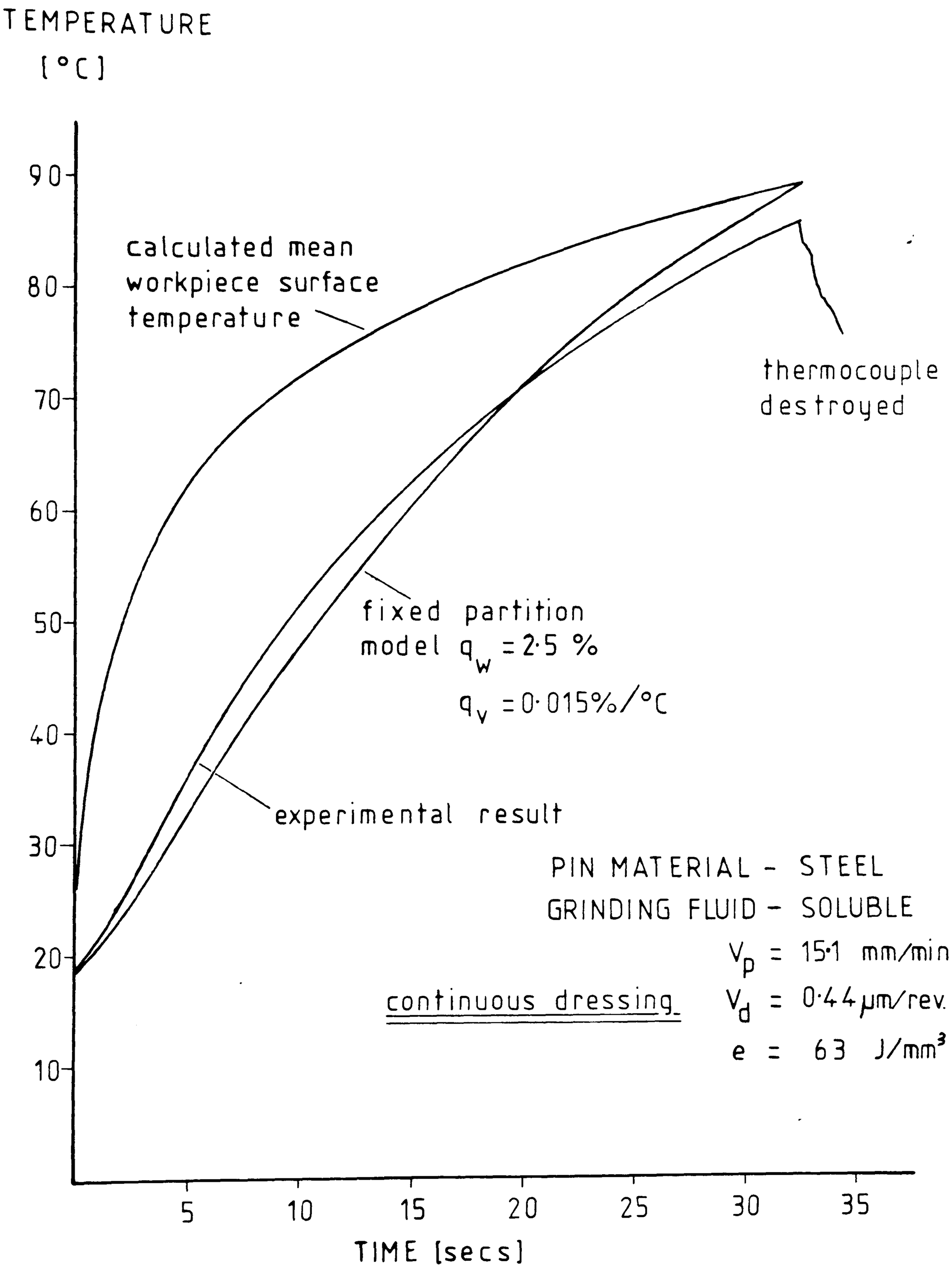

FIG 44 TEMPERATURE Vs TIME FOR AN INSULATED PIN GRINDING TEST

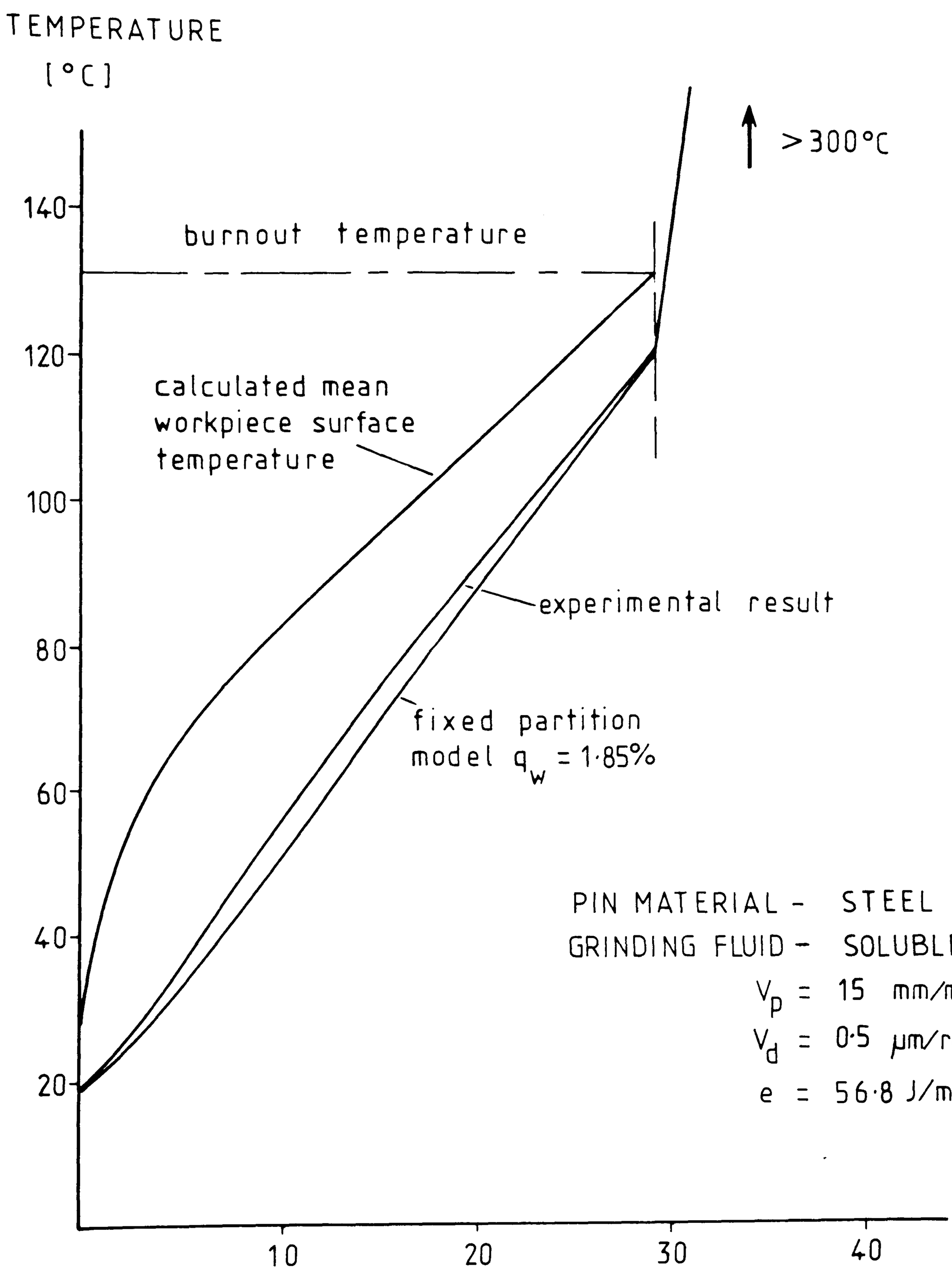

FIG 45 TEMPERATURE Vs TIME FOR AN INSULATED PIN GRINDING TEST

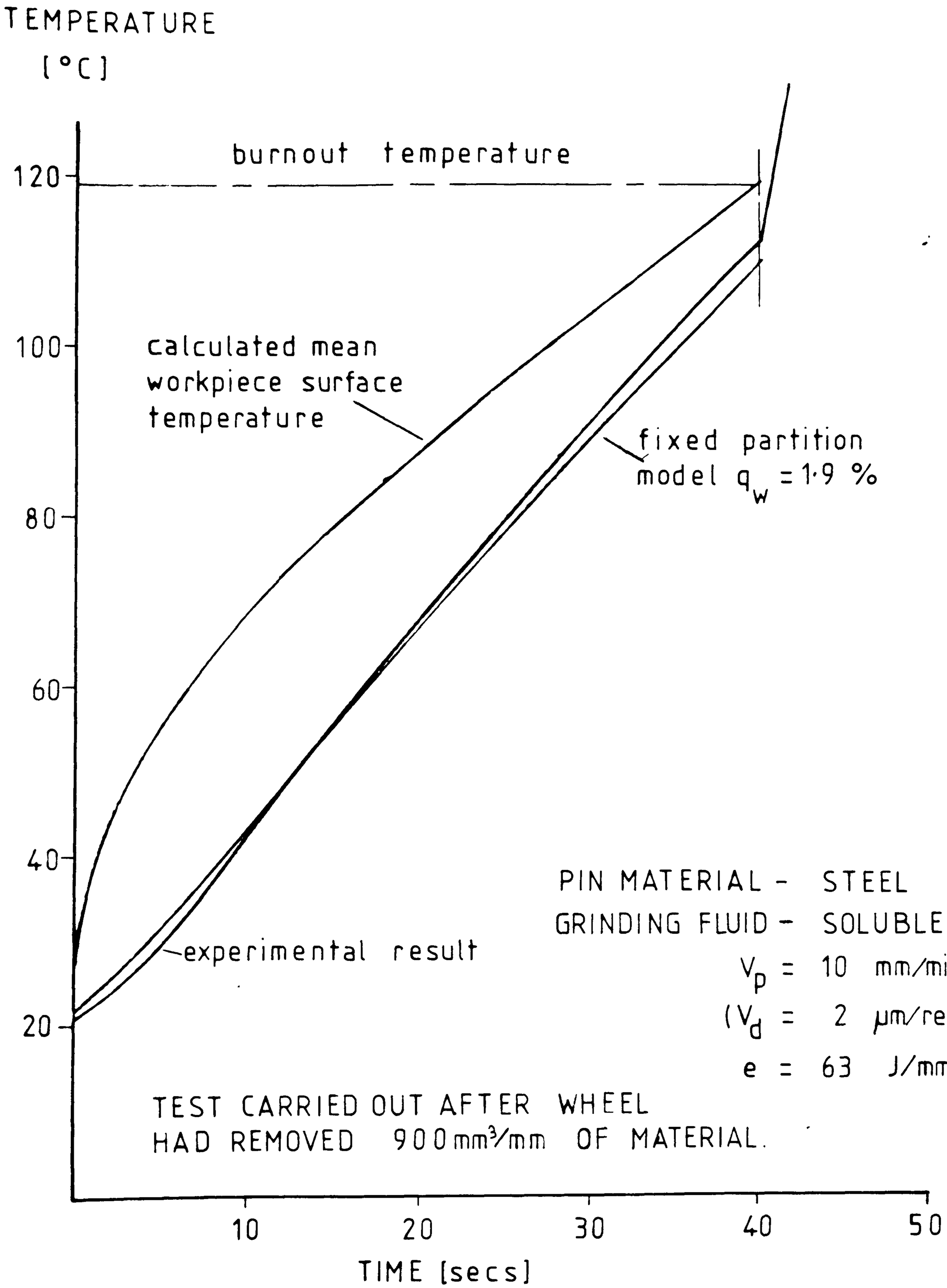

FIG 46 TEMPERATURE Vs TIME FOR AN INSULATED PIN GRINDING TEST

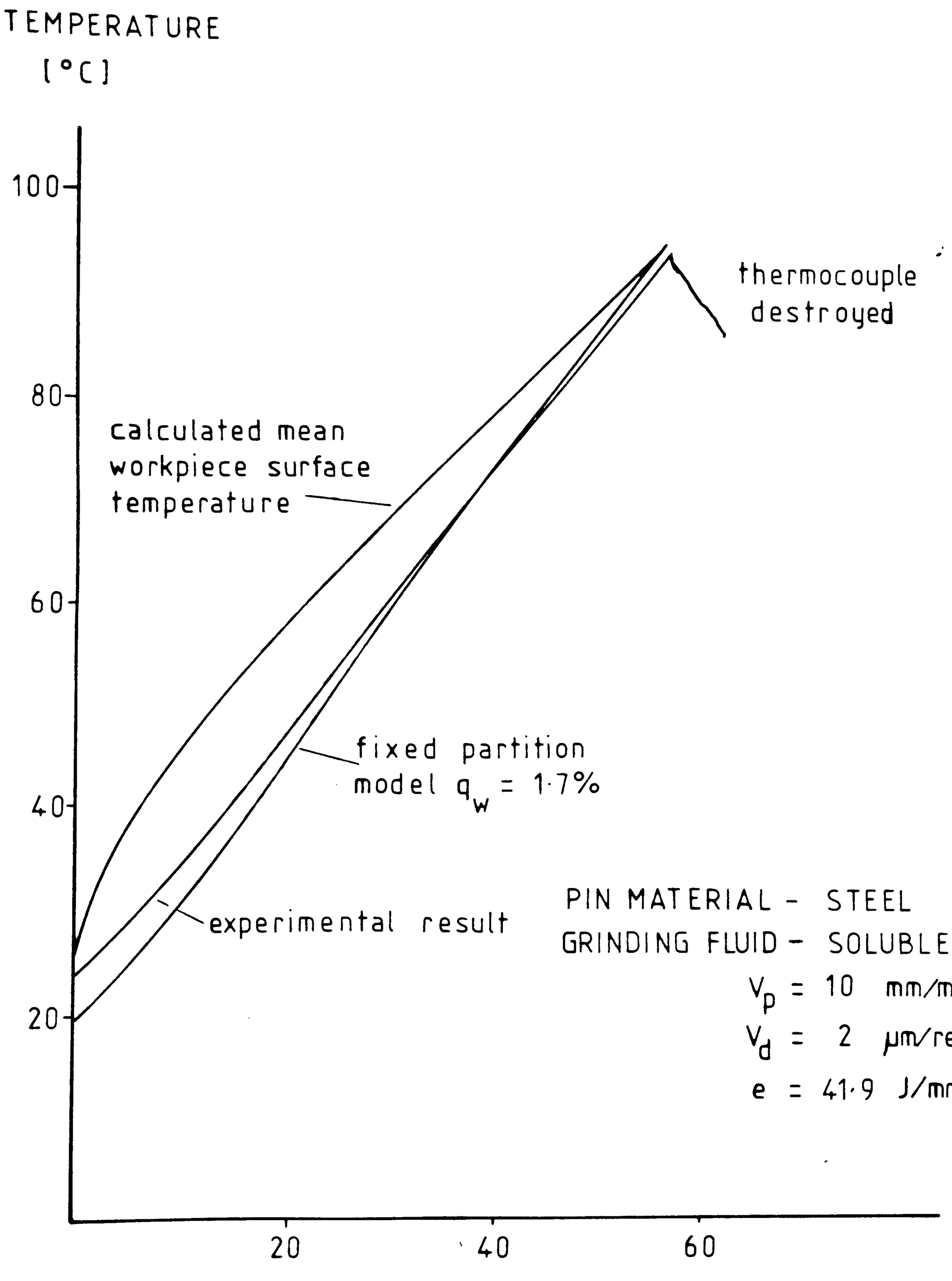

FIG 47 TEMPERATURE Vs TIME FOR AN INSULATED PIN GRINDING TEST

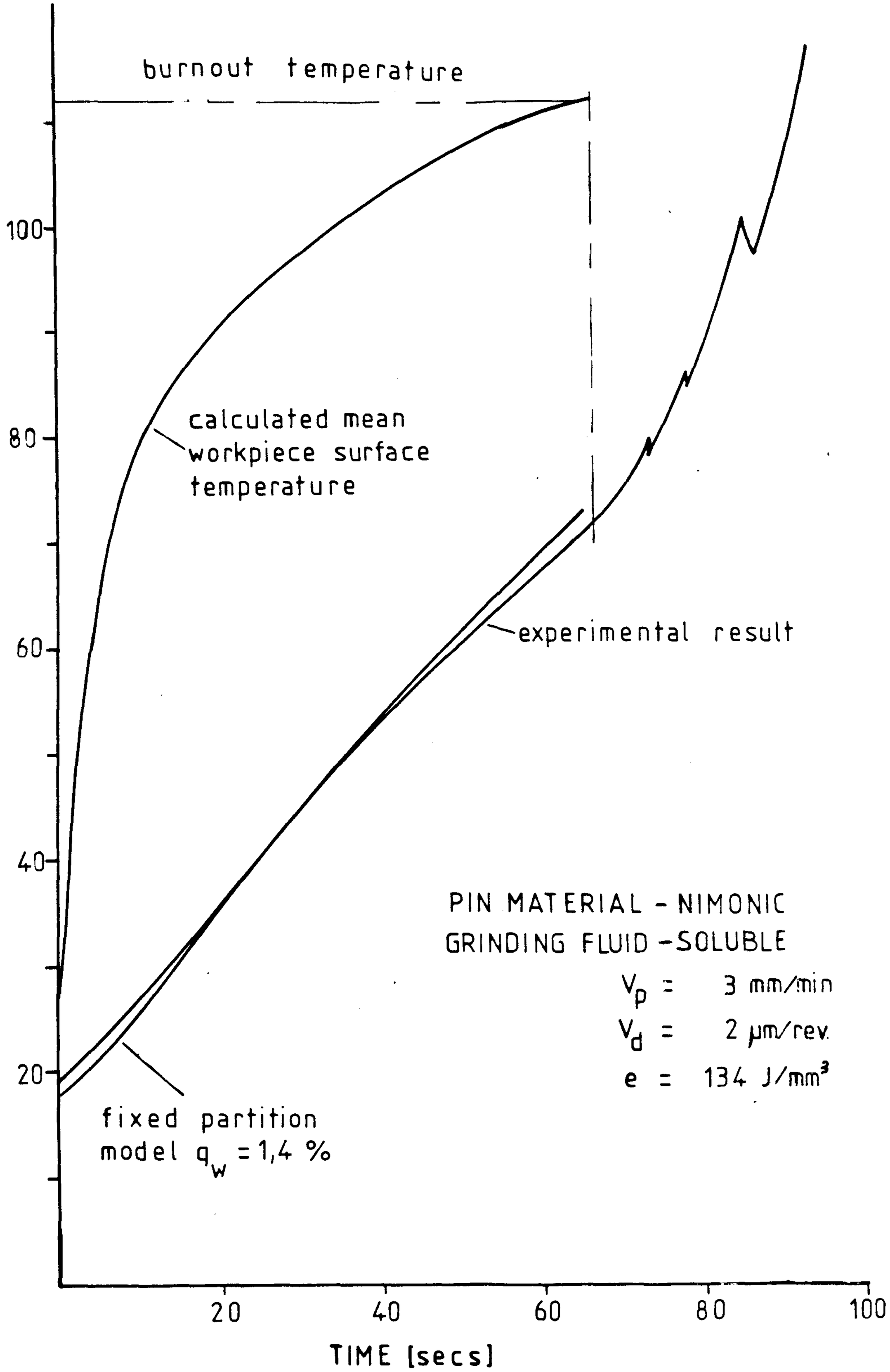

FIG 48 TEMPERATURE Vs TIME FOR AN INSULATED PIN GRINDING TEST

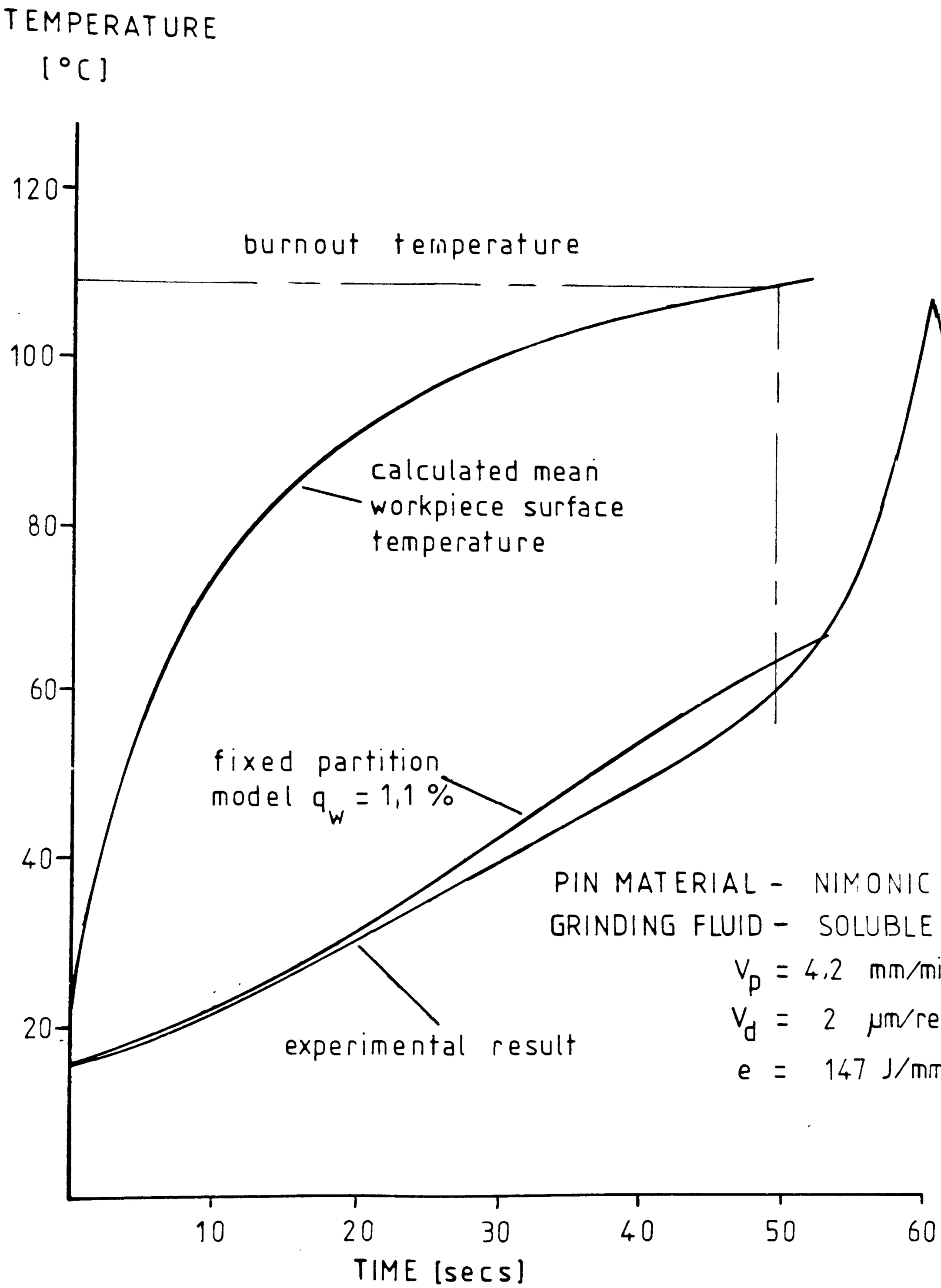

FIG 49 TEMPERATURE Vs TIME FOR AN INSULATED PIN GRINDING TEST

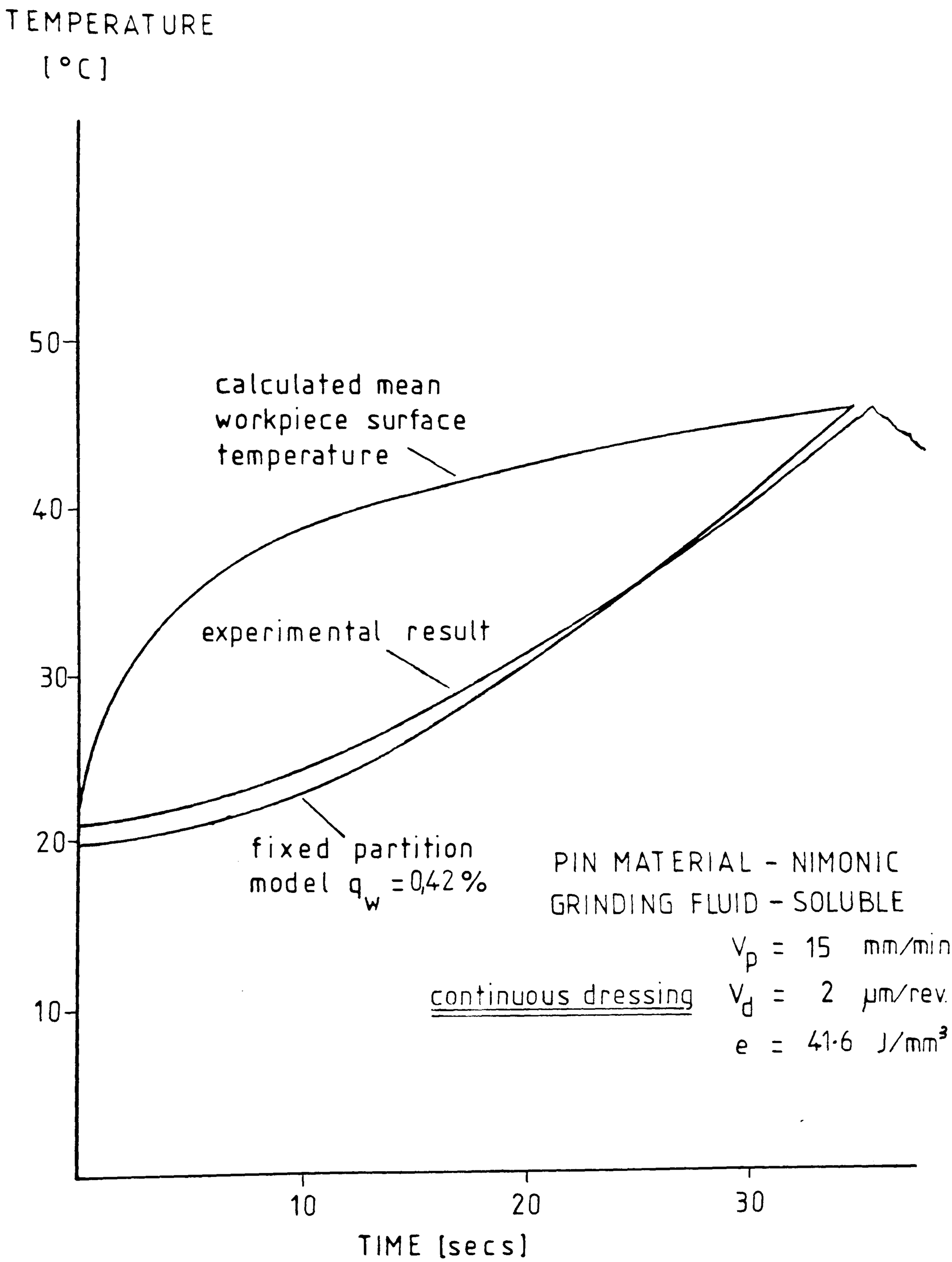

FIG 50 TEMPERATURE Vs TIME FOR AN INSULATED PIN GRINDING TEST

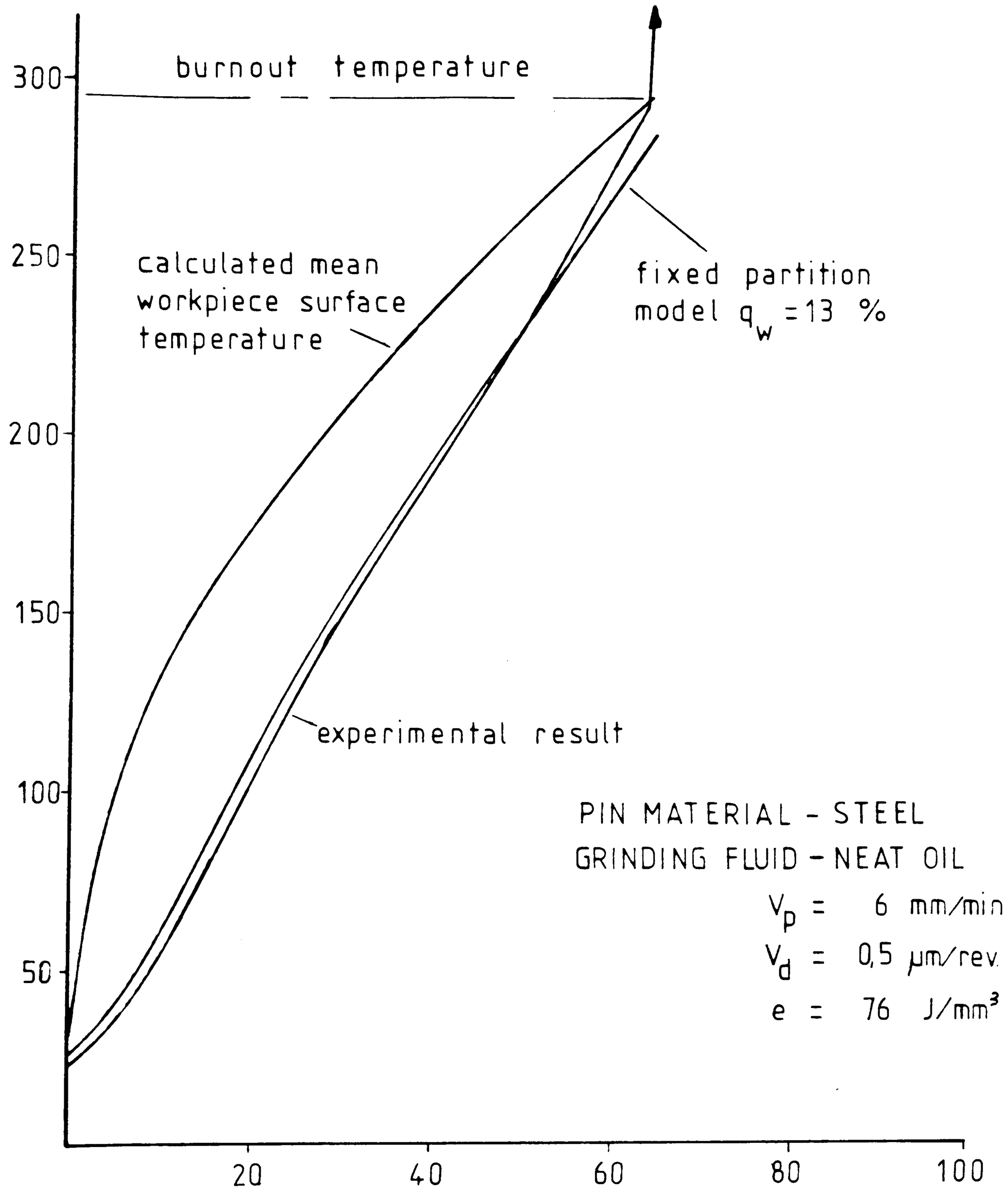

FIG 51 TEMPERATURE Vs TIME FOR AN INSULATED PIN GRINDING TEST

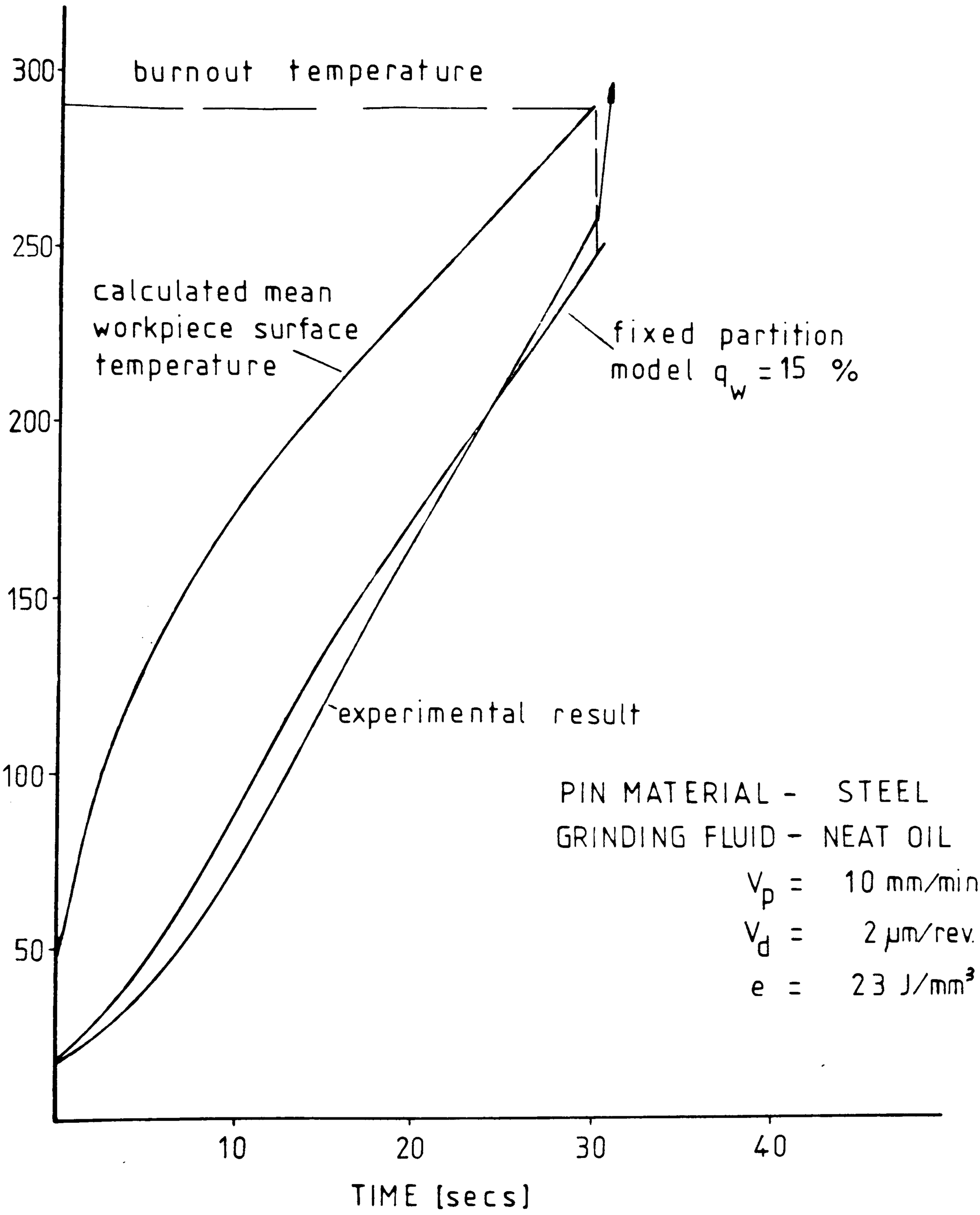

FIG 52 TEMPERATURE Vs TIME FOR AN INSULATED PIN GRINDING TEST

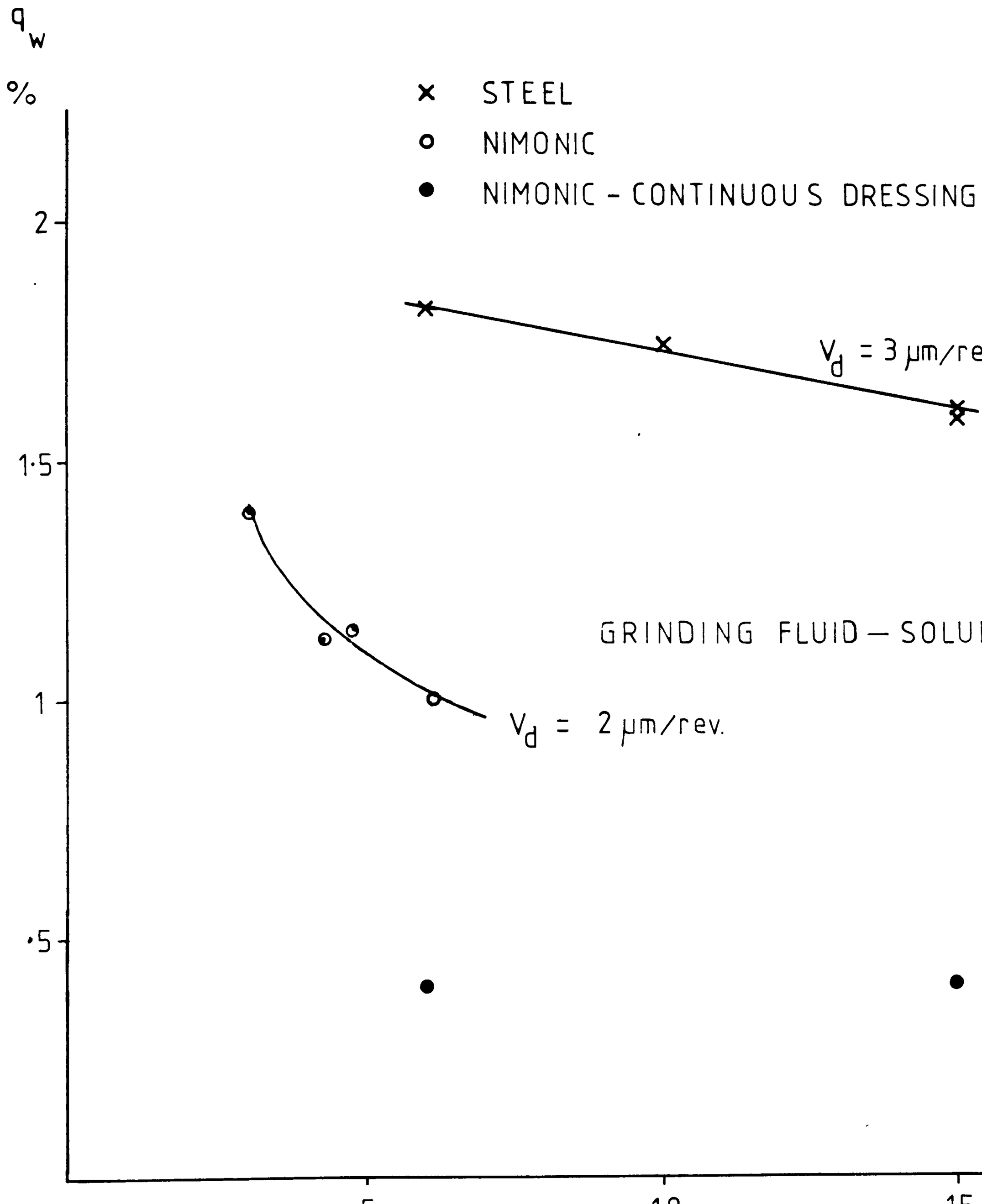

FIG 53 ENERGY PARTITIONING Vs. INFEED RATE FOR STEEL AND NIMONIC PINS

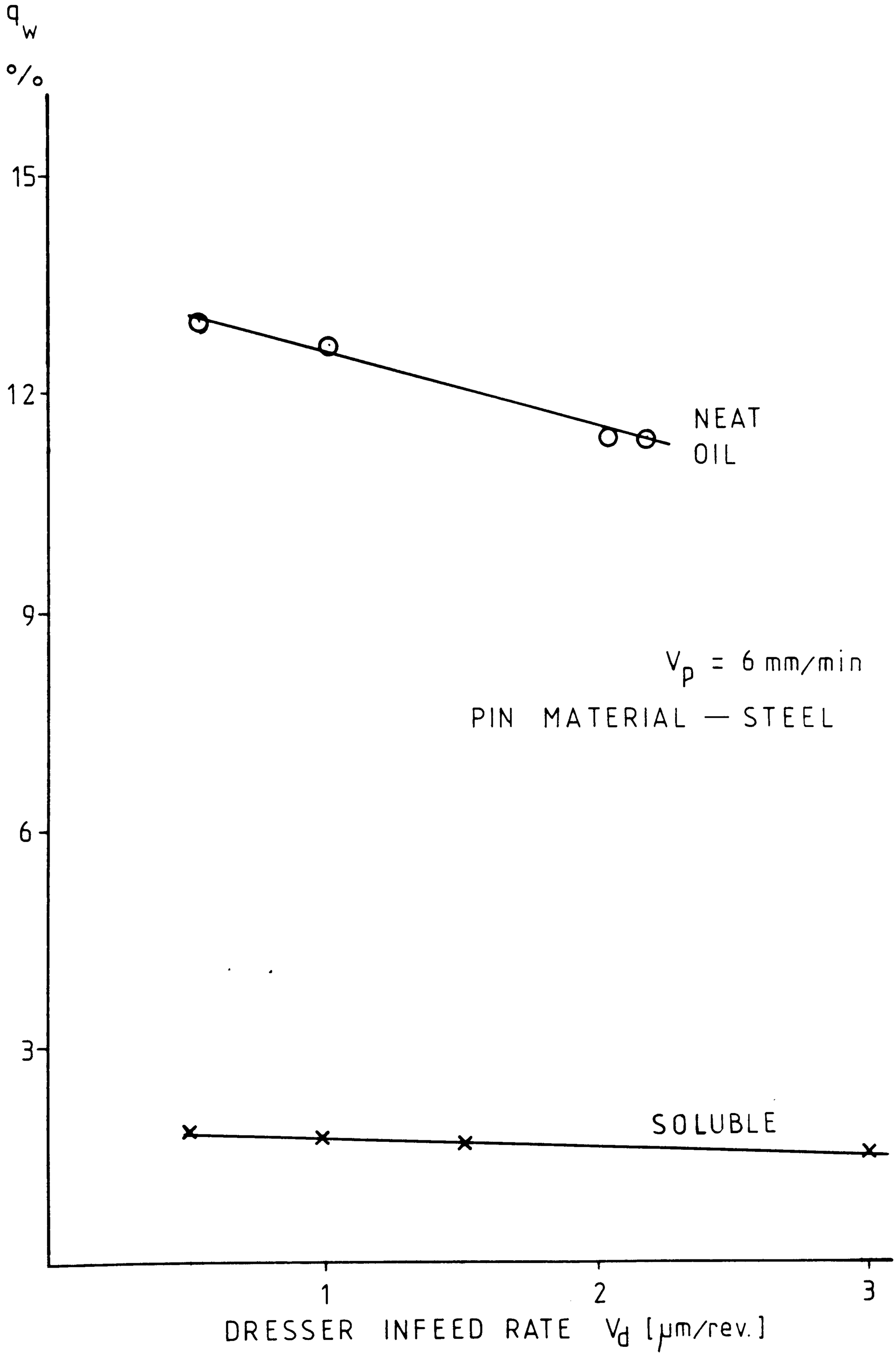

FIG 54 ENERGY PARTITIONING Vs. DRESSER INFEED RATE FOR OIL AND WATER BASED GRINDING FLUIDS

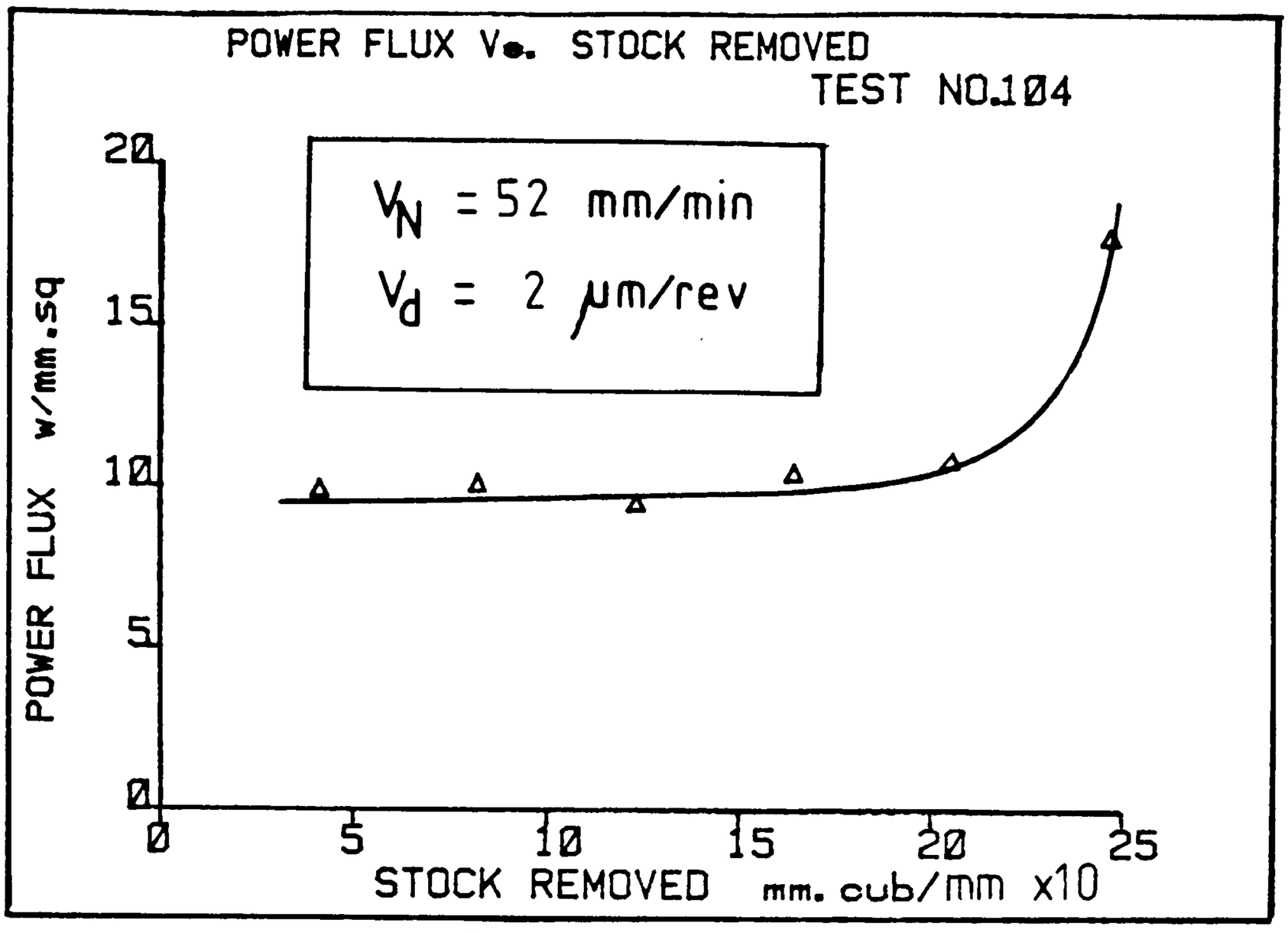

FIG 55

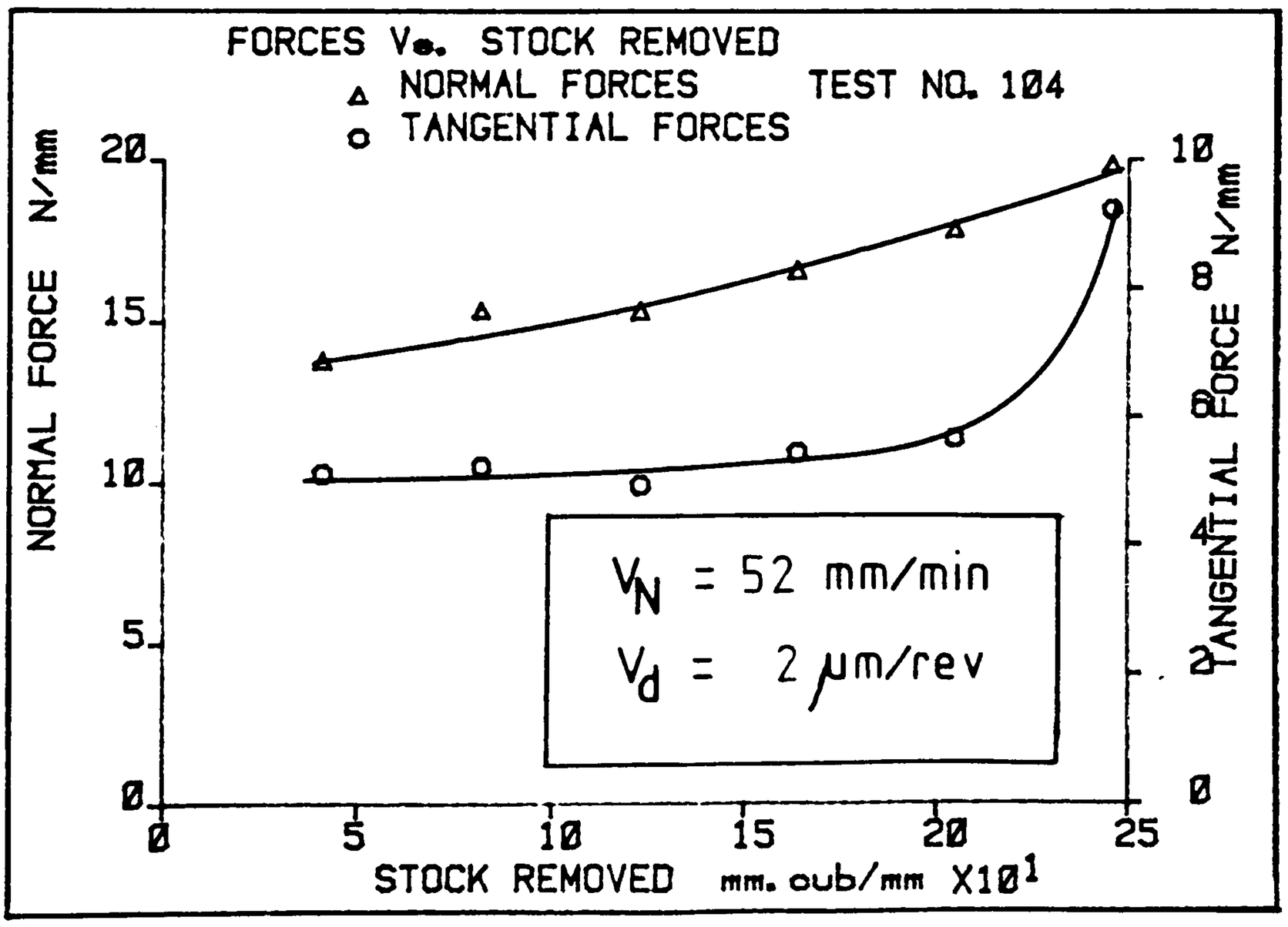

FIG 56

POWER FLUX AND GRINDING FORCES Vs. STOCK REMOVED WITH NEAT OIL GRINDING FLUID

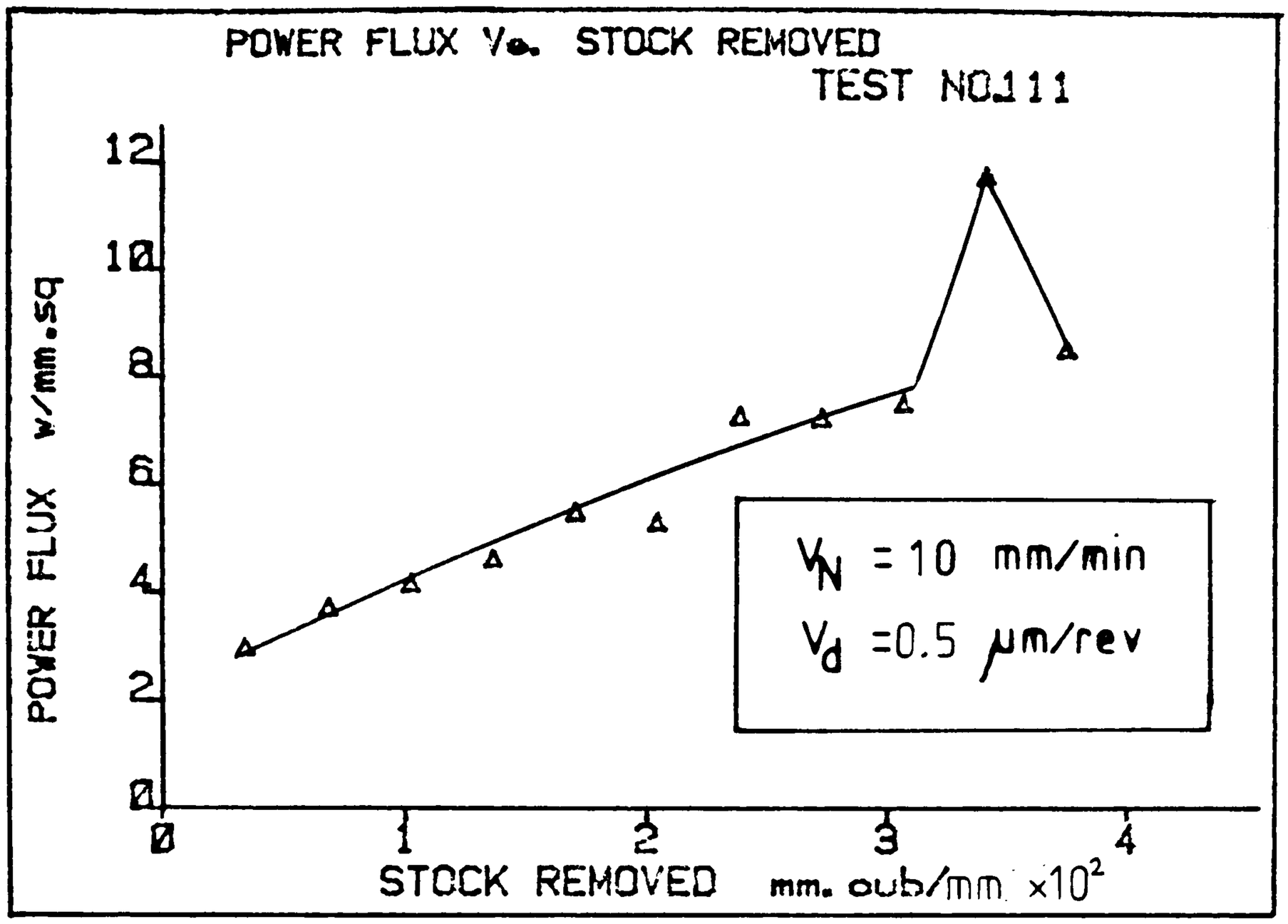

FIG 57

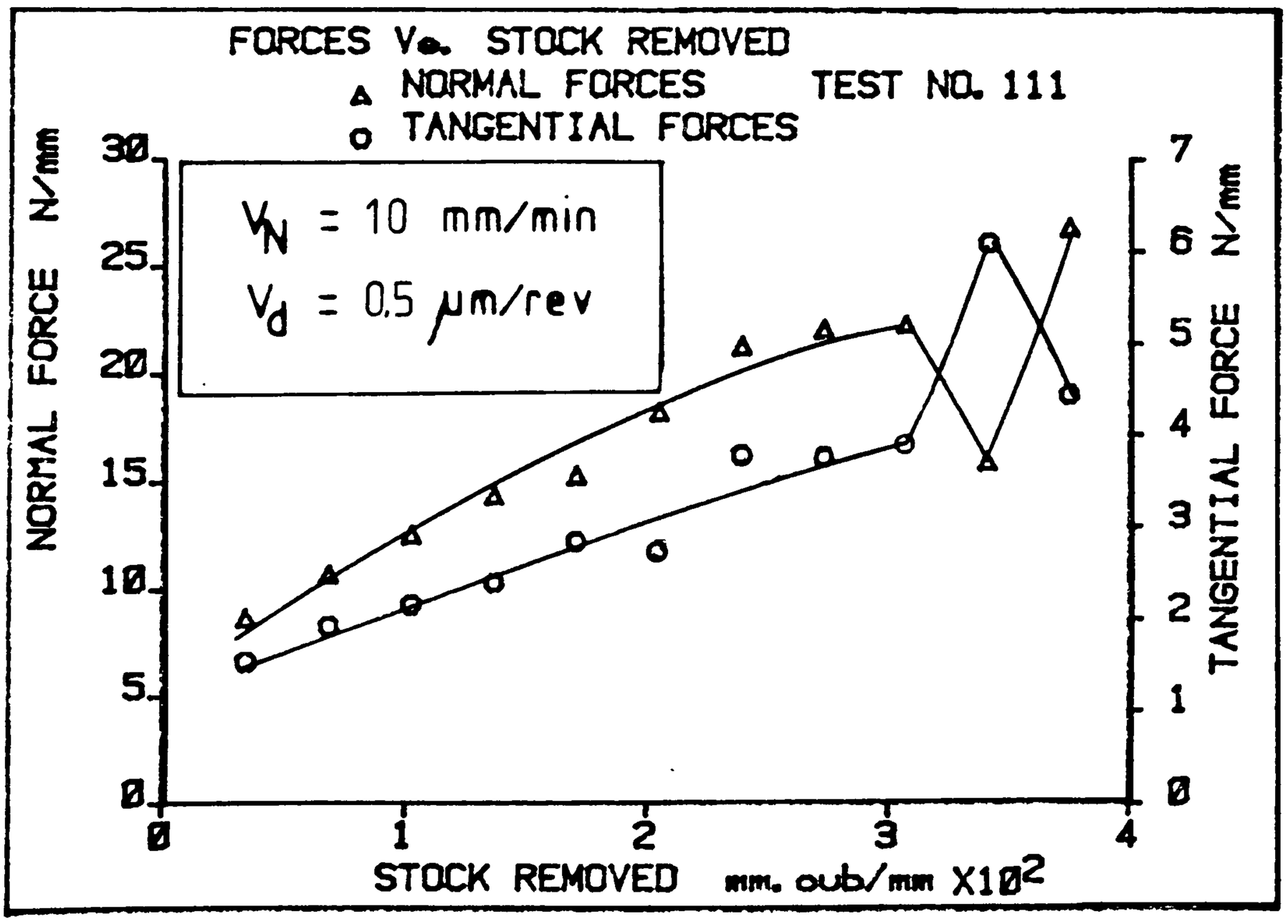

FIG 58

POWER FLUX AND GRINDING FORCES Vs. STOCK REMOVED WITH NEAT OIL GRINDING FLUID

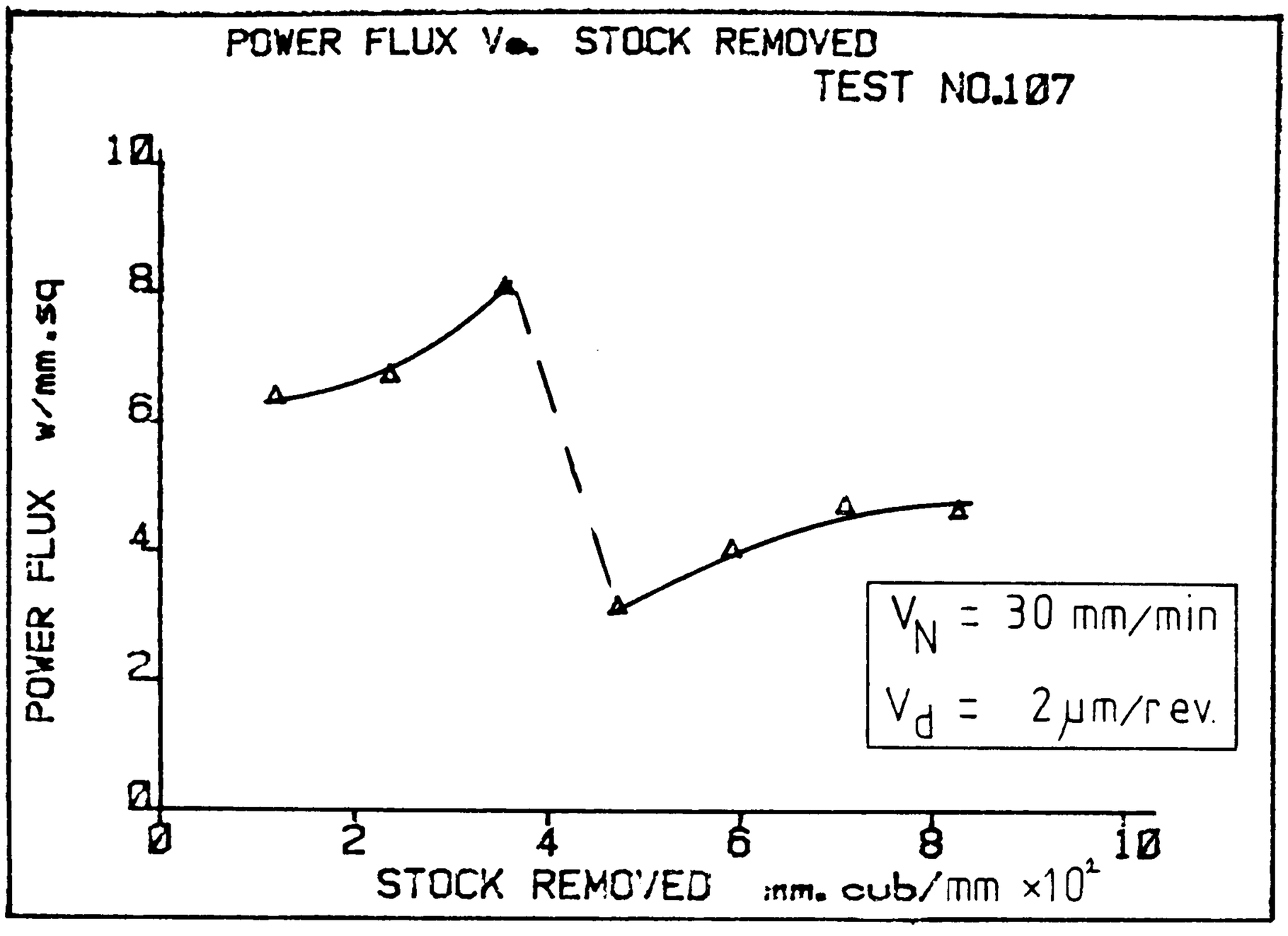

FIG 59

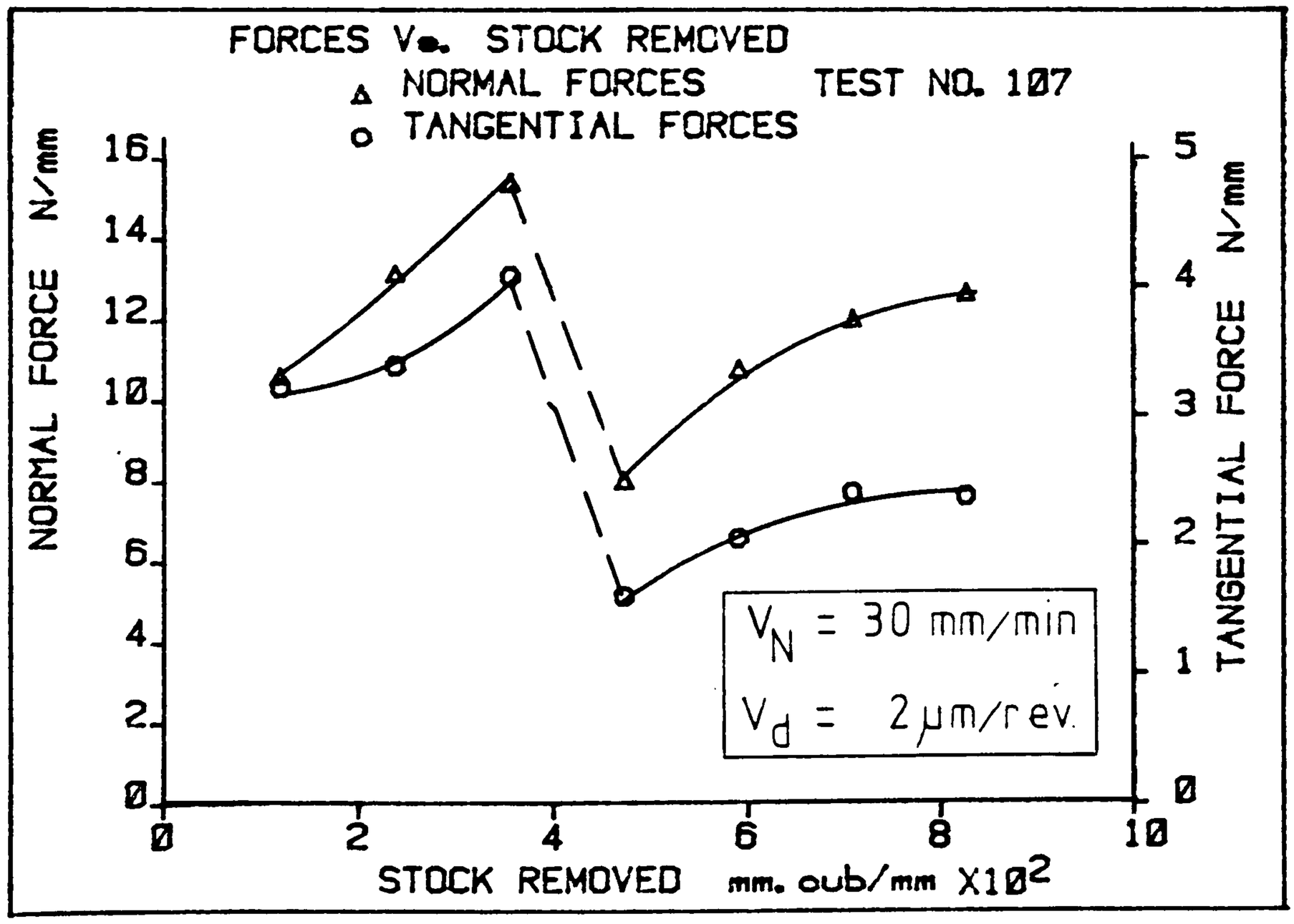

FIG 60

POWER FLUX AND GRINDING FORCES Vs. STOCK REMOVED WITH NEAT OIL GRINDING FLUID

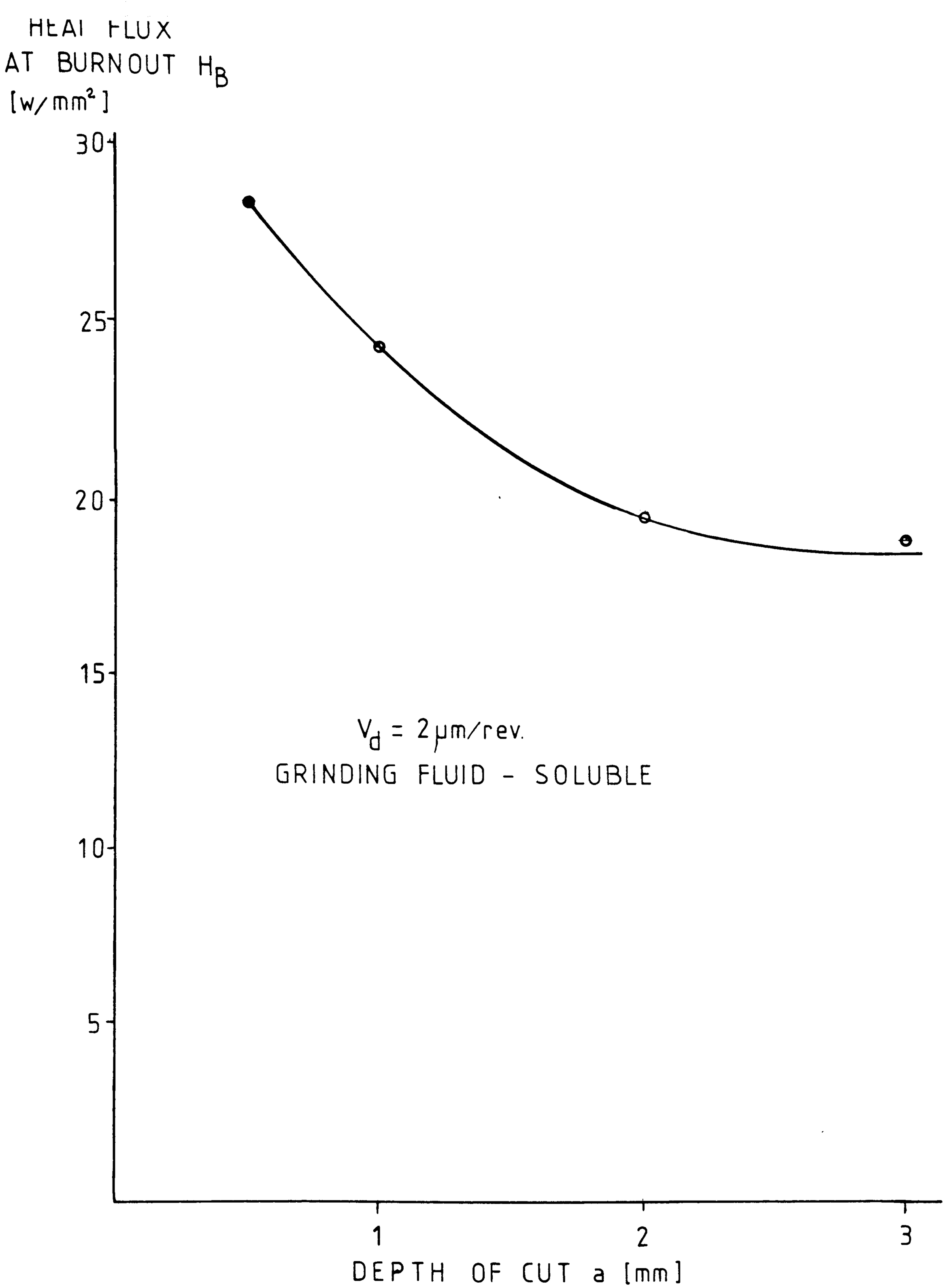

FIG 61 BURNOUT HEAT FLUX Vs. DEPTH OF CUT (EXPERIMENTAL)

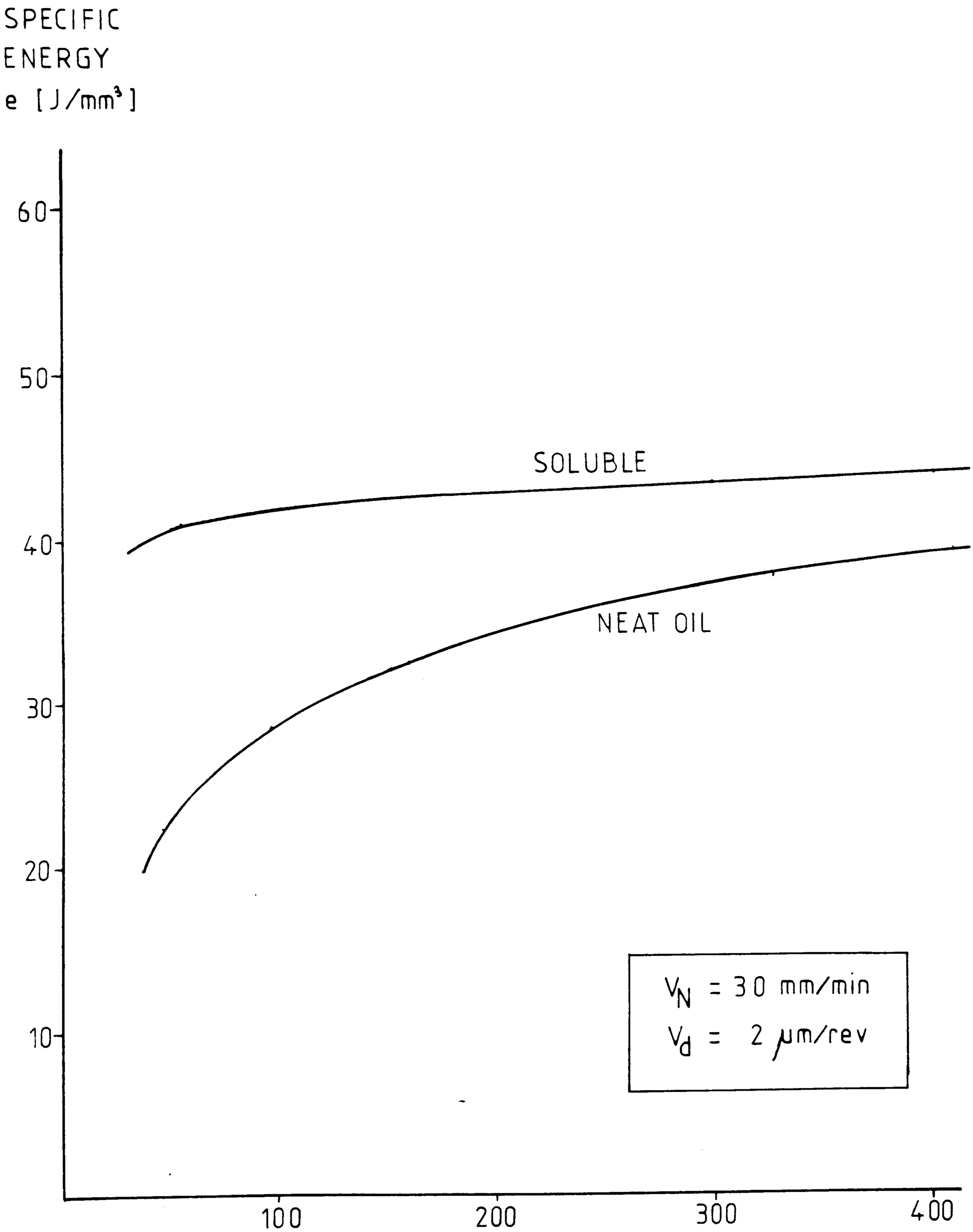

FIG 62 SPECIFIC ENERGY Vs. STOCK REMOVED FOR OIL AND WATER BASED GRINDING FLUIDS

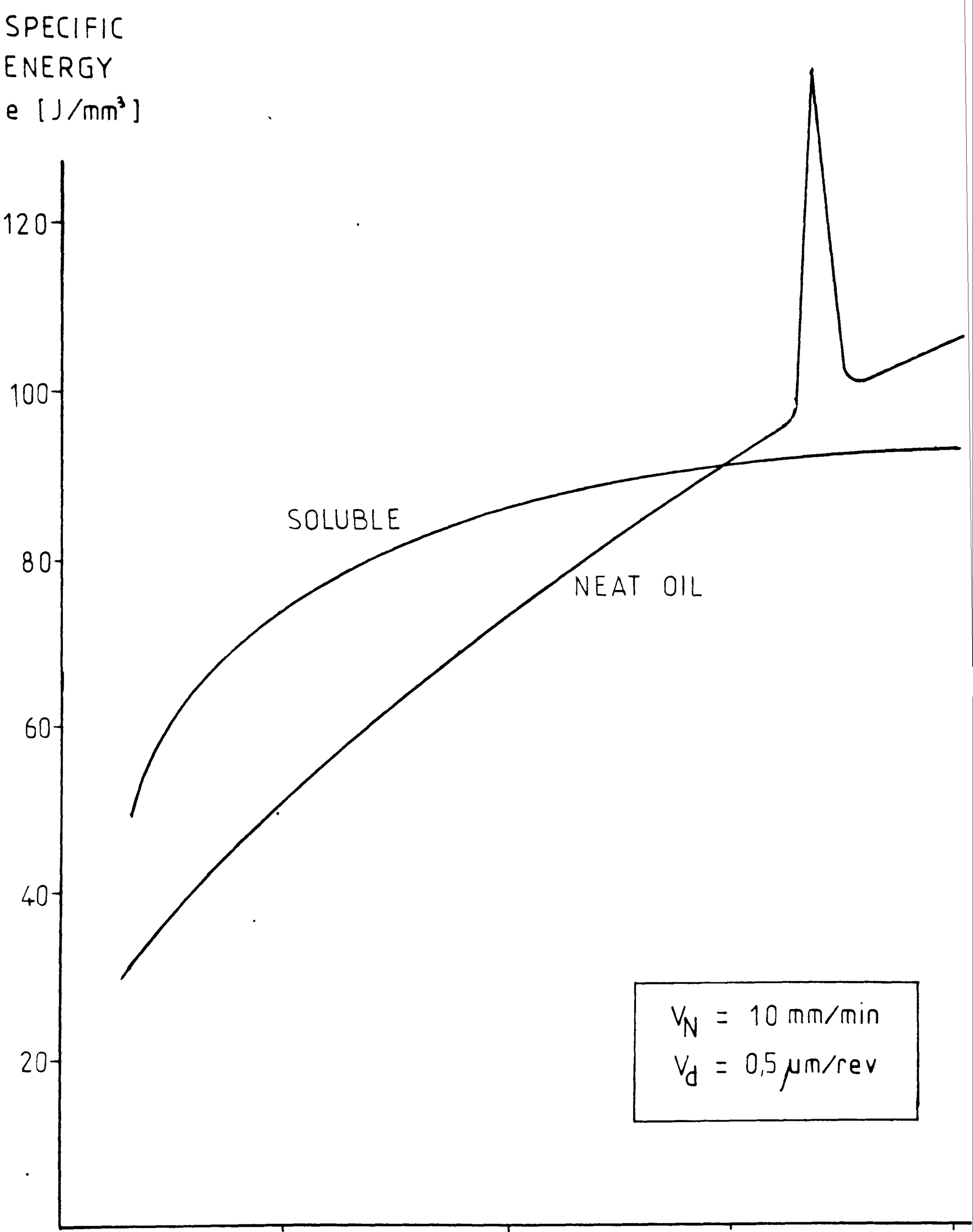

FIG 63 SPECIFIC ENERGY Vs. STOCK REMOVED FOR OIL AND WATER BASED GRINDING FLUIDS

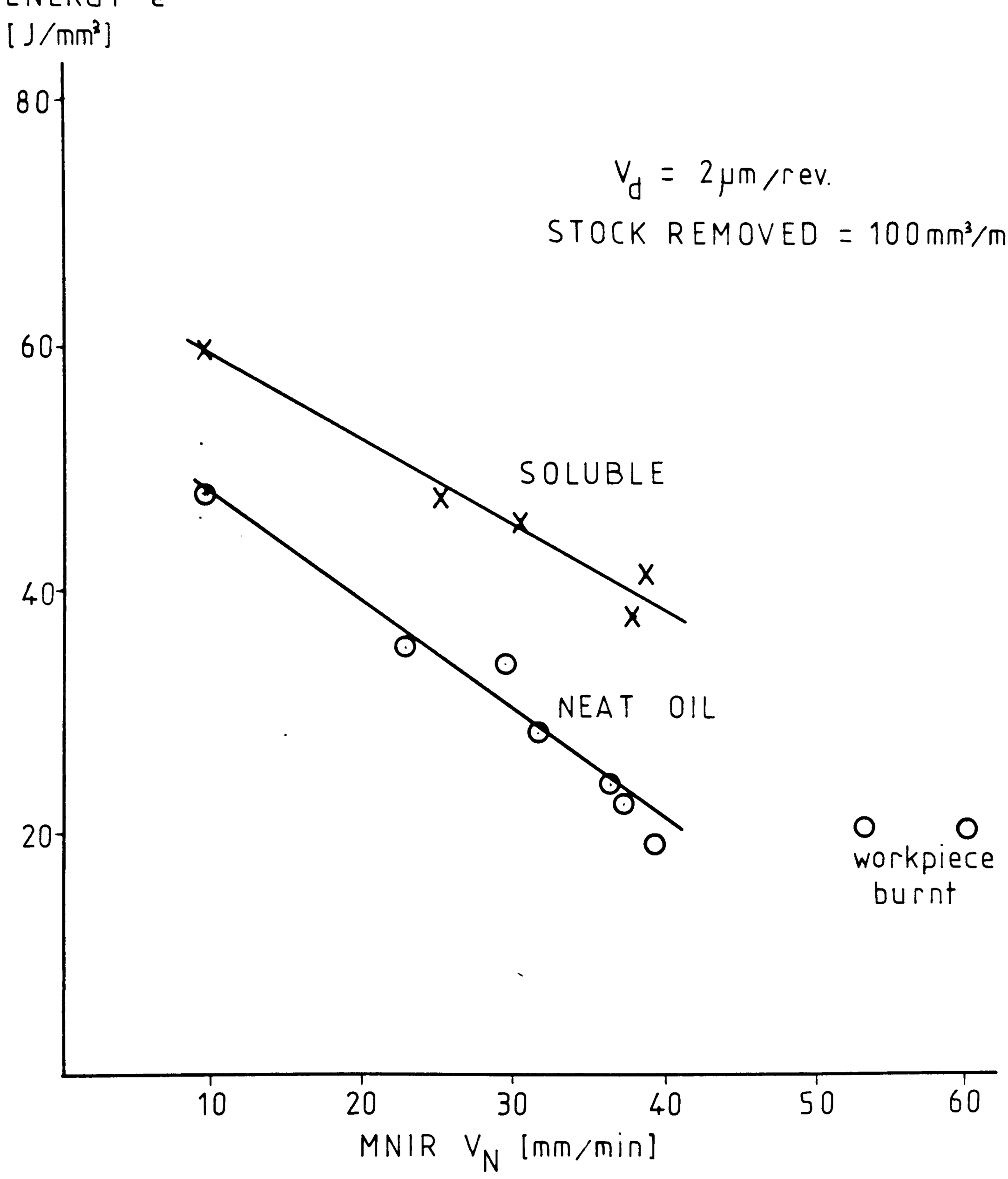

FIG 64 SPECIFIC ENERGY Vs. MNIR FOR OIL AND WATER BASED GRINDING FLUIDS

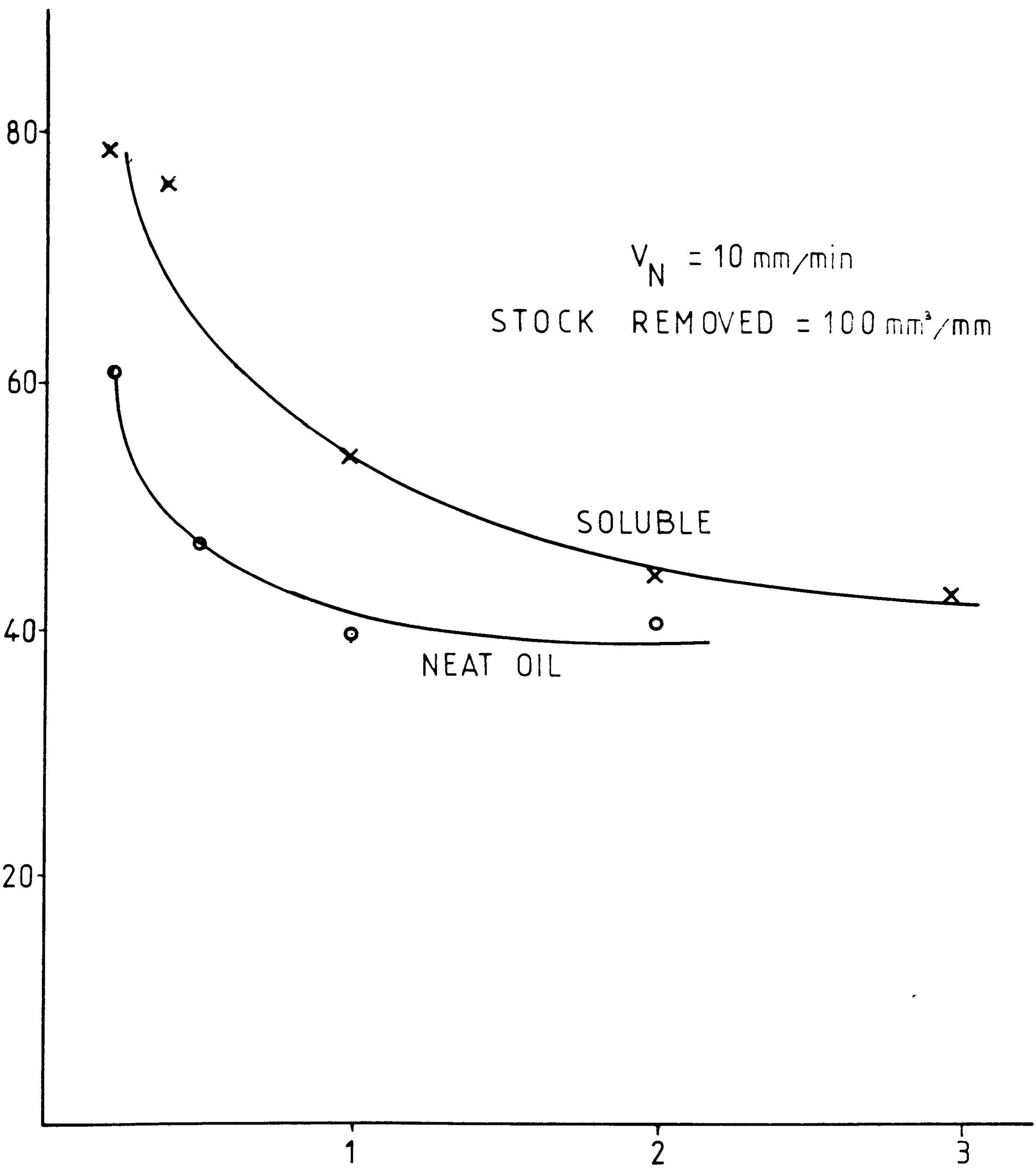

FIG 65 SPECIFIC ENERGY Vs. DRESSER INFEED RATE FOR OIL AND WATER BASED GRINDING FLUIDS

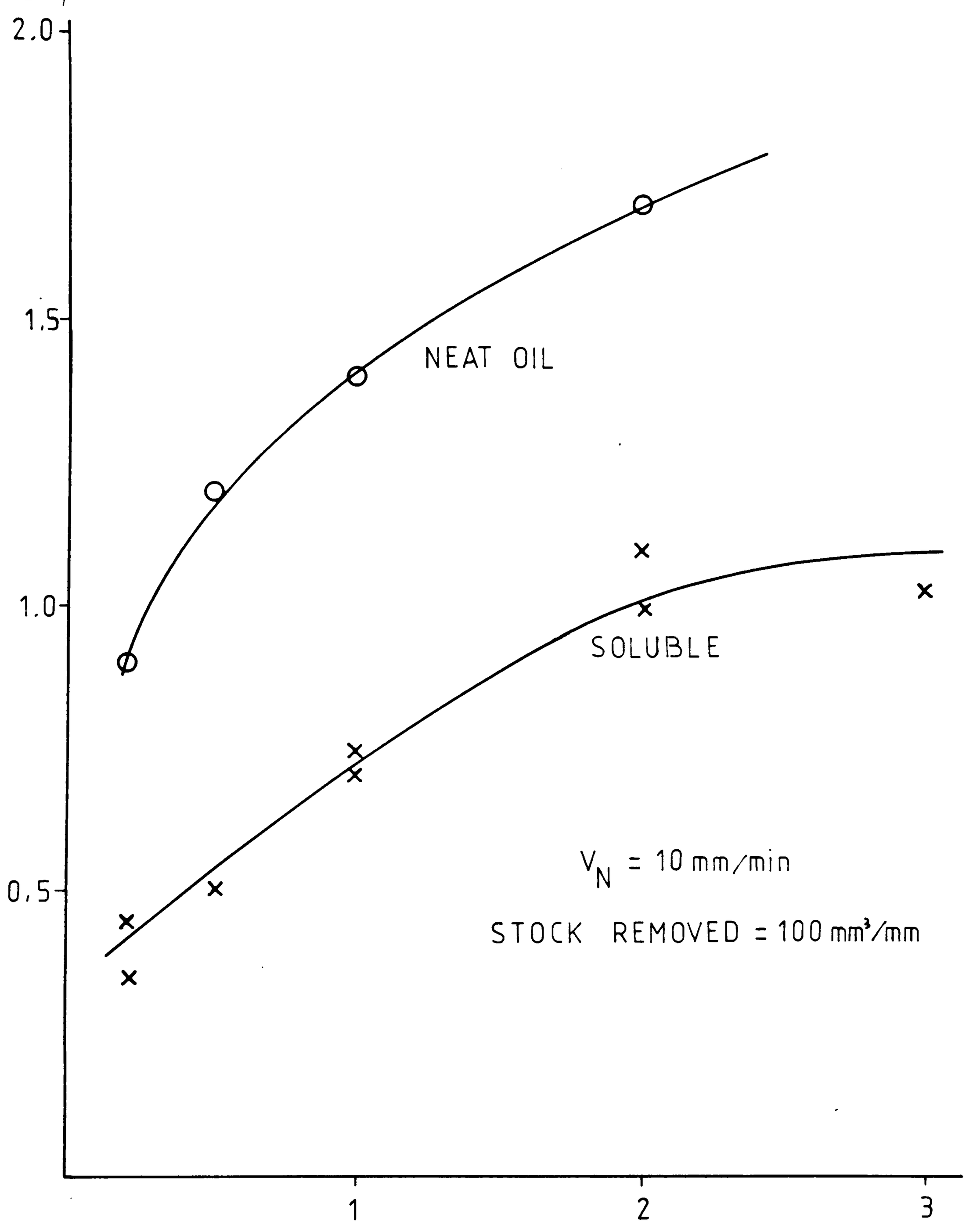

FIG 66 SURFACE FINISH Vs. DRESSER INFEED RATE FOR OIL AND WATER BASED GRINDING FLUIDS

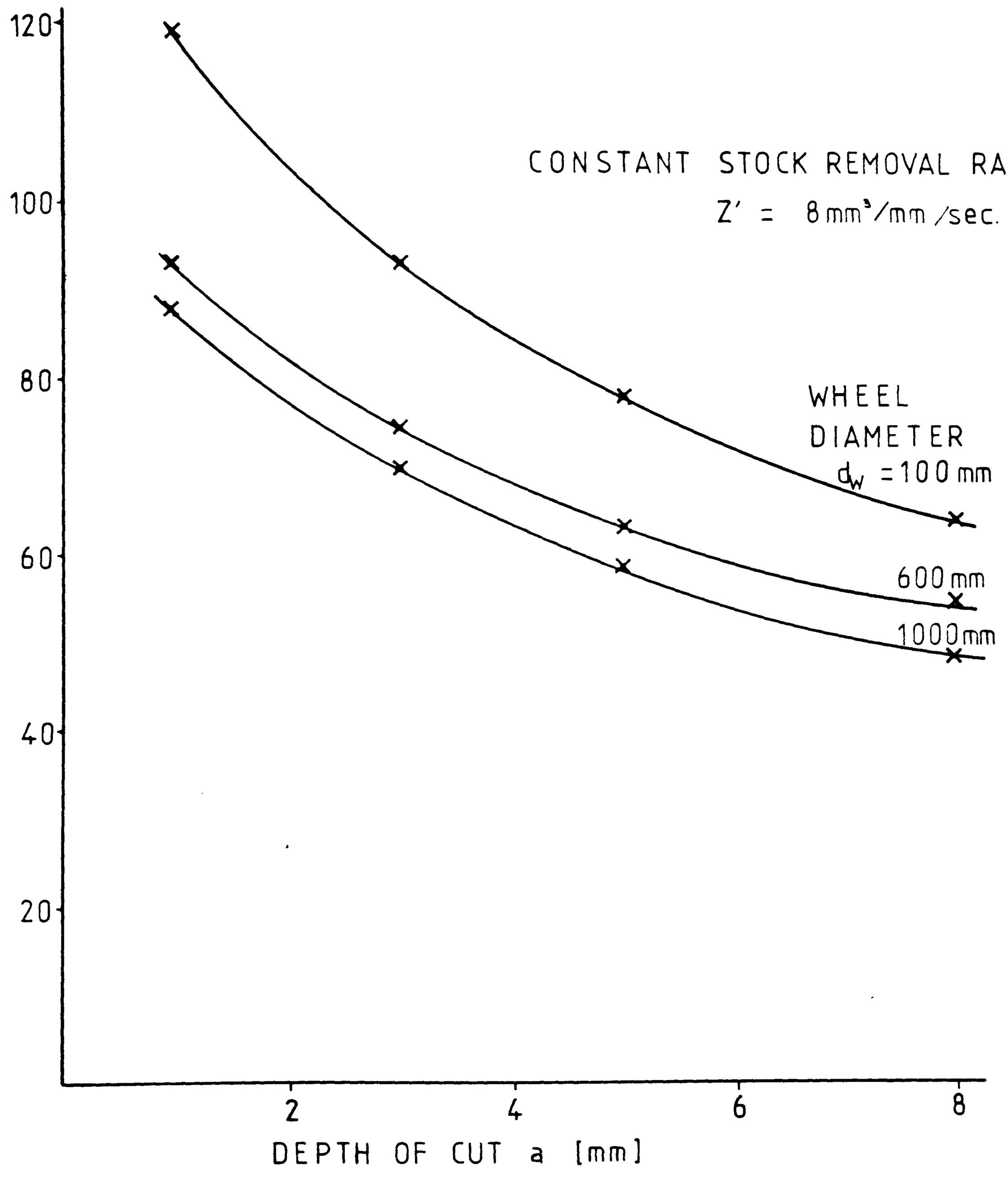

FIG 67 MAX. WORKPIECE TEMPERATURE Vs. DEPTH OF CUT FOR VARIOUS WHEEL DIAMETERS FROM FINITE ELEMENT ANALYSIS

	MATERIAL	GRINDING FLUID	q_w	T_B
A	STEEL	SOLUBLE	1·7%	130°C
B	NIMONIC	SOLUBLE	1·1%	110°C
C	STEEL	NEAT OIL	13 %	290°C

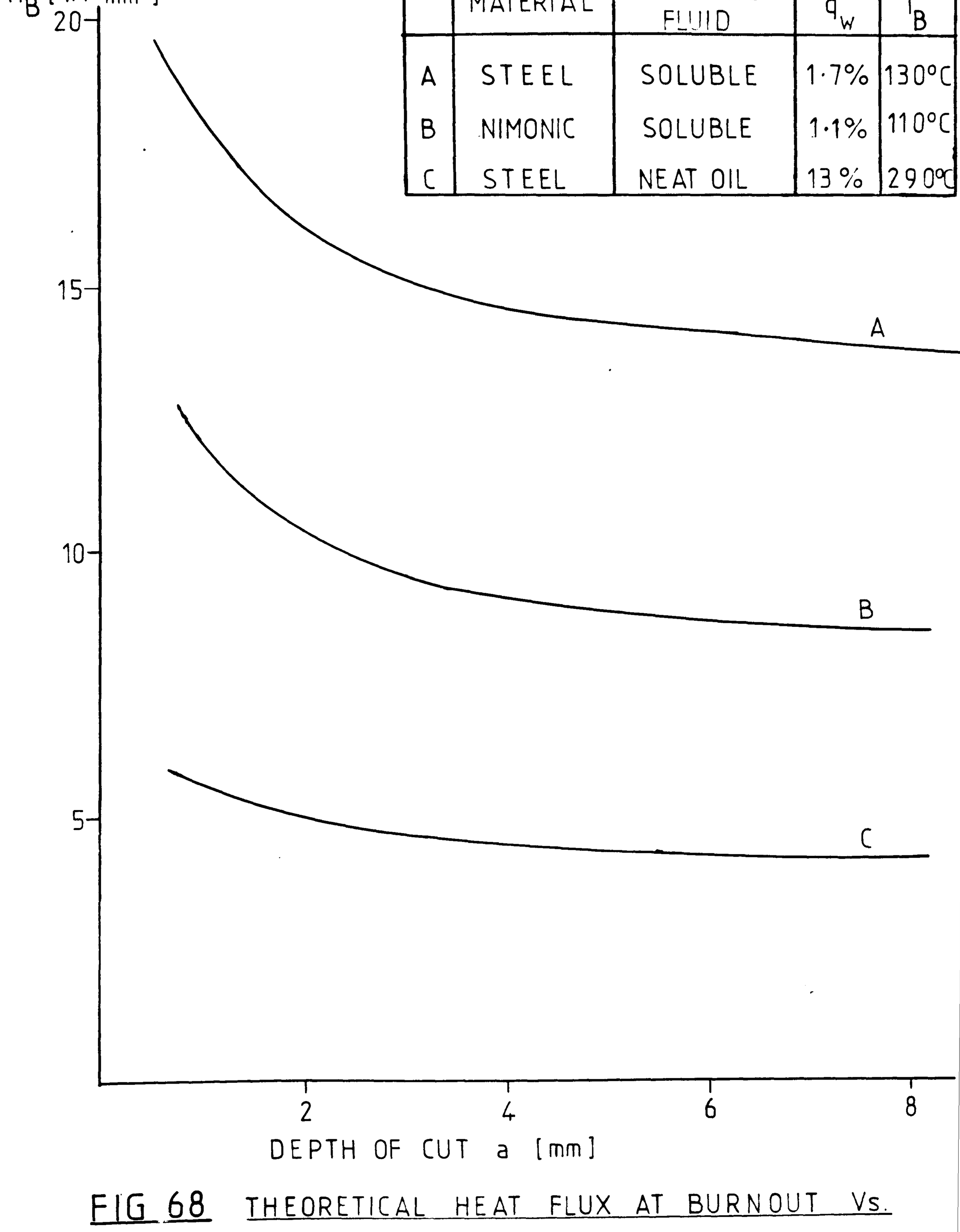

FIG 68 THEORETICAL HEAT FLUX AT BURNOUT Vs. DEPTH OF CUT [FROM FINITE ELEMENT ANALYSIS

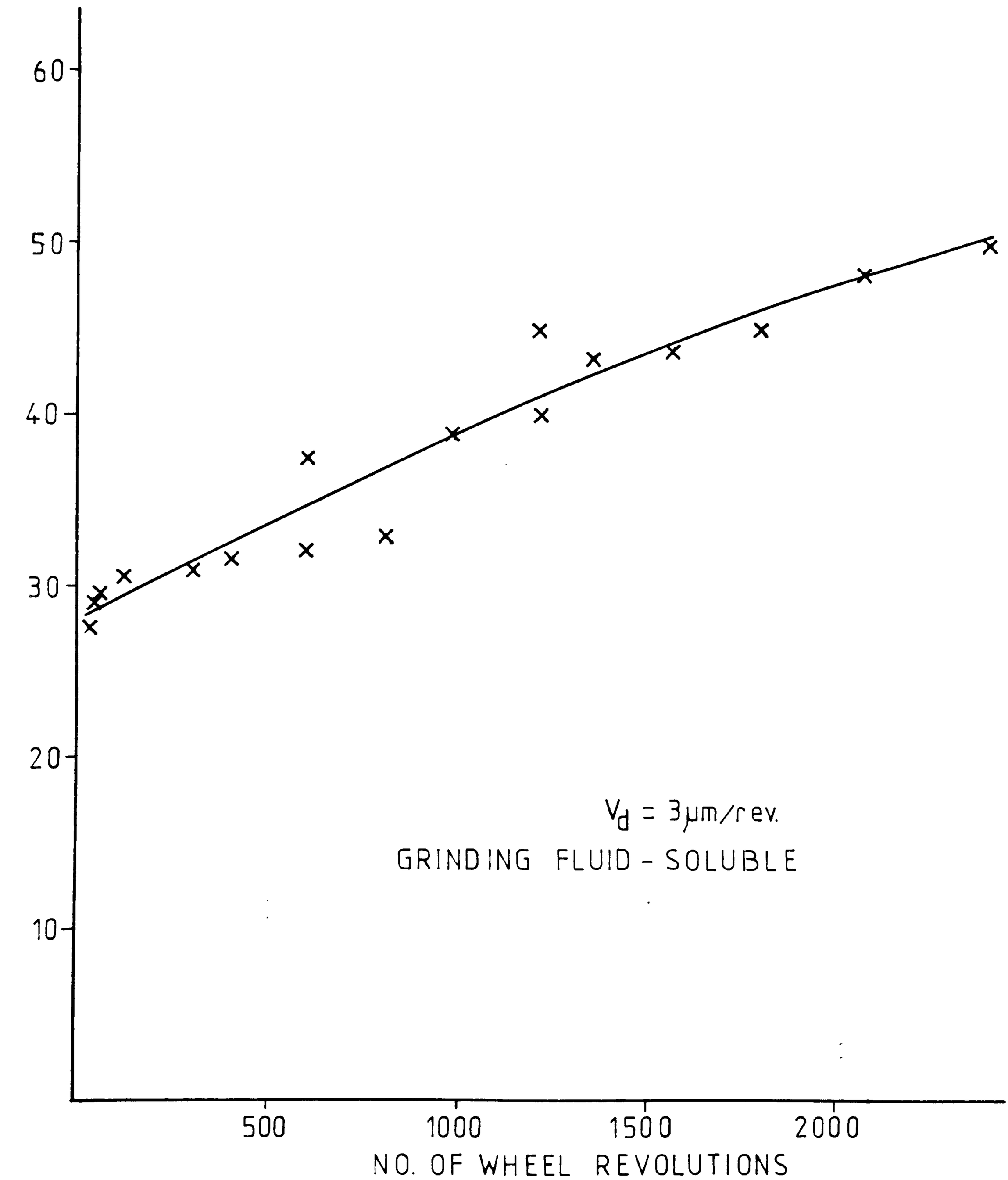

FIG 69 SPECIFIC ENERGY Vs. NUMBER OF WHEEL REVOLUTIONS FROM TESTS AT VARIOUS FEED RATES

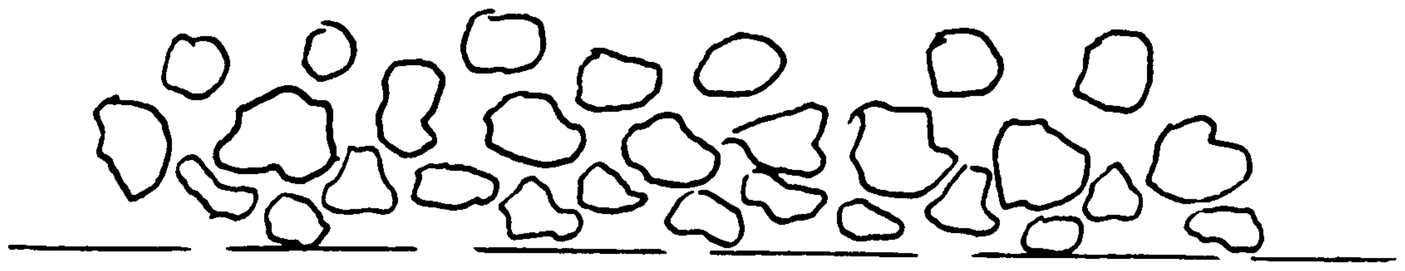

WHEEL FRESHLY DRESSED

SAME WHEEL AFTER INITIAL WEAR PHASE

FIG 70 INCREASE IN NUMBER OF ACTIVE GRITS DURING INITIAL WHEEL WEAR

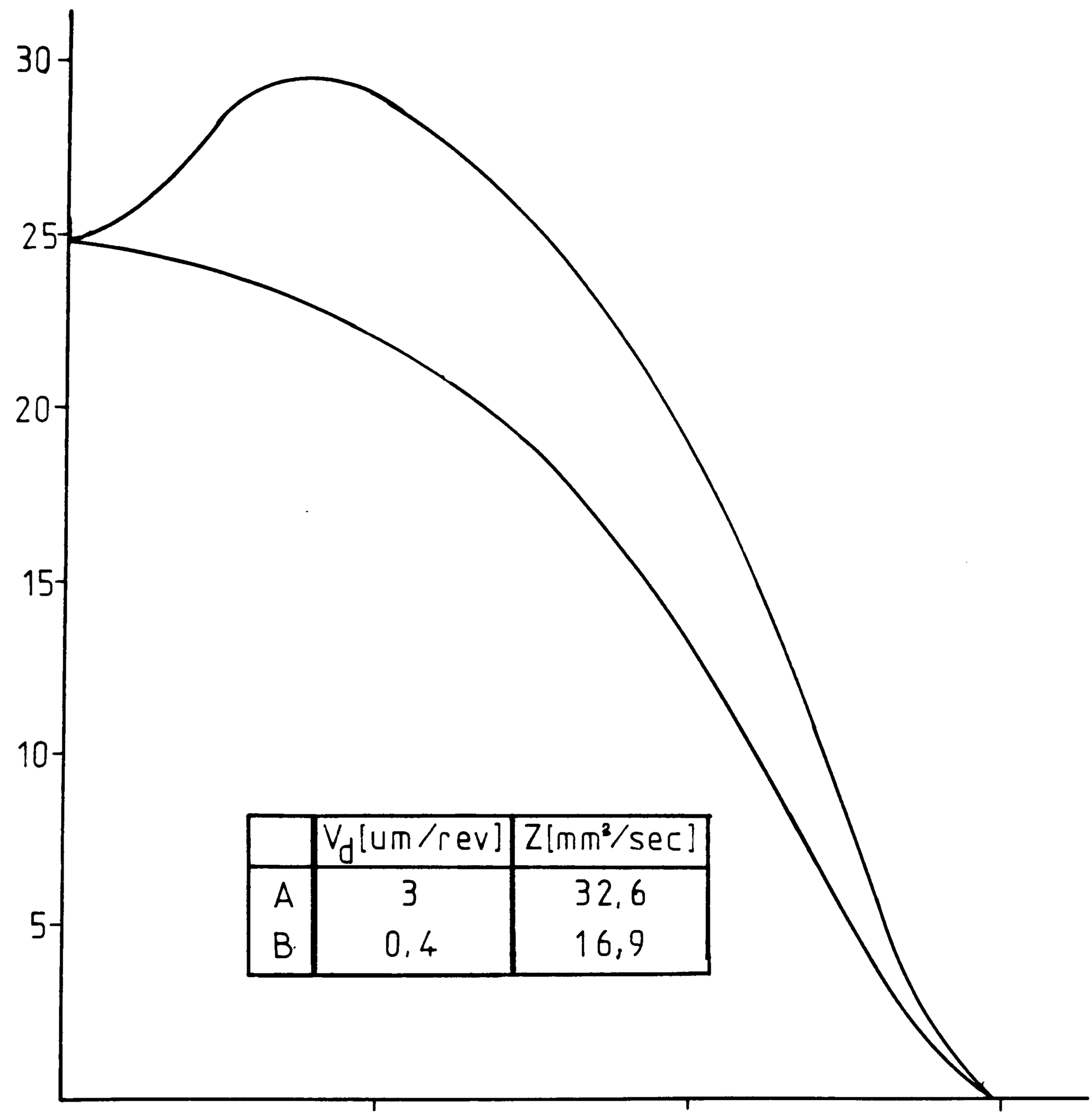

	V_d[um/rev]	Z[mm²/sec]
A	3	32,6
B	0,4	16,9

FIG 71 DISTRIBUTION OF POWER FLUX AROUND A SEMI CIRCULAR FORM

Text cut off in original

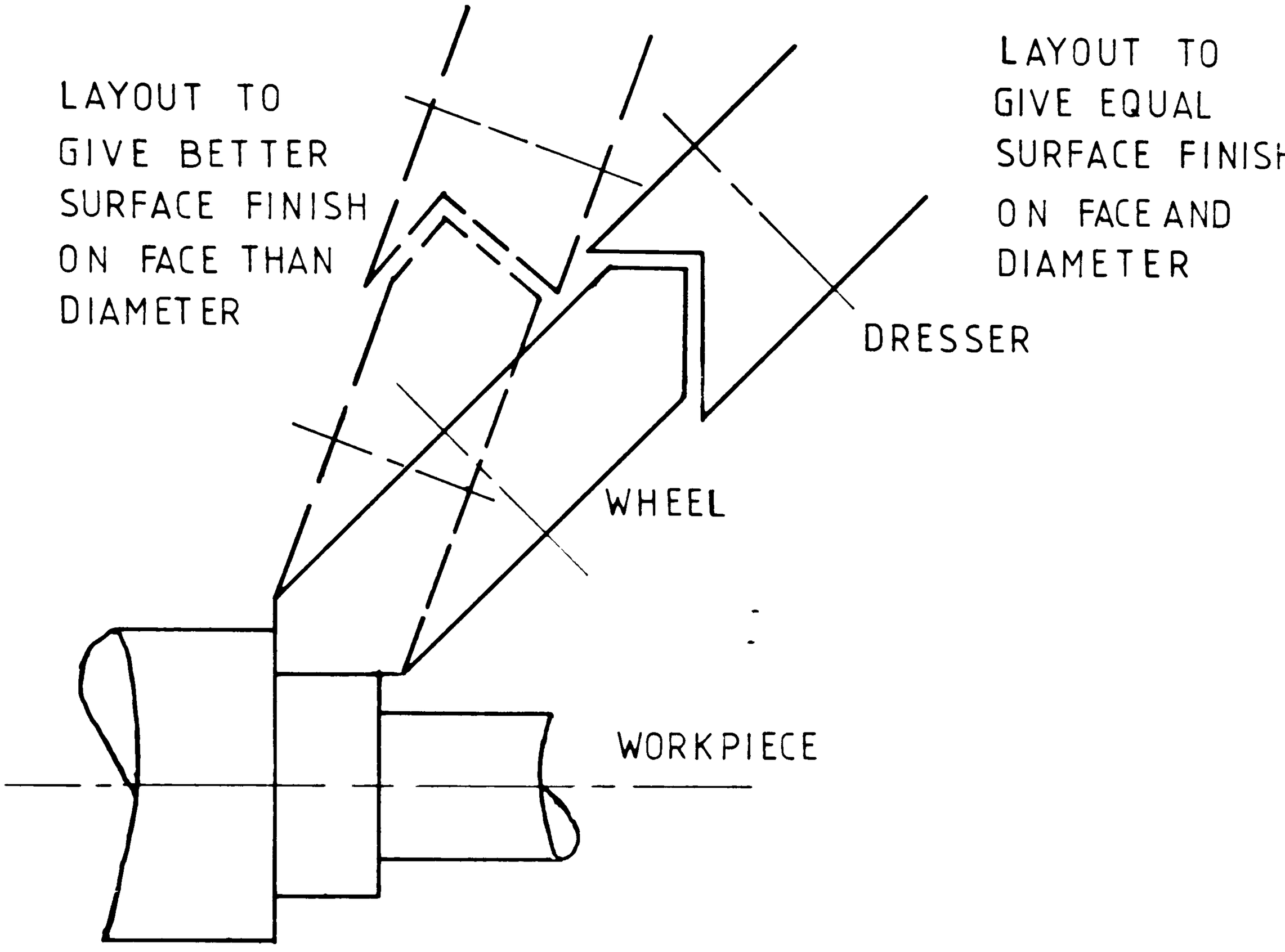

FIG 72 AN ANGLED APPROACH GRINDING OPERATION

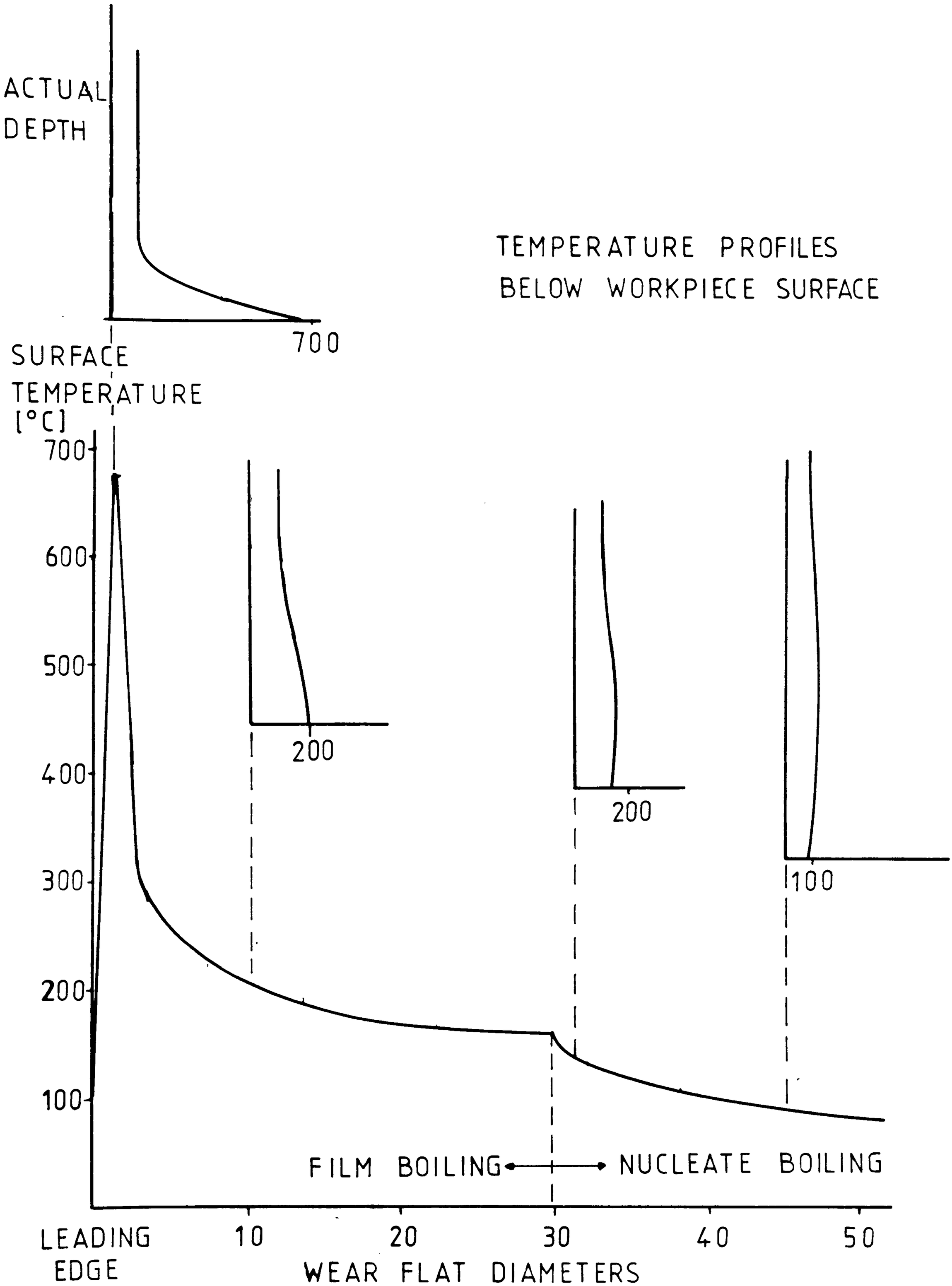

TEMPERATURE PROFILES BELOW WORKPIECE SURFACE

FIG 73 SURFACE TEMPERATURE VARIATION BEHIND AN ACTIVE GRINDING GRIT [BASED ON rIFMENTS ref. 87]

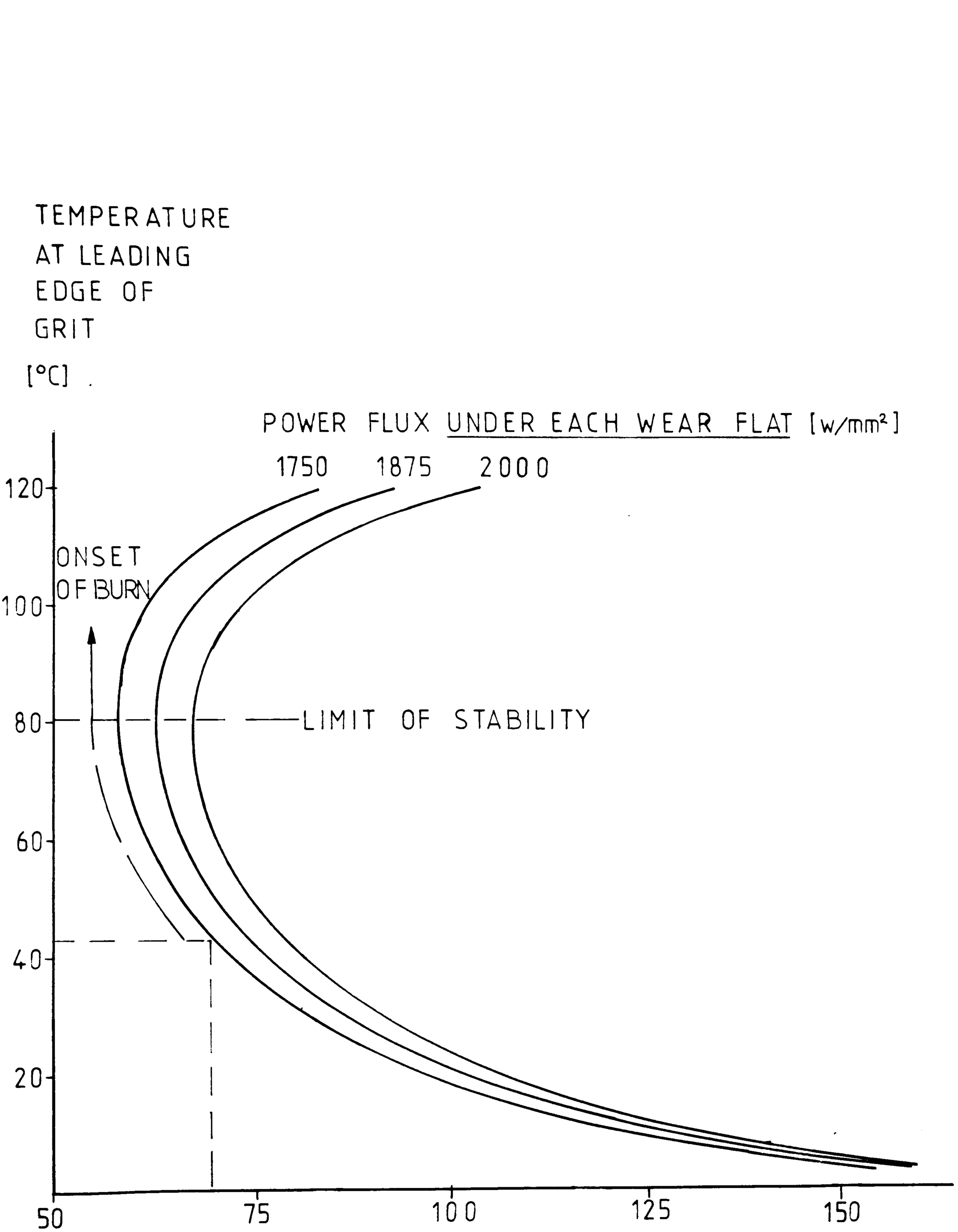

FIG 74 THERMAL STABILITY CURVES [BASED ON CLEMENTS ref 87]

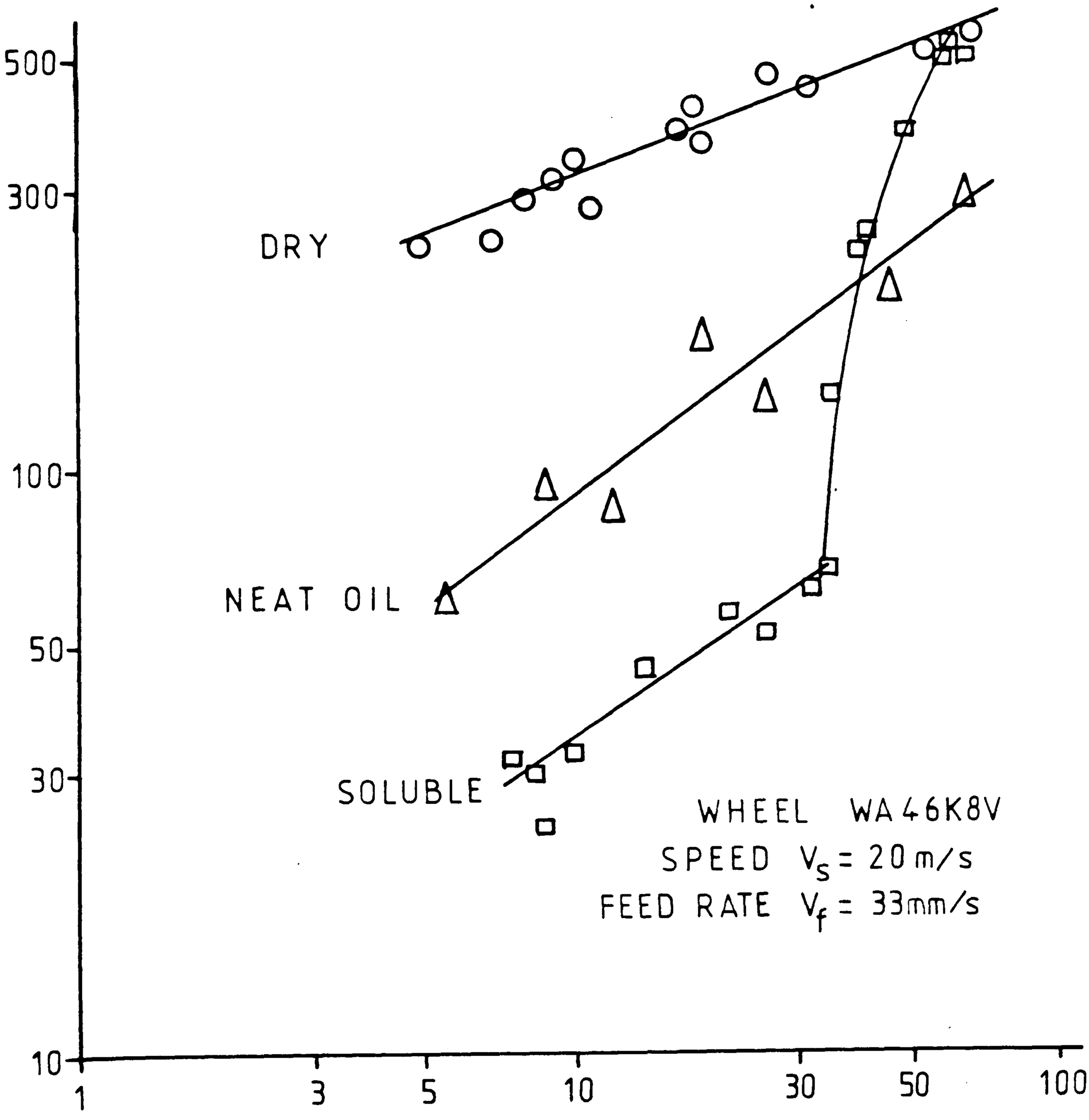

FIG 75 MAXIMUM WORKPIECE TEMPERATURE FOR DIFFERENT GRINDING FLUIDS UNDER CONVENTIONAL GRINDING CONDITIONS [AFTER YASUI AND TSUKUDA ref 59]